(2)

Theory of Pseudogap Phenomena in High-T_c Cuprates – Based on the Strong Coupling Superconductivity –

Youichi YANASE

December 27, 2000

Abstract

In this thesis we investigate the pseudogap phenomena in High-T_c superconductors. In our scenario, the superconducting fluctuations are the origin of the pseudogap. They are sufficiently strong to give rise to the pseudogap in the quasi-two dimensional strong coupling superconductors. We calculate the effects of the superconducting fluctuations on the normal state electronic structure. The pseudogap phenomena are naturally derived from the *resonance scattering* due to the superconducting fluctuations. The obtained results comprehensively explain the pseudogap phenomena in High-T_c superconductors including their doping dependence. First, we expand the reciprocal of the T-matrix with respect to the momentum and the frequency, and we discuss the properties of the expansion parameters. We estimate these parameters and carry out the calculations for the single particle self-energy using the T-matrix and the self-consistent T-matrix approximations, respectively (§3.1). The spectral weight and the density of states show the pseudogap by the effects of the resonances scattering. The critical temperature T_c is remarkably reduced owing to the fluctuations. Second, the effect of the magnetic field on the pseudogap phenomena are investigated. The obtained results well explain the experimental results including their doping and temperature dependences (§3.2). Third, the superconducting phase transition from the pseudogap state is investigated. The characteristic features of the phase transitions are naturally confirmed (§3.3). Moreover, the anomalous properties of High-T_c superconductors are investigated both in the normal state and in the superconducting state. The comprehensive understanding of the NMR, the neutron scattering, the in-plane and c-axis resistivity, the optical conductivity and the London penetration depth is obtained (§3.4). Finally, the resonance scattering scenario on the pseudogap phenomena is well justified on the basis of the Hubbard model which includes only the on-site repulsive interaction U (§4). The electronic state and the anti-ferromagnetic spin fluctuations are calculated by using the fluctuation exchange (FLEX) approximation. The T-matrix which is the propagator of the superconducting fluctuations is calculated by extending the Éliashberg equation. The self-energy due to the superconducting fluctuations is calculated by the FLEX+T-matrix approximation. The pseudogap in the single particle properties and the magnetic properties is derived. The doping dependence is well reproduced. The comprehensive explanation for the phase diagram of High-T_c cuprates is obtained. Furthermore, we apply the theory to the electron-doped cuprates and obtain the consistent results with the recent experiments. The results of the self-consistent calculation for the spin fluctuations, superconducting fluctuations and the single particle properties are carried out within the FLEX and the self-consistent T-matrix approximations. The relation between the superconducting fluctuations and the spin fluctuations are clarified. The calculated superconducting critical temperature T_c is remarkably reduced from the results of the mean field (FLEX) calculation. In particular, it is shown that the critical temperature decreases with decreasing doping concentration in the under-doped region with large U. Thus, we start from the Fermi liquid state, and succeed in describing the High-T_c cuprates including the under-doped region.

Acknowledgments

The author expresses his sincerest gratitude to Professor Kosaku Yamada for his appropriate guidance, fruitful discussions and kindhearted encouragements during the graduate course. Without his instructive suggestions, the graduate course in the four and a half years had been less meaningful. The author is impressed by his point of view, vision and insight. The instruction from Prof. K. Yamada will be a basis of the future studies of the author.

The author thanks Professor Tetsuo Ohmi for valuable discussions and comments. The author has received the knowledge on the unconventional superconductivity from the studies of Prof. T. Ohmi.

The author is most grateful to Professor Ryusuke Ikeda for many valuable comments and discussions on the superconducting fluctuations. The comments from the expert in the superconducting fluctuations have been important for the author to complete the work. The earnest attitude of Prof. R. Ikeda toward the theoretical studies have influenced the author.

The author would like to thank Dr. Satoshi Fujimoto and Dr. Hiroaki Ikeda for valuable discussions and gracious encouragements. Dr. S. Fujimoto have given the critical reading of some published papers of the author.

The author would like to thank Professor Yoshiteru Maeno and his co-workers for valuable discussions and comments from the experimental point of view.

The author greatly appreciate the valuable discussions with Professor Masao Ogata (Tokyo), his fruitful comments and the kind hospitality of the members of the Ogata group. The author expresses a genuine gratitude to Prof. M. Ogata for the new circumstance to study and a lot of kind encouragements.

The author are grateful to Prof. M. Ido, Prof. M. Oda, Dr. N. Momono (Hokkaido University), Prof. T. Takahashi, Mr. T. Sato (Tohoku University), Dr. T. Takimoto (Electrotechnical Laboratory), Prof. D. Hirashima, Dr. Y. Ohasi (University of Tsukuba), Prof. T. Moriya (Science University of Tokyo), Prof. Fukuyama, Prof. K. Ueda, Prof. M. Imada, Prof. M. Kohmoto, Dr. T. Shibauchi, Mr. S. Onoda, Mr. H. Yamase, Mr. T. Kisu (University of Tokyo), Prof. H. Kontani (Saitama University), Dr. T. Okabe (Shizuoka University), Dr. J. Kishine (Institute for Molecular Science), Prof. Y. Kuroda, Prof. Y. Tanaka, Dr. A. Kobayashi, Dr. A. Tsuruta (Nagoya University), Prof. T. Ishiguro, Prof. Kazuyoshi. Yamada, Dr. M. Fujita, Dr. S. Nakatuji (Kyoto University), Prof. H. Kohno, Dr. H. Maebashi, Dr. T. Ichinomiya, Dr. G-q. Zheng, Dr. K. Ishida, Dr. T. Mito, Dr. Y. Tokunaga (Osaka University), Dr. K. Kanki (Osaka Prefecture University) T. Ekino (Hiroshima University) for valuable discussions and comments.

Thanks are extended to all members of *Bussei Riron* group for their kind help. The author thank Dr. Sigeru Koikegami and Mr. Takanobu Jujo for fruitful discussions on the pseudogap phenomena. The especial thanks are expressed to superusers of computers for the good environment and the kind instruction. The author would like to express his genuine acknowledgments to the roommate in Room 514, Dr. Hiroya Nakao, Mr. Hideaki Ishibashi, Dr. Yutaka Sakai, Mr. Tsuyoshi Mishiro, Mr. Hiroshi Kori and Mrs. Hirono Fukazawa for their a lot of kindness.

At last, the author wishes to express his gratitude to his family, Kensuke Yanase, Yoshimi Yanase, Takakazu Izaki and Hiroko Izaki for their continuous encouragements.

Contents

Chapter 1

Introduction

Since the discovery of the high-temperature (High-T_c) superconductivity by Bednortz and Müller [1], many studies on the High-T_c superconductors have been carried out for a long time.

In the first stage, the symmetry of the Cooper pairs and the mechanism of the superconductivity have been the main issues. The symmetry of the conventional BCS superconductors is the s-wave which is mediated by the electron-phonon interaction [2]. In the early stage, some experiments indicated the s-wave superconductivity also in the High-T_c superconductivity. However, the more detailed analysis have shown the d-wave superconductivity both experimentally [3] and theoretically [4]. After that, the phase-sensitive experiments have supported the d-wave symmetry [5, 6]. The d-wave superconductivity is a common conclusion at present.

Many scenario on the mechanism of the d-wave superconductivity have been proposed by many authors. Among them, the nearly anti-ferromagnetic Fermi liquid theory [7, 8] has obtained a considerable consensus untill now. The nearly anti-ferromagnetic Fermi liquid theory starts from the Fermi liquid state and considers the strong anti-ferromagnetic spin fluctuations [9, 10]. The d-wave pairing interaction mediated by the anti-ferromagnetic spin fluctuations is a natural result of this theory [7, 8].

The other well-known starting point is the t-J Hamiltonian in which the super-exchange interaction J is included. The t-J Hamiltonian is used to descrive the resonating valence bond (RVB) theory which starts from the non-Fermi liquid state [11, 12]. The d-wave superconductivity have been shown also in the t-J Hamiltonian [13, 14, 15].

In the next stage, the anomalous properties in the normal state have been the current issues. In this context, the phrase 'anomalous' means the deviation from the conventional Fermi liquid theory. The Fermi liquid theory has shown the good success in the general description of the metals [16]. However, the many quantities including the magnetic and transport properties show the 'anomalous' behavior in the under-doped region. The pseudogap phenomena are the typical ones. With increasing the hole-doping, the anomalous behavior continuously changes to the conventional one in the Fermi liquid theory.

The electron-correlation is considered to be strong in the under-doped region which is near the metal-insulator transition. Therefore, the description of the normal state properties has been one of the main topics of the strongly correlated electron systems. Needless to say, the normal state is the stage in which the High-T_c superconductivity occurs. Therefore, it is expected that the understanding of the anomalous properties gives the comprehensive understanding of High-T_c superconductivity.

In particular, the anomalous properties have frequently lead the argument that the Fermi liquid state is completely broken in High-T_c superconductors. Many ideas for the non-Fermi liquid state

have been proposed and developed. Then, the pseudogap phenomena are the main evidence of these arguments. This is the main reason that the pseudogap phenomena have been the main issues among the anomalous properties.

The pseudogap phenomena mean the suppression of the low frequency part of the various spectrum without any long range order. In other words, the gap-like behavior is observed above T_c and called 'pseudogap'. The pseudogap phenomena are the universal phenomena observed in the various compounds of High-T_c superconductors. The pseudogap is observed in the wide temperature region in under-doped cuprates. The temperature region becomes narrow with increasing the hole-doping and becomes unobservable near the optimally-doped region (Fig. 2.2). The pseudogap phenomena are the great mysteries within the conventional Fermi liquid theory, and have been regarded as the characteristics of High-T_c superconductors.

Among the non-Fermi liquid theories, the well-known one is the RVB theory [11, 12]. The spin-charge separation is the starting point of the RVB theory and two distinct excitations 'spinon' and 'holon' are considered as the low energy excitations. The 'spinon' and 'holon' have the spin and charge, respectively. The idea contradicts the Fermi liquid theory in which the low energy excitations are the adiabatically continuated quasi-particles. In the RVB theory, the pseudogap phenomena are explained as a singlet pairing of the 'spinons'. The magnetic excitations are suppressed by the singlet pairing. Since the 'holons' couple to the 'spinons' only thorough the gauge field, the singlet pairing only weakly affects on the transport phenomena. These features are consistent with the characteristics of the pseudogap phenomena. Therefore, the pseudogap phenomena have been regarded as the evidence of the spin-charge separation. Thus, they are key issues on the argument, 'High-T_c superconductors are Fermi liquid or non-Fermi liquid ?'.

Here, we consider it natural that the anomalous properties are explained by starting from the Fermi liquid state and taking into account some characteristic factors of the systems. Such explanation is necessary for the comprehensive understanding of the High-T_c superconductors in which the anomalous behavior in the under-doped region continuously changes to the conventional behavior in the over-doped region. It should be noticed that there are no phase transition from the over-doped region to the under-doped one.

Actually, the many theoretical studies have been made from the above point of view. Most of 'anomalous' properties have already been explained by these studies. For example, the superconducting critical temperature T_c with relevant order of magnitude is obtained by starting from the Fermi liquid state. Moreover, the transport phenomena, such as T-linear resistivity $\rho(T)$, enhanced Hall coefficient $R_H(T)$ and incoherent c-axis resistivity $\rho_c(T)$ have been explained. They are the typical 'anomalous' properties which are contradictory to the conventional Fermi liquid theory. In most of these theories, the anti-ferromagnetic spin fluctuations, which are the origin of the pairing interaction, play a dominant role. Thus, many of the 'anomalous' properties are explained by the approach based on the Fermi liquid theory. However, the sufficient understanding of the pseudogap phenomena have not been obtained from these approaches. The comprehensive understanding of the phenomena have remained as the last and important problem for us.

As an approach from the Fermi liquid state, there are some scenarios on the problem. One is the magnetic scenarios which take into account the anti-ferromagnetic spin fluctuations or the anti-ferromagnetic hidden order [9, 17, 18, 19]. Another one is the pairing scenarios in which the pseudogap is a precursor of the superconductivity. The pairing scenario was proposed in the early stage [20]. This scenario became to be noticed [21] after the experiments have indicated the close relation between the pseudogap state and the superconducting one [22, 23]. However, the theories in the first stage do not correspond to the realistic situation, and therefore the sufficient

understanding has not been obtained by these theories.

In this thesis, we derive the pseudogap phenomena under the relevant situation for High-T_c superconductors [24]. It is shown by the results that the correct mechanism of pseudogap phenomena is different from that of the early theories. In our scenario, the resonance scattering due to the strong superconducting fluctuations derives the pseudogap phenomena. The validity of our scenario is shown in this thesis. We obtain the comprehensive understanding including the characteristic doping dependence, magnetic field dependence [25] and the close relation with the superconducting state [26, 27]. Moreover, the magnetic and transport properties are well explained by considering the characteristic momentum dependence of the systems [27].

We succeed in describing the pseudogap phenomena by starting from the Hubbard Hamiltonian [28]. In this calculation, we start from the repulsive Hubbard Hamiltonian, and calculate the pairing interaction within the fluctuation exchange (FLEX) approximation. We show that superconducting fluctuations arising from the pairing interaction is sufficient to give rise to the pseudogap phenomena. The doping dependence, which includes both the hole-doped and electron-doped cases, is also explained consistently. As a result, the comprehensive understanding on the basis of the pairing scenario is obtained for the pseudogap phenomena.

Hereafter, we explain our calculation and the obtained results in detail. This thesis is constructed as follows. In §2, we review the past results for the High-T_c superconductivity. The materials and the phase diagram of the High-T_c superconductors are explained in §2.1. The experimental results for the pseudogap phenomena are reviewed in §2.2. The past theories based on the pairing scenario are reviewed in §2.3. Our calculations based on the model with a d-wave attractive interaction are shown in §3. In §3.1, we give the mechanism of the pseudogap which is derived by the resonance scattering from the superconducting fluctuations. The effect of the magnetic field on the pseudogap is clarified in §3.2. The superconducting transition from the pseudogap state is investigated in §3.3. The anomalous features in the magnetic and transport properties are explained in §3.4. In §4, we explain our results based on the Hubbard Hamiltonian. The FLEX+T-matrix approximation, which is first developed here, is explained in §4.3.1. In §4.3.2, the pseudogap phenomena are derived by using the FLEX+T-matrix approximations. The doping dependence of the superconducting fluctuations is clarified in §4.3.3. The pseudogap phenomena in the magnetic properties are well explained in §4.3.4. Our theory is applied to the electron-doped cuprates in §4.3.5. Moreover, the self-consistent FLEX+T-matrix approximation is carried out in §4.4. The relation between the spin fluctuations and the superconducting fluctuations is clarified in §4.4.1. The calculated results of the single particle properties and the obtained phase diagram are shown in §4.4.2. The summary of §4 is given in §4.5. Finally, the conclusion of this thesis is given in §5.

Chapter 2

Theories and Experiments on High-T_c Superconductivity -Introduction to Pseudogap Phenomena-

2.1 Materials and Phase Diagram

Bednortz and Müller have first discovered the high temperature superconductivity in $La_{2-x}Ba_xCuO_4$ [1]. After that, many High-T_c compounds have been discovered in the Copper Oxide. The well-known compounds are $La_{2-x}Sr_xCuO_4$, $YBa_2Cu_3O_{6+\delta}$, $Bi_2Sr_2CaCu_2O_{8+\delta}$, $Tl_2Ba_2CuO_{6+\delta}$, $HgBa_2CuO_{4+\delta}$ and so on. All of these compounds have the perovskite structure (Fig. 2.1(a)), and have the CuO_2-planes (Fig. 2.1(b)). The High-T_c superconductivity essentially occurs in the two dimensional CuO_2-plane. Therefore, these compounds are generally called 'High-T_c cuprates'. This thesis also use this generic name.

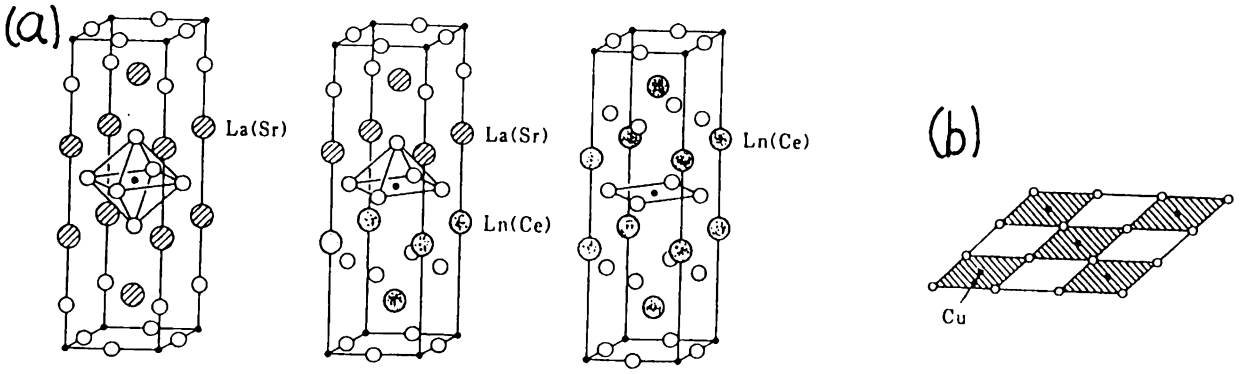

Figure 2.1: (a) The crystal structure of the typical High-T_c superconductors. (b) The CuO_2 planes.

The properties of these compounds are controlled by the carrier doping concentration δ (Fig. 2.2). The systems are half-filled without any carrier doping ($\delta = 0$). In this case, the system is an anti-ferromagnetic Mott insulator. The anti-ferromagnetic phase is suppressed by the hole-doping and the metallic phase appears. The High-T_c superconductivity occurs in the metallic phase. First, the superconducting critical temperature T_c increases with increasing the hole-doping concentration δ. This region is called 'under-doped' region. The critical temperature T_c shows its maximum around a finite doping concentration. This region is called 'optimally-doped'

region. By increasing the doping concentration more, the critical temperature decreases, and the superconductivity disappears at last. This region is called 'over-doped' region.

There are two important characteristics of the High-T_c superconductors. One is the strong electron-electron correlation. This is indicated by the phase diagram in which the metallic phase is near the Mott insulator phase. The other is the quasi-two dimensionality which results from the two-dimensional crystal structure. Both the electron correlation and the quasi-two dimensionality is expected to be strong in the under-doped region. These characteristics yield the 'anomalous' properties in the under-doped region. However, it should be noticed that there is no phase transition between the under-doped region and the over-doped one. In other words, all of the regions in the metallic phase are continuously connected. The continuity is one of the basic concept of the Fermi liquid theory. The pseudogap phenomena occur from the optimally- to under-doped region. Since the phenomena are not the phase transition, the onset line $T = T^*$ in the phase diagram (Fig. 2.2) corresponds to the crossover temperature between the pseudogap state and the non-pseudogap state.

The electron-doping ($\delta < 0$) also induces the superconductivity. However, some different features are observed in the electron-doped cuprates. For example, the anti-ferromagnetic phase is robust in these systems. The superconductivity occurs in the narrow doping region. The relatively low superconducting critical temperature is observed. The most important difference concerned with this thesis is that the pseudogap phenomena in the under-doped region *is not* observed in the electron-doped cuprates.

In this thesis, we give a comprehensive understanding of the phase diagram including both the hole- and electron-doped cases.

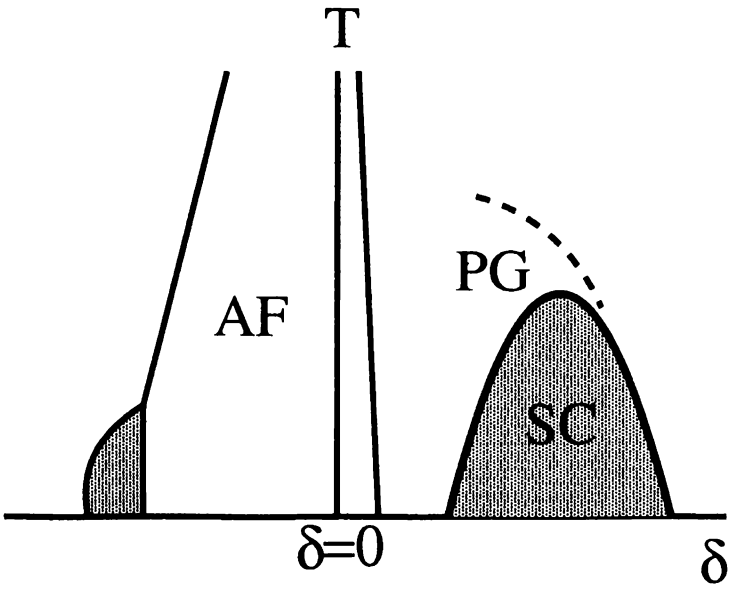

Figure 2.2: The phase diagram of the High-T_c superconductors. The horizontal axis and the vertical axis show the doping concentration and the temperature, respectively. The character 'AF', 'SC' and 'PG' mean the anti-ferromagnetic state, the superconducting state, and the pseudogap state, respectively. The onset line of the pseudogap $T = T^*$ is not the phase transition line. That shows the typical crossover temperature.

2.2 Experimental Results for the Pseudogap Phenomena

The normal state excitation gap in the under-doped cuprates has been indicated by various experiments. First, the pseudogap was found in the magnetic excitation by the nuclear magnetic resonance (NMR) experiment [30]. Therefore, the phenomena were called 'spin gap' in early years. The phrase 'spin gap' frequently implies the magnetic origin and the gap formation only in the spin channel. At present, the pseudogap phenomena have been observed in various properties which include not only the magnetic excitation [30, 31, 32, 33, 34, 35, 36], but also the transport [40, 41, 42, 43, 44, 45], optical spectrum [46, 47, 48], density of states [49, 50] electronic specific heat [51, 52], and the single particle spectral weight [22, 23]. In particular, the observation of the single particle gap has presented the important suggestion. Before explaining that, we briefly review the experimental results for High-T_c Cuprates, mainly those showing the pseudogap phenomena. The experimental results are reviewed in Ref. 53.

2.2.1 NMR

The nuclear magnetic resonance (NMR) experiments have shown the anomalous temperature dependence of the spin lattice relaxation rate $1/T_1$ (Fig. 2.3), the Knight shift K (Fig. 2.4) and the spin-echo decay rate $1/T_{2G}$ (Fig. 2.5) [30, 31, 32, 33, 34, 35, 36]. The quantity $1/T_1T$ takes a constant value independent of the temperature T in the conventional Fermi liquid theory. High-T_c cuprates shows the Curie-law of the NMR $1/T_1T$ above the pseudogap onset temperature T^*, namely $1/T_1T \propto (T+\theta)^{-1}$. The Curie-law in the metallic state is well explained by the self-consistent renormalization (SCR) theory [10] which includes the mode coupling effects of the spin fluctuations. The Curie-law indicates the existence of the strong spin fluctuations in the High-T_c cuprates. The NMR $1/T_1T$ shows the peak at T^* and decreases with decreasing the temperature below T^*. This is the well-known pseudogap phenomenon discovered first [30], and means the suppression of the magnetic excitations in the low frequency part.

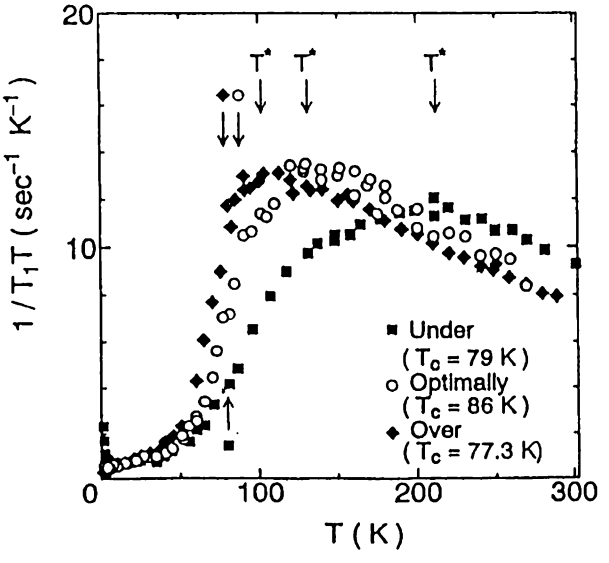

Figure 2.3: The experimental data of the NMR $1/T_1T$ [34].

The Knight shift K is proportional to the uniform susceptibility $\chi \propto K$. In the Fermi liquid theory, the uniform susceptibility χ is a constant and satisfies the Korringa-relation $K^2 \propto 1/T_1T$.

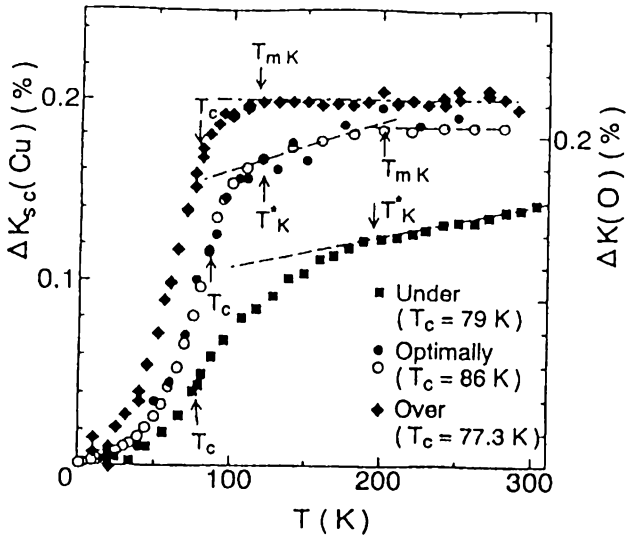

Figure 2.4: The experimental data of the Knight shift [34].

However, the Knight shift K shows the different temperature dependence from that of $1/T_1T$ in High-T_c cuprates. The former gradually decreases with decreasing the temperature below the temperature T_0 which is much higher than T^* [34]. This behavior is observed also in the direct measurement for the uniform susceptibility χ [54]. Some authors have argued from the temperature dependence that the pseudogap is not observed in the uniform susceptibility. However, the decrease of the Knight shift becomes rapid below T^* [34]. Thus, the effect of the pseudogap appears also in the uniform susceptibility, or Knight shift.

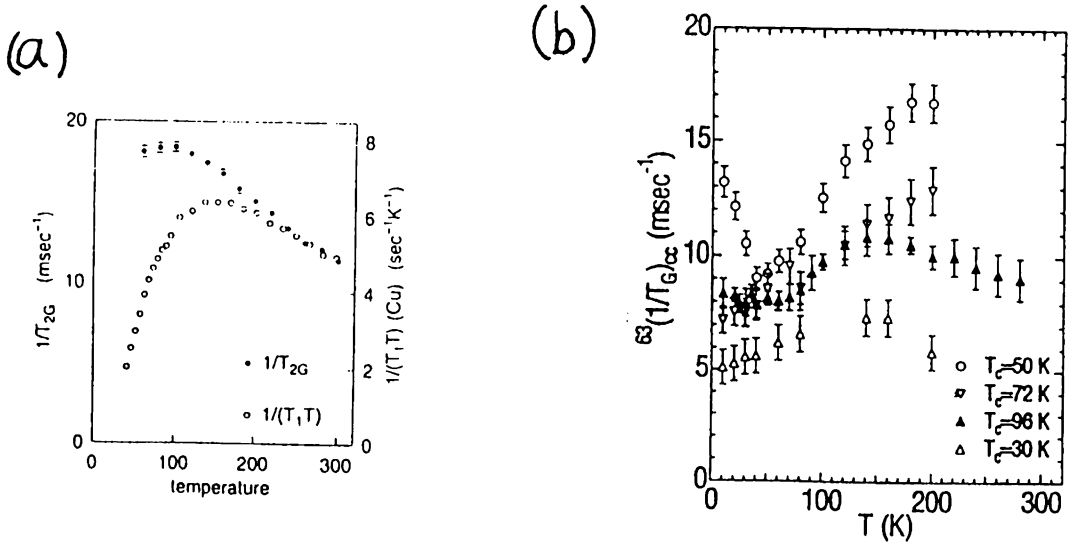

Figure 2.5: The experimental data of the NMR $1/T_{2G}$ for (a)$YBa_2Cu_3O_{6.63}$ [32] and (b)$HgBa_2CuO_{4+\delta}$ [33].

The spin echo decay rate $1/T_{2G}$ reflects the momentum sum of the static spin susceptibility $\chi(\boldsymbol{q}, 0)$. This quantity increases with decreasing the temperature above T^*. The experiments in early years have shown that the NMR $1/T_{2G}$ keep increasing also below T^* [32]. However, the recent experiments shows the different behavior of the NMR $1/T_{2G}$ for different High-T_c

compounds. In some compounds, the decrease of $1/T_{2G}$ in the pseudogap state is reported [33, 35]. There is an idea that attributes the difference to the effects of the interlayer coupling [36]. Anyway, the relatively weak effect of the pseudogap on the NMR $1/T_{2G}$ compared with the NMR $1/T_1T$ is observed in common.

2.2.2 Neutron scattering

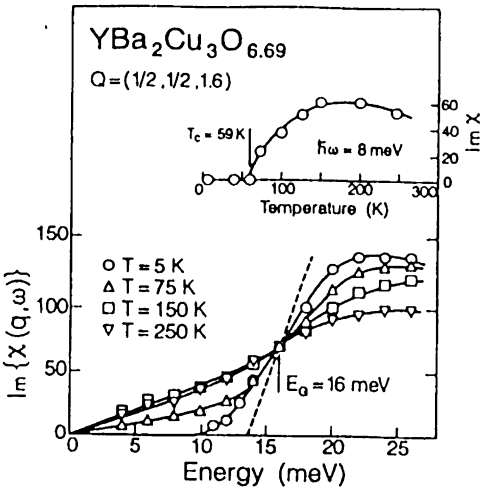

Figure 2.6: The experimental data of the dynamical spin susceptibility at the anti-ferromagnetic wave vector $\mathrm{Im}\chi(\boldsymbol{Q},\omega)$ [37].

The neutron scattering experiments have given a more direct information about the pseudogap in the magnetic excitations (Fig. 2.6) [37]. The dynamical spin susceptibility $\chi(\boldsymbol{q},\omega)$ is measured by the neutron scattering experiments. The susceptibility $\chi(\boldsymbol{q},\omega)$ grows near the anti-ferromagnetic wave vector $\boldsymbol{q} = (\pi,\pi)$ in High-T_c cuprates. This is a direct evidence of the strong anti-ferromagnetic spin fluctuations. Hereafter, we write the anti-ferromagnetic wave vector as $\boldsymbol{Q} = (\pi,\pi)$. The experimental results of the ω-dependence in $\chi(\boldsymbol{Q},\omega)$ have directly shown the pseudogap in the magnetic excitations. Generally, the spin fluctuations grows with decreasing the temperature and the weight of the spin fluctuations $\mathrm{Im}\chi(\boldsymbol{Q},\omega)$ increases in the low frequency part. However, the weight is suppressed and shifts to the high frequency part in the pseudogap state ($T_c < T < T^*$). This behavior is the pseudogap phenomena observed by the neutron scattering [37].

The other topic indicated by the neutron scattering is the incommensurate structure of the dynamical susceptibility $\chi(\boldsymbol{q},\omega)$. The incommensurability has been pointed out by the inelastic neutron scattering measurements for the Y-based compounds, and has been discussed in connection with the stripe phase [38]. The incommensurability becomes small with decreasing the temperature [39]. We give a comment on this phenomenon in §4.3.4.

2.2.3 Resistivity and Hall coefficient

Generally, the pseudogap phenomena in the transport properties are weak compared with the magnetic properties. This is a reason why the pseudogap has been called 'spin gap'. However, the transport coefficients also change their behavior at T^*, and these characteristics are well explained by our scenario.

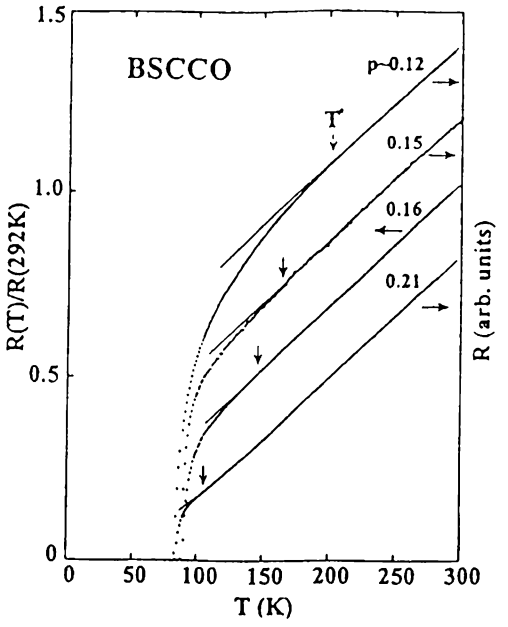

Figure 2.7: The experimental data of the in-plane resistivity [43].

In the conventional Fermi liquid, the resistivity shows the T^2-law in the low temperature region. However, the T-linear in-plane resistivity is observed in optimally- and under-doped cuprates [41]. That is anomalous at a glance, however is well explained by considering the scattering process exchanging the spin fluctuations [55, 56, 57]. The in-plane resistivity changes its slope at T^* and slightly deviates downward (Fig. 2.7) [42, 43]. This rather weak deviation have been one of the puzzle. However, that is well explained by considering the characteristic momentum dependence of High-T_c cuprates. We will explain this point in the following section (§3.4.2).

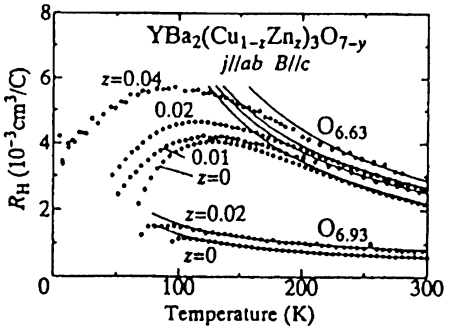

Figure 2.8: The experimental data of the Hall coefficient [42].

The Hall coefficient R_H in High-T_c cuprates show the strong temperature dependence [44], while it is temperature independent in the conventional Fermi liquid. Moreover, in under-doped cuprates, the Hall coefficient becomes much larger than that obtained by the band calculation. The enhanced Hall coefficient has been interpreted as the evidence of the low carrier density n because the relation $R_H \propto 1/n$ is derived from the Drude theory. However, this interpretation is a much superficial expectation. Since only the quasi-particles near the Fermi surface contributes to the transport, the number density n of carriers do not appear in the correct theory. Actually, the

enhanced Hall coefficient is well explained by the nearly anti-ferromagnetic Fermi liquid theory [58, 59]. Kontani and Kanki have pointed out on the basis of the Kohno's general expression [60] that the vertex correction plays an important role. The Kohno's general expression is derived from the Kubo formula and includes the vertex correction which is not included in the Boltzmann theory. The Hall coefficient remarkably deviates downward in the pseudogap state, and decreases with temperature (Fig. 2.8) [42].

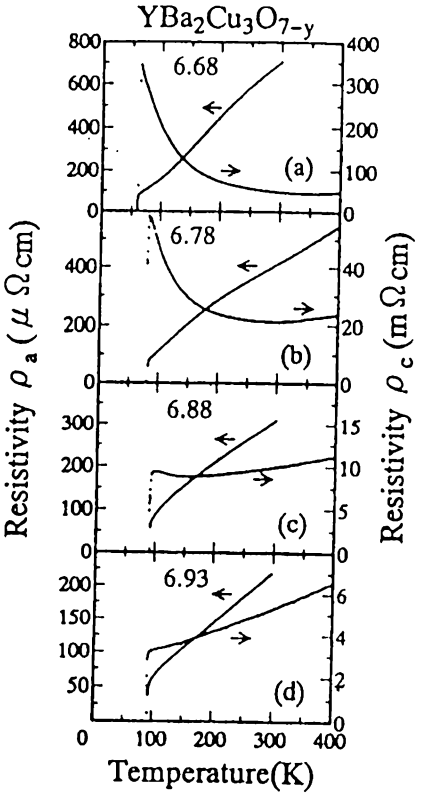

Figure 2.9: The experimental data of the c-axis resistivity [45].

The the c-axis resistivity shows the strong anisotropy ρ_c/ρ_{ab} in High-T_c cuprates (Fig. 2.9). The anisotropy becomes strong in the under-doped and/or low temperature region. Moreover, the c-axis resistivity behaves as a semiconductor in under-doped region (Fig. 2.9) [45]. The pseudogap remarkably affects on the c-axis resistivity which strongly increases in the pseudogap state [45]. This qualitatively different behavior from the in-plane resistivity will be also explained in the following section (§3.4.2) [57].

2.2.4 Optical conductivity

The c-axis optical conductivity shows no Drude peak in under-doped region (Fig. 2.10) [46, 47, 48]. That is consistent with the incoherent c-axis resistivity. The c-axis optical conductivity shows the gap structure in the pseudogap state, although the in-plane optical conductivity shows only the weak structure in the higher frequency region. The pseudogap observed in the c-axis optical conductivity smoothly changes to the superconducting gap [46, 47].

On the other hand, the in-plane optical conductivity shows the sharp Drude peak. The Drude peak remains even in the superconducting state [46, 47, 48]. That is a feature of the d-wave superconductivity. This behavior is also shown in the following section (§3.4.2).

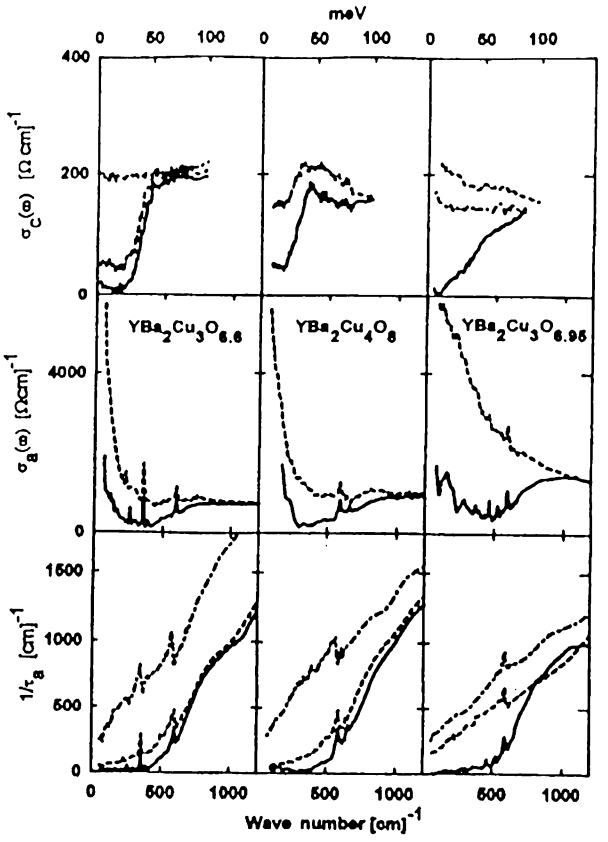

Figure 2.10: The experimental results for the optical conductivity [47].

2.2.5 Angle-resolved photo-emission spectroscopy

The angle-resolved photo-emission spectroscopy (ARPES) has shown the especially important suggestion about the pseudogap phenomena [22, 23]. The ARPES directly measures the single particle spectral weight at the selected momentum. The results have shown the leading edge gap above T_c (Fig. 2.11). In the BCS theory, the leading edge gap corresponds to the superconducting gap. Here, the leading edge gap appears without the superconducting long range order. That means the suppression of the single particle spectral weight near the Fermi energy in the normal state. The gap starts to open near T^* [54]. Thus, it has been shown that the pseudogap occurs in the single particle spectrum. Moreover, ARPES experiments have shown the following two important results. (i) The shape of the pseudogap is similar to that of the superconducting gap. That is to say, the pseudogap has the d-wave form. (ii) The magnitude of the pseudogap does not change thorough the superconducting transition [22, 23]. Below T_c, the coherent quasi-particle peak appears at the gap edge, and the gap structure becomes sharp. However, the energy scale of the gap does not change. This behavior is naturally understood in our scenario (§3.3).

Thus, the close relation between the pseudogap and the superconductivity is suggested by ARPES experiments. These results have remarkably encouraged the pairing scenario, and therefore many theoretical studies have been done on the basis of the scenario.

2.2.6 Tunneling spectroscopy

The tunneling spectroscopy directly measures the electronic density of states (DOS). The suppression of the DOS near the Fermi level is shown above T_c (Fig. 2.12) [49, 50]. The energy scale of the

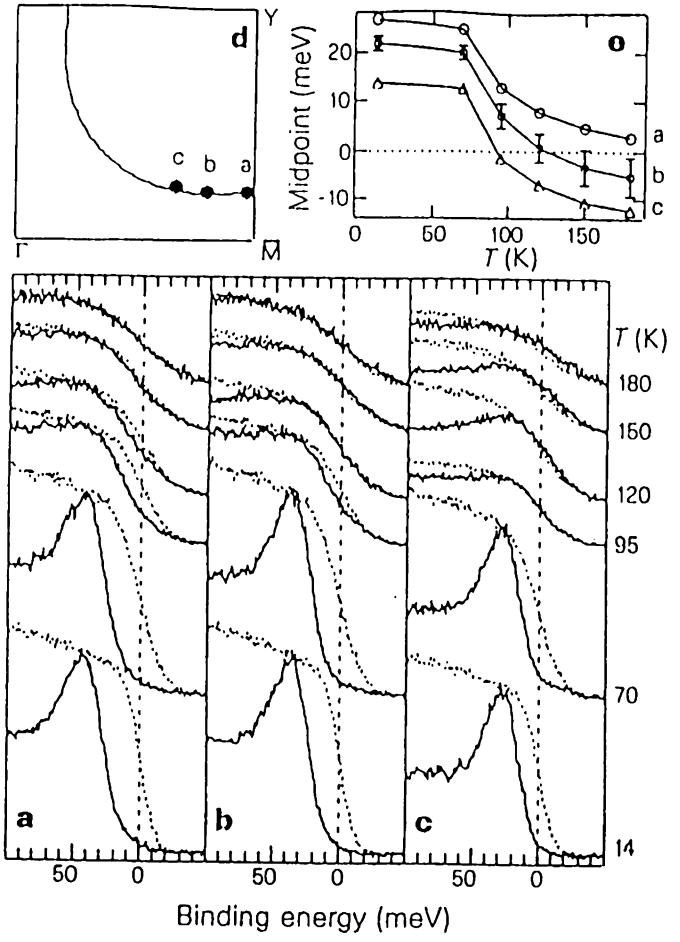

Figure 2.11: The results of the ARPES [22]. The leading edge gap is observed above T_c. The pseudogap shows the same momentum dependence as that of the superconducting gap.

pseudogap in the DOS is nearly the same as that of the superconducting gap. The gap structure becomes sharp below T_c. The results are consistent with the ARPES, and have supported the pairing scenario similarly [49].

In this connection, the gap-like structure which is similar to the normal state pseudogap is observed in vortex cores in the superconducting state [61]. Although the zero bias peak in the vortex core is shown theoretically for the pure d-wave case [62, 63], that is not observed experimentally [61, 64, 65]. The authors have indicated that the pre-formed pairs exist in the vortex core [61]. We think, this conclusion is still uncertain. Another proposal on the problem is that the other component participates in the $d_{x^2-y^2}$-wave component of the superconducting order parameter. For example, the possibility of $d_{x^2-y^2} + is$-wave [66] or $d_{x^2-y^2} + id_{xy}$-wave [62] is investigated. In these cases, the superconductivity becomes node-less near the vortex cores. Therefore, the bound state appears around the vortex cores. The other proposal is that the momentum dependence of the c-axis hopping matrix $t_\perp(\boldsymbol{k})$ suppresses the zero bias peak. The momentum dependence is indicated by the band calculation [68]. This is the origin of the incoherent c-axis transport which will be explained in the following section (§3.4.2) [57, 69].

2.2.7 Electronic specific heat

The electronic specific heat C is proportional to the temperature $C \propto \gamma T$ in the Fermi liquid theory. The coefficient γ is proportional to the quasi-particle density of state which is enhanced

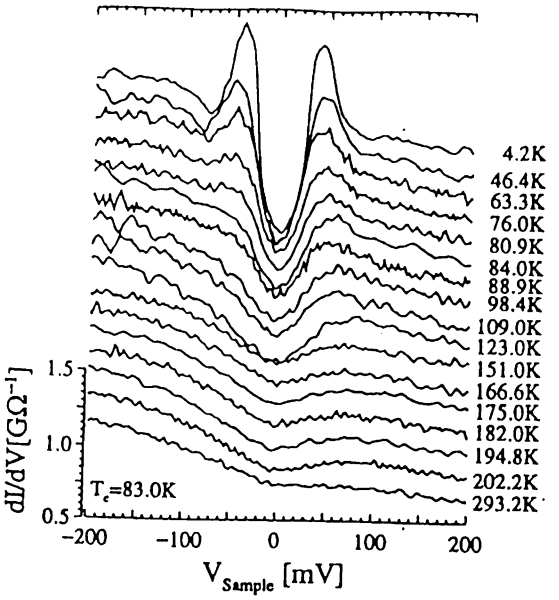

Figure 2.12: The results of the tunneling spectroscopy [49].

by the electron correlation. The experimental results show the temperature dependence of the coefficient γ in the under-doped region [51]. The coefficient γ is reduced with decreasing the temperature and/or the doping concentration. The reduction occurs well above T_c and T^*. The step height at T_c becomes small in under-doped cuprates. This behavior is inconsistent with the simple expression for the strongly correlated electron systems. Generally speaking, the electron correlation enhances the specific heat as is observed in the heavy-fermion systems. However, since the momentum dependence is one of the characteristics of the low dimensional systems, it is natural that the simple theory neglecting the momentum dependence is not applicable to these systems. The similar behavior to the cuprates is observed also in the organic superconductor κ-(BEDT-TTF) compounds. These results mean that the entropy has been already lost at rather high temperature. Generally speaking, the entropy in the strongly correlated electron systems mainly originates from the freedom of spins. Therefore, we think that the development of the spin correlation reduces the entropy and the specific heat.

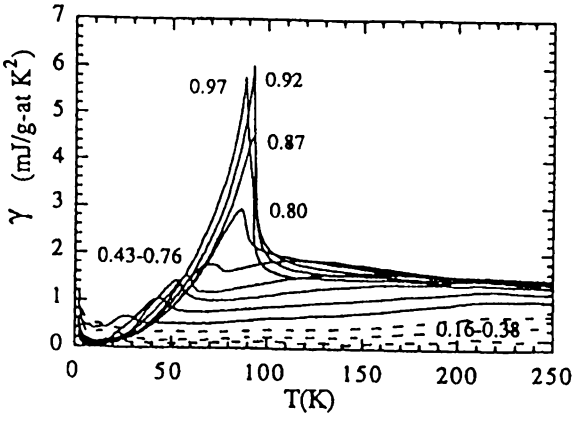

Figure 2.13: The results for the heat coefficient γ [51].

The recent experiment has shown that the coefficient γ shows a weak change near T^* and

decreases more rapidly below T^* [52]. It should be considered that this decreases is a result of the suppressed DOS in the pseudogap state.

2.2.8 Phase diagram

As is explained in this subsection, the pseudogap is observed by various measurements. It is shown that the onset temperature T^* measured by the above experiments is similar and shows the same doping dependence. One important result is that the onset temperature T^* is proportional to the amplitude of the superconducting gap (Fig. 2.14) [70]. Although the critical temperature T_c decreases with under-doping, the superconducting gap increases. Namely, the superconducting gap seems to have a close relation with T^* rather than T_c. This relation also indicates the close relation between the pseudogap phenomena and the superconductivity. Thus, the pairing scenario is expected to give an comprehensive understanding of the phase diagram of High-T_c cuprates.

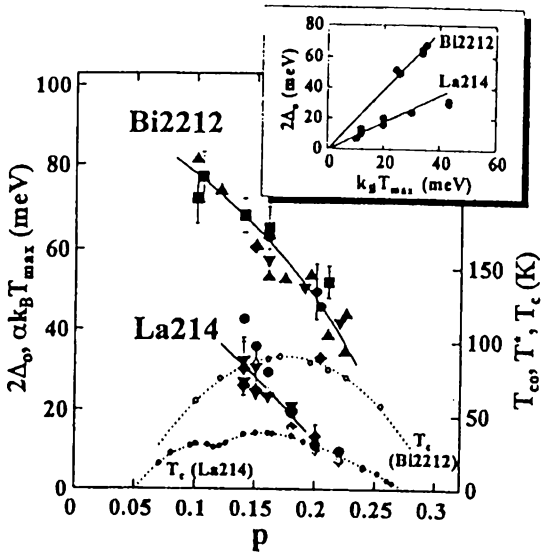

Figure 2.14: The phase diagram. The doping dependence of the pseudogap onset temperature T^* and the superconducting gap Δ are plotted [70].

2.3 Pairing Scenario and Strong Coupling Superconductivity

In this thesis, we develop a theory of the pseudogap phenomena on the basis of the strong superconducting fluctuations [24, 25, 26, 27, 28]. We consider that the strong fluctuations originates from the strong coupling superconductivity and the quasi-two dimensionality. This theory belongs to the pairing scenario. However, the pairing scenario is classified into some types. Many of them are different from ours and do not correspond to the realistic situation. First, we explain the strong coupling superconductivity and review some types of the pairing scenario for the pseudogap phenomena.

Generally, the mean field theory based on the BCS theory [2] assume that the superconducting critical temperature T_c is much smaller than the effective Fermi energy ε_F. Therefore, the BCS theory is called the weak coupling theory. The effective Fermi energy ε_F is the typical energy

scale of the electron system. This assumption is generally justified in the conventional superconductors in which the electron-phonon interaction is the pairing interaction. In other words, the pairing interaction is sufficiently small compared with the kinetic energy of the electron systems. Therefore, it is considered that the superconducting fluctuations are sufficiently weak in the conventional superconductors. The *Strong Coupling Superconductivity* means that the assumption is violated and therefore the superconducting fluctuations play an important role. The correction on the two-body correlation function resulting from the superconducting fluctuations has been investigated within the weak coupling theory [71, 72]. However, the superconducting fluctuations strongly affects the single particle properties in the strong coupling case [24].

The strength of the superconducting coupling is indicated by the ratio $T_{\rm c}^{\rm MF}/\varepsilon_{\rm F}$. Here, $T_{\rm c}^{\rm MF}$ is the superconducting critical temperature obtained by the mean field theory. The assumption of the weak coupling is written as $T_{\rm c}^{\rm MF}/\varepsilon_{\rm F} \ll 1$ which is justified in conventional superconductors. There are two important factors in order to realize the strong coupling superconductivity in High-$T_{\rm c}$ cuprates. (i) The effective Fermi energy $\varepsilon_{\rm F}$ is renormalized by the electron-electron correlation. In this sense, the strong coupling superconductivity is a characteristic phenomenon in the strongly correlated electron systems. (ii) The high critical temperature $T_{\rm c}$ itself which is derived by the pairing interaction mediated by the anti-ferromagnetic spin fluctuations [7, 8]. The strong coupling superconductivity generally induces the strong fluctuations. Moreover, the quasi-two dimensionality enhances the superconducting fluctuations still more. The above factors, strong renormalization, High-$T_{\rm c}$ and the quasi-two dimensionality are the characteristics of the systems. Thus, it is natural to consider the strong superconducting fluctuations in High-$T_{\rm c}$ cuprates.

The well-known theory describing the strong coupling superconductivity is the Nozières and Schmitt-Rink (NSR) theory [73, 74]. The NSR theory describes the crossover from the weak coupling BCS superconductivity to the Bose Einstein condensation of the pre-formed pairs. First, the ground state in the strong coupling superconductors is formulated by Leggett [73]. In his procedure, the BCS wave function in the ground state is used. He have shown that the crossover is described by the shift of the chemical potential μ. The wave function changes with the shift which is included in the coefficients u_k, and v_k in the ordinary notation.

Nozières and Schmitt-Rink have extended the formulation to the finite temperature. The concept of the NSR theory [74] is taking account of the corrections of the pair fluctuations to the thermodynamic potential Ω shown in Fig. 2.15. The correction is written as,

$$\Omega_{\rm b} = T \sum_{\boldsymbol{q},{\rm i}\Omega_n} \log[1 + \chi_{\rm p0}(\boldsymbol{q}, {\rm i}\Omega_n)], \tag{2.1}$$

$$\chi_{\rm p0}(\boldsymbol{q}, \Omega) = \sum_{\boldsymbol{k}} V_{\boldsymbol{k},\boldsymbol{k}} \frac{1 - f(\varepsilon_{\boldsymbol{k}+\boldsymbol{q}/2}) - f(\varepsilon_{-\boldsymbol{k}+\boldsymbol{q}/2})}{\varepsilon_{\boldsymbol{k}+\boldsymbol{q}/2} + \varepsilon_{-\boldsymbol{k}+\boldsymbol{q}/2} - \Omega}. \tag{2.2}$$

Here, $V_{\boldsymbol{k},\boldsymbol{k}}$ is the pairing interaction which is $V_{\boldsymbol{k},\boldsymbol{k}} = V < 0$ in the s-wave case. The function $\chi_{\rm p0}(\boldsymbol{q}, \Omega)$ is the bare pairing susceptibility. It should be noticed that the notation of $\chi_{\rm p0}(\boldsymbol{q}, \Omega)$ is different from that used by us in the following section.

In the next procedure, the correction to the fermion number density is calculated by the following formula.

$$N_{\rm b} = -\frac{\partial}{\partial \mu}\Omega_{\rm b} = T \sum_{\boldsymbol{q},{\rm i}\Omega_n} \frac{-\partial \chi_{\rm p0}(\boldsymbol{q}, {\rm i}\Omega_n)/\partial \mu}{1 + \chi_{\rm p0}(\boldsymbol{q}, {\rm i}\Omega_n)}, \tag{2.3}$$

$$\sim T \sum_{\boldsymbol{q},{\rm i}\Omega_n} \frac{-\partial \chi_{\rm p0}(\boldsymbol{0}, 0)/\partial \mu}{1 + \chi_{\rm p0}(\boldsymbol{q}, {\rm i}\Omega_n)}. \tag{2.4}$$

The total fermion density is obtained by adding it to the free fermion part $N_{\rm f}$ as $N = N_{\rm f} + N_{\rm b}$. These procedures of the NSR theory correspond to counting the number of the bosonic pre-formed pairs. In the NSR theory, the chemical potential μ is determined self-consistently so as to fix the total fermion density N. Thus, the essence of the NSR theory is included in the shift of the chemical potential μ. The NSR theory describes the crossover between the BCS superconductivity $\mu \sim \varepsilon_{\rm F}$, $N \sim N_{\rm f}$ to the BE condensation of the pre-formed pairs $\mu \sim V$, $N \sim N_{\rm b}$. The applicability of the NSR formalism to the two-dimensional systems have been investigated [75, 76], because the fluctuations in the two-dimensional systems reduces the critical temperature $T_{\rm c} = 0$ even in the weak coupling limit. This is caused by the singularity due to the two-dimension. It should be noticed that the NSR theory is justified in the low density limit [74] as is explained later.

We can understand this fact by considering the following easy question. The effects considered in the NSR theory cancel in the particle-hole symmetric case. Even in this case, the two-dimensionality is sure to reduce the critical temperature $T_{\rm c} = 0$ unless we consider the Kosterlitz-Thouless transition. What is the origin ? The answer is the higher order corrections of the superconducting fluctuations.

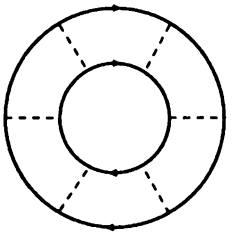

Figure 2.15: The correction to the thermodynamic potential calculated in the Nozières and Schmitt-Rink theory.

The pairing scenario based on the strong coupling superconductivity was first proposed by Randeria *et al* [20]. The proposal is also based on the NSR theory. In the NSR theory, the gap opens in the single particle spectrum in the strong coupling case. That is a natural result because the fermions are tightly bound by the strong pairing interaction. In that case, the low energy excitation is the motion of the center of mass of the pre-formed pairs. The phase transition is the BE condensation of the pre-formed pairs.

The pseudogap in High-$T_{\rm c}$ cuprates has lead to the studies based on the NSR theory and the BCS-BE crossover [20, 77, 78, 79, 80, 82, 83]. In these studies, the pseudogap state has been regarded as the intermediate regime of the BCS-BE crossover. Many of them calculated the s-wave case, such as the attractive Hubbard model. For example, the Ginzburg-Landau theory is derived by Stintzing and Zwerger [79]. One feature of the GL theory is that the dissipation term becomes exponentially small in the BE regime. This is because the DOS of the fermions is completely gaped. The reduced dissipation has pointed out by other The NSR formalism has been applied to the d-p model by Koikegami and Yamada [82] and Kobayashi *et al* [83]. The self-consistent T-matrix calculation has been carried out [77, 78, 80, 81], first by Haussman [77]. The above calculations have treated the Fermi gas model or the low density model. It should be noticed that the self-consistent T-matrix approximation describes the same scenario as the NSR theory, when the fermion density is chosen to be low density. Although we will use the self-consistent T-matrix approximation, the different situation results in the different scenario.

Some authors have also proposed the phenomenological model in which the fermions and the

pre-formed bosons coexist [84, 85, 86]. This situation corresponds to an intermediate regime in the NSR theory. Geshkenbein *et al.* [84] have proposed the phenomenology with reference to the sign problem of the fluctuational Hall effect [87]. We briefly discuss the problem later.

However, the NSR theory is justified in the low density limit and not in High-T_c cuprates. This is because they are nearly half-filled lattice system and should be regarded as the rather high density system. Moreover, since the pseudogap phenomena take place near the Fermi surface, the situation in which the Fermi surface remarkably changes and disappears at last is not realistic. Actually, it is shown that the pseudogap phenomena are naturally derived by the self-energy correction due to the strong superconducting fluctuations [24, 88]. The resonance scattering by the low energy superconducting fluctuations gives rise to the anomalous features of the self-energy and leads to the pseudogap. The self-energy is sufficiently small in the weak coupling case, and therefore usually neglected. However, the self-energy remarkably affects the electronic state in the strong coupling case. This scenario is different from the NSR scenario. The resonance scattering plays an important role in high density systems, although the shift of the chemical potential is dominant in low density systems. First, the importance of the resonance scattering has been pointed out by Janko *et al* [88]. However, their calculation is also based on the Fermi gas model with the s-wave pairing interaction. Therefore, their calculation also describes the NSR scenario and the BCS-BE crossover at last. In this thesis, we derive the pseudogap phenomena on the basis of the resonance scattering scenario in the relevant situation for High-T_c cuprates. It is shown that the shift of the chemical potential, which is included in our calculation, is actually small [24]. It should be noticed that the effective Fermi energy ϵ_F in High-T_c cuprates is reduced by the electron-electron correlation and not by the low density.

The other approach belonging to the pairing scenario is the phase fluctuation scenario. The scenario has been proposed by Emery and Kivelson [21] and calculated by other authors [89, 90]. Their calculations are based on the Kosterlitz-Thouless (KT) transition in the two-dimensional system. In the procedures, the vortex excitation plays an important role. The situation may exist near the critical temperature. Actually, the recent experiment on the thermal conductivity has indicated the vortex excitation [91]. However, the situation in which the amplitude is fixed in the wide region of the pseudogap state is inappropriate. Since the real systems are weakly three-dimensional, the description of the situation is important and difficult problem for the phase fluctuation scenario.

Chapter 3

Theory of Pseudogap Phenomena on the Basis of the Strong Coupling Superconductivity [24, 25, 26, 27]

In this chapter, we clarify the mechanism of the pseudogap on the basis of the model with the d-wave attractive interaction [24, 25, 27, 26]. Our scenario for the pseudogap phenomena will be justified in §4 by using the Hubbard model. However, the fundamental features of the superconducting fluctuations and the pseudogap phenomena are included in this attractive model.

In §3.1, the basic formalism describing the mechanism of the pseudogap phenomena are explained. The important factors for realizing the pseudogap is clarified. In §3.2, the effects of the magnetic field on the pseudogap phenomena are calculated. The obtained results well explain the high field NMR measurements including their doping dependence. The comprehensive understanding from the over-doped to under-doped region is shown. In §3.3, the properties of the superconducting transition from the pseudogap phenomena are investigated. The relevant understanding of the smooth change from the pseudogap state to the superconducting one are obtained. In §3.4, the various quantities, such as the magnetic and transport properties, are calculated in the pseudogap state and in the superconducting state. The characteristic behavior in each quantities is explained by considering the characteristic momentum dependence of High-T_c cuprates.

3.1 Mechanism of the Pseudogap Phenomena [24]

In this section, we derive the pseudogap phenomena caused by the superconducting fluctuations which are enhanced in the quasi-two dimensional strong coupling superconductors.

This section is constructed as follows. In §3.1.1, we give a model Hamiltonian and explain the basic formalism adopted in this chapter. In §3.1.2 and §3.1.3, we explicitly calculate the single particle self-energy corresponding to the T-matrix and the self-consistent T-matrix approximations, respectively. In §3.1.4, we explain the important factors for the pseudogap phenomena and discuss the possibility of the pseudogap phenomena in other compounds.

3.1.1 Theoretical Framework

In this section, we describe the basic formalism of the idea 'resonances scattering' due to the low energy superconducting fluctuations. The formalism is based on the time-dependent-Ginzburg-Landau (TDGL) expansion for the superconducting fluctuations and the T-matrix and self-consistent T-matrix approximations for the self-energy of electrons. We show that the strong

coupling superconductivity leads to the anomalous normal state properties above the superconducting critical temperature. Hereafter, we adopt the unit $\hbar = c = k_B = 1$.

We adopt the following two-dimensional model Hamiltonian which has a $d_{x^2-y^2}$-wave superconducting ground state.

$$H = \sum_{\boldsymbol{k},s} \varepsilon_{\boldsymbol{k}} c^{\dagger}_{\boldsymbol{k},s} c_{\boldsymbol{k},s} + \sum_{\boldsymbol{k},\boldsymbol{k}',\boldsymbol{q}} V_{\boldsymbol{k}-\boldsymbol{q}/2,\boldsymbol{k}'-\boldsymbol{q}/2} c^{\dagger}_{\boldsymbol{q}-\boldsymbol{k}',\uparrow} c^{\dagger}_{\boldsymbol{k}',\uparrow} c_{\boldsymbol{k},\uparrow} c_{\boldsymbol{q}-\boldsymbol{k},\uparrow}, \tag{3.1}$$

where $V_{\boldsymbol{k},\boldsymbol{k}'}$ is the $d_{x^2-y^2}$-wave separable pairing interaction,

$$V_{\boldsymbol{k},\boldsymbol{k}'} = g\varphi_{\boldsymbol{k}}\varphi_{\boldsymbol{k}'}, \tag{3.2}$$

$$\varphi_{\boldsymbol{k}} = \cos k_x - \cos k_y. \tag{3.3}$$

Here, g is negative and $\varphi_{\boldsymbol{k}}$ is the $d_{x^2-y^2}$-wave form factor. The form factor is a constant in the conventional s-wave case. We consider the dispersion $\varepsilon_{\boldsymbol{k}}$ given by the tight-binding model for a square lattice including the nearest- and next-nearest-neighbor hopping t, t', respectively,

$$\varepsilon_{\boldsymbol{k}} = -2t(\cos k_x + \cos k_y) + 4t' \cos k_x \cos k_y - \mu. \tag{3.4}$$

We fix the lattice constant $a = 1$. We adopt $t = 0.5$eV and $t' = 0.45t$. These parameters well reproduce the Fermi surface of the typical High-T_c cuprates, $YBa_2Cu_3O_{6+\delta}$ and $Bi_2Sr_2CaCu_2O_{8+\delta}$. We choose the chemical potential μ so that the filling $n = 0.9$, which corresponds to the hole doping $\delta = 0.1$. The Fermi surface is shown in Fig. 3.1.

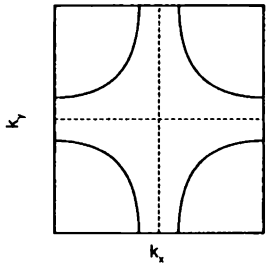

Figure 3.1: The Fermi surface adopted in this chapter.

Since the Brillouin zone edge acts as a natural momentum cut-off, we do not have to use the renormalization methods in order to remove the ultraviolet divergences which exist in the Fermi gas model. [20]

The above Hamiltonian is an effective model in which the paring interaction affects the renormalized quasi-particles. Since the energy scale in the above model is the renormalized Fermi energy ε_F, the relatively large paring interaction is considered. The realistic energy scale for cuprates is obtained by considering the renormalization as $\cong 1/10$ which is a relevant order in d-electron systems.

Actually, the origin of the pairing interaction should be considered to be the anti-ferromagnetic spin fluctuations [7, 8]. The calculation dealing with the pairing correlations obtained by the spin fluctuations on the basis of the fluctuation exchange (FLEX) approximation is carried out in the next chapter [28]. Here, adopt the simplified model and show the essential points of the pseudogap phenomena derived by the superconducting fluctuations. There is a feedback effect on

the pairing interaction arising from the pseudogap. The pseudogap suppresses the low frequency component of the spin fluctuations. However, the pairing interaction is mainly caused by the high frequency component compared with the energy scale of the superconducting fluctuations. Therefore, qualitatively the same results are obtained from the model with a fixed attractive interaction.

First of all, we consider the properties of the scattering vertex arising from the superconducting fluctuations, $\Gamma(\boldsymbol{k}, \boldsymbol{q}-\boldsymbol{k} : \boldsymbol{k}', \boldsymbol{q}-\boldsymbol{k}' : \mathrm{i}\Omega_n)$. The vertex is described by the ladder diagrams (T-matrix) in the particle-particle interaction channel (Fig. 3.2.).

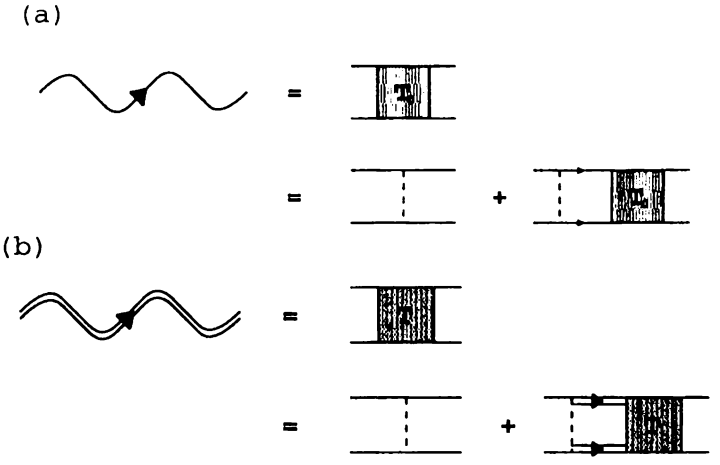

Figure 3.2: The scattering vertex represented by the ladder diagrams in the particle-particle channel (T-matrix). The dashed lines represent the attractive interaction $V_{\boldsymbol{k},\boldsymbol{k}'}$. The single and double solid lines represent the propagator of the bare and renormalized fermions, respectively. The single and double wavy lines represent the propagator of the bare and renormalized superconducting fluctuations, respectively.

It is factorized into $\Gamma(\boldsymbol{k}, \boldsymbol{q}-\boldsymbol{k} : \boldsymbol{k}', \boldsymbol{q}-\boldsymbol{k}' : \mathrm{i}\Omega_n) = \varphi_{\boldsymbol{k}-\boldsymbol{q}/2} t(\boldsymbol{q}, \mathrm{i}\Omega_n) \varphi_{\boldsymbol{k}'-\boldsymbol{q}/2}$, where

$$t(\boldsymbol{q}, \mathrm{i}\Omega_n) = [g^{-1} + \chi_{\mathrm{p0}}(\boldsymbol{q}, \mathrm{i}\Omega_n)]^{-1}, \tag{3.5}$$

$$\chi_{\mathrm{p0}}(\boldsymbol{q}, \mathrm{i}\Omega_n) = T \sum_{\boldsymbol{k}', \omega_m} G(\boldsymbol{k}', \mathrm{i}\omega_m) G(\boldsymbol{q}-\boldsymbol{k}', \mathrm{i}\Omega_n - \mathrm{i}\omega_m) \varphi^2_{\boldsymbol{k}'-\boldsymbol{q}/2}. \tag{3.6}$$

Here, $\omega_m = 2\pi(m+\frac{1}{2})T$ and $\Omega_n = 2\pi n T$ are the fermionic and bosonic Matsubara frequencies, respectively. As a result of the analytic continuation, $\chi_{\mathrm{p0}}(\boldsymbol{q}, \Omega)$ is expressed as

$$\chi^{\mathrm{R}}_{\mathrm{p0}}(\boldsymbol{q}, \Omega) = \sum_{\boldsymbol{k}} \int \frac{\mathrm{d}\omega}{\pi} [f(\omega - \Omega) \mathrm{Im} G^{\mathrm{R}}(\boldsymbol{q}-\boldsymbol{k}, \Omega - \omega) G^{\mathrm{R}}(\boldsymbol{k}, \omega) \tag{3.7}$$

$$- f(\omega) G^{\mathrm{R}}(\boldsymbol{q}-\boldsymbol{k}, \Omega - \omega) \mathrm{Im} G^{\mathrm{R}}(\boldsymbol{k}, \omega)] \varphi^2_{\boldsymbol{k}-\boldsymbol{q}/2}. \tag{3.8}$$

Here, $Z_{\mathrm{sc}} = (1 + g\chi_{\mathrm{p0}}(\boldsymbol{q}, \Omega))^{-1}$ is regarded as a enhancement factor for the superconducting susceptibility $\chi_{\mathrm{sc}}(\boldsymbol{q}, \Omega)$. When $1 + g\chi_{\mathrm{p0}}(\boldsymbol{0}, 0) = 0$, the susceptibility $\chi_{\mathrm{sc}}(\boldsymbol{0}, 0)$ diverges and the superconductivity occurs. This is the well-known Thouless criterion which is equivalent to the BCS theory in the weak coupling limit. [74] The T-matrix $t(\boldsymbol{q}, \Omega)$ can be regarded as a propagator of the fluctuating Cooper pairs. The momentum and the frequency $\boldsymbol{q}$ and Ω represent the motion of the center of mass. The Thouless criterion corresponds to the situation in which $t(\boldsymbol{q}, \Omega)$ has its pole at $\boldsymbol{q} = \Omega = 0$.

Here, we are interested in the normal state near the superconducting critical point, where the Z_{sc} grows and the superconducting fluctuations are enhanced. Even in the weak coupling limit, this divergence affects the various physical quantities [71, 72], and the several studies have been given for High-T_c on the basis of such a framework [92, 93, 94, 95, 96, 97]. However, in the strong or intermediate coupling region, the superconducting fluctuations more seriously affect the electronic states. We will show that below.

Because the T-matrix $t(\boldsymbol{q},\Omega)$ is strongly enhanced around $\boldsymbol{q} = \Omega = 0$, its contribution to the single particle self-energy $\Sigma(\boldsymbol{k},\omega)$ is mainly from the vicinity of $\boldsymbol{q} = \Omega = 0$. Therefore, we expand the reciprocal of the T-matrix $t^{-1}(\boldsymbol{q},\Omega)$ in the vicinity of $\boldsymbol{q} = \Omega = 0$. The expansion is described as follows,

$$t(\boldsymbol{q},\Omega) = \frac{g}{t_0 + b\boldsymbol{q}^2 - (a_1 + \mathrm{i}a_2)\Omega}. \tag{3.9}$$

This expansion corresponds to the time-dependent-Ginzburg-Landau (TDGL) expansion. In the above description, $t_0 = 1 + g\chi_{\mathrm{p0}}(\boldsymbol{0},0)$. The other parameters b, $a_1 + \mathrm{i}a_2$ are obtained by the differentiation of $g\chi_{\mathrm{p0}}(\boldsymbol{q},\Omega)$ with respect to the momentum and frequency, respectively. Later, we explicitly estimate $\chi_{\mathrm{p0}}(\boldsymbol{q},\Omega)$ and the TDGL expansion parameters by using the bare Green function $G^{\mathrm{R(0)}}(\boldsymbol{k},\omega) = (\omega - \varepsilon_{\boldsymbol{k}} + \mathrm{i}\delta)^{-1}$ in §2.2, the renormalized Green function $G^{\mathrm{R}}(\boldsymbol{k},\omega) = (\omega - \varepsilon_{\boldsymbol{k}} - \Sigma^{\mathrm{R}}(\boldsymbol{k},\omega))^{-1}$ in §2.3, respectively. These estimations correspond to the T-matrix approximation (see Fig. 3.3(a)) and the self-consistent T-matrix approximation (see Fig. 3.3(b)), respectively.

In this section, we explain the general properties of the TDGL parameters, and calculate the contribution of the superconducting fluctuations to the single particle self-energy $\Sigma^{\mathrm{R}}(\boldsymbol{k},\omega)$.

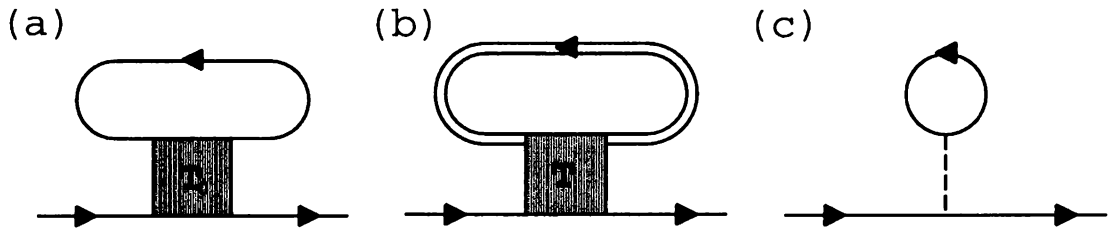

Figure 3.3: The diagrams of the single particle self-energy based on (a) the T-matrix approximation and (b) the self-consistent T-matrix approximation, respectively. (c) The Hartree-Fock term which we exclude afterward. This term should be included in the dispersion relation $\varepsilon_{\boldsymbol{k}}$ from the beginning.

First, we describe the expression in the weak coupling limit. In this case, we can use the bare Green function $G^{\mathrm{R(0)}}$. The bare pair susceptibility $\chi_{\mathrm{p0}}(\boldsymbol{q},\Omega)$ is expressed as follows:

$$\chi_{\mathrm{p0}}(\boldsymbol{q},\Omega) = \sum_{\boldsymbol{k}} \frac{1 - f(\varepsilon_{\boldsymbol{k}+\boldsymbol{q}/2}) - f(\varepsilon_{-\boldsymbol{k}+\boldsymbol{q}/2})}{\varepsilon_{\boldsymbol{k}+\boldsymbol{q}/2} + \varepsilon_{-\boldsymbol{k}+\boldsymbol{q}/2} - \Omega}\varphi_{\boldsymbol{k}}^2, \tag{3.10}$$

where $f(\varepsilon)$ is the Fermi distribution function. The TDGL parameters are expressed as follows:

$$t_0 = 1 + g\int \mathrm{d}\varepsilon \frac{\tanh(\frac{\varepsilon}{2T})}{2\varepsilon}\rho_{\mathrm{d}}(\varepsilon) \cong |g|\rho_{\mathrm{d}}(0)\frac{T - T_{\mathrm{c}}}{T_{\mathrm{c}}}, \tag{3.11}$$

$$b = |g|\int \mathrm{d}\varepsilon \frac{\rho_{\mathrm{d}}(\varepsilon)\bar{v}_{\mathrm{F}}^2}{16\varepsilon}\frac{\partial^2 f(\varepsilon)}{\partial\varepsilon^2} \cong |g|\rho_{\mathrm{d}}(0)\frac{7\zeta(3)}{32(\pi T)^2}\bar{v}_{\mathrm{F}}^2, \tag{3.12}$$

$$a_1 = |g| \int d\varepsilon \frac{\tanh(\frac{\varepsilon}{2T})}{(2\varepsilon)^2} \rho_{\rm d}(\varepsilon) \cong \frac{1}{2}\rho'_{\rm d}(0)/\rho_{\rm d}(0) \cong \frac{1}{2}|g| \frac{\partial \chi_{\rm p0}(\mathbf{0},0)}{\partial \mu}, \tag{3.13}$$

$$a_2 = |g| \rho_{\rm d}(0) \frac{\pi}{8T}. \tag{3.14}$$

Here, $\zeta(3)$ is the Riemann's zeta function and $\bar{v}_{\rm F}$ is the mean value of the quasi-particle's velocity on the Fermi surface. Here, we have defined the effective DOS for the $d_{x^2-y^2}$-wave symmetry.

$$\rho_{\rm d}(\varepsilon) = \sum_{\boldsymbol{k}} \rho_{\boldsymbol{k}}(\varepsilon) \varphi_{\boldsymbol{k}}^2, \tag{3.15}$$

where, $\rho_{\boldsymbol{k}}(\varepsilon)$ is the single particle spectral weight $\rho_{\boldsymbol{k}}(\varepsilon) = A_{\boldsymbol{k}}(\varepsilon) = -\frac{1}{\pi}{\rm Im}G^{\rm R}(\boldsymbol{k},\varepsilon)$. The first derivative of the effective DOS is expressed as $\rho'_{\rm d}(0)$. It should be noticed that $\rho_{\rm d}(\varepsilon)$ is more sensitive to the pseudogap formation rather than the DOS $\rho(\varepsilon) = \sum_{\boldsymbol{k}} \rho_{\boldsymbol{k}}(\varepsilon)$. In the pseudogap state, the spectral weight near the Fermi level is suppressed around the momentum $(\pi, 0)$ where the form factor $\varphi_{\boldsymbol{k}}$ is large. One the other hand, the quasi-particle peak remains in the vicinity of $(\pi/2, \pi/2)$. However, this area contributes little to the effective DOS $\rho_{\rm d}(\varepsilon)$ because of the small form factor $\varphi_{\boldsymbol{k}}$. Therefore, the pseudogap remarkably suppresses $\rho_{\rm d}(0)$ rather than $\rho_{\rm d}(0)$. In this sense, the difference between the s-wave case and the d-wave one is small.

The properties of the TDGL parameters are explained in the following way. The parameter $t_0 = 1 + g\chi_0(\mathbf{0}, 0)$ represents the distance to the phase transition, and is sufficiently small near the critical point $T = T_{\rm c}$. The parameter b is generally related to the coherence length ξ_0, $b \propto \xi_0^2$. The small b generally means the strong fluctuations. The parameter a_2 expresses the time scale of the fluctuations. This is the dissipation term of the fluctuations. Roughly speaking, the parameters a_2 and b are described as, $a_2 \propto \rho_{\rm d}(0)/T$ and $b \propto \rho_{\rm d}(0)/T^2$. Because of the high critical temperature $T_{\rm c}$ and the renormalization effect by the pseudogap, both a_2 and b become small in the strong coupling superconductivity. The renormalization effect on the dissipation term has been pointed out by the other calculation [98]. These features of the TDGL parameters indicate that the scattering vertex due to the superconducting fluctuations is remarkably enhanced.

The parameter a_1 is determined by the particle-hole asymmetry of each system. That is understood by considering it is proportional to the first derivative $\rho'_{\rm d}(0)$ and $\frac{\partial \chi_{\rm p0}(\mathbf{0},0)}{\partial \mu}$ [99]. The cancelation in the particle-hole symmetric case is robust even in the strong coupling case. In the weak coupling limit, the real part a_1 is higher order than the imaginary part a_2 with respect to the small parameter $T_{\rm c}^{\rm MF}/\varepsilon_{\rm F}$. Therefore, the parameter a_1 has usually been neglected. However, the real part a_1 should not be neglected for High-$T_{\rm c}$ cuprates. One reason is that the superconductivity is expected to be in the intermediate or strong coupling region. In that case, the ratio $T_{\rm c}^{\rm MF}/\varepsilon_{\rm F}$ increases with the coupling constant $|g|$. The other reason is the strongly asymmetric band structure of the systems. It should be noticed that a_1 is not so reduced even in the case of the strong coupling superconductivity. Because the relatively large momentum space contributes to the parameter a_1, it is not so affected by the pseudogap formation. Therefore, it is possible that the real part a_1 is the same order of the imaginary part a_2.

As a result of the above discussion, the extreme condition $|a_1| \geq a_2$ can be realized near the critical point in the strong coupling limit. This expectation is confirmed by our explicit self-consistent calculation in §2.3. In this case, the superconducting fluctuations have a propagative character, although they are over-damped diffusive mode in the conventional weak coupling theory. It should be noticed that it is a character of the collective mode and does not mean the tightly bound pairs supposed in the NSR scenario [74]. The suppression of the dissipation term a_2 has the different origin from that in the NSR theory [79]. Especially, the phase transition is the

superconductivity, not the Bose condensation in the sense of the NSR theory. The finite a_1 induces the asymmetry of the T-matrix. Actually, the particle-hole asymmetry is not necessary but advantageous to the pseudogap state in the self-consistent solution (§2.3).

As is explained before, the sign of a_1 depends on the band structure. The sign of a_1 is negative in case of under-doped High-T_c cuprates. This fact indicates that the superconducting fluctuations have hole-like character in the under-doped region. The sign of a_1 determines the sign of the correction of the superconducting fluctuations on the Hall coefficient [99]. It has been pointed out [87] that the experimental results of the Hall coefficient in High-T_c cuprates under the high magnetic field is not consistent with the above general expression. The sign-reversal of the Hall coefficient occurs in under-doped cuprates. The result means that the electron-like contribution is given by the superconducting fluctuations. That is inconsistent with the negative sign of a_1. Geshkenbein *et al.* phenomenologically assumed that the pre-formed pairs are electron-like in order to explain the sign problem [84]. However, the sign of a_1 is negative even in the strong coupling region. Moreover, the pre-formed pairs are hole-like even in the NSR scenario. Thus, the assumption by Geshkenbein *et al.* is not justified by the simple strong coupling theory.

In the remaining part of this section, we calculate the single particle self-energy corresponding to the one-loop diagram (Fig. 3.3(a)) on the basis of the above TDGL expansion for the T-matrix. Here, we phenomenologically define the TDGL parameters and use the bare Green function for simplicity. This calculation corresponds to the T-matrix approximation. Hereafter, we choose the TDGL parameter t_0 as a small parameter. Therefore, our theory is an approach starting from the actual critical point.

The self-energy is given by

$$\Sigma(\boldsymbol{k}, \mathrm{i}\omega_n) = T \sum_{\boldsymbol{q}, \mathrm{i}\Omega_m} t(\boldsymbol{q}, \mathrm{i}\Omega_m) G(\boldsymbol{q}-\boldsymbol{k}, \mathrm{i}\Omega_m - \mathrm{i}\omega_n) \varphi^2_{\boldsymbol{k}-\boldsymbol{q}/2}. \tag{3.16}$$

After the analytic continuation, we obtain

$$\begin{aligned} \Sigma^{\mathrm{R}}(\boldsymbol{k}, \omega) &= \sum_{\boldsymbol{q}} \int \frac{\mathrm{d}\Omega}{\pi} [b(\Omega) \mathrm{Im} t(\boldsymbol{q}, \Omega) G^{\mathrm{A}}(\boldsymbol{q}-\boldsymbol{k}, \Omega-\omega) - f(\Omega) t(\boldsymbol{q}, \Omega+\omega) \mathrm{Im} G^{\mathrm{R}}(\boldsymbol{q}-\boldsymbol{k}, \Omega)] \\ &\quad \times \varphi^2_{\boldsymbol{k}-\boldsymbol{q}/2}, \end{aligned} \tag{3.17}$$

$$\mathrm{Im}\Sigma^{\mathrm{R}}(\boldsymbol{k}, \omega) = -\sum_{\boldsymbol{q}} \int \frac{\mathrm{d}\Omega}{\pi} [b(\Omega+\omega) + f(\Omega)] \mathrm{Im} t(\boldsymbol{q}, \Omega+\omega) \mathrm{Im} G^{\mathrm{R}}(\boldsymbol{q}-\boldsymbol{k}, \Omega) \varphi^2_{\boldsymbol{k}-\boldsymbol{q}/2}. \tag{3.18}$$

Here $b(\Omega)$ is the Bose distribution function. In the conventional Fermi liquid theory, the factor $[b(\Omega+\omega) + f(\Omega)]$ gives the common relation $\mathrm{Im}\Sigma^{\mathrm{R}}(\boldsymbol{k}, \omega) \propto \omega^2 + (\pi T)^2$. However, in this case, the strong $\boldsymbol{q}$- and Ω-dependence of the T-matrix $t(\boldsymbol{q}, \Omega)$ give rise to the anomalous features as we show below.

Assuming $|a_1| \gg a_2$ which is expected in the strong coupling limit, we can describe the imaginary part of the T-matrix in the following way,

$$\mathrm{Im} t(\boldsymbol{q}, \Omega) = g \frac{\pi}{a_1} \delta(\Omega - \Omega_{\boldsymbol{q}}) \tag{3.19}$$

Here, we have defined the dispersion relation of the fluctuating Cooper pairs $\Omega_{\boldsymbol{q}} = (t_0 + b\boldsymbol{q}^2)/a_1$. Because the parameter a_1 is negative in our case, the pole of the T-matrix is also negative $\Omega_{\boldsymbol{q}} < 0$. This shows that the superconducting fluctuations are not electron-like but hole-like. By substituting eq. 3.19 into eq. 3.17, we obtain

$$\mathrm{Re}\Sigma^{\mathrm{R}}(\boldsymbol{k}, \omega) = \sum_{\boldsymbol{q}} g [\frac{1}{a_1} b(\Omega_{\boldsymbol{q}}) \mathrm{Re} G^{\mathrm{R}}(\boldsymbol{q}-\boldsymbol{k}, \Omega_{\boldsymbol{q}} - \omega)$$

$$-\int \frac{d\Omega}{\pi} f(\Omega-\omega)\frac{1}{t_0+bq^2-a_1\Omega}\mathrm{Im}G^{\mathrm{R}}(\boldsymbol{q}-\boldsymbol{k},\Omega-\omega)]\varphi^2_{\boldsymbol{k}-\boldsymbol{q}/2}. \quad (3.20)$$

$$\mathrm{Im}\Sigma^{\mathrm{R}}(\boldsymbol{k},\omega) = -\sum_{\boldsymbol{q}}\frac{g}{a_1}[b(\Omega_{\boldsymbol{q}})+f(\Omega_{\boldsymbol{q}}-\omega)]\mathrm{Im}G^{\mathrm{R}}(\boldsymbol{q}-\boldsymbol{k},\Omega_{\boldsymbol{q}}-\omega)\varphi^2_{\boldsymbol{k}-\boldsymbol{q}/2}. \quad (3.21)$$

We can see from the above expressions that the singular contribution in the small t_0 limit arises from the terms proportional to $b(\Omega_{\boldsymbol{q}})$. Therefore, we estimate the singular terms by linearizing the bare Green function as, $G^{(0)\mathrm{R}}(\boldsymbol{q}-\boldsymbol{k},\omega) = (\omega-\varepsilon_{\boldsymbol{k}}+v_{\boldsymbol{k}}\boldsymbol{q}+\mathrm{i}\delta)^{-1}$. Because the singular contribution arises from the vicinity of $\boldsymbol{q}=0$, we restrict the $\boldsymbol{q}$-sum to the region $|\Omega_{\boldsymbol{q}}|\leq T$, and use the approximate relation $b(\Omega_{\boldsymbol{q}})\sim\frac{T}{\Omega_{\boldsymbol{q}}}$. Since only the small region in the vicinity of $\boldsymbol{q}=0$ contributes to the self-energy, we can neglect the $\boldsymbol{q}$-dependence of the form factor $\varphi_{\boldsymbol{k}-\boldsymbol{q}/2}$. By using the above procedures, we exactly calculate the $\boldsymbol{q}$-sum. Since the results are very complicated, we show the approximate results as follows,

$$\mathrm{Re}\Sigma^{\mathrm{R}}(\boldsymbol{k},\omega) = \begin{cases} -g\varphi^2_{\boldsymbol{k}}\frac{T}{4\pi b}\frac{1}{\alpha}\log[\frac{a_1}{t_0}\min(T,\alpha,\alpha^2b/|a_1|v^2_{\boldsymbol{k}})] & (|\alpha|\gg\frac{t_0}{|a_1|}) \\ -g\varphi^2_{\boldsymbol{k}}\frac{T}{2\pi a_1 v^2_{\boldsymbol{k}}}(\frac{a_1}{t_0}\alpha-1) & (|\alpha|\sim\frac{t_0}{|a_1|}), \end{cases} \quad (3.22)$$

$$\mathrm{Im}\Sigma^{\mathrm{R}}(\boldsymbol{k},\omega) = \begin{cases} g\varphi^2_{\boldsymbol{k}}\frac{T}{4b}(\alpha^2+\frac{v^2_{\boldsymbol{k}}}{b}t_0)^{-\frac{1}{2}} & (|\alpha|\leq T) \\ 0 & (\alpha\geq\frac{|a_1|v^2_{\boldsymbol{k}}}{4b}-\frac{t_0}{|a_1|}), \end{cases} \quad (3.23)$$

where we have defined as $\alpha=\omega+\varepsilon_{\boldsymbol{k}}$.

We show the typical features of $\mathrm{Re}\Sigma^{\mathrm{R}}(\boldsymbol{k},\omega)$, $\mathrm{Im}\Sigma^{\mathrm{R}}(\boldsymbol{k},\omega)$ and $\pi A(\boldsymbol{k},\omega)=-\mathrm{Im}G^{\mathrm{R}}(\boldsymbol{k},\omega)$ in Fig. 3.4.

It is notable that the real part of the self-energy has the positive slope in the vicinity of $\alpha=0$, and the imaginary part of the self-energy has the sharp peak at $\alpha=0$ in its absolute value. The both features are anomalous compared with the conventional Fermi liquid theory. These anomalous features should be regarded as the effects of the resonance scattering of the quasi-particles by the thermally fluctuating Cooper pairs. Such drastic phenomena take place on the condition $|\Omega_{\boldsymbol{0}}|\ll T$. Of course, the characteristics of the strong coupling superconductivity are included in the properties of the TDGL parameters. As the coupling constant $|g|$ increases and therefore the critical temperature T_{c} increases, the effects of the resonance scattering become remarkable. On the other hand, these effects are sufficiently weak in the weak coupling case. Although we have used the assumption $|a_1|\gg a_2$ in the above analytic calculation, the results change little even in the conventional case $|a_1|\leq a_2$. The only change is that the particle-hole asymmetric structure is weakened. However, the large dissipation term a_2 reduces the absolute value of the self-energy.

It should be noticed that the self-energy essentially has the asymmetric structure, which arises from the hole-like features of the superconducting fluctuations. For example, the imaginary part has the long tail on the negative frequency side.

Norman *et al.* [100] have used the assumption $\Sigma^{\mathrm{R}}(\boldsymbol{k},\omega)\propto\frac{1}{\omega+\varepsilon_{\boldsymbol{k}}+\mathrm{i}\Gamma_0}$ in order to explain the data of the ARPES experiments. Our results are qualitatively consistent with the assumption. However, we shall point out in §2.3 that the slight break down of the assumption which originates from the asymmetric structure is important for the self-consistent solution.

The result for the single particle spectral weight $A(\boldsymbol{k},\omega)$ is shown in Fig. 3.4(c). According to Fig. 3.4(a), there are three solutions of the equation $\omega-\varepsilon_{\boldsymbol{k}}-\mathrm{Re}\Sigma^{\mathrm{R}}(\boldsymbol{k},\omega)=0$. However, since the imaginary part of the self-energy is extremely large in the vicinity of $\alpha=0$, the middle solution

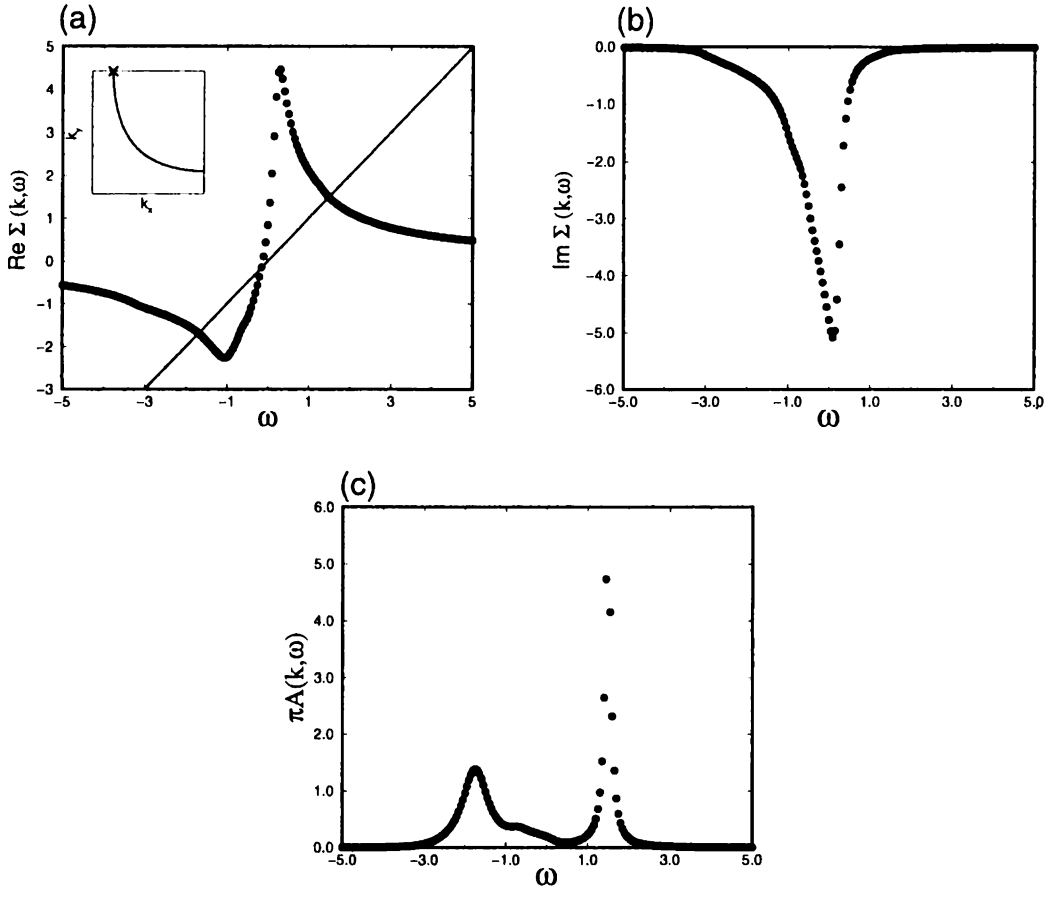

Figure 3.4: (a) The real part of the self-energy given by the one loop diagram in Fig. 3.3(a). The solid line shows the condition $\omega - \varepsilon_{\boldsymbol{k}} - \mathrm{Re}\Sigma^{\mathrm{R}}(\boldsymbol{k},\omega) = 0$. (b) The imaginary part of the self-energy. (c) The spectral weight. For all figures, the $\boldsymbol{k}$-point is chosen so as to be on the Fermi surface near $(0,\pi)$. (see inset in (a)). Here, the coupling constant and the TDGL parameters are chosen as $g = -2.0$, $a_1 = -1.0$, $a_2 = 0.2$, $b = 0.2$, $t_0 = 0.03$, $T = 0.2$.

in Fig. 3.4(a) disappears. Therefore, the spectral weight shows the gap-like two peak structure at

$$E = \pm\sqrt{\varepsilon_{\boldsymbol{k}}^2 + \Delta_{\boldsymbol{k}}^2}, \tag{3.24}$$

$$\Delta_{\boldsymbol{k}}^2 = |g|\varphi_{\boldsymbol{k}}^2 \frac{T}{4\pi b}\log[T/\frac{t_0}{a_1}]. \tag{3.25}$$

This spectrum is similar to that of the superconducting state. Although the gap amplitude is related to the condensed Cooper pairs in the superconducting state, here, $\Delta_{\boldsymbol{k}}^2$ is proportional to the total weight of the superconducting fluctuations. That is regarded as the number of the thermally fluctuating Cooper pairs, $n_{\rm B} \propto \sum_{\boldsymbol{q}} b(\Omega_{\boldsymbol{q}})$ in the strong coupling limit.

Furthermore, the spectral weight also has the asymmetric structure. The spectrum has the relatively broad peak on the negative frequency side and the sharp peak on the positive frequency side. Randeria *et al.* [101] have proposed the assumption of the particle-hole symmetry for the spectral weight, and actually Norman *et al.* [22] carried out the analysis for the ARPES data on the basis of the assumption. We consider that this analysis is qualitatively relevant. However, our calculation shows that this assumption is necessarily broken in the strong coupling superconductors, because the particle-hole asymmetry clearly appear in that case. Indeed, the particle-hole asymmetry plays an important role in stabilizing the self-consistent calculation in §2.3.

We shall numerically carry out the explicit calculation for the TDGL parameters and the single-particle self-energy corresponding to the T-matrix (in §2.2) and the self-consistent T-matrix (in §2.3) approximations in the following sections.

It should be pointed out that there is a logarithmic singularity of the self-energy and $\Delta_{\boldsymbol{k}}$ near the critical point. This singularity is a characteristic feature of the two-dimensional systems. Strictly speaking, the singularity reduces the critical temperature $T_{\rm c}$ to 0. The result is well-known as the Marmin-Wagner's theorem. The NSR theory for two-dimensional systems [75, 76] has the similar singularity, and the critical temperature $T_{\rm c} = 0$. However, there is not such a singularity in the layered systems. Although the quasi-two dimensionality enhances the effects of the fluctuations, the weak three-dimensionality is sure to remove the singularity. [94]

Here, we briefly comment on the Nozières and Schmitt-Rink theory. The NSR theory takes account of the shift of the chemical potential by the creation of the bosonic particles, and decides the critical temperature $T_{\rm c}$ using the Thouless criterion for the shifted chemical potential. It should be noticed that the chemical potential shifts upward in case of High-$T_{\rm c}$ cuprates because the superconducting fluctuations are not electron-like, but hole-like. It is the opposite direction compared to the Fermi gas model or the low density lattice model. (see Fig. 3.5.) We can understand this result by considering eqs. (1.3) and (2.13). The derivative of the thermodynamic potential with respect to the chemical potential μ is related to the TDGL parameter a_1. In the relation $2a_1 = |g|\frac{\partial \chi_{\rm p0}(\mathbf{0},0)}{\partial \mu}$, the factor 2 corresponds to the two electrons composing the Cooper pairs. In the low density case $\frac{\partial \chi_{\rm p0}(\mathbf{0},0)}{\partial \mu} > 0$, and in case of the under-doped cuprates, $\frac{\partial \chi_{\rm p0}(\mathbf{0},0)}{\partial \mu} < 0$. The upward shift is a natural result because the DOS decreases in that direction.

We can understand from the above calculations that the NSR scenario is justified in the low density limit. In the low density limit, a strong attractive interaction easily creates the bosonic pre-formed pairs which can move almost freely. The chemical potential shifts remarkably in that case. There is no serious effects on the fermion system except for the shift of the chemical potential μ. This insight is justified by the results in this section that the self-energy is proportional to the number of bosons $n_{\rm B}$ in rough estimate. Because the number of bosons $n_{\rm B}$ can not exceed the total fermion density, the effects of the resonance scattering do not appear in the low density limit. On the other hand, the effects of the resonance scattering are dominate the shift of the

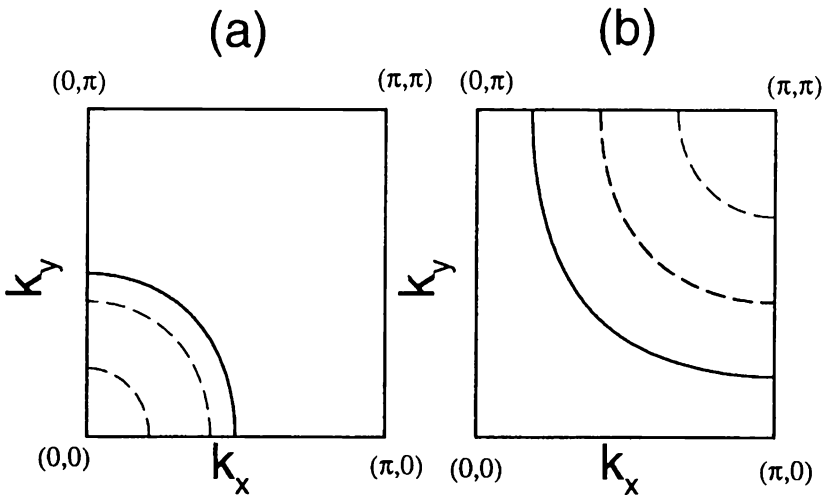

Figure 3.5: The schematic figures of the transformation of the Fermi surface by the shift of the chemical potential, which is the dominant effect in the NSR theory. The solid line shows the original Fermi surface, and the long-dashed line shows the shifted Fermi surfaces. (a) The case of the Fermi gas model, or the low density lattice model. The chemical potential shifts downward. (b) The case of High-T_c cuprates. The chemical potential shifts upward.

chemical potential in high density systems. Therefore, the chemical potential actually shifts even in the high density systems, that is not a dominant effect. The shift of the chemical potential is included in our calculation. However, we will not pay attention to it in the following sections.

3.1.2 Lowest Order Calculation

In this section we explicitly calculate the single particle self-energy on the basis of the formalism described in the previous section.

First, we calculate the T-matrix around $\boldsymbol{q} = \Omega = 0$ by using the non-interacting Green function $G^{\mathrm{R}(0)}(\boldsymbol{k}, \omega) = (\omega - \varepsilon_{\boldsymbol{k}} + \mathrm{i}\delta)^{-1}$. We expand the reciprocal of the T-matrix, $t(\boldsymbol{q}, \Omega)^{-1}$ and estimate the TDGL expansion parameters. Of course, the results are equivalent to eq. 3.11.

Secondly, we calculate the single particle self-energy corresponding to the diagram shown in Fig. 3.3(a), using eq. 3.17. This calculation corresponds to the T-matrix approximation. We exclude the trivial Hartree-Fock term shown in Fig. 3.3(c).

Because we use the non-interacting Green function, the superconducting critical temperature T_c is the same as that obtained by the BCS mean field theory, T_c^{MF}. Therefore, our calculation in this section is carried out above T_c^{MF}. We show the results for the single particle self-energy in Fig. 3.6. The self-energy shows the same features as we have calculated analytically in §2.1. The effects of the resonance scattering clearly appear.

The results for the spectral weight is shown in Fig. 3.7 for various temperatures. The spectral weight has the two peak and shows the gap structure clearly near the critical point. As the temperature increases, the gap structure is filled up. Thus, the quasi-particles of the normal Fermi liquid, which is realized at higher temperature, become unstable near the superconducting critical temperature $T_c = T_c^{\mathrm{MF}} = 0.185$ where the superconducting fluctuations are strong. Thus, the resonance scattering produce the pseudogap in the single particle spectral weight.

The momentum dependence of the spectral weight is shown in Fig. 3.8. We can see that the

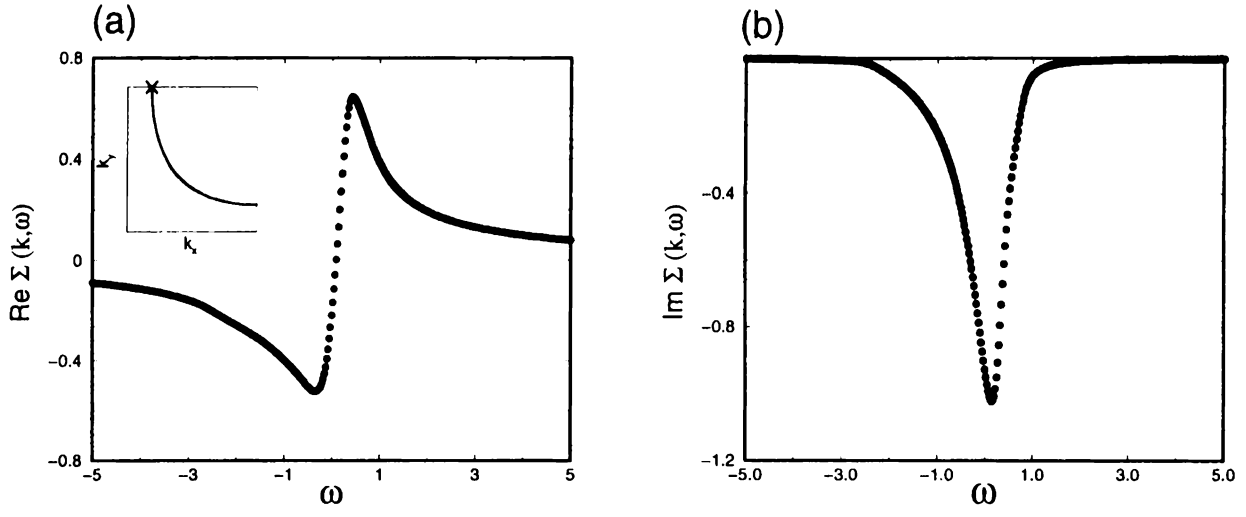

Figure 3.6: The single particle self-energy on the Fermi surface near $(0, \pi)$ obtained by the lowest order calculation. (a)The real part. (b)The imaginary part. Here, $\boldsymbol{k} = (0.589, \pi)$, $g = -1.0$, and $T = 0.21$. The $\boldsymbol{k}$-point is shown in the inset of (a). Here, $T_c = T_c^{\mathrm{MF}} = 0.185$.

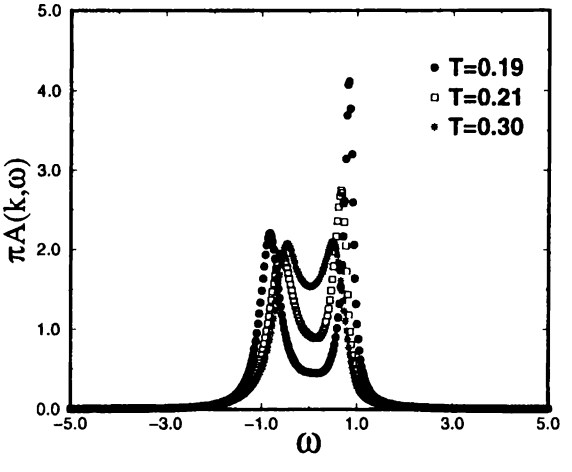

Figure 3.7: The spectral weight for various temperatures $T = 0.19$(circles), $T = 0.21$(squares), $T = 0.30$(stars). The other parameters are the same as those in Fig. 3.6.

amplitude of the gap is large in the vicinity of $(0, \pi)$, and decreases as the momentum approaches $(\pi/2, \pi/2)$. Furthermore, the single peak structure of quasi-particles appears in the vicinity of $(\pi/2, \pi/2)$. These features are consistent with the ARPES experiments [22, 23]. The momentum dependence is mainly owing to the $d_{x^2-y^2}$-wave form factor $\varphi_{\boldsymbol{k}}$. Thus, it is naturally led from our formalism that the pseudogap has the same shape as that of the superconducting gap. Since the attractive interaction is small in the vicinity of $(\pi/2, \pi/2)$, quasi-particles are not affected by the superconducting fluctuations.

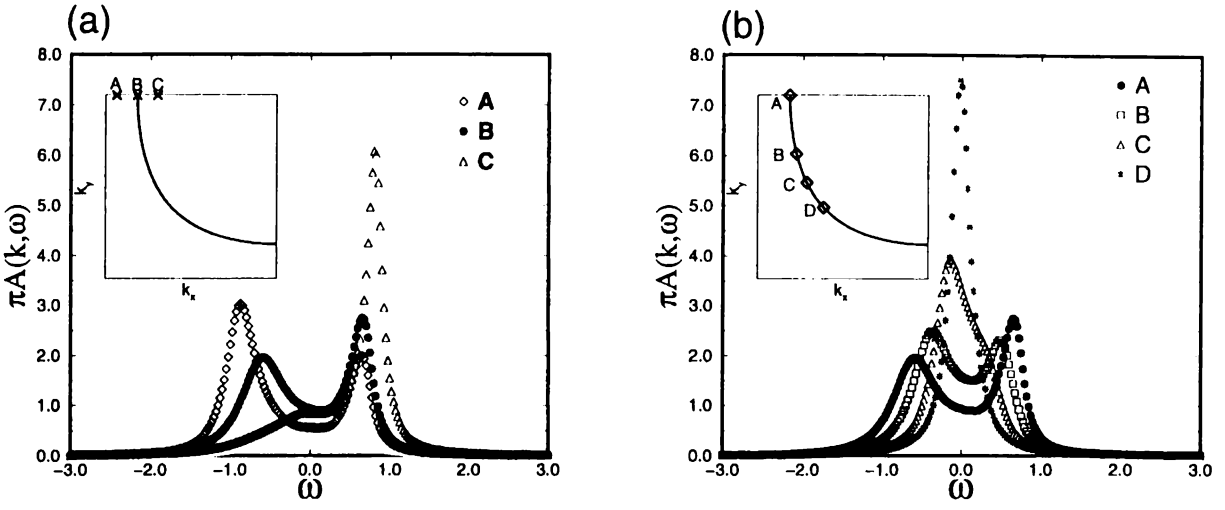

Figure 3.8: The momentum dependence of the spectral weight (a) across the Fermi surface near $(0, \pi)$ (b) along the Fermi surface. The respective $\boldsymbol{k}$-points are shown in the inset. The other parameters are the same as those in Fig. 3.6.

The results for the DOS $\rho(\varepsilon)$ is shown in Fig. 3.9. The pseudogap clearly appear in the density of state. Our calculation is carried out only for the $\boldsymbol{k}$-points in the vicinity of the Fermi surface. Because the quasi-particles far from the Fermi surface are not so affected by the superconducting fluctuations, we do not pay attention to them. The DOS in Fig. 3.9 is obtained by summing up the momentum on the calculated area. Therefore, the peak position is artificial and depends on the summed area. Only the suppression of the density of state near the Fermi level is essential.

Because the quasi-particles exist around $(\pi/2, \pi/2)$, the gap structure of the DOS is not so clear compared with that in the superconducting states. These results are consistent with the results of the tunneling spectroscopy [49].

Thus, most of the features related to the pseudogap phenomena are understood from the above lowest order calculation. From the above results, we conclude at least that the strong coupling superconductivity in the quasi-two dimensional system makes the Fermi liquid state unstable near the mean field superconducting critical temperature T_c^{MF}.

As we have pointed out before, the above calculation is applicable to the higher temperature than T_c^{MF}. In practice, the effects of the superconducting fluctuations remarkably suppress the critical temperature. Indeed, we have an interest in the temperature region in which the superconductivity is suppressed by the fluctuations. In order to treat this region explicitly, we must carry out the self-consistent calculation using the renormalized Green function. We will carry out the self-consistent calculation in the next section, §2.3. Although there are some differences, the essential results, such as the gap structure and so on, do not change even in the self-consistent

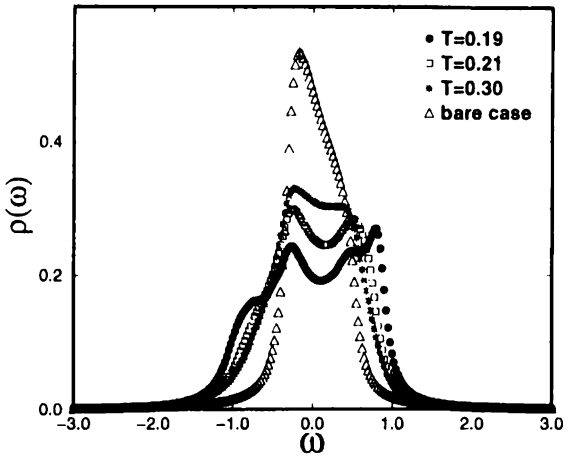

Figure 3.9: The DOS $\rho(\varepsilon)$ for various temperatures. The parameters and the marks are the same as those in Fig. 3.6. The triangles show the non-interacting DOS. Since we calculate only in the vicinity of the Fermi surface, the peak position is not exact. The suppression of the DOS at the low energy is essential.

calculation.

3.1.3 Self-Consistent Calculation

In this section, we self-consistently calculate the single particle self-energy and the TDGL parameters on the basis of the formalism described in §2.1. Furthermore, we calculate the superconducting critical temperature suppressed by the effects of the fluctuations, and determine the phase diagram.

To begin with, we explain our method of the numerical calculation used in this section. We restrict the $\boldsymbol{k}$- points for which the self-energies are calculated to the region close to the Fermi surface. The restricted region is shown in Fig. 3.10. As we have mentioned in the previous section, the effects of the superconducting fluctuations (resonance scattering) are important in the vicinity of the Fermi surface, and are not important far from the Fermi surface. Except for a_1, the TDGL parameters mainly determined by the electronic states near the Fermi surface. Furthermore, the important Green functions for the self-consistent calculation of the self-energy $\Sigma^{\mathrm{R}}(\boldsymbol{k},\omega)$ have the momentum in the vicinity of $\boldsymbol{k}$, because the main contribution is given by the small momentum of the center of mass $\boldsymbol{q} \sim 0$. Therefore, we have only to consider the self-energy near the Fermi surface. Thus, our restriction for the momentum space is justified. The other justification of the above procedure is obtained in the following way. Generally speaking, the renormalized quasi-particles give rise to the superconductivity in the strongly correlated electron systems. The renormalized quasi-particles are well defined only near the Fermi surface. Therefore, order parameter is expected to be sufficiently small far from the Fermi surface and the electronic state is not so affected by the superconducting fluctuations. Since these features are no included in the effective model adopted in this chapter, we phenomenologically introduce the features by the above procedure.

We estimate the TDGL parameters by eq. 3.7 for the renormalized Green function $G^{\mathrm{R}}(\boldsymbol{k},\omega) = (\omega - \varepsilon_{\boldsymbol{k}} - \Sigma^{\mathrm{R}}(\boldsymbol{k},\omega))^{-1}$, and self-consistently calculate the single particle self-energy $\Sigma^{\mathrm{R}}(\boldsymbol{k},\omega)$,

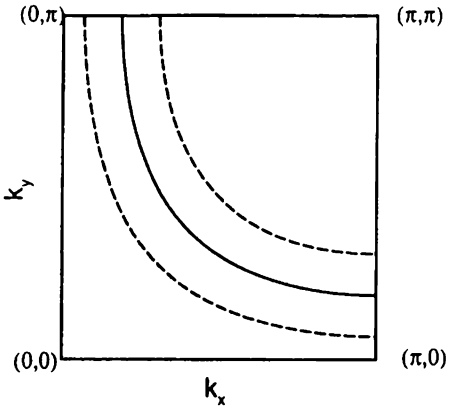

Figure 3.10: In this section, the self-energy is calculated in the region between the dashed lines.

using eq. 3.17 (see Fig. 3.3(b)). Here, we exclude the Hartree-Fock term corresponding to the diagram in Fig. 3.3(c), as we have done in the lowest order calculation in §2.2. This calculation corresponds to the self-consistent T-matrix approximation.

For the purpose of the self-consistent calculation, we divide the Brillouin zone as shown in Fig. 3.10, and put $\Sigma^{\mathrm{R}}(\boldsymbol{k},\omega) = 0$ outside of the dashed lines. As we have described before, this approximation does not change the electronic structure near the Fermi surface and is appropriate to discuss the pseudogap phenomena. Furthermore, we introduce the cutoff parameters for the integrations by Ω and $\boldsymbol{q}$, because the main contribution is obtained from the integrations around $\boldsymbol{q} = \Omega = 0$. The TDGL expansion is not so reliable for large $\boldsymbol{q}$ and Ω. Owing to the cutoff, we might slightly underestimate the effects of the superconducting fluctuations. However, the cutoff procedure has no significant effect on our results.

It should be noticed that we fix the parameter t_0 in this self-consistent calculation instead of the coupling constant g. Although the final self-consistent results are identical, the convergence of the solution is remarkably improved by using this method. In particular, we need to adopt this method in order to calculate near the critical point where the superconducting fluctuations are strong. The parameter t_0 represents the distance from the superconducting critical point. Therefore, if the parameter t_0 is varied, the situation remarkably changes. As a result, the solution fluctuates and the calculation is impossible near the critical point for the g-fixed calculations in many cases [102, 103]. Thus, because of the convenience of the numerical calculation, not the coupling constant g but the temperature T and the parameter t_0 are fixed in our calculation. The coupling constant g is determined by the result of the self-consistent calculation. We do not positively change the chemical potential so as to conserve the particle number. However, we have verified that the particle number is almost conserved in this calculation. This is an evidence of that the NSR scenario is not justified in this case.

Strictly speaking, the superconducting transition does not occur in the two-dimensional systems. The fact is well known as the Marmin-Wagner's theorem. Our calculations also satisfy the theorem, and the critical temperature is zero $T_{\mathrm{c}} = 0$ in our formalism. This is because of the logarithmic singularity of the self-energy which arises from the two-dimensionality. However, the weak three-dimensionality is sure to remove these singularities in the layered systems. [94] Therefore, we phenomenologically introduce the three-dimensionality and define the superconducting critical temperature as the temperature in which $1 + g\chi_{\mathrm{p0}}(\mathbf{0}, 0) = 0.01$. This condition corresponds to

the 100 times enhancement of the superconducting susceptibility. The phase diagram does not depend on the details of this definition, qualitatively.

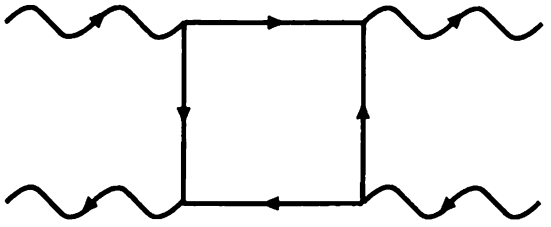

Figure 3.11: The diagram representing the mode coupling effect in the lowest order. The wavy and solid lines represent the propagator of the fluctuating Cooper pairs and that of the fermions, respectively.

It should be noticed that the self-consistently calculated T-matrix includes the renormalization effects of the superconducting fluctuations through the self-energy $\Sigma^{\mathrm{R}}(\boldsymbol{k},\omega)$. The renormalization effects include the mode coupling effect. The forth order term in the Ginzburg-Landau action is expressed by the diagram shown in Fig. 3. 11, which indicates the repulsive interaction between the fluctuating Cooper pairs (that is the lowest order mode coupling term). The effect of the mode coupling term is included in the self-consistent T-matrix calculation at least in the Hartree-Fock approximation. Thus, the self-consistent T-matrix calculation is a method introducing the criticality of the superconducting fluctuations. Furthermore, the microscopic renormalization effects are included through the single particle properties. They have been discussed in §2.1. Then, the properties of the calculated TDGL parameters well reproduce our argument in §2.1. The renormalization effects enhance the scattering vertex originated from the superconducting fluctuations and accelerate the pseudogap formation. The critical temperature T_{c} is reduced by the fluctuations. The reduced T_{c} is due to the reduced density of states (DOS) by the pseudogap. The reduced T_{c} can be regarded as a result of the wide critical region, simultaneously. The reduction is remarkable in the strong coupling superconductivity, while it is neglected in the weak coupling one.

We show the results of the spectral weight for various t_0 and temperatures in Fig. 3.12. The pseudogap structure exists in the small t_0 cases, and becomes clear as t_0 decreases. Because the parameter t_0 shows the distance to the superconducting critical point, this behavior are natural. The effects of the resonance scattering are rather drastic in case of the high temperature, that is to say, large $|g|$ where the thermal fluctuations are rather strong.

In particular, the plural peak structure appears in the small t_0 and large T cases. This complicated structure is also understood on the basis of the formalism as we have have explained below. For example, we show the self-energy for $T = 0.10$, $t_0 = 0.01$ in Fig. 3.13. In this case, the spectral weight shows the three peak structure.

It should be noticed that the electronic structure around $(-\boldsymbol{k},-\omega)$ plays an important role for the estimate of the self-energy $\Sigma^{\mathrm{R}}(\boldsymbol{k},\omega)$. It is because the main contribution comes from the integrations in the vicinity of $\boldsymbol{q} = \Omega = 0$. Therefore, if the spectral weight has its peak at $\omega = \omega_{\mathrm{p}}$, the real part of the self-energy has the positive slope at $\omega = -\omega_{\mathrm{p}}$, and the imaginary part has the peak at $\omega = -\omega_{\mathrm{p}}$ in its absolute value. In rough estimate, the relation $\mathrm{Im}\Sigma^{\mathrm{R}}(\boldsymbol{k},\omega) \propto A(\boldsymbol{k},-\omega)$ is expected.

To put it in detail, the left peak and the middle peak yield the positive slope of the real part on

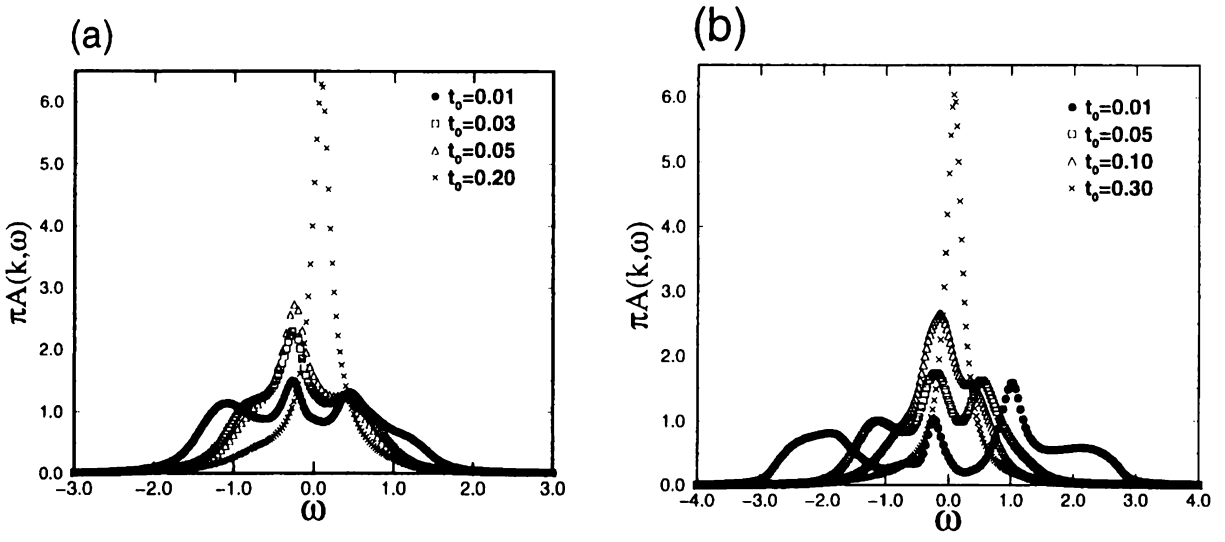

Figure 3.12: The single particle spectral weight on the Fermi surface near $(0, \pi)$ obtained by the self-consistent calculation. (a)$T = 0.10$. t_0 is varied as $0.01, 0.03, 0.05, 0.20$. (b)$T = 0.15$. t_0 is varied as $0.01, 0.05, 0.10, 0.30$. The calculated points are shown in the phase diagram (Fig. 3.16). The $\boldsymbol{k}$-point is the same as that in Fig. 3.6.

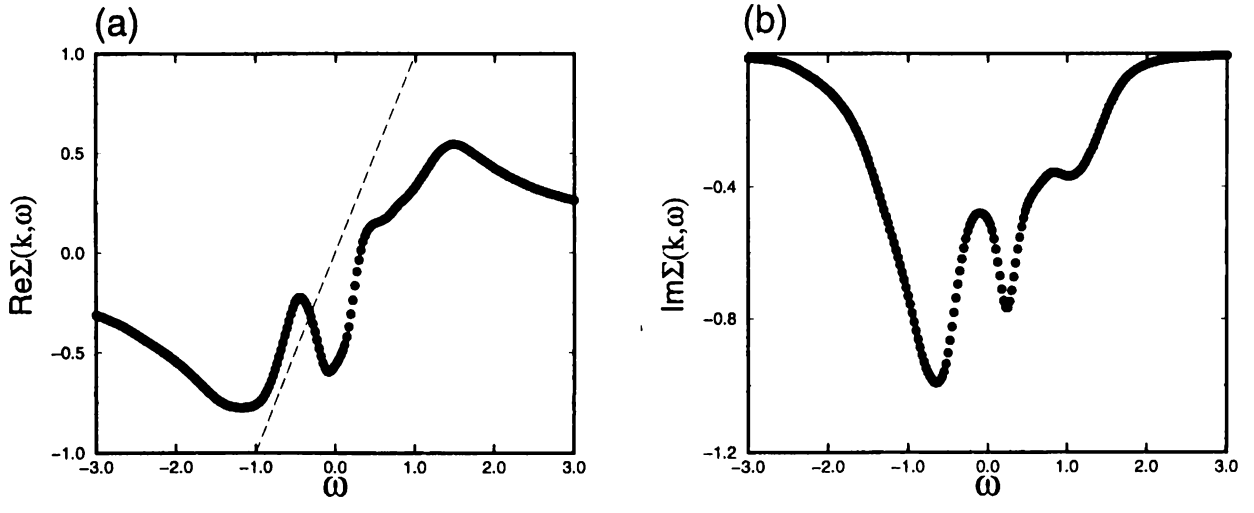

Figure 3.13: The single particle self-energy on the Fermi surface near $(0, \pi)$. Here, $T = 0.10$, $t_0 = 0.01$. (a)The real part. The long-dashed line is described in order to show the line $\omega - \varepsilon_{\boldsymbol{k}} - \mathrm{Re}\Sigma^{\mathrm{R}}(\boldsymbol{k}, \omega = 0$. (b)The imaginary part. The $\boldsymbol{k}$-point is the same as that in Fig. 3.6.

the positive frequency side, and yield the right peak. The right peak yields the positive slope of the real part on the negative frequency side. Consequently the negative slope is formed at the small negative frequency. The only solution $\omega - \varepsilon_{\boldsymbol{k}} - \mathrm{Re}\Sigma^{\mathrm{R}}(\boldsymbol{k},\omega) = 0$ exists here. This corresponds to the middle peak. Moreover, the right peak yields the sharp peak of $-\mathrm{Im}\Sigma^{\mathrm{R}}(\boldsymbol{k},\omega)$ at the negative frequency side. The peak yields the double peak structure on the negative frequency side. They correspond to the left and middle peaks. It should be noticed that such an asymmetric structure stabilizes the self-consistent solution. Because of the rough relation $\mathrm{Im}\Sigma^{\mathrm{R}}(\boldsymbol{k},\omega) \propto A(\boldsymbol{k},-\omega)$, the peak of the spectral weight at $\omega = \omega_{\mathrm{p}}$ suppresses the weight at $\omega = -\omega_{\mathrm{p}}$. Thus, the symmetric structure is unstable in the self-consistent solution. In particular, the spectral weight at the Fermi energy $\omega = 0$ is necessarily suppressed.

The particle-hole asymmetry is not necessary but advantageous for the pseudogap state in the self-consistent solution. As we mentioned in §2.1, the particle-hole asymmetry naturally exists in the systems and plays an important role for the self-consistent solution to be stabilized. Furthermore, High-T_{c} cuprates are the strongly asymmetric systems because of existence of the Van-Hove singularity at $(\pi, 0)$. It is notable that these results are not consistent with the assumption by Norman *et al.* [100] and Maly *et al.* [88]. The assumed self-energy by them does not satisfy the self-consistency.

Here, we pay attention to the change of the spectral weight, once more. In the phase diagram (Fig. 3.16), we show the parameters for which we show the spectral weight or the DOS.

When t_0 is large and the temperature T is higher than the mean field critical temperature $T_{\mathrm{c}}^{\mathrm{MF}}$, the spectral weight has the sharp single peak structure. This structure is common in the conventional Fermi liquid theory. As t_0 decreases and the temperature becomes lower than $T_{\mathrm{c}}^{\mathrm{MF}}$, the peak shifts to the negative frequency side and has the long tail to the positive frequency side. In this region, as the momentum is varied from $(0,\pi)$ to (π,π), the peak shifts to positive frequency side and cross the Fermi level $\omega = 0$. However, as a result of the resonance scattering, the damping rate $-\mathrm{Im}\Sigma^{\mathrm{R}}(\boldsymbol{k},\omega)$ is large at the Fermi level and the spectral weight is suppressed there. Therefore, the DOS is reduced at the Fermi level. The superconducting fluctuations are gradually affected by the reduced DOS. As t_0 decreases further and the system approaches to the critical point, the spectral weight shows the plural peak structure. This behavior is quite different from that of the conventional Fermi liquid theory.

Here, we show the DOS for $T = 0.10$ and various t_0 in Fig. 3.14. As we mentioned above, the DOS at the Fermi level is reduced by the superconducting fluctuations. In particular, in case of $t_0 = 0.10$, the spectral weight has a sharp single peak in the vicinity of the Fermi surface. However, we can see clearly the suppression of the DOS. Generally speaking, the suppression becomes distinguished near the mean field critical temperature $T = T_{\mathrm{c}}^{\mathrm{MF}}$. The suppression becomes more remarkable, as t_0 decreases and the system approaches the critical point. In the vicinity of the critical point, the DOS at the Fermi level is mainly given by the contribution from the quasi-particles near $(\pi/2, \pi/2)$. Therefore, $\rho_{\mathrm{d}}(0)$ is more remarkably reduced by the resonance scattering due to the superconducting fluctuations.

In Fig. 3.15, we show the momentum dependence of the spectral weight in the pseudogap state. In Fig. 3.15(a), the momentum is varied across the Fermi surface near $(0,\pi)$. Below the original Fermi surface, the spectral weight transfers to the left peak. On the other hand, it transfers to the right peak on the opposite above the original Fermi surface. All peaks shift to the positive frequency side with increasing k_x. It should be noticed that the middle peak shifts and is found at the Fermi level $\omega = 0$ when the momentum slightly deviates from the original Fermi surface (represented as C in the inset). However, it is remarkably reduced by the effects

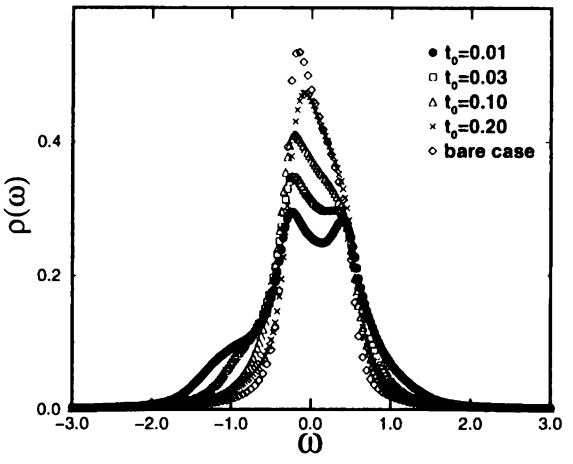

Figure 3.14: The DOS $\rho(\omega)$ for $T = 0.10$. t_0 is varied as $0.01, 0.03, 0.10, 0.20$. The diamonds show the non-interacting DOS. Since we calculate only the states in the vicinity of the Fermi surface, the peak position is not exact. The suppression of the DOS near the Fermi energy is essential.

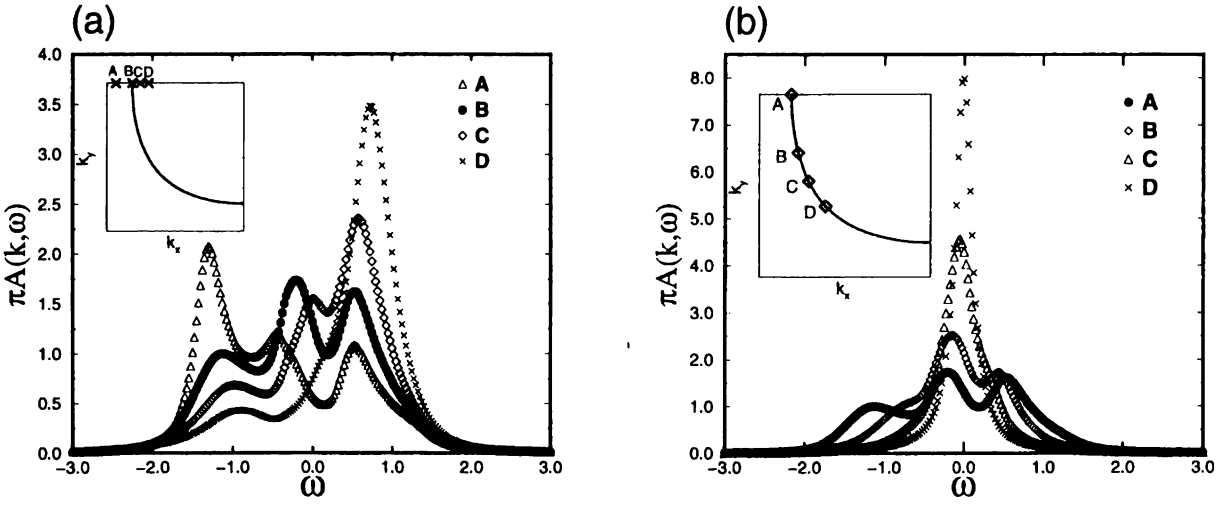

Figure 3.15: The momentum dependence of the spectral weight. Here, $T = 0.15$, $t_0 = 0.05$. The momentum is varied (a)across the Fermi surface near $(0, \pi)$ (b)along the Fermi surface. The respective $\boldsymbol{k}$-points are shown in the inset.

of the superconducting fluctuations. With increasing k_x, this peak cannot cross the Fermi level $\omega = 0$ and disappears at last. Thus, the spectral weight shows the double peak structure at the momentum D (see the inset).

In Fig. 3.15(b), the momentum is varied along the Fermi surface. We can see that the gap structure is clear in the vicinity of $(0, \pi)$ where the attractive interaction is strong, and becomes inconspicuous as the momentum approaches to $(\pi/2, \pi/2)$. Furthermore, the single peak of quasi-particles exists in the vicinity of $(\pi/2, \pi/2)$. This fact shows that the Fermi liquid like behavior exists in this region. Thus, the d-wave superconducting fluctuations necessarily give rise to the pseudogap with the same shape as the superconducting gap. The results are consistent with the ARPES experiments [22, 23].

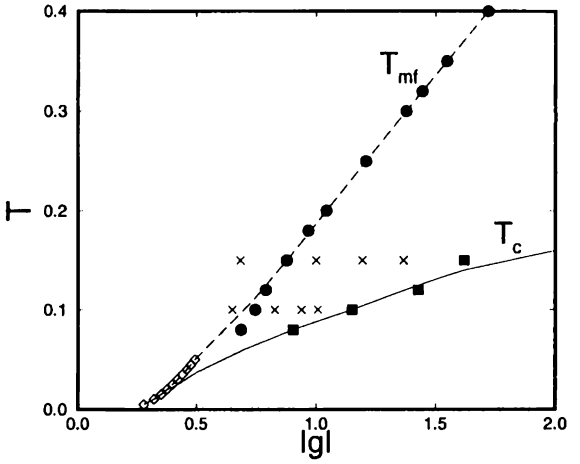

Figure 3.16: The phase diagram obtained in this section. The circles and diamonds show the superconducting critical temperature based on the mean field theory (T_c^{MF}). The circles are obtained by using the discrete momentum used in our self-consistent calculation. The diamonds are obtained by the explicit calculation for eq. 3.10. The circles at the low temperature are slightly off by the numerical error. The squares show the actual critical temperature (T_c) reduced by the fluctuations. The reduction becomes stronger in the strong coupling region. The marks $\times$ show the points where we have shown the spectral weight or the DOS. They correspond to $t_0 = 0.20$, $t_0 = 0.10$, $t_0 = 0.05$, $t_0 = 0.03$ from left to right for the temperature $T = 0.10$, and $t_0 = 0.30$, $t_0 = 0.10$, $t_0 = 0.05$, $t_0 = 0.03$ for $T = 0.15$, respectively. We determine the critical temperature T_c by the condition $t_0 = 0.01$. Here, the condition $t_0 = 0$ corresponds to the Thouless criterion, and the parameter t_0 represents the distance to the superconducting critical point.

At the last of this section, we show the obtained phase diagram in Fig. 3.16. We show the mean field critical temperature T_c^{MF} and the critical temperature T_c reduced by the fluctuations. The critical temperature is remarkably reduced by the fluctuations. This effect is mainly caused by the suppression of the DOS. As the coupling constant increases, the reduction of the critical temperature becomes remarkable. It should be noticed that this effect is different from that of the Nozières and Schmitt-Rink theory. According to the NSR theory, the critical temperature is reduced by the shift of the chemical potential. The chemical potential shifts so as to decrease the density of state. In our formalism, the DOS is reduced by the effects of the resonance scattering arising from the superconducting fluctuations.

Roughly speaking, the pseudo-gap phenomena occurs in the region between T_c^{MF} and T_c. This

region is extremely wide in the strong coupling case. The DOS starts to decrease, near $T = T_c^{MF}$. Most of the physical quantities measured by the various experiments, such as NMR [30, 31, 32, 33, 34, 35, 36], optical conductivity, [46, 47, 48] tunneling spectroscopy [49, 50], specific heat [51, 52] and so on, reflect the density of state. Therefore, their experiments are expected to show some changes near T_c^{MF}. Actually, various changes around T_c^{MF} are reported by various experiments [54].

Moreover, the ARPES experiments directly reflect the spectral weight. Our calculation shows the plural peak structure of the spectral weight. However, since the spectral weight is extremely broad when the plural peak structure appears, such a structure may not be observed actually. Moreover, by summing up the momentum around the measured momentum, corresponding to the experimental resolving power, the plural peak structure may disappear. The reduction of the spectral weight at the Fermi energy $\omega = 0$ is essential. In this sense, our calculation is consistent with the ARPES experiments.

3.1.4 Discussions

In this section, we have calculated the effects of the strong coupling superconductivity on the normal state electronic structure. We have considered that the strong coupling superconductivity takes place in under-doped High-T_c cuprates and the pseudogap phenomena are its precursor.

Considering that the band width ε_F is renormalized by the electron-electron correlation, the ratio T_c^{MF}/ε_F is increased by the renormalization. As the doping quantity decreases, the system approaches to the Mott insulator. Therefore, it is natural to consider that the renormalization effects are enhanced with decreasing doping concentration. Since the anti-ferromagnetic spin fluctuations are enhanced at the same time, the attractive interaction becomes strong in the under-doped region. Therefore, the superconductivity effectively becomes strong coupling with decreasing doping concentration. It should be noticed that the superconducting coupling is represented by the ratio T_c^{MF}/ε_F, and not by the critical temperature T_c which is suppressed by the fluctuations. Because of the renormalization of the effective Fermi energy ε_F and the enhanced fluctuations, the superconducting coupling becomes strong with under-doping in spite of the reduced T_c. Thus, our theory appropriately explains the pseudogap phenomena in High-T_c cuprates including their doping dependence.

It should be noticed that both T_c and T_c^{MF} are scaled by the band width ε_F. By considering these facts, it is naturally understood that critical temperature T_c decreases with the doping concentration, although T^* doesn't. Since T_c/ε_F is almost independent of the coupling constant $|g|$ in the strong coupling region, T_c decreases with ε_F in the under-doped region. On the other hand, T_c^{MF}/ε_F increases with $|g|$. Therefore, T_c^{MF} increases with the attractive interaction $|g|$ in spite the decrease of the effective band width ε_F in the under-doped region.

Here, we mention the important condition for the pseudogap phenomena derived from the superconducting fluctuations. Of course, the strong coupling superconductivity is most essential. The coupling constant g does not appear in the formulation explicitly. However, it is included in the properties of the TDGL parameters. In particular, the essential factor is that b and a_2 are reduced in the strong coupling superconductivity. There are two factors to make the superconducting coupling strong. One is the strong electron correlation which renormalize the energy scale of the quasi-particles. The other is the high critical temperature which is expected in the non electron-phonon mechanism.

In addition to that, there are some important factors for the pseudogap. The high density is one of them because the NSR theory dominates the resonance scattering in the low density case.

High-T_c cuprates are high density because they are near the half-filling in the lattice system. The particle-hole asymmetry is also important to stabilize the self-consistent solution.

The quasi-two dimensionality plays an essential role because it leads to the strong fluctuations which are characteristics of the low-dimensional systems. Such strong fluctuations are not expected in the isotropic three dimensional systems. The importance of the two dimensionality is shown by the calculation in the following way. Jujo *et al* have applied the T-matrix approximation to the model with an inter-layer hopping t_z (Fig. 3.17). The results have shown that the anomalous features of the self-energy disappear in the three-dimensional systems and the typical behavior in the Fermi liquid theory is revived.

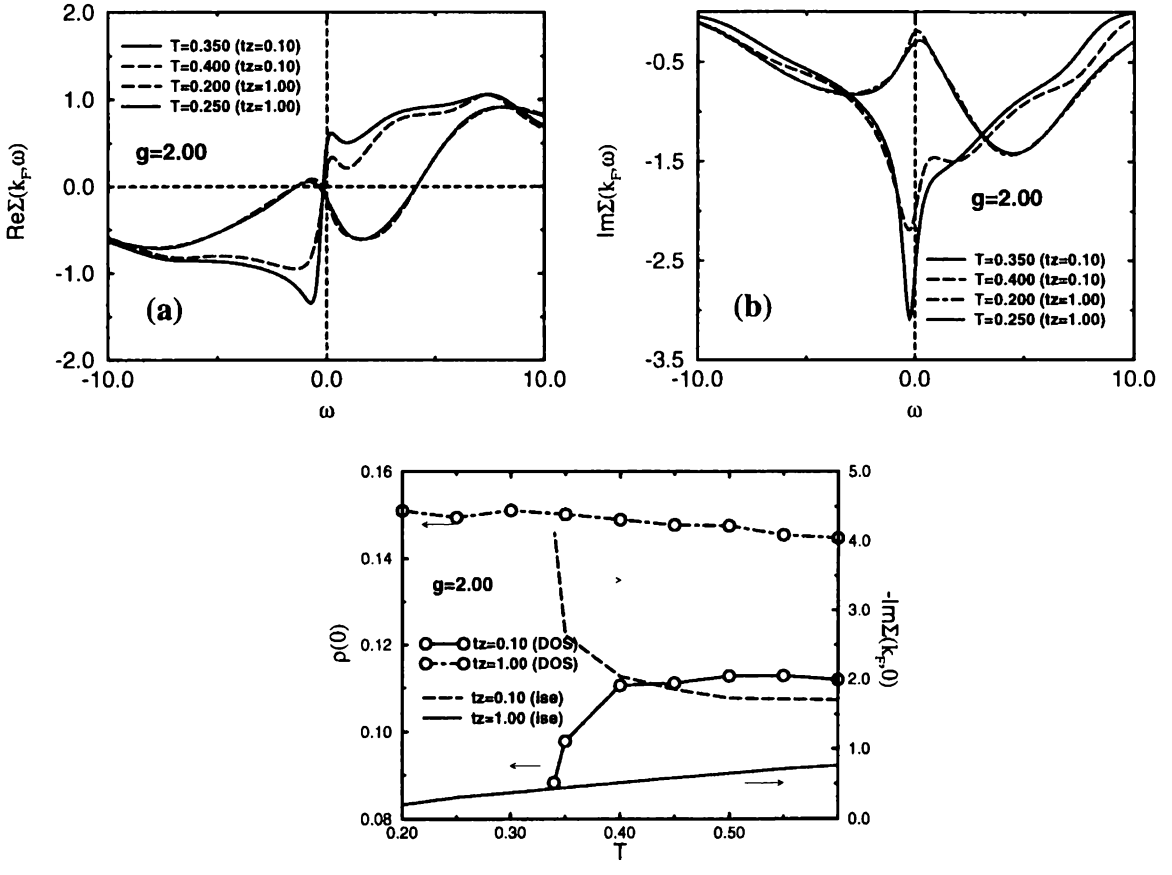

Figure 3.17: (a) The real part and (b) The imaginary part of the self-energy. Here, the inter-layer hopping t_z is chosen as $t_z/t = 0.10$ or $t_z/t = 1.0$. (c) The temperature dependence of the density of state $\rho(0)$ and the damping rate $-\mathrm{Im}\Sigma^{\mathrm{R}}(\boldsymbol{k},\omega)$ at the Fermi level. The results are cited from Ref.105.

These factors properly reflect the characteristics of High-T_c cuprates. Thus, the realistic treatment carried out in this thesis is necessary for the pseudogap phenomena. In other words, the pseudogap phenomena well represent the characteristics of High-T_c cuprates.

It is notable that the organic superconductor κ-(BEDT-TTF) compounds also satisfies the above conditions. The compounds are quasi-two dimensional systems and have relatively high critical temperature near the Mott transition [104]. The pseudogap phenomena are observed also in these compounds, although the experimental evidences are not sufficient. The possibility of the pseudogap phenomena arising from the superconducting fluctuations has been pointed out for

these compounds [105].

3.1.5 Observability of the Superconducting Fluctuations

In the recent letter [106], Jankó *et al.* have proposed an experiment as a direct probe into the superconducting fluctuations. The measurement of the incoherent pair tunneling directly gives the imaginary part of the pair susceptibility (T-matrix) in the normal state. The conductance due to the incoherent pair tunneling has been calculated a long time ago [107]. Jankó *et al.* have shown that the measurement is possible by using the appropriate tunneling junction involving the under-doped cuprates, the insulator and the optimally-doped cuprates. We consider that this will be an important measurement, if it is experimentally achieved. Not only the incoherent pair tunneling is an direct evidence of the paring scenarios but also it specifies the correct scenarios from them.

In this section, we have argued the importance of the strong thermal superconducting fluctuations, which necessarily arise as a result of the strong coupling superconductivity and the quasi-two dimensionality of High-T_c cuprates. In this case, the superconducting fluctuations show the particle-hole asymmetric structure near the critical point $T = T_c$.

The I-V characteristic of the pair tunneling measurements give us the direct information for the pair susceptibility. The contribution from the pair tunneling on the conductance is expressed as,

$$I(V) \propto \mathrm{Im}t(\mathbf{0}, 2eV). \tag{3.26}$$

Thus, the I-V characteristic is proportional to the imaginary part of the T-matrix.

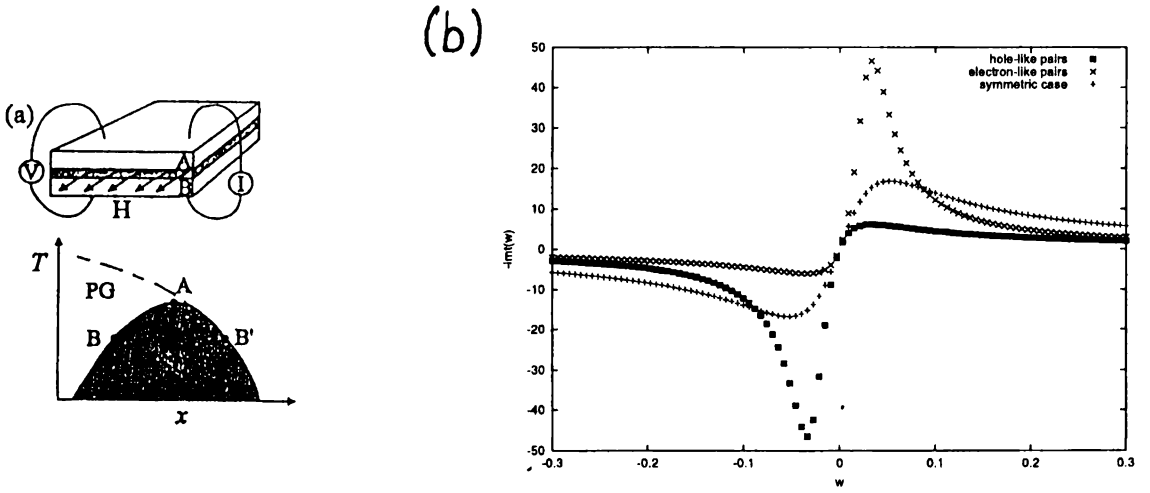

Figure 3.18: (a) The schematic figure of the pair tunneling experiments (b) The imaginary part of the pair susceptibility which is proportional to the tunneling current $I(V)$. The closed squares show the hole-like case obtained by our results. The times ($\times$) show the electron-like case proposed by Jankó *et al.* [88]. The pluses (+) shows the particle-hole symmetric case which corresponds to the conventional weak coupling theory.

The reciprocal of the T-matrix is described in a TDGL expansion form as $gt^{-1}(\boldsymbol{q}, \Omega) = t_0 + b\boldsymbol{q}^2 - (a_1 + ia_2)\Omega$. The real part a_1 is is usually neglected in the conventional weak coupling theory. However, in the strong coupling case, a_1 is the same order as a_2 and plays an important role. The parameter a_1 induces the asymmetry of the pair susceptibility. Since Jankó *et al.* consider the

electron gas model, the superconducting fluctuations have the electron-like character ($a_1 > 0$) [88]. However, the superconducting fluctuations should have the hole-like character ($a_1 < 0$) in High-T_c cuprates as is shown by our explicit calculation taking account of the realistic band structure (see §3.1.1). The sign of a_1 is determined by the asymmetry of the band structure. For High-T_c cuprates, there is a large contribution to a_1 from the vicinity of the Van Hove singularity. This contribution is not so influenced by the pseudogap and leads to the hole-like character of the superconducting fluctuations. As a result, the imaginary part of the pair susceptibility should behave as the closed squares in Fig. 3.18(b). The tunneling current has the large absolute value under the negative bias. This asymmetry is opposite to that proposed by Jankó *et al.* [88].

Generally speaking, this experiment is difficult because the quasi-particles contribute to the tunneling current more remarkably. Therefore, somewhat ingenious method by which the pair tunneling process is drawn is desirable. We consider that the asymmetric structure of the pair tunneling current will be a strong evidence for the pairing scenario based on the strong coupling superconductivity.

3.2 Pseudogap Phenomena in the Magnetic Field [25]

3.2.1 Introduction

Recently, the magnetic field effects on the NMR spin-lattice relaxation rate $1/T_1$ have been measured and discussed by several groups to determine the correct scenarios for the pseudogap phenomena [108, 109, 110]. The experimental results are interpreted as follows. The magnetic field effects cannot be observed in under-doped cuprates in which the strong pseudogap phenomena occurs in the wide temperature region [108, 109]. In particular, the onset temperature T^* does not vary. On the other hand, the magnetic field effects are visible near the optimally-doped region in which only the weak pseudogap phenomena are observed in the narrow temperature region [110].

In this section, we point out that the magnetic field effects are naturally and continuously understood from under-doped to over-doped cuprates on the basis of our resonance scattering scenario. In particular, there is an interpretation that regards the experimental results for under-doped systems as a negative evidence for the pairing scenario [108]. It is generally considered that the superconducting fluctuations are remarkably influenced by the magnetic field, while the effects of the magnetic field on the spin-fluctuations are considered to be small. Therefore, the experimental results have been interpreted as an evidence for the magnetic scenario for the pseudogap. Our results conclude that this interpretation is inappropriate. The misinterpretation is caused by the loss of the understanding for the strong coupling superconductivity. Therefore, we give an explanation for the magnetic field effects on the pseudogap phenomena on the basis of the strong coupling superconductivity. Actually, the experimental results including their doping dependence rather support our scenario for the pseudogap phenomena.

This section is constructed as follows. In §3.2.2, we explain the theoretical framework in order to calculate the pseudogap in the magnetic field. In §3.2.3, we explicitly calculate the single particle self-energy $\Sigma^{\mathrm{R}}(\boldsymbol{k},\omega)$, DOS $\rho(\varepsilon)$, NMR spin-lattice relaxation rate $1/T_1T$ and their magnetic field dependences. In §3.2.4, we give an comprehensive understanding of the phase diagram in High-T_c cuprates. It is shown that the doping dependence of the magnetic field effects well support our scenario.

3.2.2 Theoretical Framework on the magnetic field effects

In this section, we use the same model and the formulation as in §3.1. Here, we consider the magnetic field applied along the c-axis, $B \parallel \vec{c}$. The main effect of the magnetic fields is the Landau level quantization for the superconducting fluctuations. It corresponds to the quantization of the orbital motion of the fluctuating Cooper pairs. The quantization is expressed by the replacement of the quadratic term of the momentum as $\boldsymbol{q}^2 \Rightarrow 4eB(n+\frac{1}{2})$ [97].

The Landau quantization has the following two important effects. One is the Landau degeneracy which generally enhances the fluctuations. The Landau degeneracy reduces the effective dimension of the fluctuations. The other is the suppression of the superconductivity. The pseudogap is suppressed by this effect, since the distance to the critical point increases as $t_0 \Rightarrow t_0 + 2beB$, The parameter corresponds to the energy level of the Lowest Landau level. When considering at the fixed temperature, the dominant effect is the latter. We can see that the characteristic magnetic field $B_{\rm ch}$ for the pseudogap phenomena is scaled by the quantity t_0/b, that is $B_{\rm ch} \propto t_0/b$. The ratio b/t_0 corresponds to the square of the GL correlation length $\xi_{\rm GL}$ for the superconducting fluctuations, that is, $b/t_0 = \xi_{\rm GL}^2$. The magnetic field effects are scaled by the quantity $B\xi_{\rm GL}^2$. Thus, the superconducting fluctuations and the pseudogap are affected by the magnetic field according to the magnetic flux penetrating the correlated area $\xi_{\rm GL}^2$.

As we mentioned above, the parameter b is small in case of the strong coupling superconductivity. Moreover, the fact that the pseudogap phenomena take place in the wide temperature region means that the parameter t_0 is large near the pseudogap onset temperature T^*. As a result, the characteristic magnetic field $B_{\rm ch}$ is remarkably large, especially near T^*. In other words, the magnetic field effects are remarkably small in case of the strong coupling superconductivity. Especially, the onset temperature T^* does not vary. On the other hand, the magnetic field effects are sure to appear near $T_{\rm c}$ since the correlation length $\xi_{\rm GL}$ diverges at the critical temperature $T_{\rm c}$. However, the region in which the effects appear is remarkably small.

In the relatively weak coupling case, the magnetic field dependence is large and the onset temperature T^* may be reduced. These features well explain the results of the high field NMR measurements including their doping dependence. [108, 109, 110]

Here, we have neglected the Zeeman coupling term. Although the Zeeman coupling term plays an important role at the low temperature in superconducting state [111]. it has only higher order correction in the fluctuating regime. This fact can be simply understood as follows. The lowest order correction of the Zeeman coupling term on the superconducting fluctuations is the second order and described as $4eB(n+\frac{1}{2}) \Rightarrow 4eB(n+\frac{1}{2}) + \frac{8}{v^2}(\mu B)^2$. Here, v is a mean value of the quasi-particle velocity on the Fermi surface. $\mu = g\mu_{\rm B}/2$ is the magnetic moment of the electrons. Here, g is the g-value and $\mu_{\rm B}$ is the Bohr magneton. Thus, the Zeeman coupling term slightly weaken the superconducting fluctuations. However, it has only higher order effect with respect to the magnetic field compared with the Landau quantization. Therefore, the effect of the Zeeman coupling term is extraordinary small in the weak coupling limit since the typical magnetic field is small. Also in High-$T_{\rm c}$ cuprates, it is higher order and remarkably small compared with the effect of the Landau quantization in the magnetic field of the experimentally relevant order. Actually, the magnetic field adopted in this thesis is the order of $eB \sim 10^{-2}$ in our unit. That corresponds to $B \sim 10$Tesla. In this case, the effect of the Zeeman coupling term is higher order than that of Landau quantization of the order 10^{-2}. Thus, the justification to neglect the Zeeman coupling term is obtained. Of course, we cannot neglect the Zeeman coupling term under the extraordinary high magnetic field in the strong coupling limit. However, such an extreme situation is not realistic.

When the magnetic field is applied perpendicular to the c-axis $B \perp \vec{c}$, effects of the Zeeman

coupling term is relatively important because the coherence length along the c-axis ξ_c is small. Therefore, the effects arising from the Landau quantization and those from the Zeeman coupling can be separated by changing the direction of the magnetic field.

3.2.3 Magnetic Field Dependence of the NMR $1/T_1T$

In this section, we actually calculate the NMR spin-lattice relaxation rate $1/T_1T$ under the magnetic field with the recent high field NMR measurements in mind. We calculate $1/T_1T$ by using the general expression,

$$1/T_1T = \sum_{\boldsymbol{q}} |A(\boldsymbol{q})|^2 [\frac{1}{\omega} \mathrm{Im}\chi_s^{\mathrm{R}}(\boldsymbol{q},\omega) \mid_{\omega\to 0}]. \tag{3.27}$$

Here, we neglect the momentum dependence of the hyperfine coupling $A(\boldsymbol{q})$ for simplicity, which does not affect the magnetic field dependence of $1/T_1T$.

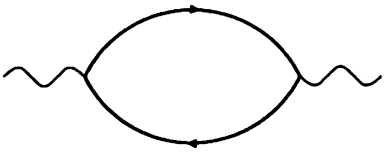

Figure 3.19: The diagram representing the dynamical spin susceptibility $\chi_s^{\mathrm{R}}(\boldsymbol{q},\omega)$

We calculate the spin susceptibility $\chi_s^{\mathrm{R}}(\boldsymbol{q},\omega)$ which corresponds to the two-body correlation function shown in Fig. 3.19. Here, the solid lines are the renormalized Green function $G^{\mathrm{R}}(\boldsymbol{k},\omega) = (\omega - \varepsilon_{\boldsymbol{k}} - \Sigma^{\mathrm{R}}(\boldsymbol{k},\omega))^{-1}$. The self-energy $\Sigma^{\mathrm{R}}(\boldsymbol{k},\omega)$ is calculated by using the T-matrix approximation as we described before. The effects of the superconducting fluctuations are included in the self-energy. In calculating the self-energy $\Sigma^{\mathrm{R}}(\boldsymbol{k},\omega)$, we linearize the dispersion relation as $\varepsilon_{\boldsymbol{k}-\boldsymbol{q}} = \varepsilon_{\boldsymbol{k}} - \boldsymbol{v}_{\boldsymbol{k}}\boldsymbol{q}$. This linearization is justified because the only small region around $\boldsymbol{q} = 0$ contributes to the self-energy. We replace the quadratic term as $\boldsymbol{q}^2 \Rightarrow 4eB(n + \frac{1}{2})$. This process corresponds to the Landau level quantization for the superconducting fluctuations.

From eq.(3.1), $1/T_1T$ is expressed as,

$$1/T_1T = -\sum_{\boldsymbol{k},\boldsymbol{q}} \int \frac{\mathrm{d}\omega}{\pi} f'(\omega) \mathrm{Im}G^{\mathrm{R}}(\boldsymbol{k},\omega) \mathrm{Im}G^{\mathrm{R}}(\boldsymbol{k}+\boldsymbol{q},\omega) \tag{3.28}$$

$$= \pi \int \mathrm{d}\omega (-f'(\omega)) \rho(\omega)^2. \tag{3.29}$$

Here, $f'(\omega)$ is the first derivative of the Fermi distribution function. This expression is reduced to the well-known expression $1/T_1T = \pi\rho(0)^2$ at $T = 0$. After all, we calculate the decrease of $1/T_1T$ by the suppression of the DOS.

Generally speaking, we can consider the Aslamazov-Larkin term (AL term) and the Maki-Thompson term (MT term) as corrections by the fluctuations on the two-body correlation function [71, 72]. However, the AL term dose not exist in calculating the spin susceptibility $\chi_s^{\mathrm{R}}(\boldsymbol{q},\omega)$. We can understand this fact by considering the spin index for the spin singlet pairing [97]. The contribution from the MT term is small in case of the d-wave pairing, and is suppressed by the slight elastic scattering [97]. Therefore, we have only to calculate the decrease of $1/T_1T$ by the pseudogap as the effect of the superconducting fluctuations.

Of course, we have to take account of the anti-ferromagnetic spin-fluctuations in order to describe the whole temperature dependence of $1/T_1T$. $1/T_1T$ increases owing to the anti-ferromagnetic spin fluctuations in the normal phase ($T > T^*$), and decreases owing to the superconducting fluctuations in the pseudogap phase ($T^* > T > T_c$). Generally speaking, the magnetic field is considered to have a remarkable effect on the superconducting fluctuations, while the effect on the spin-fluctuations is comparatively small. Because we pay attention to the magnetic field dependence in this thesis, we have only to calculate the decrease of $1/T_1T$ due to the superconducting fluctuations and its magnetic field dependence. Actually, the misinterpretation for the experimental results is caused by the loss of the understanding of the magnetic field effect on the superconducting fluctuations in case of the strong coupling superconductivity. Our calculation gives a clear understanding about the magnetic field dependence of the pseudogap phenomena.

Even if the effect of the exchange enhancement is taken into account, the results for the magnetic field effect do not change, qualitatively. At the last of this section, we actually calculate the effect of the exchange enhancement within the random phase approximation (RPA). Qualitatively the same results are obtained there.

The calculated results are shown in Figs. 3.20-23. In all figures, the magnetic field is varied as $4eB = 0.01, 0.02, 0.05$ and 0.1 in our unit. The horizontal axis is the temperature scaled by the zero-field critical temperature T_{c0}. All results can be understood by considering the characteristic magnetic field we have mentioned in the previous section,

$$B_{ch} \propto t_0/b = \xi_{GL}^{-2}. \tag{3.30}$$

The results for the relatively weak coupling case $g = -0.5$ are shown in Fig. 3.20. In this case, only the weak pseudogap is observed in the narrow temperature region. This case corresponds to the slightly over-doped or optimally-doped cuprates. The magnetic field dependence of $1/T_1T$ is clearly observed and T^* varies. This behavior is consistent with the NMR experiments in the slightly over-doped cuprates. [110]

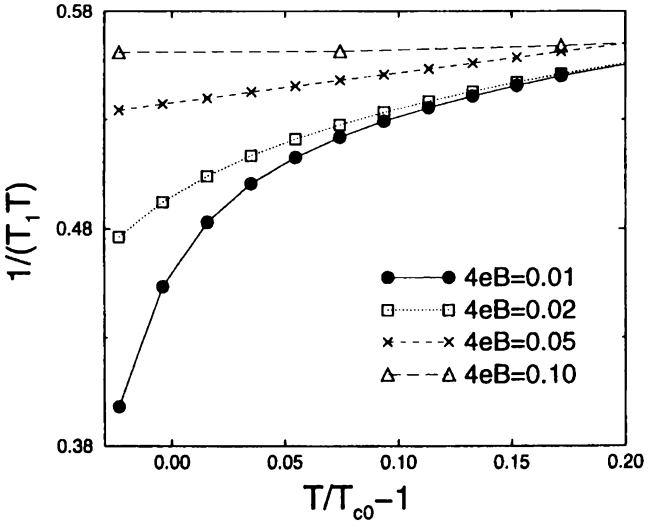

Figure 3.20: The calculated results for $1/T_1T$ under the various magnetic field $4eB = 0.01, 0.02, 0.05, 0.1$. The weak pseudogap case $g = -0.5$.

In case of $g = -0.8$, the magnetic field dependence is weak since the parameter b decreases (Fig.

3.21). In particular, $1/T_1T$ is almost independent of the magnetic field near the onset temperature T^* where the parameter t_0 is large. On the other hand, the magnetic field dependence can be observed in the vicinity of the critical temperature T_c, since the parameter t_0 is small there.

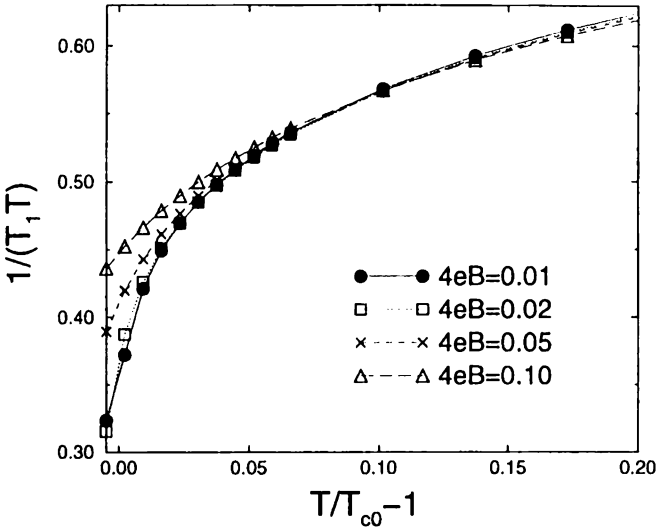

Figure 3.21: The calculated results for $1/T_1T$ under the magnetic field. The magnetic field is chosen as the same as that in Fig. 3.20. The relatively strong pseudogap case $g = -0.8$.

We can see the different magnetic field dependences of the density of states according to the distance to the critical point (Fig. 3.22). The magnetic field effect is visible just above T_c (Fig. 3.22(a)). The DOS near the Fermi energy are recovered with increasing the magnetic field. On the other hand, the effect is almost invisible when the temperature is apart form T_c (Fig. 3.22(b)).

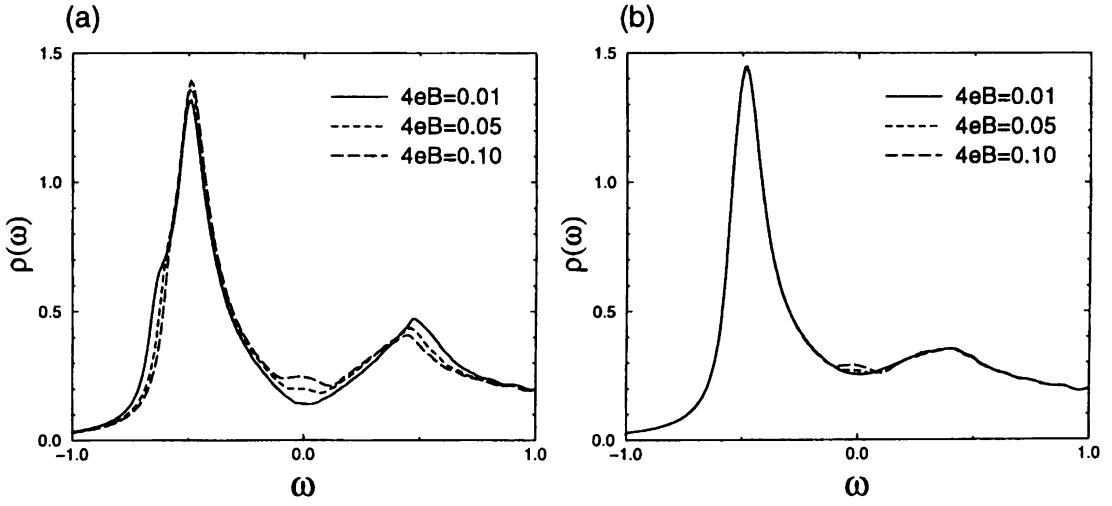

Figure 3.22: The magnetic field dependence of the DOS. Here, $g = -0.8$ and $T_{c0} = 0.1407$. The magnetic field is varied as $4eB = 0.01, 0.05, 0.1$. (a) in the vicinity of T_c, $T = 0.141$. (b) apart from T_c, $T = 0.15$.

The results for the considerably strong coupling case $g = -1.0$ is shown in Fig. 3.23. In this

case, the strong pseudogap anomaly exists in the wide temperature region. The magnetic field effects become still weaker. The magnetic field dependence is narrowly observed in the vicinity of T_c. We consider that these strong coupling cases correspond to the under-doped cuprates. This

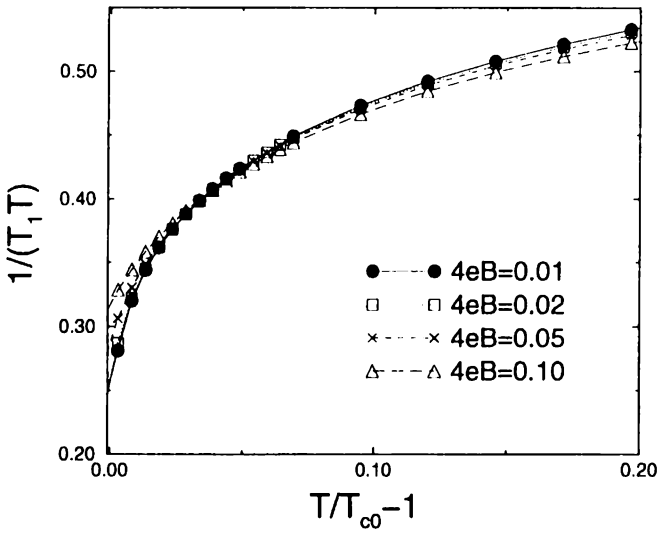

Figure 3.23: The calculated results for $1/T_1T$ under the magnetic field. The magnetic field is chosen as the same as that in Fig. 3.20. The strong pseudogap case $g = -1.0$.

behavior well explain the experimental results in the under-doped cuprates [108, 109]. The weak effect in the vicinity of T_c is also observed in the experimental results [108]. Thus, the interpretation of the experimental results as a negative evidence for the pairing scenario is inappropriate.

It should be noticed that the strength of the superconducting coupling is indicated by the ratio T_c^{MF}/ε_F. The ratio increases due to the mass renormalization arising from the electron-electron correlation. It should be considered that the mass renormalization is enhanced with decreasing the doping concentration. The attractive interaction becomes strong at the same time, since the anti-ferromagnetic spin fluctuations are enhanced. Therefore, it is naturally expected that the superconductivity becomes the strong coupling as the doping concentration decreases. Thus, the strength of the superconducting coupling changes with the doping in accordance with our expectation. It should be noticed that the change of the magnetic field effects is continuous from weak to strong coupling. In other words, the calculated results explain the NMR measurements continuously and entirely from over-doped cuprates to under-doped ones. Therefore, the recent high field NMR measurements including their doping dependence are regarded as an affirmative evidence for the pairing scenario.

In order to confirm the effect of the Landau degeneracy to enhance the fluctuations, we show the Fig. 3.24. In Fig. 3.24, the horizontal axis is scaled by the critical temperature under the magnetic field T_{cH}. By keeping the distance to the critical point, we can remove the effect of the suppression of the superconductivity. Therefore, we can see the effect of the Landau degeneracy which reduces the effective dimension.

The results show that $1/T_1T$ decreases with increasing the magnetic field. It is because of the Landau degeneracy. The Landau degeneracy enhances the superconducting fluctuations and make the pseudogap stronger. Then, $1/T_1T$ is still more reduced. Therefore, even in the rather weak pseudogap case, the pseudogap may be observed clearly under the high magnetic field. In other words, the magnetic field makes the pseudogap visible in more over-doped cuprates. These features

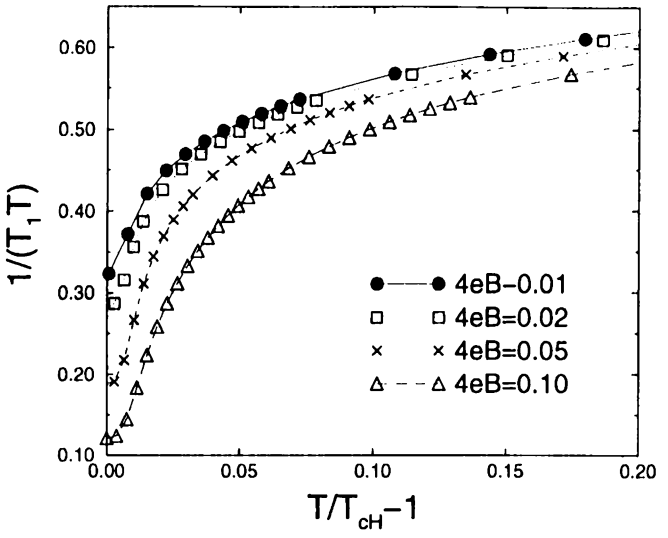

Figure 3.24: The results for $1/T_1T$ in which the temperature is scaled by the critical temperature under the magnetic field T_{cH}. The magnetic field is chosen as the same as that in Fig. 3.24. Here, $g = -0.8$.

are actually observed in the experimental data [110]. The enhancement of the fluctuations by the magnetic field affects the actual critical temperature T_c. The critical temperature is reduced by the fluctuations even under the zero magnetic field. It is expected that the enhanced fluctuations reduces the critical temperature still more. Therefore, the magnetic field dependence of the critical temperature is more drastic than that expected by the mean field theory. We consider that the difference between T_c and T^* about its magnetic field dependence are explained by the discussion. The actual calculation is necessary for the detailed explanation.

At the last of this section, we consider the effect of the exchange enhancement. The exchange enhancement is taken into account within the random phase approximation (RPA). The basic results about the magnetic field effects are not changed. However, it is definitely shown that the peak of $1/T_1T$ ($T = T^*$) does not change in the strong coupling case, while the peak changes in the weak coupling case. The dynamical spin susceptibility $\chi_{\rm RPA}(\boldsymbol{k},\omega)$ calculated by the RPA is expressed as follows.

$$\chi^{\rm R}_{\rm RPA}(\boldsymbol{q},\omega) = \frac{\chi^{\rm R}_0(\boldsymbol{q},\omega)}{1 - U\chi^{\rm R}_0(\boldsymbol{q},\omega)}, \tag{3.31}$$

$$\chi_0(\boldsymbol{q},\mathrm{i}\omega_n) = -T\sum_{\boldsymbol{k},\omega_m} G(\boldsymbol{k},\mathrm{i}\omega_m)G(\boldsymbol{k}+\boldsymbol{q},\mathrm{i}\Omega_m+\mathrm{i}\omega_n). \tag{3.32}$$

We fix the enhancement parameter $U = 1.5$ afterward. The relaxation rate $1/T_1T$ is calculated by eq.(3.1). Here, we take into account the momentum dependence of the hyperfine coupling $|A(\boldsymbol{q})|^2 = \frac{1}{2}[\{A_1+2B(\cos(q_x)+\cos(q_y))\}^2+\{A_2+2B(\cos(q_x)+\cos(q_y))\}^2]$. The hyperfine coupling constants A_1, A_2 and B is evaluated as $A_1 = 0.84B$ and $A_2 = -4B$ [112]. The following results are not affected by the choice of the parameters, qualitatively.

The calculated results are shown in Figs. 3.25 and 3.26. In the high temperature region, $1/T_1T$ is enhanced owing to the exchange enhancement. Near the critical temperature, $1/T_1T$ is reduced owing to the superconducting fluctuations. As a result, $1/T_1T$ shows its peak at $T = T^*$ above T_c. It is a well-known pseudogap phenomenon in the NMR measurements.

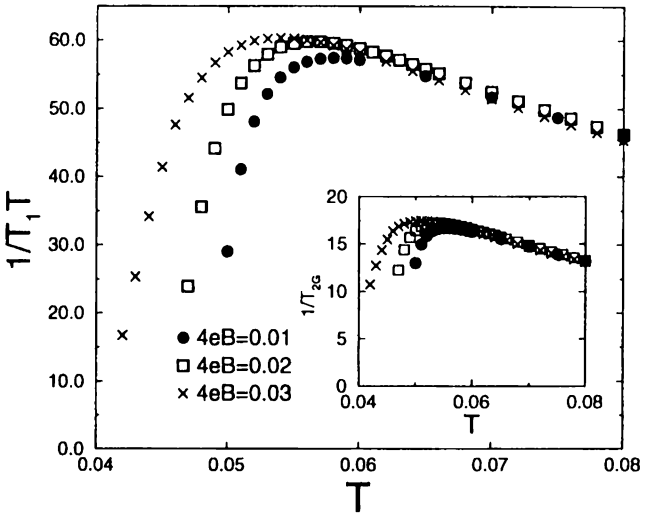

Figure 3.25: The results for $1/T_1T$ including the effects of the exchange enhancement. The weak pseudogap case $g = -0.5$. The magnetic field is varied as $4eB = 0.01, 0.02$, and 0.03 in our unit. The inset shows the results for the spin echo decay rate $1/T_{2G}$.

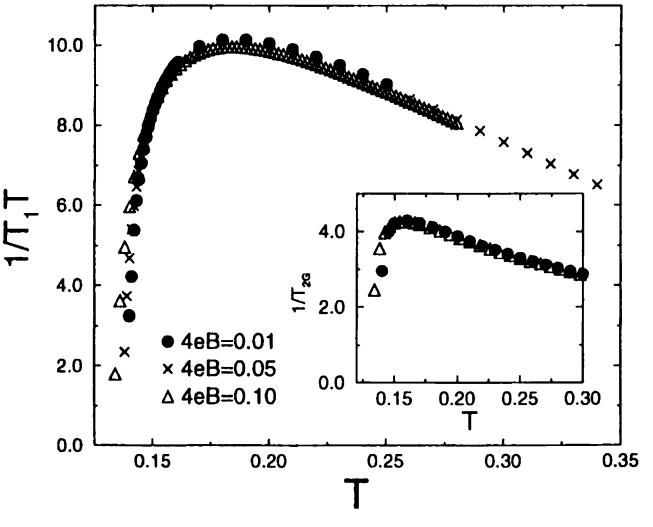

Figure 3.26: The results for $1/T_1T$ including the effects of the exchange enhancement. The relatively strong pseudogap case $g = -0.8$. The magnetic field is varied as $4eB = 0.01, 0.05$, and 0.1 in our unit. The inset shows the results for $1/T_{2G}$.

In the weak coupling case $g = -0.5$ (Fig. 3.25), the effect of the magnetic field is clearly observed. The onset temperature T^* is lowered by the magnetic field. On the other hand, in the relatively strong coupling case $g = -0.8$ (Fig. 3.26), the effect of the magnetic filed is remarkably small. In particular, the onset temperature T^* is not changed by the magnetic field. In this case, $1/T_1T$ shows the magnetic filed dependence only in the vicinity of the critical temperature T_c. Needless to say, these features are the same as those derived by the calculation without the exchange enhancement.

The results for the spin-echo decay rate $1/T_{2G}$ are shown in the inset of Figs. 3.25 and 3.26. $1/T_{2G}$ is calculated by the following expression.

$$1/T_{2G}^2 = \sum_{\boldsymbol{q}} [|A_{\parallel}(\boldsymbol{q})|^2 \mathrm{Re}\chi_s^{\mathrm{R}}(\boldsymbol{q},0)]^2 - [\sum_{\boldsymbol{q}} |A_{\parallel}(\boldsymbol{q})|^2 \mathrm{Re}\chi_s^{\mathrm{R}}(\boldsymbol{q},0)]^2. \tag{3.33}$$

Here, the dynamical spin susceptibility is calculated by RPA, and the hyperfine coupling is expressed as $|A_{\parallel}(\boldsymbol{q})|^2 = \{A_2 + 2B(\cos(q_x) + \cos(q_y))\}^2$ [112]. The spin echo decay rate $1/T_{2G}$ also shows the pseudogap phenomena. However, the effect of the pseudogap on $1/T_{2G}$ is weaker than that on $1/T_1T$. The pseudogap appears in the narrower temperature region. $1/T_{2G}$ shows its peak below the pseudogap onset temperature T^* in $1/T_1T$. These results are consistent with the experimental results [35].

These results indicate that the effects of the pseudogap are weak on the real part of the spin susceptibility rather than on the imaginary part at the low frequency. The dissipation (imaginary part) directly reflects the density of state near the Fermi level. However, the static properties (real part) do not necessarily so. In other wards, the pseudogap suppresses the weight of the spin fluctuations at low frequency. However, the effect on the total weight is rather small. In particular, the d-wave pseudogap only weakly affects the real part near the anti-ferromagnetic wave vector $\boldsymbol{q} = (\pi, \pi)$. The momentum dependence of the hyperfine coupling $A_{\parallel}(\boldsymbol{q})$ reduces the effect of the pseudogap on $1/T_{2G}$ still more. The above features are in common with the superconducting state [113]. That is natural because the pseudogap and the superconducting gap have the same $d_{x^2-y^2}$-wave form and the same energy scale. The magnetic field dependence of $1/T_{2G}$ has the same features as those of $1/T_1T$.

3.2.4 Discussions

In this section, we have shown that the pairing scenario based on the strong coupling superconductivity well explains the effects of the magnetic field on the pseudogap phenomena in High-T_c cuprates. There is an interpretation that the magnetic field independence of the pseudogap phenomena in under-doped cuprates is an evidence denying the pairing scenarios for the pseudogap [108]. However, the pairing scenario based on the resonance scattering well explains the experiments.

By considering that the effective Fermi energy ε_F decreases and the attractive interaction increases with decreasing the doping concentration, the calculated results well explain the high field NMR measurements including their doping dependence and the temperature dependence. The comprehensive understanding from over-doped to under-doped cuprates is obtained. Moreover, the continuous understanding in the phase diagram rather support the pairing scenario. In the pseudogap phase, the self-energy correction due to the superconducting fluctuations is a common mechanism in reducing the DOS and $1/T_1T$. Because the pseudogap phenomena continuously take place from slightly over-doped to under-doped cuprates, their magnetic field dependences should be continuously understood. The pseudogap becomes strong as the doping concentration

decreases. The magnetic field dependence of the weak pseudogap case can be understood within the conventional weak coupling theory for the superconducting fluctuations [97, 110]. Our theory is an extension of the theory. This fact indicates the correctness of our description for the pseudogap phenomena in under-doped cuprates on the basis of the strong coupling superconductivity.

On the other hand, it is not clear whether the magnetic origin may be consistent with the magnetic field dependence, especially in the weak pseudogap case. It is because the magnetic exchange coupling J is the order of $J \sim 1000$K and the applied magnetic field is the order of $\mu_B B \sim 10$K.

Here, we give a brief discussion on the self-consistent calculation. In the self-consistent calculation the pseudogap is described in a similar way. The fundamental picture does not change also in the self-consistent calculation, although the renormalization effects on the TDGL parameters exist. As we have described before, the self-consistent T-matrix calculation is a method treating the critical fluctuations. The criticality makes the magnetic field dependence still smaller. To put it in detail, in the self-consistent calculation the parameter t_0 depends on the magnetic field. As the magnetic field suppresses the pseudogap, $t_0(B)$ is reduced. Therefore, the distance to the superconductivity $t_0(B) + 2beB$ varies more slowly than $t_0(0) + 2beB$. Thus, the magnetic field dependence is reduced in the critical fluctuation regime. Anyway, the strong coupling superconductivity is the essential factor for the magnetic field independence, as we have described in this section. The existence of the wide critical region is a result of the strong coupling superconductivity.

The more systematic measurements of the magnetic field dependences in the various doping concentration will be an important verification to determine the origin of the pseudogap phenomena in High-T_c cuprates.

3.3 Superconducting Phase Transition from the Pseudogap State [26, 27]

3.3.1 Introduction

The direct measurements of the electronic spectrum, such as ARPES [22, 23] and tunneling spectroscopy[49] have indicated the similarity between the pseudogap and the superconducting gap. In particular, the same energy scale and the same momentum dependence between the two gaps have been indicated. Thus, the electronic structure changes continuously from the pseudogap state to the superconducting state. This important observations have strongly suggested that the pseudogap is a precursor of the superconductivity. The same energy scale of the two gaps are self-evident in the NSR theory because the energy scale is the binding energy of the pre-formed bosons. However, it is not so self-evident in our scenario and should be confirmed by the calculations. Furthermore, the similarity and the difference between the pseudogap state and the superconducting state have been reported from the various experiments. The comprehensive explanation for the characteristic properties of the phase transition is desired.

In this section, we extend the self-consistent T-matrix calculation to the superconducting state. Our main purpose in this section is to understand the superconducting transition from the pseudogap state. The close relation indicated by the spectroscopic experiments are confirmed by our calculation.

In this section, we do not use the TDGL expansion because it is not justified in the ordered state. The main results obtained in §3.1 are confirmed by the calculation in this section. Moreover,

the characteristic properties in the ordered state, such as the order parameter Δ and the single particle spectral weight are given by the self-consistent T-matrix calculation extended to the superconducting state.

3.3.2 Theoretical Framework

In this subsection, we describe the theoretical framework in this section. Hereafter, we adopt the unit $\hbar = c = k_B = 1$. In this section, we use the same model and the formulation as in §3.1. The calculation is based on the self-consistent T-matrix calculation. The Green function G is expressed as $G(\boldsymbol{k}, i\Omega_n) = (\omega - \varepsilon_{\boldsymbol{k}} - \Sigma(\boldsymbol{k}, i\Omega_n))^{-1}$. The self-energy Σ is given by the self-consistent T-matrix calculation, (Fig. 3.3(b))

$$\Sigma(\boldsymbol{k}, i\omega_m) = T \sum_{\boldsymbol{q}, i\Omega_n} t(\boldsymbol{q}, i\Omega_m) G(\boldsymbol{q} - \boldsymbol{k}, i\Omega_n - i\omega_m) \varphi^2_{\boldsymbol{k}-\boldsymbol{q}/2}. \tag{3.34}$$

In §3.1 and §3.2, we have expanded the reciprocal of the T-matrix $t^{-1}(\boldsymbol{q}, \Omega)$ around $\boldsymbol{q} = \Omega = 0$. This expansion corresponds to the time-dependent-Ginzburg-Landau (TDGL) expansion,

$$T(\boldsymbol{q}, \omega) = \frac{g}{t_0 + b\boldsymbol{q}^2 - (a_1 + ia_2)\Omega}. \tag{3.35}$$

The detailed properties of the TDGL parameters are discussed in §3.1.1. In this section, we do not use the TDGL expansion with reference to the Landau singularity in the ordered state [114]. We explicitly calculate the T-matrix around $\boldsymbol{q} = \Omega = 0$. The obtained results confirm the above behavior of the T-matrix including the renormalization effects. The pseudogap state is obtained similarly. We restrict the integrated area for $\boldsymbol{q}$ and Ω, as is done in §3.1. Namely, the meaningful region as a superconducting fluctuation is picked up. There is no qualitative difference by the details of the calculation.

Here, we extend the self-consistent T-matrix calculation to the superconducting state. The T-matrix is described as the following 2×2 matrix in the superconducting state. (Fig. 3.27(a))

$$\boldsymbol{T}(\boldsymbol{q}, i\Omega_n) = [g^{-1}\mathbf{1} + \boldsymbol{\chi}_{p0}(\boldsymbol{q}, i\Omega_n)]^{-1}, \tag{3.36}$$

$$\boldsymbol{\chi}_{p0}(\boldsymbol{q}, i\Omega_n) = \begin{pmatrix} K(\boldsymbol{q}, i\Omega_n) & L(\boldsymbol{q}, i\Omega_n) \\ L^*(\boldsymbol{q}, i\Omega_n) & K(-\boldsymbol{q}, -i\Omega_n) \end{pmatrix}, \tag{3.37}$$

where,

$$K(\boldsymbol{q}, i\Omega_n) = T \sum_{\boldsymbol{k}', \omega_m} G(\boldsymbol{k}', i\omega_m) G(\boldsymbol{q} - \boldsymbol{k}', i\Omega_n - i\omega_m) \varphi^2_{\boldsymbol{k}'-\boldsymbol{q}/2}, \tag{3.38}$$

$$L(\boldsymbol{q}, i\Omega_n) = -T \sum_{\boldsymbol{k}', \omega_m} F(\boldsymbol{k}', i\omega_m) F(\boldsymbol{q} - \boldsymbol{k}', i\Omega_n - i\omega_m) \varphi^2_{\boldsymbol{k}'-\boldsymbol{q}/2}, \tag{3.39}$$

and $\mathbf{1}$ is the unit matrix.

Here, $G(\boldsymbol{k}, i\omega_m)$ and $F(\boldsymbol{k}, i\omega_m)$ are normal and anomalous Green functions including the self-energy $\Sigma(\boldsymbol{k}, i\omega_m)$, respectively.

$$G(\boldsymbol{k}, i\omega_m) = \frac{i\omega_m + \varepsilon_{\boldsymbol{k}} + \Sigma(-\boldsymbol{k}, -i\omega_m)}{[i\omega_m - \varepsilon_{\boldsymbol{k}} - \Sigma(\boldsymbol{k}, i\omega_m)][i\omega_m + \varepsilon_{\boldsymbol{k}} + \Sigma(-\boldsymbol{k}, -i\omega_m)] - \Delta^2_{\boldsymbol{k}}}, \tag{3.40}$$

$$F(\boldsymbol{k}, i\omega_m) = \frac{-\Delta_{\boldsymbol{k}}}{[i\omega_m - \varepsilon_{\boldsymbol{k}} - \Sigma(\boldsymbol{k}, i\omega_m)][i\omega_m + \varepsilon_{\boldsymbol{k}} + \Sigma(-\boldsymbol{k}, -i\omega_m)] - \Delta^2_{\boldsymbol{k}}}. \tag{3.41}$$

The normal self-energy $\Sigma(\boldsymbol{k}, \mathrm{i}\omega_m)$ is given by the self-consistent T-matrix approximation (Fig. 3.27(b)).

$$\Sigma(\boldsymbol{k}, \mathrm{i}\omega_m) = T \sum_{\boldsymbol{q}, \mathrm{i}\Omega_n} T_{11}(\boldsymbol{q}, \mathrm{i}\Omega_m) G(\boldsymbol{q} - \boldsymbol{k}, \mathrm{i}\Omega_n - \mathrm{i}\omega_m) \varphi^2_{k-q/2}. \tag{3.42}$$

Here, the trivial Hartree-Fock term is excluded (Fig. 3.27(c)).

The d-wave order parameter $\Delta_{\boldsymbol{k}} = \Delta\varphi_{\boldsymbol{k}}$ is determined by the gap equation.

$$\Delta_{\boldsymbol{k}} = -gT \sum_{\boldsymbol{k}', \mathrm{i}\Omega_m} F(\boldsymbol{k}', \mathrm{i}\omega_m) \varphi_{\boldsymbol{k}'} \varphi_{\boldsymbol{k}}. \tag{3.43}$$

The effects of the fluctuations on the gap equation are included in the normal self-energy in the anomalous Green function $F(\boldsymbol{k}, \mathrm{i}\omega_m)$.

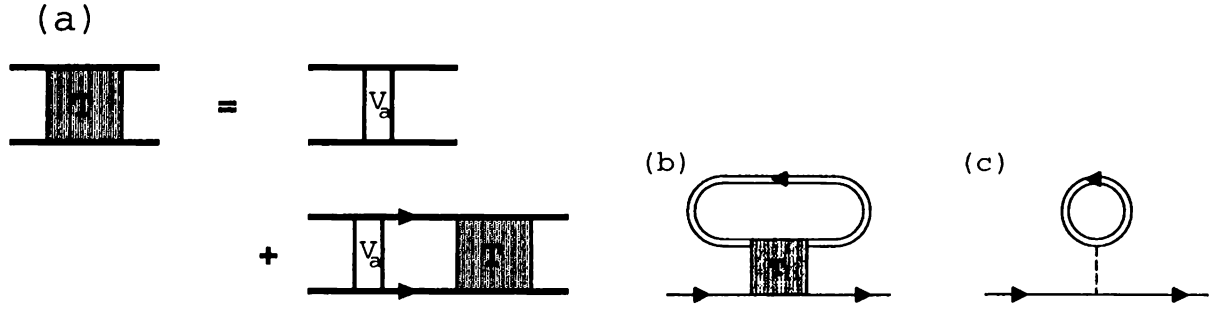

Figure 3.27: (a) The diagonal component of the T-matrix in the superconducting state. The double solid lines represent the normal and anomalous Green functions of the fermions. (b) The normal self-energy calculated by the self-consistent T-matrix approximation. (c) The Hartree-Fock term which we exclude.

The T-matrix corresponds to the propagator of the pair field $\eta(\boldsymbol{q}, \mathrm{i}\Omega_n) = \Delta(\boldsymbol{q}, \mathrm{i}\Omega_n) - \Delta$ [115]. By describing the pair field by the amplitude mode $\lambda(\boldsymbol{q}, \mathrm{i}\Omega_n)$ and the phase mode $\theta(\boldsymbol{q}, \mathrm{i}\Omega_n)$ as $\eta(\boldsymbol{q}, \mathrm{i}\Omega_n) = \lambda(\boldsymbol{q}, \mathrm{i}\Omega_n) + \mathrm{i}\theta(\boldsymbol{q}, \mathrm{i}\Omega_n)$, the effective Gaussian action for the pair field is expressed as,

$$S_2(\lambda, \theta) = \frac{1}{2} T \sum_{\boldsymbol{q}, \mathrm{i}\Omega_n} (\lambda^*, \theta^*) \begin{pmatrix} 1/|g| - K_+ - L & -\mathrm{i}K_- \\ \mathrm{i}K_- & 1/|g| - K_+ + L \end{pmatrix} \begin{pmatrix} \lambda \\ \theta \end{pmatrix}. \tag{3.44}$$

Here, $K_+ = (K(\boldsymbol{q}, \mathrm{i}\Omega_n) + K(-\boldsymbol{q}, -\mathrm{i}\Omega_n))/2$ and $K_- = (K(\boldsymbol{q}, \mathrm{i}\Omega_n) - K(-\boldsymbol{q}, -\mathrm{i}\Omega_n))/2$. We omitted the indices $\boldsymbol{q}$ and Ω_n. The condition $1/|g| - K(\boldsymbol{0}, 0) + L(\boldsymbol{0}, 0) = 0$ is equivalent to the gap equation and is realized in the superconducting state. This fact indicates the existence of the gap-less phase mode which corresponds to the Bogoliubov-Anderson mode at the zero temperature [116]. However, the phase mode have a dissipation due to the quasi-particle excitations at the finite temperature.

In the particle-hole symmetric case, $K(\boldsymbol{q}, \mathrm{i}\Omega_n) = K(-\boldsymbol{q}, -\mathrm{i}\Omega_n)$ is satisfied, and the off-diagonal component K_- vanishes. Therefore, the phase mode and the amplitude mode are completely decoupled. However, High-T_c cuprates are strongly particle-hole asymmetric systems, as we have emphasized. Therefore, the phase and amplitude fluctuations couples with each other through the off-diagonal component. Anyway, since the off-diagonal component vanishes at $\boldsymbol{q} = \mathrm{i}\Omega_n = 0$, the T-matrix has a pole at $\boldsymbol{q} = \mathrm{i}\Omega_n = 0$ in the superconducting state (This is the Thouless criterion for T_c). Thus, the T-matrix in the superconducting state include both the phase and amplitude modes.

We consider the effects of the superconducting fluctuations on the electronic state which are the origin of the pseudogap. In the superconducting state the effects are mainly from the phase mode. However, the effects are small compared to those in the normal state. Although the self-energy correction makes the spectrum broad, the effects make no significant difference in the low energy properties because the large superconducting gap rapidly grows below T_c. (See Fig. 3.29 in the next subsection.)

After carrying out the analytic continuation for the above expressions eqs. (3.35-42), we self-consistently determine the self-energy $\Sigma^R(\boldsymbol{k},\omega)$, the order parameter Δ_k, normal and anomalous Green functions $G^R(\boldsymbol{k},\omega)$, $F^R(\boldsymbol{k},\omega)$ and 2×2 T-matrix on the real frequency. The calculation is carried out both in the normal state and in the superconducting state.

Since the effects of the superconducting fluctuations are included in the self-energy $\Sigma^R(\boldsymbol{k},\omega)$, our formalism reduces to the BCS mean field theory by neglecting the self-energy. In the normal state, off-diagonal components Δ_k, $F(\boldsymbol{k},i\omega_n)$ and $L(\boldsymbol{q},i\Omega_n)$ vanish. In this case, it can be easily confirmed that the above set of equations are reduced to the self-consistent T-matrix calculation used in the normal state. The self-consistent T-matrix calculation gives a unified description for the pseudogap state, the superconducting state and their phase transition, although it is not precise on the critical point. As we have done in the previous section §3.1, we keep the $\alpha = 1 + gK(\boldsymbol{0},0) - gL(\boldsymbol{0},0)$ as small value $\alpha = 0.01$ in the superconducting state in order to avoid the singularity from the two-dimensionality. This operation is justified in the quasi-two dimensional systems which High-T_c cuprates are considered to be, because the weak three dimensionality surely remove the singularity. The finite critical temperature is obtained by this operation. The critical temperature T_c is more reduced as α is decreased. That is a natural result because the value α represents the three-dimensionality of the systems. The choice of the value α makes no qualitative difference on the calculated results in this thesis.

3.3.3 Order Parameter

Hereafter, we show the results of the self-consistent calculations for the set of equations in §3.3.1. In the main part of this section, we choose the coupling constant $g = -1.0$, or $g = -2.0$. Both cases give the qualitatively same results. In case of $g = -1.0$, mean field critical temperature $T_c\mathrm{MF} = 0.194$, and the calculated critical temperature $T_c = 0.099$. In case of $g = -2.0$, $T_c^{\mathrm{MF}} = 0.472$, and $T_c = 0.212$. The obtained phase diagram is shown in Fig. 3.28, which is similar to Fig 3.16. Here, we have determined the critical temperature T_c as the highest temperature where the solution for the superconducting state is obtained.

The suppression of T_c from T_c^{MF} becomes remarkable with increasing the coupling constant $|g|$. In the strong coupling case, the pseudogap state appears in the wide temperature region. We show the region where $0 \le 1/|g| - \chi_{\mathrm{p0}}(\boldsymbol{0},0) \le 0.1$ in Fig. 3.28. In case of the Gaussian fluctuation, $1/|g| - \chi_{\mathrm{p0}}(\boldsymbol{0},0) \cong \rho_{\mathrm{d}}(0)\frac{T-T_c}{T_c}$. Therefore, the width of the region is scaled by T_c. Our result shows that the region is enlarged in the strong coupling case. This indicates the wide critical region and the wide pseudogap region.

Once the superconducting order occurs, the effects of the fluctuations are drastically suppressed. The main reason is the following two points. The amplitude mode is suppressed owing to the growth of the order parameter. Moreover, the weight of the phase mode shifts to high frequency because the dissipation is reduced in the ordered state. As a result, the order parameter $\Delta_k = \Delta\varphi_k$ grows more rapidly than the result of the BCS theory. The temperature dependence of the order parameter is shown in Fig. 3.29. The rapid growth of the order parameter is a

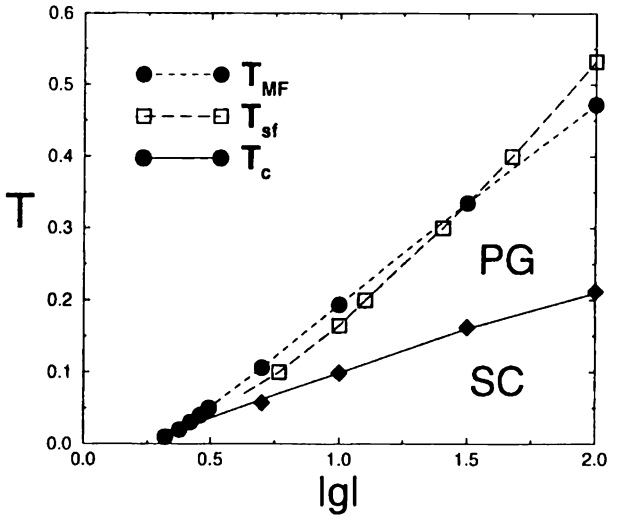

Figure 3.28: The obtained phase diagram. The closed circles show the critical temperature based on the mean field theory (T_c^{MF}). The closed diamonds show the critical temperature (T_c) suppressed by the fluctuations. The suppression becomes remarkable in the strong coupling region. There are slight differences from Fig. 3.16 because the different calculation is adopted in this section. The open squares correspond to the temperature T_{sf} where $1/|g| - \chi_{p0}(\mathbf{0}, 0) = 0.10$.

common feature of the theories including the critical fluctuations. It should be noticed that the dissipation of the two modes is reduced at the low temperature in accordance with the power law, $\mathrm{Im}K(\boldsymbol{q}, \Omega) \pm \mathrm{Im}L(\boldsymbol{q}, \Omega) \propto \Omega^4$, while it is exponentially reduced in the s-wave superconductor. The power law is due to the gap node. Thus, the dissipation remains in the d-wave case more than in the s-wave case.

The rapid growth of the order parameter should be seen in various probes. For example, the London penetration depth is a typical one (see §3.4.2). However, the rapid growth is a more general feature of the superconductivity caused by the electron correlation. For example, the rapid growth of the order parameter is also shown in the FLEX calculation [117]. We consider that the rapid growth obtained by the FLEX calculation is caused by the suppression of the de-pairing effect arising from the low frequency spin fluctuations. This effect is different from that calculated in this thesis. Both effects exist in High-T_c cuprates. Since the de-pairing effect from the spin fluctuations is suppressed by the pseudogap and the pseudogap becomes clear with decreasing the doping concentration, it is expected that the effect shown in this thesis becomes dominant with under-doping.

3.3.4 Single Particle Properties

Next, we show the results for the single particle properties. The single particle spectral weight $A(\boldsymbol{k}, \omega) = -\frac{1}{\pi}\mathrm{Im}G^{\mathrm{R}}(\boldsymbol{k}, \omega)$ is shown in Fig. 3.30. The pseudogap appears in the normal state $T \geq T_c$. Since the calculation using the TDGL expansion is inappropriate in the high frequency region, the structure at high frequency is different from the results from the previous section §3.1. However, the broad and asymmetric structure of the pseudogap at the low frequency is obtained similarly. As is pointed out in §3.1, the asymmetric structure is essential for the self-consistent solution showing the pseudogap. On the other hand, the gap structure becomes clear and symmetric below T_c. This is a usual feature of the superconducting gap. This change is smooth, but rapid

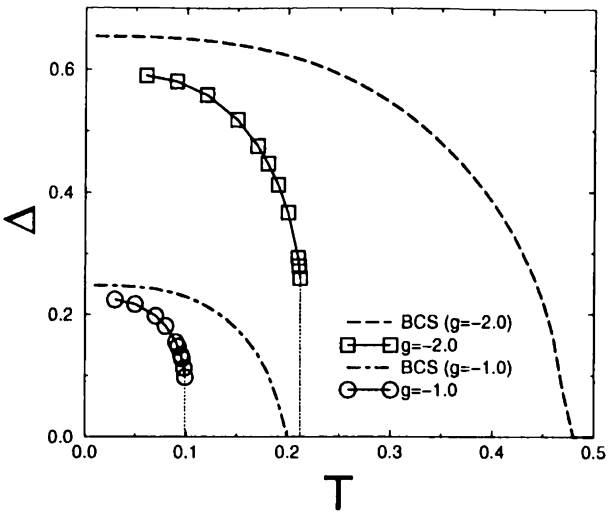

Figure 3.29: The growth of the order parameter Δ. The open circles and the open squares are the calculated results for $g = -1.0$ and $g = -2.0$, respectively. The dashed-dotted and long-dashed lines show the results of the d-wave BCS theory for $g = -1.0$ and $g = -2.0$, respectively. The order parameter grows more rapidly than the BCS result.

because of the rapid growth of the order parameter. The pseudogap is caused by the self-energy correction due to the superconducting fluctuations, while the superconducting gap is caused by the superconducting order. The self-energy correction is reduced in the superconducting state because the fluctuations are suppressed.

It should be noticed that the energy scale of the pseudogap and that of the superconducting gap are similar including their momentum dependences. The broad pseudogap, the sharp superconducting gap and the same energy scale are the important properties observed by ARPES [22, 23]. However, ARPES experiments can not refer to the asymmetric or symmetric structure, since ARPES measures only the spectrum below the Fermi energy. Moreover, the asymmetric structure disappears by summing up the momentum corresponding to the experimental resolving power.

Here, we briefly comment on the properties of the T-matrix in the pseudogap state. The calculation in this thesis justifies the calculation using the TDGL expansion in the pseudogap state (§3.1). In the TDGL expansion, we have neglected the quadratic term in Ω which is emphasized as the lowest order term in the particle-hole symmetric case [98]. However, the quadratic term can be neglected near T_c because it is a higher order term than the linear term which is present here. Moreover, our calculation shows that the quadratic term is reduced by the renormalization effect. The coefficient of the quadratic term a_3 is proportional to the parameter b, $a_3 = (2/\bar{v}^2)b$ in the Gaussian fluctuation. Here, $\bar{v}$ is the mean value of the quasi-particle velocity on the Fermi surface. The coefficient a_3 are reduced by the pseudogap with the parameter b. Therefore, the quadratic term is not important in the pseudogap state. On the other hand, The quadratic term is restored in the superconducting state, although the sign is opposite to that above T_c. Therefore, the T-matrix becomes symmetric in the superconducting state. That is a natural result because the superconductivity mixes the particle and the hole.

We can see more clearly the character of the phase transition from the pseudogap state to the superconducting state by showing the DOS in Fig. 3.31. The DOS $\rho(\omega) = \sum_{\boldsymbol{k}} A(\boldsymbol{k},\omega)$ shows the broad pseudogap in the normal state. The DOS remains near the Fermi level to some extent.

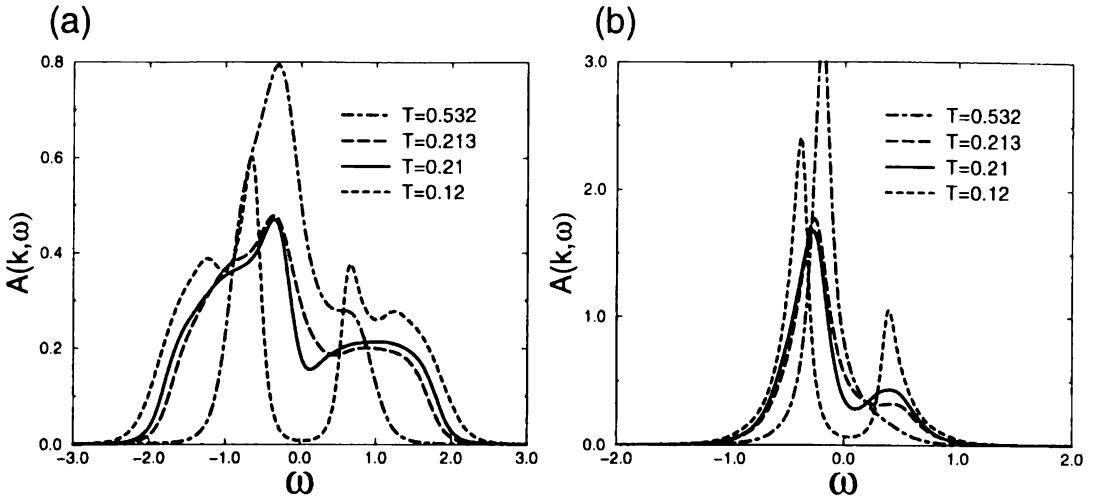

Figure 3.30: The single particle spectral weight at (a) $\boldsymbol{k} = (\pi, 0.15\pi)$, (b) $\boldsymbol{k} = (0.5\pi, 0.25\pi)$, just bellow the Fermi level. The dash-dotted ($T = 0.532$) and long-dashed ($T = 0.213$) lines are the results above T_c. $T = 0.213$ is just above T_c and corresponds to the pseudogap state. The solid ($T = 0.21$) and the dashed lines ($T = 0.12$) are results below T_c. The pseudogap smoothly changes to the superconducting gap. The gap structure becomes sharp and symmetric in the superconducting state.

These features reflect the broad and asymmetric structure of the single particle spectral weight $A(\boldsymbol{k}, \omega)$. The pseudogap grows with approaching the critical point. The superconducting phase transition takes place by the remained DOS. It should be noticed that the phase transition is superconductivity, and is not the Bose Einstein condensation in the NSR theory. The shift of the chemical potential is actually small. Once the superconducting order occurs, the gap becomes sharp with the rapid growth of the order parameter. The change is rapid but smooth across T_c. The DOS shows the linear energy dependence $\rho(\omega) \propto \omega$ at the low temperature. This is a characteristic feature of the $d_{x^2-y^2}$-wave superconductivity.

It should be noticed that the energy scale of the pseudogap and that of the superconducting gap are almost the same. When the coupling constant $|g|$ increases, the energy scale of the pseudogap increases with that of the superconducting gap. The energy scale is almost independent of the temperature. These features are consistent with the important results of the spectroscopic measurements [22, 23, 49]. The same gap scale is not so obvious in the resonance scattering scenario, while it is obvious in the NSR scenario. However, the same gap scale is an expected result because the two phenomena, the pseudogap and the superconductivity, have the same origin in our scenario. This is actually confirmed by the above results.

3.3.5 Discussions

In this section, the pseudogap state and the superconducting state in High-T_c cuprates have been investigated. It should be noticed that the system is not the low density system. Therefore, our scenario is based on the resonance scattering and is not based on the NSR theory. [74] Namely, the mechanism of the phase transition should be considered as the superconductivity, and is not the Bose Einstein condensation in the sense of the NSR theory. The characteristics of the pseudogap state and the superconducting state have been investigated on the basis of the calculated results.

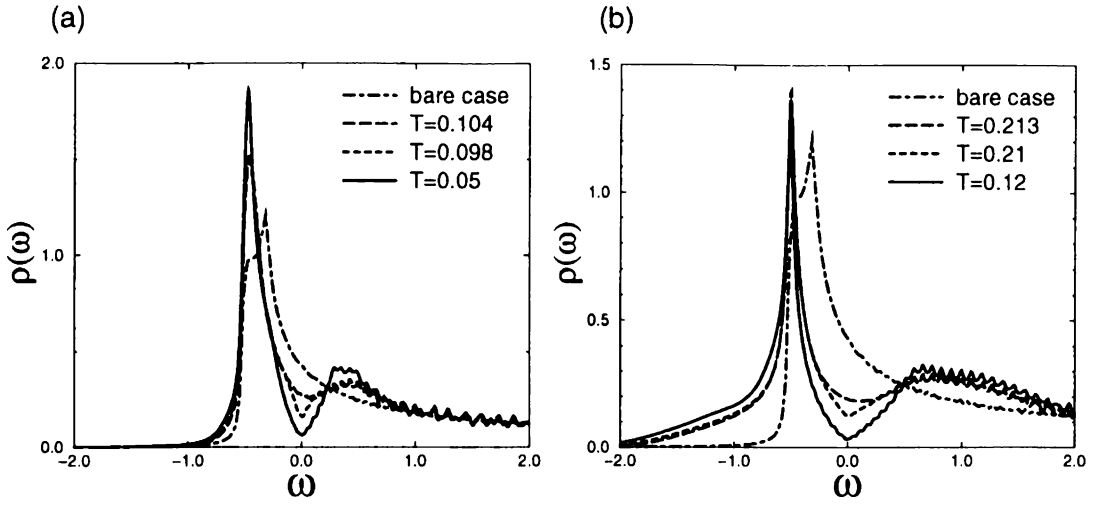

Figure 3.31: The DOS for (a) $g = -1.0$ and (b) $g = -2.0$. The dash-dotted lines show the non-interacting DOS. The long-dashed lines ((a) $T = 0.104$ (b) $T = 0.213$) show the pseudogap state above T_c. The dashed ((a) $T = 0.098$ (b) $T = 0.21$) and solid ((a) $T = 0.05$ (b)$T = 0.12$) lines are the results bellow T_c. It should be noticed that the gap scale is almost the same between in the pseudogap state and in the superconducting state.

The calculated results well explain the experimental results. The smooth change observed in the electronic spectrum has been reproduced. The same energy scale is not so self-evident in the resonance scattering scenario, compared with the NSR theory. However, our results have actually confirmed the important character. This fact means that the energy gain due to the formation of the gap around the Fermi energy is common to both of the pseudogap and the superconductivity.

In the above sections, we have emphasized the importance of the comprehensive explanation of the phase diagram in order to understand the overview of the High-T_c superconductivity. The pseudogap is an especially important character of the High-T_c cuprates. The following two points are important to understand the pseudogap and the phase diagram.

One is the continuity with respect to the hole doping. The pseudogap phenomena take place from slightly over-doped region to under-doped one. The pseudogap gradually develops with decreasing the doping concentration. Our scenario based on the resonance scattering scenario is properly consistent with the doping dependence. The typical change due to the doping is clearly observed in the magnetic field dependence of the pseudogap phenomena [108, 109, 110]. The scenario based on the resonance scattering well explains the doping dependent character of the pseudogap continuously from the slightly over-doped to under-doped region (§3.2) The comprehensive understanding strongly supports our scenario.

The other important point is the close relation between the pseudogap state and the superconducting state. It is natural to consider the pairing scenario for the pseudogap which develops with approaching the critical point and smoothly changes to the superconducting gap. In this thesis, the same aspects between the pseudogap state and the superconducting state are confirmed in detail. The results support our scenario more clearly.

3.3.6 Comment on the Magnetic Scenarios

Here, we give a discussion on the magnetic scenarios for the pseudogap phenomena. The magnetic scenarios based on the anti-ferromagnetic hidden order or the anti-ferromagnetic fluctuations have been proposed for the pseudogap phenomena. [9, 18, 19] The RVB theory is also included in the magnetic scenario because the spin singlet pairing is caused by the magnetic interaction (super-exchange interaction). We also think it possible that the strong spin fluctuations near the magnetic critical point reduce the electronic DOS. However, it is difficult to give a comprehensive understanding of the phase diagram on the basis of the magnetic scenario. First, the same energy scale of the pseudogap and the superconducting gap is unnatural in the magnetic scenario. This is because the spin fluctuations (or the anti-ferromagnetism) and the superconductivity have considerably different energy scale. Next, it is not clear whether the magnetic scenario may be consistent with the magnetic field dependence, especially in the weak pseudogap case. It is because the magnetic exchange coupling J is the order of $J \sim 1000$K and the applied magnetic field is the order of $\mu_B B \sim 10$K. Therefore, we think that the magnetic scenario is inappropriate to explain the pseudogap phenomena in High-T_c cuprates.

Moreover, we comment on the spin-fluctuation-induced pseudogap. There is a calculation treating the pseudogap phenomena as a precursor of the magnetic instability (anti-ferromagnetism) [18, 19]. In these theories, 'hot spot', which is a part of the Fermi surface in the vicinity of the anti-ferromagnetic Brillouin zone, exists near $(0, \pi)$ and plays an especial role. Since the quasi-particles at 'hot spot' are strongly scattered by the anti-ferromagnetic spin fluctuations, the gap structure appears at 'hot spot'. Since the spin fluctuations lead to the transformation of the Fermi surface, 'hot spot' comes to exist in the wide region near $(0, \pi)$ [57]. Therefore, the gap structure would have a similar shape to the $d_{x^2-y^2}$-wave superconducting gap. However, the scenario is difficult to induce the clear pseudogap. Since the interaction caused by the superconducting fluctuations is strong in the vicinity of $\boldsymbol{q} = (0, 0)$, the important $\boldsymbol{k}$-points for the self-energy on the Fermi surface are sure to be on the Fermi surface. On the other hand, in case of the anti-ferromagnetic spin fluctuations, the interaction is strong in the vicinity of $\boldsymbol{Q} = (\pi, \pi)$. Therefore, the important $\boldsymbol{k}$-points for the quasi-particles with the momentum $\boldsymbol{k}$ exist in the vicinity of $\boldsymbol{k} + \boldsymbol{Q}$. They are on the Fermi surface only when $\boldsymbol{k}$ is on the 'hot spot'. As a result, the quasi-particles slightly apart from 'hot spot' are not directly scattered by the strong fluctuations. Thus, the pseudogap is not impossible but difficult to be attributed to the magnetic interaction on the quantitative point of view. Moreover, since the phase transition which really occurs is the superconductivity, the superconducting critical phenomena necessarily take place. It is not obvious how the critical spin fluctuations can exist even in the critical region of the superconductivity. Indeed, the spin fluctuations are reduced in the pseudogap region [30, 31, 32, 33, 34, 35, 36].

On the other hand, a slight suppression of the DOS with large energy scale has been indicated. This phenomenon appears at the rather higher temperature than T^* and is called 'large pseudogap' [49, 118]. We expect that the 'large pseudogap' results from the magnetic origin. In this case, the pseudogap discussed in this thesis results from the origin with more small energy scale. A clear understanding is obtained by considering that the origin is the *superconductivity*. Thus, the pairing scenario gives the comprehensive understanding of the High-T_c superconductivity, more clearly than the magnetic scenarios.

3.4 Anomalous Properties in the Pseudogap State [27]

In this section, we investigate the magnetic and transport properties which show the pseudogap phenomena. The pseudogap phenomena observed in each probe are explained by considering the characteristic momentum and frequency dependence of High-T_c cuprates. We calculate the behavior of some quantities from the pseudogap state to the superconducting state. The self-consistent T-matrix approximation is used in this section. The TDGL expansion is not used because the calculation is carried out in the ordered state [114]. Our results give qualitatively consistent explanation for the experimental results.

3.4.1 Magnetic Properties

In this subsection, we show the results for the magnetic properties. The magnetic field dependence has already been calculated in §3.2. In this subsection the properties are investigated in more detail. We calculate the dynamical spin susceptibility $\chi_s(\boldsymbol{k},\omega)$ by using the random phase approximation (RPA). The exchange enhancement is taken into account within the RPA.

$$\chi_s^{\mathrm{R}}(\boldsymbol{q},\omega) = \frac{\chi_0^{\mathrm{R}}(\boldsymbol{q},\omega)}{1-U\chi_0^{\mathrm{R}}(\boldsymbol{q},\omega)}, \tag{3.45}$$

$$\chi_0(\boldsymbol{q},\mathrm{i}\omega_n) = -T\sum_{\boldsymbol{k},\omega_m}[G(\boldsymbol{k},\mathrm{i}\omega_m)G(\boldsymbol{k}+\boldsymbol{q},\mathrm{i}\Omega_m+\mathrm{i}\omega_n)+F(\boldsymbol{k},\mathrm{i}\omega_m)F(\boldsymbol{k}+\boldsymbol{q},\mathrm{i}\Omega_m+\mathrm{i}\omega_n)] \tag{3.46}$$

Here, the expression includes the anomalous Green function F because the calculation is extended to the superconducting state. We fix the enhancement parameter $U = 1.5$, afterward. The following results are not affected by the choice of the parameter, qualitatively. As is explained in §3.2.2, we can neglect the correction to the two-body correlation function by the superconducting fluctuations (AL term and MT term). The effects of the superconducting fluctuations are included in the normal and anomalous Green function G and F thorough the self-energy correction.

The NMR spin-lattice relaxation rate $1/T_1$ and spin-echo decay rate $1/T_{2G}$ are calculated by the following expressions.

$$1/T_1T = \sum_{\boldsymbol{q}} F_\perp(\boldsymbol{q})[\frac{1}{\omega}\mathrm{Im}\chi_s^{\mathrm{R}}(\boldsymbol{q},\omega)\mid_{\omega\to 0}], \tag{3.47}$$

$$1/T_{2G}^2 = \sum_{\boldsymbol{q}}[F_{\|}(\boldsymbol{q})\mathrm{Re}\chi_s^{\mathrm{R}}(\boldsymbol{q},0)]^2 - [\sum_{\boldsymbol{q}} F_{\|}(\boldsymbol{q})\mathrm{Re}\chi_s^{\mathrm{R}}(\boldsymbol{q},0)]^2. \tag{3.48}$$

Here, $F_\perp(\boldsymbol{q}) = \frac{1}{2}[\{A_1+2B(\cos q_x+\cos q_y)\}^2+\{A_2+2B(\cos q_x+\cos q_y)\}^2]$ and $F_{\|}(\boldsymbol{q}) = \{A_2+2B(\cos q_x+\cos q_y)\}^2$. The hyperfine coupling constants A_1, A_2 and B are evaluated as $A_1 = 0.84B$ and $A_2 = -4B$ [112]. The above expression is the same as that used in §3.2.3.

The calculated results are shown in Fig. 3.32. In the normal state far above T_c, $1/T_1T$ increases with lowering the temperature owing to the exchange enhancement. It shows a peak above T_c and decreases with lowering the temperature below T^*. The decrease is an effect of the superconducting fluctuations. It is the well-known pseudogap phenomena in NMR $1/T_1T$ [30, 31, 32, 33, 34, 35, 36]. The superconducting fluctuations give rise to the pseudogap in the DOS, and reduce the weight of the spin fluctuations at the low frequency. Thus, the pseudogap observed in NMR $1/T_1T$ takes place through the single particle pseudogap. However, the decrease in the pseudogap state is rather moderate than in the superconducting state. With the growth of the sharp superconducting gap, $1/T_1T$ decreases rapidly. The BCS-like behavior is obtained in the superconducting state since the superconducting gap opens clearly. These features are consistent with the experimental results.

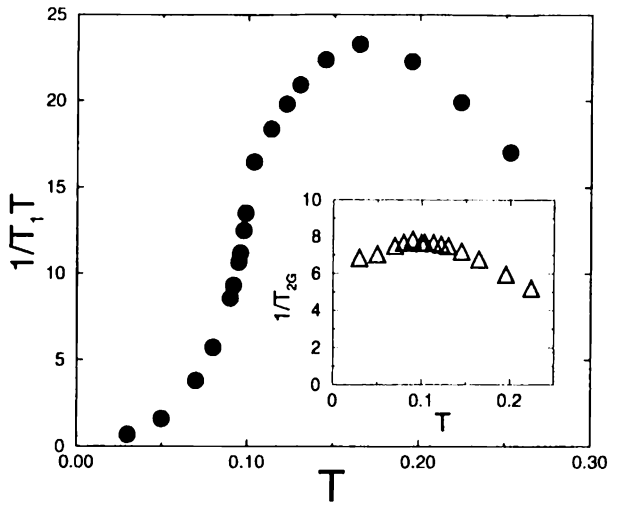

Figure 3.32: The results for $1/T_1T$. Here, $g = -1.0$. The peak appears above $T_c = 0.099$. $1/T_1T$ is reduced by the pseudogap and decreases with approaching the critical point. The inset shows the result for $1/T_{2G}$.

On the other hand, NMR $1/T_{2G}$ shows rather weak temperature dependence both in the pseudogap state and in the superconducting state (see the inset of Fig. 3.32). NMR $1/T_{2G}$ increases with decreasing temperature in the normal state far above T_c owing to the exchange enhancement. The pseudogap also affects the NMR $1/T_{2G}$. The increase of $1/T_{2G}$ becomes moderate in the pseudogap state. Near T_c, NMR $1/T_{2G}$ is almost independent of the temperature. These are the effects of the pseudogap. However, the effects on $1/T_{2G}$ are weaker than those on $1/T_1T$. In the superconducting state, $1/T_{2G}$ decreases moderately with decreasing the temperature as a characteristic result of the d-wave pairing.

Since $1/T_{2G}$ reflects the total weight of the spin fluctuations, the effect of the pseudogap is weak on $1/T_{2G}$. In particular, the static susceptibility $\mathrm{Re}\chi_s^R(\boldsymbol{q}, 0)$ around $\boldsymbol{q} = \boldsymbol{Q} = (\pi, \pi)$ is not reduced so much by the d-wave pseudogap, while it is remarkably reduced around $\boldsymbol{q} = (0, 0)$. The momentum dependence of the hyperfine coupling $F_{\|}(\boldsymbol{q})$ further weaken the effects of the pseudogap on $1/T_{2G}$. The above features are in common with those in the superconducting state [113]. That is a natural result because the pseudogap and the superconducting gap have the same $d_{x^2-y^2}$-wave form.

It is natural that the scaling law for the spin fluctuations is violated by the pseudogap, because it is violated in the superconducting state. The above results are qualitatively consistent with the features indicated by the NMR experiments [30, 31, 32, 33, 34, 35, 36]. Minutely speaking, the different behavior of $1/T_{2G}$ has been reported for different High-T_c compounds. [32, 33, 35, 36] There is an idea that attributes the difference to the effects of the interlayer coupling [36]. The difference of the hyperfine coupling is also the origin of the different behavior. Anyway, the relatively weak effect of the pseudogap on $1/T_{2G}$ than on $1/T_1T$ is observed in common. The qualitatively consistent results are obtained here.

The remaining part of this subsection is concerned with the neutron resonance peak observed by the neutron scattering experiments [119, 120]. The neutron resonance peak is observed in the superconducting state from optimally-doped to under-doped region. The recent measurements have found the development of the weak resonance peak in the pseudogap state [120]. The reso-

nance peak in the superconducting state is attributed to the interplay of the anti-ferromagnetic correlation and the d-wave superconductivity [117, 121, 122]. Our result shows the sharp resonance peak in the superconducting state, which is caused by the same mechanism. Moreover, we investigate the behavior of the resonance peak in the pseudogap state. The neutron scattering intensity is proportional to the imaginary part of the spin susceptibility, $\mathrm{Im}\chi_s^{\mathrm{R}}(\boldsymbol{q},\omega)$. We show the calculated results for $\mathrm{Im}\chi_s^{\mathrm{R}}(\boldsymbol{q},\omega)$ at $\boldsymbol{q} = \boldsymbol{Q}$ in Fig. 3.33. Here, $\mathrm{Im}\chi_s^{\mathrm{R}}(\boldsymbol{Q},\omega)$ is expressed as follows,

$$\mathrm{Im}\chi_s^{\mathrm{R}}(\boldsymbol{Q},\omega) = \frac{\mathrm{Im}\chi_0^{\mathrm{R}}(\boldsymbol{Q},\omega)}{[1 - U\mathrm{Re}\chi_0^{\mathrm{R}}(\boldsymbol{Q},\omega)]^2 + [U\mathrm{Im}\chi_0^{\mathrm{R}}(\boldsymbol{Q},\omega)]^2}. \tag{3.49}$$

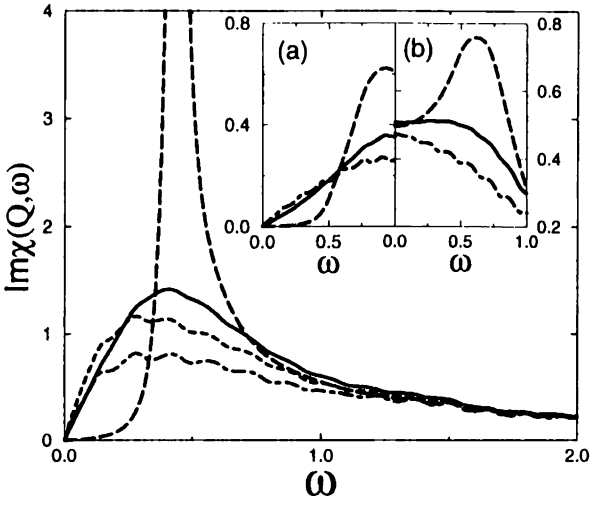

Figure 3.33: The results for $\mathrm{Im}\chi_s^{\mathrm{R}}(\boldsymbol{Q},\omega)$. Here, $g = -1.0$. The inset shows (a) $\mathrm{Im}\chi_0^{\mathrm{R}}(\boldsymbol{Q},\omega)$ and (b) $\mathrm{Re}\chi_0^{\mathrm{R}}(\boldsymbol{Q},\omega)$, respectively. The long-dashed lines, the solid lines, the dashed-lines and the dash-dotted lines correspond to $T = 0.050$ (superconducting state), $T = 0.104$ (pseudogap state), $T = 0.165$ and $T = 0.253$, respectively.

In the superconducting state, the real part $\mathrm{Re}\chi_0^{\mathrm{R}}(\boldsymbol{Q},\omega)$ increases with ω and the imaginary part $\mathrm{Im}\chi_0^{\mathrm{R}}(\boldsymbol{Q},\omega)$ is suppressed in the low frequency region $\omega < 2\Delta_{\mathrm{max}}$. Here, Δ_{max} is the maximum gap energy. Therefore, there is a point $\omega = \omega_{\mathrm{r}}$ where the denominator of eq.(4.5) is remarkably small, when the system is near the anti-ferromagnetic instability, $1 - U\mathrm{Re}\chi_0^{\mathrm{R}}(\boldsymbol{Q},0) \ll 1$. Then, the sharp resonance peak appears at $\omega = \omega_{\mathrm{r}}$. In the pseudogap state, the dynamical susceptibility χ_0 behaves similarly. $\mathrm{Re}\chi_0^{\mathrm{R}}(\boldsymbol{Q},\omega)$ has the positive slope with respect to ω. The dissipation $\mathrm{Im}\chi_0^{\mathrm{R}}(\boldsymbol{Q},\omega)$ is reduced in the low frequency region. This behavior is an essential result of the pseudogap as a precursor of the superconductivity. However, the features are rather weak compared to the superconducting state. In particular, the finite dissipation remains in the pseudogap state because of the remained DOS near the Fermi energy. As a result, the weight of the spin fluctuations shifts to the high frequency. This is a precursor of the resonance peak, however it is weak and broad. The peak appears at the slightly lower frequency than ω_{r}. The peak smoothly develops to the sharp peak in the superconducting state. Far above T_c, the conventional behavior of the normal state is obtained. We can see that the low frequency component of the spin fluctuations is suppressed by the pseudogap, however, the weight is transfered to the high frequency. This behavior is not obtained by considering the spin fluctuations alone. The transfered high frequency component is effective as the pairing interaction, and contribute to the NMR $1/T_{2G}$ as we have explained before.

3.4.2 Transport Properties

The transport phenomena are interesting enough to be discussed here, because they reflect the characteristic momentum dependences of High-T_c cuprates and the relationship between the spin fluctuations and the superconducting fluctuations. In this subsection, we investigate the transport phenomena in High-T_c cuprates.

First, we describe how the transport phenomena in under-doped cuprates are understood in the normal state ($T > T^*$). They are anomalous at a glance, and therefore regarded as an evidence of the 'anomalous metal'. However, we can understand them by considering the magnetic interaction caused by the anti-ferromagnetic spin fluctuations [56, 57, 58, 59].

The momentum dependence of the lifetime of quasi-particles is important to understand the transport properties. The momentum dependent lifetime is due to the scattering by the anti-ferromagnetic spin fluctuations [56, 57]. The 'hot spot' means the part of the Fermi surface in which $\varepsilon_{\boldsymbol{k}} = \varepsilon_{\boldsymbol{k}+\boldsymbol{Q}}$ [56]. Here, $\boldsymbol{Q}$ is a anti-ferromagnetic wave vector $\boldsymbol{Q} = (\pi, \pi)$. At the 'hot spot', quasi-particles directly suffer an scattering by the anti-ferromagnetic spin fluctuations at $\boldsymbol{q} = \boldsymbol{Q}$. The 'cold spot' is the area on the Fermi surface far from the 'hot spot'. There, quasi-particles do not directly scattered by the spin fluctuations. Therefore, the lifetime of the quasi-particles is long at the 'cold spot' and short at the 'hot spot'. This momentum dependent lifetime is a general property of the systems with an strong anti-ferromagnetic spin fluctuations [123]. For High-T_c cuprates, the 'hot spot' is located near $(\pi, 0)$ and its symmetric points. The 'cold spot' is located near $(\pi/2, \pi/2)$. This momentum dependence of the lifetime is observed experimentally [124]. At the same time, the pseudogap is large at the 'hot spot' and small at the 'cold spot' because of its $d_{x^2-y^2}$-wave shape.

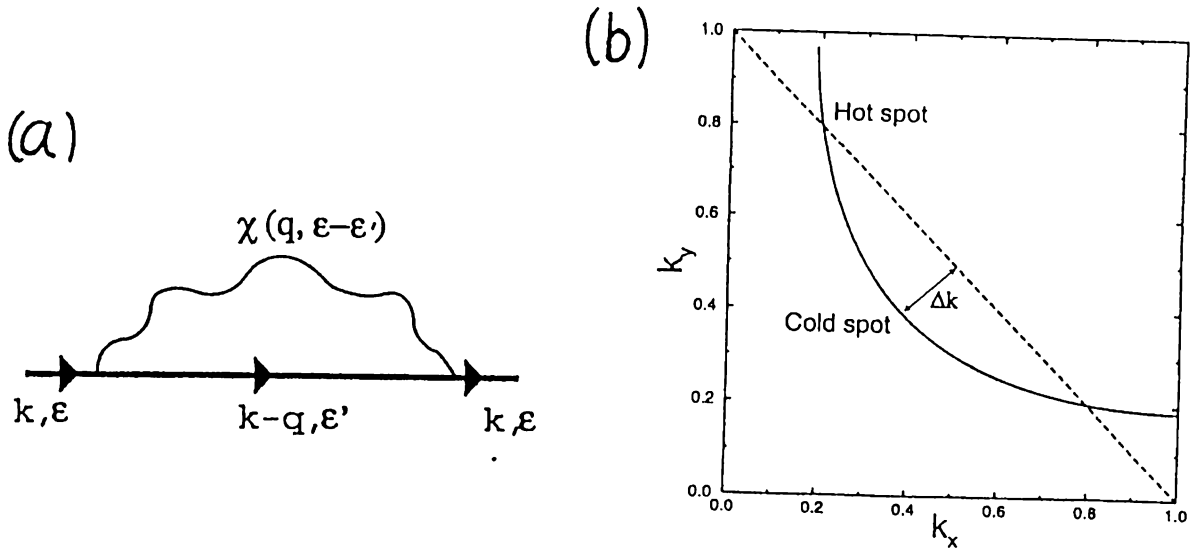

Figure 3.34: (a) The self-energy due to the spin fluctuations within the one loop approximation. (b) The 'hot spot' and 'cold spot' of the Fermi surface.

The 'hot spot' does not contribute to the in-plane conductivity, because the conductivity is almost determined by the most easily flowing quasi-particles. The in-plane conductivity is mainly determined by the 'cold spot'. The quasi-particles at 'cold spot' are sure to have the T^2-damping rate at the low temperature limit which is consistent with the conventional Fermi liquid theory. However, they have the T-linear damping rate above the crossover temperature ($T > T_{cr}$). It is because of the low energy magnetic excitations. The transformation of the Fermi surface which

leads to a form more appropriate to the nesting reduces the crossover temperature $T_{cr} \simeq \omega_0(\Delta k)^2$. Here, the parameter Δk is shown in Fig. 3.34(b). The transformation itself is due to the anti-ferromagnetic spin fluctuations [57].

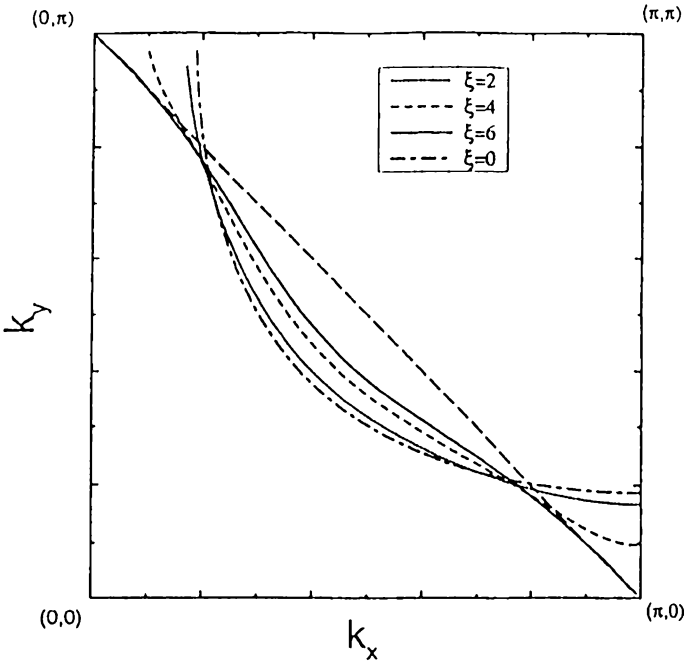

Figure 3.35: The transformed Fermi surface for $\xi = 0$ (dot-dashed line), $\xi = 2$ (dotted line), $\xi = 4$ (dashed line) and $\xi = 6$ (solid line), respectively. Here, the parameter ξ is the anti-ferromagnetic correlation length. As ξ increases, the Fermi surface at 'hot spot' approaches to the anti-ferromagnetic Brillouin zone.

As a result, the in-plane resistivity shows a T-linear law in the under-doped region ($T > T^* > T_{cr}$). It should be noticed that T-linear resistivity is not due to the Curie-Weiss law $\chi_s(\boldsymbol{Q}) \propto 1/(T+\theta)$, or $1/T_1T \propto 1/(T+\theta)$. The calculations inappropriately treating the momentum dependent lifetime attribute the T-linear resistivity to the Curie-Weiss law [7, 125] For example, the approximate relation between the in-plane resistivity ρ_{ab} and $1/T_1T$, $\rho_{ab} \propto T^2/(T_1T)$ is derived [125]. If appropriately considering the 'hot spot' and the 'cold spot', the T-linear resistivity is realized more generally, but in more high temperature region [57]. This generality is important to understand the T-linear in-plane resistivity in the pseudogap state in which the Curie-Weiss law is violated.

The other important character of High-T_c cuprates is a momentum dependence of the interlayer hopping matrix element $t_\perp(\boldsymbol{k})$. The band calculation has shown that the dispersion along the c-axis is large at the 'hot spot' and is nearly 0 at the 'cold spot' [68]. The hopping matrix element $t_\perp(\boldsymbol{k})$ is approximately expressed as [68, 69].

$$t_\perp(\boldsymbol{k}) = t_c(\frac{\cos k_x - \cos k_y}{2})^2. \tag{3.50}$$

Since the quasi-particle velocity along the c-axis is nearly 0 at the 'cold spot', the 'cold spot' does not contribute to the c-axis conductivity. On the other hand, the contribution from 'hot spot' is reduced by the short lifetime, in spite of the large velocity along the c-axis. As a result, the c-axis transport becomes incoherent. Thus, we can understand the coherent in-plane conductance and the incoherent c-axis conductance at the same time [57].

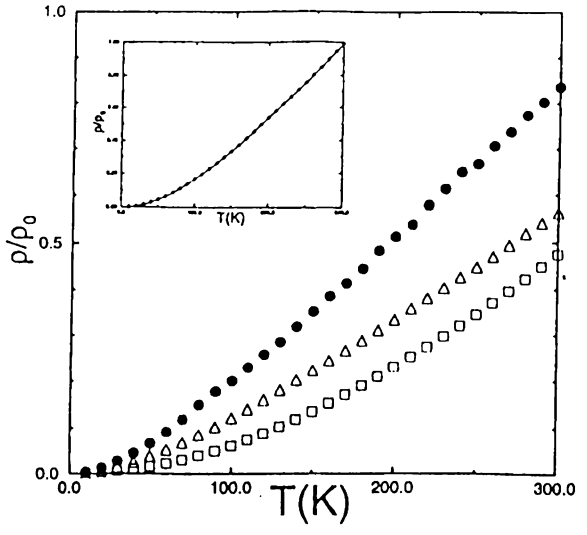

Figure 3.36: The temperature dependence of the in-plane resistivity. The marks of •, △ and □ correspond to under-doped, optimally-doped and over-doped cuprates, respectively. The inset is the in-plane resistivity of under-doped cuprates without the transformation of the Fermi surface. It doesn't show T-linear law up to rather high temperature.

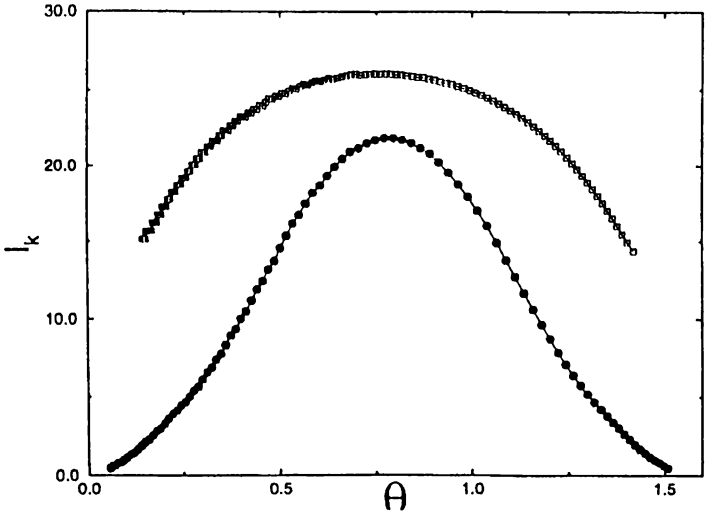

Figure 3.37: The momentum dependence of the mean free path. The marks of •, and □ correspond to under-doped and over-doped cuprates, respectively. Here, $\theta = \mathrm{Arctan}(k_y/k_x)$. The under-doped case shows the strong anisotropy.

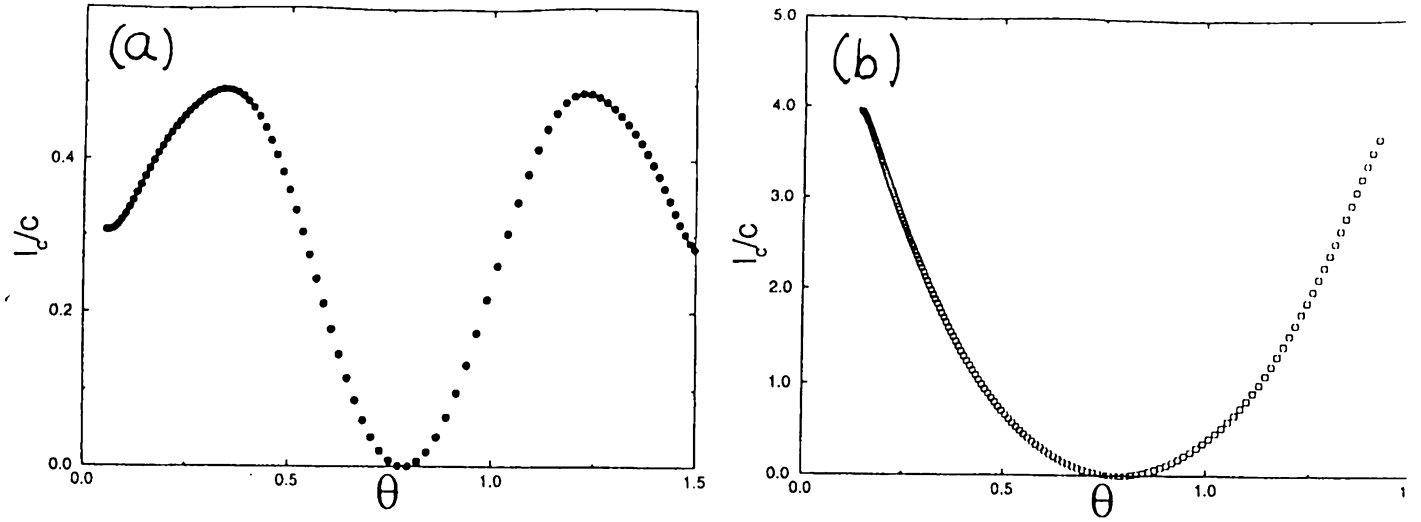

Figure 3.38: The mean free path along the c-axis for (a) the under-doped cuprates and (b)the over-doped cuprates. Here, $\theta = \mathrm{Arctan}(k_y/k_x)$, and c is a lattice space along the c-axis.

The momentum dependent lifetime enhances the Hall coefficient $R = \sigma_{xy}/\sigma_{xx}^2 H$ [57]. This is because the effective DOS for the in-plane transport is reduced. However, the vertex correction plays a more important role for the Hall coefficient [58, 59]. The effect is results from the momentum derivative of the total current J_ν in the general formula given by Kohno and Yamada [60]. The Hall coefficient is strongly enhanced by the vertex correction. In the conventional metals, the vertex correction gives only an constant factor arising from the Umklapp scattering and has no significant effect [126]. The significance of the vertex correction is also due to the anti-ferromagnetic spin fluctuations. The vertex correction is not so important for the longitudinal conductivity even in the systems with spin fluctuations [58, 59].

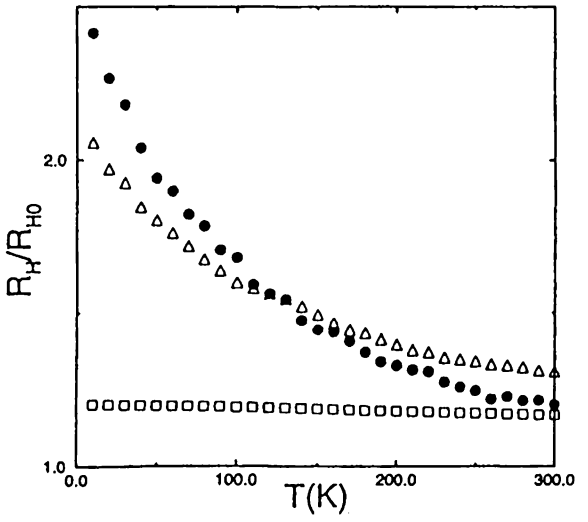

Figure 3.39: The temperature dependence of the Hall coefficient calculated in Ref 57. The marks are the same as Fig. 3.36. R_{H0} is the Hall coefficient without the transformation of the Fermi surface and the momentum dependence of the mean free path.

Hereafter, we investigate the effects of the pseudogap and the superconductivity on the trans-

port phenomena. The experimental results clearly show the pseudogap phenomena in the c-axis transport [45, 46] On the other hand, the in-plane transport does not clearly show the pseudogap. The different effects of the pseudogap on the in-plane and c-axis transport are understood by considering the momentum dependence of the interlayer hopping $t_\perp(\boldsymbol{k})$. Although the in-plane transport phenomena are dominated by the contribution from the 'cold spot', the c-axis transport is mainly determined by the 'hot spot'. Therefore, the qualitatively different properties between the in-plane and c-axis transport are yielded. Since the pseudogap and the superconducting gap are large at the 'hot spot', the c-axis transport reflects the pseudogap more clearly than the in-plane transport.

The experimental results have actually indicated so. The c-axis resistivity increases with decreasing temperature in the pseudogap state, while the in-plane resistivity keeps the T-linear law and slightly deviates downward [42, 43]. The c-axis optical conductivity shows the gap structure in the pseudogap state, although the in-plane optical conductivity shows only the weak structure in the higher frequency region [46]. The pseudogap observed in the c-axis optical conductivity smoothly changes to the superconducting gap [46]. This fact also indicates the close relation between the pseudogap and the superconductivity. However, the pseudogap in the c-axis optical conductivity has never been explained on the basis of the pairing scenario.

Here, we calculate the conductivity by neglecting the vertex corrections. The conductivity $\sigma_{\rm tot}(\omega)$ is described by the normal fluid part and the superfluid part in the low frequency region, $\sigma_{\rm tot}(\omega) = \sigma(\omega) + {\rm i}/4\pi\lambda^2(\omega + {\rm i}\delta)$. The second term is proportional to the London constant (or the superfluid density), $\Lambda = 1/4\pi\lambda^2$ and appears in the superconducting state. Here, λ is the London penetration depth which we calculate later. The in-plane and c-axis optical conductivity at the finite frequency is expressed by the normal fluid part in the following way,

$$\begin{aligned}
\sigma_{\rm ab}(\omega) &= -\frac{e^2}{d}\frac{1}{\omega}\sum_{\boldsymbol{k}} v^2(\boldsymbol{k}) \int \frac{{\rm d}\omega'}{\pi}[f(\omega'+\omega) - f(\omega')] \\
&\quad \times ({\rm Im}G^{\rm R}(\boldsymbol{k},\omega'){\rm Im}G^{\rm R}(\boldsymbol{k},\omega+\omega') + {\rm Im}F^{\rm R}(\boldsymbol{k},\omega'){\rm Im}F^{\rm R}(\boldsymbol{k},\omega+\omega')), \qquad (3.51) \\
\sigma_{\rm c}(\omega) &= -4de^2\frac{1}{\omega}\sum_{\boldsymbol{k}} t_\perp^2(\boldsymbol{k}) \int \frac{{\rm d}\omega'}{\pi}[f(\omega'+\omega) - f(\omega')] \\
&\quad \times ({\rm Im}G^{\rm R}(\boldsymbol{k},\omega'){\rm Im}G^{\rm R}(\boldsymbol{k},\omega+\omega') + {\rm Im}F^{\rm R}(\boldsymbol{k},\omega'){\rm Im}F^{\rm R}(\boldsymbol{k},\omega+\omega')). \qquad (3.52)
\end{aligned}$$

Here, d is the interlayer distance, and $v(\boldsymbol{k}) = \sqrt{v_x^2 + v_y^2}$ is the in-plane velocity, where $v_\mu = \partial\varepsilon_{\boldsymbol{k}}/\partial k_\mu$. The velocity $v(\boldsymbol{k})$ is almost independent of the momentum on the Fermi surface in our model. We have neglected the weak k_z dependence of the electronic state. This procedure corresponds to the lowest order calculation with respect to $t_{\rm c}$. We have neglected the term proportional to the delta function $\delta(\omega)$ which comes from the superfluid part.

Here, we comment on the vertex correction neglected here. In particular, the AL term is considered to be important for the transport [71]. We think that the effect of the AL term does not appear except for the narrow region near $T_{\rm c}$. This expectation is explained as follows. The current vertex in the AL term parallel to the plane $J_{ab}(\boldsymbol{q})$ is proportional to the TDGL parameter b, $J_{ab}(\boldsymbol{q}) \propto b\boldsymbol{q}$. This corresponds to the velocity of the fluctuating Cooper pairs and is small in the strong coupling case. Thus, the small b indicates the small velocity of the fluctuating Cooper pairs as well as the strong fluctuations. The factors b from the current vertex and from the pair propagator cancel each other in two-dimension. The contribution from the AL term is expressed as $\sigma_{\rm AL} \propto 1/t_0$ [71]. On the other hand, the effects on the single particle properties are estimated as $1/\tau_{\boldsymbol{k}} = -{\rm Im}\Sigma^{\rm R}(\boldsymbol{k},0) \propto 1/\sqrt{bt_0}$. Since the singularity with respect to the parameter t_0 is stronger

in the AL term $\sigma_{\rm AL}$ than in the damping rate $1/\tau_k$, and since the parameter b is large, the AL term is more important than the latter in the weak coupling limit. However, the situation is quite different in the strong coupling case. The effects on the single particle properties can appear at T^* before the AL term dominate the large conductivity from the 'cold spot'.

On the other hand, the conductivity is small along the c-axis. However, we can neglect the AL term along the c-axis in the quasi-two dimensional systems because the AL term along the c-axis is a higher order term with respect to the anisotropy t_c/t. It is because the current vertex $J_c(\boldsymbol{q})$ is quadratic with respect to t_c $J_c(\boldsymbol{q}) \propto t_c^2$, although the quasi-particle velocity is linear $v_c \propto t_c$. The MT term is considered to be suppressed by the elastic scattering in the d-wave case. The vertex correction arising from the spin fluctuations is shown to be not important for the longitudinal conductivity [58, 59]. Thus, it is justified to neglect the vertex correction.

Hereafter, we normalize the conductivity by the constant factor as $\sigma_c(\omega) = \sigma_c(\omega)/\sigma_c^0$ and $\sigma_{\rm ab}(\omega) = \sigma_{\rm ab}(\omega)/\sigma_{\rm ab}^0$, where $\sigma_c^0 = de^2$ and $\sigma_{\rm ab}^0 = e^2/d$. In this subsection we fix the coupling constant $g = -2.0$ and $t_c = 0.1$.

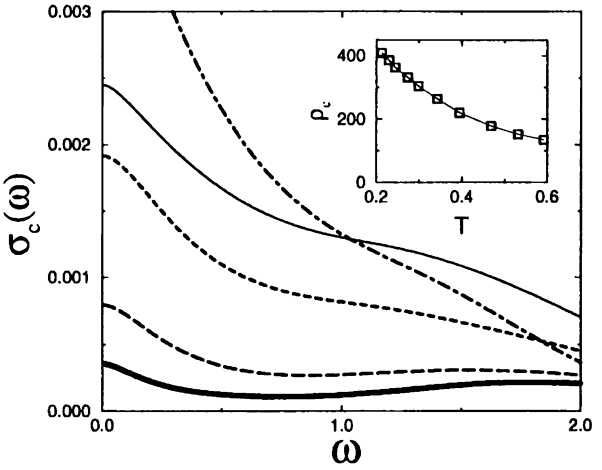

Figure 3.40: The c-axis optical conductivity due to the coherent process for $T = 0.395$ (dash-dotted line), $T = 0.213$ (thin solid line), $T = 0.20$ (dashed line), $T = 0.15$ (long-dashed line) and $T = 0.12$ (thick solid line). The Drude peak is suppressed in the pseudogap state ($T = 0.213$) and the superconducting state ($T = 0.20$,$T = 0.15$,$T = 0.12$). The inset shows the normal state c-axis resistivity ρ_c.

The calculated results are shown in Figs. 3.40 and 3.41. First, the c-axis resistivity shows a semi-conductive behavior in the pseudogap state (the inset in Fig. 3.40). This is because the scattering due to the superconducting fluctuations increases with approaching the critical point. Next, the results for the c-axis optical conductivity are shown in Fig. 3.40. The Drude peak is remarkably suppressed by the pseudogap. In other words, the coherent picture of the c-axis transport is broken by the pseudogap. In the superconducting state, the c-axis optical conductivity is suppressed furthermore and shows the gap structure at low temperatures. It should be noticed that the above results in the superconducting state are different from the expectation of the conventional d-wave BCS theory. Since the gap node does not contribute to the c-axis transport, the c-axis transport behaves like a s-wave superconductor in the ordered state.

The results for the in-plane optical conductivity are shown in Fig. 3.41. The Drude peak remains even in the deeply superconducting state and the gap structure does not appear. These

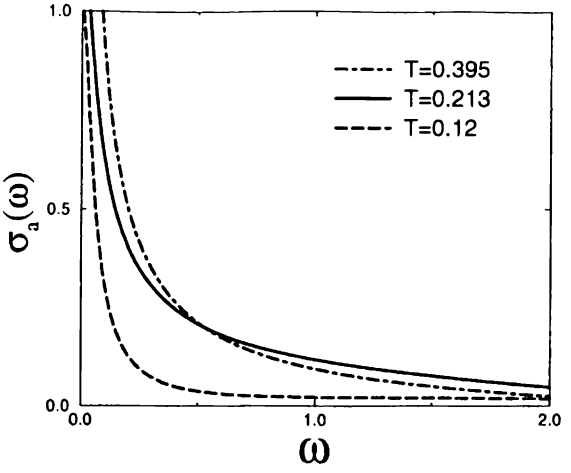

Figure 3.41: The in-plane optical conductivity in the normal state $T = 0.395$ (dash-dotted line), the pseudogap state $T = 0.213$ (solid line) and the superconducting state $T = 0.12$ (long-dashed line), respectively. The Drude peak remains in all temperature range.

features are characteristics of the d-wave superconductivity and due to the contribution from the gap node. The sharp Drude peak appears in the in-plane optical conductivity in the pseudogap state, owing to the contribution from the 'cold spot' similarly. The qualitatively different results in the c-axis transport originate in the momentum dependence of the interlayer hopping $t_\perp(\boldsymbol{k})$. Thus, the coherent in-plane transport and the incoherent c-axis transport in the pseudogap state are understood simultaneously in a consistent way.

The detailed properties of the in-plane longitudinal transport in the pseudogap state are explained by considering the feedback effect of the pseudogap on the low frequency spin fluctuations [57]. The superconducting fluctuations remarkably affects the quasi-particles near the 'hot spot'. However, these quasi-particles contribute little to the in-plane transport from the beginning. Therefore, the pseudogap affects on the in-plane transport thorough the feedback effect on the spin fluctuations. the quasi-particle damping at the 'cold spot' is caused by the low frequency part of the anti-ferromagnetic spin fluctuations. Therefore, the quasi-particle damping at the 'cold spot' is affected by the pseudogap. The in-plane resistivity slightly deviates downward owing to the feedback effect (Fig. 3.42) [57]. This behavior is observed in many under-doped compounds and the downward deviation coincides with the pseudogap [43]. The only slight deviation in the pseudogap state can not be understood by the phenomenological relation, $\rho_{\rm ab} \propto T^2\chi_{\rm s}(\boldsymbol{Q})$ or $\rho_{\rm ab} \propto T^2/(T_1T)$. Thus, the calculation appropriately treating the momentum dependence well explain the experimental results. The optical conductivity in the pseudogap state has been explained by considering the feedback effects [127].

Moreover, the behavior of the Hall coefficient is also explained by the feedback effects. The vertex correction due to the spin fluctuations plays an important role for the strong enhancement of the Hall coefficient [58, 59] The vertex correction is also reduced by the feedback effect on the spin fluctuations. Moreover, since the effects of the vertex correction is remarkable at 'hot spot' where the pseudogap is large, the pseudogap itself reduces the vertex correction. Therefore, the Hall coefficient is expected to be reduced by the pseudogap. The reduction is actually observed in the experiments [44]. The detailed calculation is an important future problem.

As we can see from Fig. 3.40, the coherent part for the c-axis transport is small in the pseu-

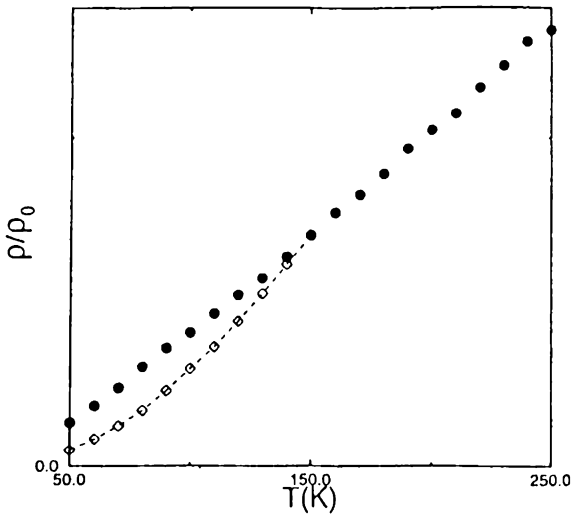

Figure 3.42: The in-plane resistivity for the under-doped cuprates. The marks • and ◇ correspond to the non-pseudogap and the pseudogap case, respectively. The pseudogap case shows a downward deviation.

dogap state. Therefore, we can not neglect the incoherent process, especially in under-doped cuprates. The tunneling process is considered to be a typical incoherent process, although there are many other incoherent processes. The contribution from the incoherent process have been discussed by Hirschfeld *et. al* [128]. According to their formalism, we obtain the following expression for the conductivity from the tunneling process $\sigma_{\rm inc}(\omega)$.

$$\sigma_{\rm inc}(\omega) = -de^2 t_{\rm inc}^2 \frac{1}{\omega} \sum_{\boldsymbol{k},\boldsymbol{k}'} \int \frac{{\rm d}\omega'}{\pi} [f(\omega'+\omega) - f(\omega')] {\rm Im} G^{\rm R}(\boldsymbol{k},\omega') {\rm Im} G^{\rm R}(\boldsymbol{k}',\omega+\omega'). \qquad (3.53)$$

Here, we have neglected the momentum dependence of the tunneling matrix element $t_{\rm inc}$ for simplicity. The above expression corresponds to the diffusive hopping process in which the information for the in-plane momentum is lost. The contribution from the anomalous Green function $F^{\rm R}(\boldsymbol{k},\omega)$ vanishes due to the d-wave symmetry.

The results are shown in Fig. 3.43. We show the results normalized by the constant factor as $\sigma_{\rm inc}(\omega) = \sigma_{\rm inc}(\omega)/\sigma_{\rm inc}^0$, where $\sigma_{\rm inc}^0 = de^2 t_{\rm inc}^2$. Here, $\sigma_{\rm inc}(\omega)$ is suppressed at the low frequency by the pseudogap and shows the weak gap structure with the energy scale of $2\Delta_{\rm eff}$. Here, $\Delta_{\rm eff}$ is the energy scale of the pseudogap. In the superconducting state, the gap structure becomes sharp, and the frequency scale of the gap does not change. This is a natural result because the same energy scale between the pseudogap and the superconducting gap is shown in the DOS (Fig. 3.31). These features are qualitatively consistent with the experimental results [46]. Thus, our scenario for the pseudogap phenomena well explains the pseudogap observed in the c-axis optical conductivity and its smooth change to the superconducting gap. Of course, the dc-conductivity from the incoherent process shows a semi-conductive behavior.

Recently, the c-axis optical conductivity has been discussed in connection with the violation of the f-sum rule [129]. The f-sum rule along the c-axis is violated in the under-doped cuprates, although it is satisfied from the over- to optimally-doped region. The violation has been attributed to the effects of the phase fluctuations [129]. Moreover, the manifestation of the quantum fluctuations has been pointed out [129]. It is natural that the quantum fluctuations develop with under-doping. However, we think that the more detailed discussion is necessary for the interpre-

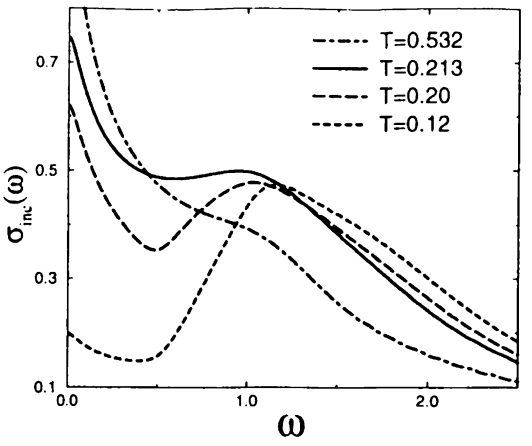

Figure 3.43: The c-axis optical conductivity due to the incoherent process for $T = 0.526$ (dash-dotted line), $T = 0.213$ (solid line), $T = 0.20$ (long-dashed line), and $T = 0.12$ (dashed line). The weak gap structure is shown in the pseudogap state. In the superconducting state, the gap becomes deep with the same energy scale.

tation of the experimental results, since the contribution from the incoherent process violates the f-sum rule easily.

3.4.3 London Penetration Depth

In this subsection, we show the results for the London penetration depth and discuss the anomalous behavior at the low temperature. The London penetration depth is related with the imaginary part of the conductivity as $1/4\pi\lambda^2 = \omega \mathrm{Im}\sigma_{\mathrm{tot}}(\omega)\ |_{\omega\to 0}$. This quantity is proportional to the superfluid density and the phase stiffness. Therefore, the London penetration depth characterizes the electrodymanics of the superconductor. Here, we calculate the London penetration depth when the system goes into the superconducting state from the pseudogap state. In other words, we investigate the properties of the superconducting transition which is suppressed by the fluctuations. Because the pseudogap exists above the critical point, we can not probe the order parameter by measuring the excitation gap. However, because the London constant characterizes the Meissner effect, the development of the order parameter is probed by the London penetration depth λ.

The expression for the London constant $1/4\pi\lambda^2$ is derived by subtracting the paramagnetic term $\propto \sum v^2(GG + FF)$ from the diamagnetic term $\propto \sum v^2(GG - FF)$. Here, the in-plane and c-axis London penetration depth is expressed as,

$$\frac{1}{4\pi\lambda_{\mathrm{ab}}^2} = 2\frac{e^2}{d}T \sum_{\boldsymbol{k},\mathrm{i}\omega_n} v^2(\boldsymbol{k})|F(\boldsymbol{k},\mathrm{i}\omega_n)|^2, \tag{3.54}$$

$$\frac{1}{4\pi\lambda_{\mathrm{c}}^2} = 8de^2T \sum_{\boldsymbol{k},\mathrm{i}\omega_n} t_\perp^2(\boldsymbol{k})|F(\boldsymbol{k},\mathrm{i}\omega_n)|^2. \tag{3.55}$$

Here, we have used the same approximation as used in §3.4.2. The contribution from the incoherent process does not exist because of the d-wave symmetry and the momentum independence of the tunneling matrix. Actually, the incoherent process contributes in the under-doped region by the momentum dependence of the tunneling matrix [128].

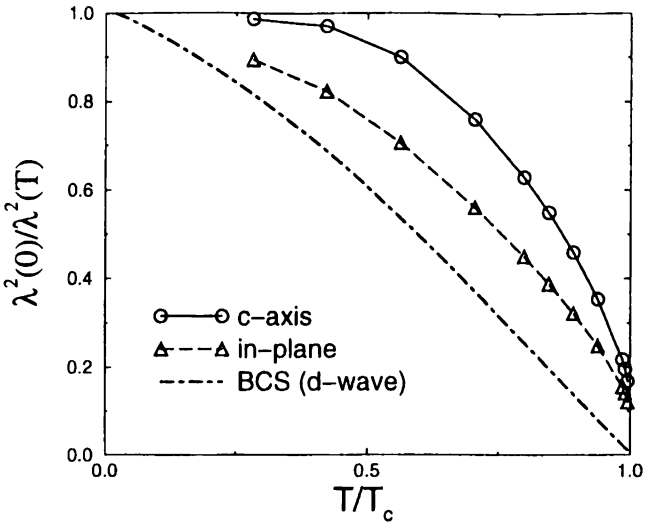

Figure 3.44: The temperature dependence of $\lambda^2(0)/\lambda^2(T)$. The open circles and the open triangles show the results along the c-axis and along the ab-axis, respectively. The dash-dotted line shows a result of the d-wave BCS theory. Here, $\lambda(0)$ is derived by the extrapolation. $1/\lambda^2(T)$ grows rapidly near T_c with the rapid growth of the order parameter. The rapid growth is more remarkable along the c-axis.

We show the temperature dependence of the in-plane and c-axis London penetration depth in Fig. 3.44. The inverse square of the London penetration depth $1/\lambda^2$ has almost linear temperature dependence within the d-wave BCS theory. The linear dependence in the low temperature region is due to the quasi-particle excitation near the gap node. Near the critical temperature T_c, the temperature dependence of the order parameter $\Delta \propto (T_c - T)^{1/2}$ causes the linear dependence in the BCS theory. Our calculation shows the more rapid increase of $1/\lambda^2$ near T_c owing to the rapid growth of the order parameter. The rapidness is more remarkable along the c-axis because the quasi-particle excitation near the gap node does not contribute. In other words, the paramagnetic current is rapidly suppressed along the c-axis. As a result, the temperature dependence of $1/\lambda_c^2$ is rather weak than that of $1/\lambda_{ab}^2$ at the low temperature. The expression of $t_\perp(\boldsymbol{k})$ in eq.(3.49) causes T^5-law, $\lambda_c^2(0)/\lambda_c^2(T) = 1 - aT^5$ in the low temperature region [130]. This behavior is qualitatively consistent with the experiment for the several under-doped or optimally-doped cuprates [130, 131]. although our calculation can not expect the precise temperature dependence near the critical point.

In this subsection, we have investigated the temperature dependence of the London constant $\Lambda(T) \propto 1/\lambda(T)^2$. We think that the low temperature behavior of the London constant is interesting as a typical problem of the superconductivity in the strongly correlated electron systems. [132, 133, 134, 135, 136] In particular, the strongly anisotropic High-T_c cuprates are expected to have the characteristic temperature and doping dependences. The Uemura plot is a typical one [132]. Moreover, the inconsistency of the value $\Lambda(0)$ at the ground state and the coefficient of the T-linear term of $\Lambda(T)$ has been pointed out [133, 134, 135]. The absolute value $\Lambda(0)$ decreases with under-doping, while the coefficient of the T-linear term is almost independent of the doping [133]. Their discussion is based on the analogy of the result for the isotropic system.

We consider that the inconsistency is understood by considering the momentum dependence of the current vertex J_ν which is remarkably anisotropic in this systems. The current vertex J_ν is renormalized by the quasi-particle mass renormalization, and includes the back flow due to the residual interaction [136, 137, 138]. The absolute value $\Lambda(0)$ is determined by the total quasi-

particles near the Fermi surface, while the T-linear term is determined by the quasi-particles near the gap node. The London constant is reduced by the mass renormalization which is is large near $(\pi, 0)$ and is small near $(\pi/2, \pi/2)$ [57]. The cancellation due to Fermi liquid effect does not occur in the anisotropic systems [136, 137, 138]. Therefore, the London constant $\Lambda(0)$ is roughly scaled by the effective Fermi energy $\varepsilon_{\rm F}$. By considering that the critical temperature $T_{\rm c}$ is also scaled by the effective Fermi energy $\varepsilon_{\rm F}$ in the strong coupling region (§3), we can understand the Uemura plot $T_{\rm c} \propto \Lambda(0)$ [21, 132] observed in the under-doped region. We consider that the vertex correction (that is to say, the Fermi liquid effects) reduces the current vertex furthermore. By considering the Bethe-Salpeter equation for the current vertex [137, 138], we can see that the current vertex is reduced by the vertex correction exchanging the anti-ferromagnetic spin fluctuations. It should be noticed that the vertex correction is different from that for calculating the Hall coefficient. The former corresponds to the non-dissipative regime and the latter corresponds to the hydrodynamic regime. The vertex correction for the London constant is related to the real part of the susceptibility $\chi_{\rm s}(\boldsymbol{q}, \omega)$, while that for the Hall coefficient is related to the imaginary part. Therefore, the correction for the London constant remains even in the superconducting state. The vertex correction is also large at 'hot spot' and small at 'cold spot'. Therefore, the Fermi liquid effect makes the system more anisotropic. As a result, the strong correlation reduces the absolute value, while the T-linear term is not reduced so much. The detailed calculation is an important future problem.

Chapter 4

Pseudogap Phenomena and Superconducting Fluctuations in Hubbard Model [28]

4.1 Introduction

In the previous chapter, the pseudogap phenomena are well explained on the basis of the resonance scattering scenario. Our calculations are based on the effective model in which the d-wave attractive interaction affects the renormalized quasi-particles [24, 25, 26, 27, 105]. The superconducting coupling has been effectively adjusted by the coupling constant $|g|$. There are two important factors in order to realize the strong coupling superconductivity in High-T_c cuprates. One is that the effective Fermi energy ε_F is renormalized by the electron-electron correlation. In this sense, the strong coupling superconductivity is a characteristic phenomenon in the strongly correlated electron systems. The other is that the high critical temperature T_c is obtained by the pairing interaction mediated by the anti-ferromagnetic spin fluctuations [7, 8]. The anti-ferromagnetic spin fluctuations also result from the strong electron-electron correlation. Thus, both factors are derived from the electron-electron correlation and should be described in a unified way.

Therefore, it is an important issue to derive the pseudogap phenomena from the model including only the on-site repulsive interaction. It should be confirmed that the superconducting coupling is strong enough to lead to the pseudogap phenomena in the under-doped region, and also that the doping dependence of the High-T_c cuprates are reproduced. In this chapter, we derive the pseudogap phenomena from the Hubbard model which is a typical model for the strongly correlated electron systems. Some authors have calculated the pseudogap phenomena by starting from the model with an repulsive interaction [103, 154, 155]. However, the sufficient results describing the pseudogap phenomena without any phenomenology have not been obtained.

In this chapter, we describe the quasi-particles in the Fermi liquid and the anti-ferromagnetic spin fluctuations by using the FLEX approximation. The characteristic momentum dependence of the quasi-particles due to the anti-ferromagnetic spin fluctuations [56, 57] are described by the FLEX approximation. The superconducting fluctuations are derived from the pairing interaction mediated by the spin fluctuations. We describe the superconducting fluctuations including the characteristic momentum and frequency dependence of the spin fluctuations. The self-energy due to the superconducting fluctuations is obtained by the one-loop approximation (T-matrix approximation). As a result, the comprehensive understanding on the basis of the resonance scattering scenario is obtained for the pseudogap phenomena. The doping dependence which

includes the electron-doped cuprates is also explained consistently.

This chapter is constructed as follows. In §4.2, we explain the Hubbard Hamiltonian and the FLEX approximation. In §4.3.1, we explain the formalism which describes the superconducting fluctuations arising from the spin fluctuations and the self-energy due to the superconducting fluctuations. In §4.3.2 the calculated results for the single particle properties are shown. In §4.3.3 we show the characteristics of the superconducting fluctuations including their doping dependence. In §4.3.4, the magnetic properties in the pseudogap state are explained. The consistent results with the NMR and the neutron scattering experiments are obtained. In §4.3.5, the theory of the superconductivity and the pseudogap phenomena is applied to the electron-doped cuprates. The relevant results including the particle-hole asymmetry are obtained. In §4.4.1, we clarify the relation between the superconducting fluctuations and the spin fluctuations in details. In §4.4.2, we show the results of the self-consistent calculation including the spin fluctuations, the superconducting fluctuations and the single particle properties. The pseudogap phenomena is derived by the superconducting fluctuations, similarly. The critical temperature reduced by the fluctuations are calculated. The appropriate phase diagram is obtained. In particular, we show that the critical temperature decreases with decreasing the doping concentration in the underdoped region. In §4.5, we summarize the obtained results in this chapter.

4.2 Hubbard Model and FLEX Approximation

First, we explain the Hubbard model and the FLEX approximation. The Hubbard model has been used for a long time as one of the typical models describing the strongly correlated electron systems. The Hamiltonian is described as,

$$H = \sum_{\boldsymbol{k},s} \varepsilon_{\boldsymbol{k}} c^{\dagger}_{\boldsymbol{k},s} c_{\boldsymbol{k},s} + U \sum_{\boldsymbol{k},\boldsymbol{k}',\boldsymbol{q}} c^{\dagger}_{\boldsymbol{q}-\boldsymbol{k}',\downarrow} c^{\dagger}_{\boldsymbol{k}',\uparrow} c_{\boldsymbol{k},\uparrow} c_{\boldsymbol{q}-\boldsymbol{k},\downarrow}. \tag{4.1}$$

The first term is the kinetic term. In this chapter, we adopt the two-dimensional dispersion relation $\varepsilon_{\boldsymbol{k}}$ given by the tight-binding model for a square lattice including the nearest- and next-nearest-neighbor hopping t, t', respectively,

$$\varepsilon_{\boldsymbol{k}} = -2t(\cos k_x + \cos k_y) + 4t' \cos k_x \cos k_y - \mu. \tag{4.2}$$

We fix $t = 0.5$, $t' = 0.25t$ and the lattice constant $a = 1$. The chemical potential μ is determined for the filling n. These parameters well reproduce the typical Fermi surface of High-T_c cuprates. We define the hole-doping concentration $\delta = 1 - n$. The main part of this chapter is concerned with the hole-doped cuprates $\delta > 0$. A brief application to the electron-doped cuprates $\delta < 0$ will be carried out in §4.3.5. The nearly half-filling systems, which are interested here, should be regarded as high-density systems. Therefore, the NSR scenario is not justified in High-T_c cuprates. The second term in eq. (4.1) expresses the on-site repulsive interaction between the electrons. All of the phenomena described in this chapter result from the electron correlation effects.

The FLEX approximation has been used in order to describe the strongly correlated electron systems near the anti-ferromagnetic instability [139]. The FLEX approximation is a conserving approximation [140] and describes the anti-ferromagnetic spin fluctuations including the mode coupling effects partly [10, 141]. It has been shown that the superconducting critical temperature with a relevant order $T_c \sim 100$K is obtained by the FLEX approximation for High-T_c cuprates [142, 143, 144, 145, 146, 147, 148]. The relevant results are also obtained for the organic superconductor κ-(BEDT-TTF) compounds [149, 150, 151] and for the ladder type compound

$Sr_{14-x}Ca_xCu_{24}O_{41}$ [152]. Moreover, the FLEX approximation is used to explain the anomalous properties resulting from the anti-ferromagnetic spin fluctuations, such as the Hall coefficient [59], the neutron resonance peak and the dip-hump structure in ARPES [117].

The self-energy given by the FLEX approximation $\Sigma_{\rm F}(\boldsymbol{k}, \mathrm{i}\omega_n)$ is expressed by the one-loop diagram exchanging the normal vertex $V_{\rm n}(\boldsymbol{q}, \mathrm{i}\Omega_n)$ (Fig. 4.1(a)).

$$\Sigma_{\rm F}(\boldsymbol{k}, \mathrm{i}\omega_n) = T \sum_{\boldsymbol{q}, \mathrm{i}\Omega_n} V_{\rm n}(\boldsymbol{q}, \mathrm{i}\Omega_n) G(\boldsymbol{k} - \boldsymbol{q}, \mathrm{i}\omega_n - \mathrm{i}\Omega_n). \tag{4.3}$$

The normal vertex is expressed as follows,

$$V_{\rm n}(\boldsymbol{q}, \mathrm{i}\Omega_n) = U^2 [\frac{3}{2} \chi_{\rm s}(\boldsymbol{q}, \mathrm{i}\Omega_n) + \frac{1}{2} \chi_{\rm c}(\boldsymbol{q}, \mathrm{i}\Omega_n) - \chi_0(\boldsymbol{q}, \mathrm{i}\Omega_n)]. \tag{4.4}$$

Here, $\chi_{\rm s}(\boldsymbol{q}, \mathrm{i}\Omega_n)$ and $\chi_{\rm c}(\boldsymbol{q}, \mathrm{i}\Omega_n)$ represent the spin and charge susceptibility, respectively,

$$\chi_{\rm s}(\boldsymbol{q}, \mathrm{i}\Omega_n) = \frac{\chi_0(\boldsymbol{q}, \mathrm{i}\Omega_n)}{1 - U\chi_0(\boldsymbol{q}, \mathrm{i}\Omega_n)}, \quad \chi_{\rm c}(\boldsymbol{q}, \mathrm{i}\Omega_n) = \frac{\chi_0(\boldsymbol{q}, \mathrm{i}\Omega_n)}{1 + U\chi_0(\boldsymbol{q}, \mathrm{i}\Omega_n)}, \tag{4.5}$$

and $\chi_0(\boldsymbol{q}, \mathrm{i}\Omega_n)$ is the irreducible susceptibility,

$$\chi_0(\boldsymbol{q}, \mathrm{i}\Omega_n) = -T \sum_{\boldsymbol{k}, \mathrm{i}\omega_n} G(\boldsymbol{k}, \mathrm{i}\omega_n) G(\boldsymbol{k} + \boldsymbol{q}, \mathrm{i}\omega_n + \mathrm{i}\Omega_n). \tag{4.6}$$

Figure 4.1: (a) The normal self-energy and (b) the anomalous self-energy obtained by the FLEX approximation.

Here, $G(\boldsymbol{k}, \mathrm{i}\omega_n)$ is the dressed Green function $G(\boldsymbol{k}, \mathrm{i}\omega_n) = (\mathrm{i}\omega_n - \varepsilon_{\boldsymbol{k}} - \Sigma_{\rm F}(\boldsymbol{k}, \mathrm{i}\omega_n))^{-1}$. The first order term in $V_{\rm n}(\boldsymbol{q}, \mathrm{i}\Omega_n)$ with respect to U is eliminated because it gives only the trivial Hartree-Fock term. In the FLEX approximation, the self-energy and the spin susceptibility are determined self-consistently. Equations (4.3-6) are self-consistently solved by the numerical calculation. In the main part of this chapter, we divide the first Brillouin zone into 64 × 64 lattice points for the numerical calculation. The spin susceptibility given by the FLEX approximation $\chi_{\rm s}(\boldsymbol{q}, \mathrm{i}\Omega_n)$ is enhanced near the anti-ferromagnetic wave vector $\boldsymbol{Q} = (\pi, \pi)$. The anti-ferromagnetic spin fluctuations described by $\chi_{\rm s}(\boldsymbol{q}, \mathrm{i}\Omega_n)$ play a dominant role in the FLEX approximation. The characteristic results of the nearly anti-ferromagnetic Fermi liquid theory [7, 8, 9, 10, 56, 57, 58, 59, 153] are qualitatively reproduced within the FLEX approximation.

The superconducting critical temperature $T_{\rm c}$ is determined as the temperature below which the linearized Dyson-Gor'kov equation has a non-trivial solution (Fig. 4.1(b)). The criterion for $T_{\rm c}$ is described by the Éliashberg equation which is the following eigenvalue equation,

$$\lambda \phi(\boldsymbol{k}, \mathrm{i}\omega_n) = -T \sum_{\boldsymbol{p}, \mathrm{i}\omega_m} V_{\rm a}(\boldsymbol{k} - \boldsymbol{p}, \mathrm{i}\omega_n - \mathrm{i}\omega_m) |G(\boldsymbol{p}, \mathrm{i}\omega_m)|^2 \phi(\boldsymbol{p}, \mathrm{i}\omega_m). \tag{4.7}$$

Here, $V_{\rm a}(\boldsymbol{q}, {\rm i}\Omega_n)$ is the anomalous vertex for the singlet channel. This is given by the FLEX approximation as follows,

$$V_{\rm a}(\boldsymbol{q}, {\rm i}\Omega_n) = U^2[\frac{3}{2}\chi_{\rm s}(\boldsymbol{q}, {\rm i}\Omega_n) - \frac{1}{2}\chi_{\rm c}(\boldsymbol{q}, {\rm i}\Omega_n)] + U. \tag{4.8}$$

The critical temperature $T_{\rm c}$ is obtained as the temperature where the maximum eigenvalue $\lambda_{\rm max}$ becomes the unity. The eigenfunction $\phi_{\rm max}(\boldsymbol{p}, {\rm i}\omega_m)$ corresponding to the eigenvalue $\lambda_{\rm max}$ is the wave function of the Cooper pairs. In this chapter, the symmetry of the superconductivity is always the $d_{x^2-y^2}$-wave.

Here, we show the typical results of the FLEX approximation in Figs. 4.2, 4.3 and 4.4. The results for the analytically continuated self-energy $\Sigma_{\rm F}^{\rm R}(\boldsymbol{k}, \omega)$ are shown in Fig. 4.2. In this chapter, the analytic continuation is carried out by using the Padé approximation. The real part ${\rm Re}\Sigma_{\rm F}^{\rm R}(\boldsymbol{k}, \omega)$ shows the negative slope and the imaginary part ${\rm Im}\Sigma_{\rm F}^{\rm R}(\boldsymbol{k}, \omega)$ has the minimum absolute value at the Fermi level. They are the characteristic features of the Fermi liquid theory which is violated in the pseudogap state (§3).

Some notable features are present in the self-energy. The imaginary part shows the ω-linear dependence near the Fermi level contrary to the ω-square dependence in the conventional Fermi liquid theory. The behavior has the same origin as that of the T-linear resistivity [56, 57]. The imaginary part at $\omega = 0$, that is the quasi-particle's damping is large near $(\pi, 0)$ ('hot spot') and is small near $(\pi/2, \pi/2)$ ('cold spot'). The above momentum dependence plays a crucial role in the coherent in-plane transport and the incoherent c-axis transport. [27, 57, 69] The renormalization factor $Z_{\boldsymbol{k}}^{-1} = 1 - \partial {\rm Re}\Sigma_{\rm F}^{\rm R}(\boldsymbol{k}, \omega)/\partial\omega$ has the same feature as the quasi-particle's damping. A lot of the low energy states near $(\pi, 0)$ arise from the Van Hove singularity and the large renormalization factor $Z_{\boldsymbol{k}}^{-1}$. The above features are the characteristics of the nearly anti-ferromagnetic Fermi liquid [7, 8, 9, 10, 56, 57, 58, 59, 153].

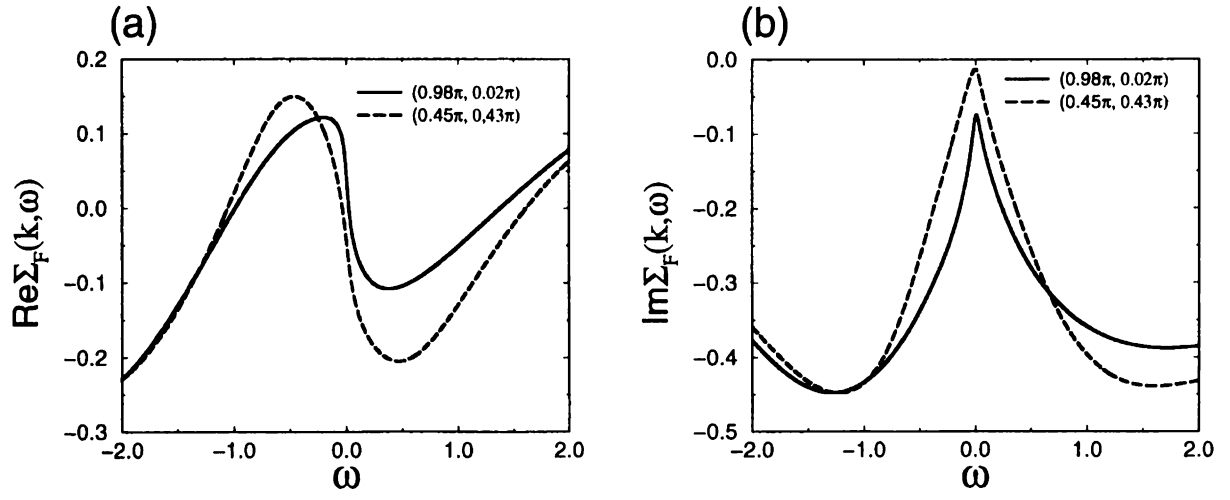

Figure 4.2: The self-energy obtained by the FLEX approximation. (a) The real part. (b) The imaginary part. Here, $U = 1.6$, $\delta = 0.095$ and $T = 0.010$. The solid line and the long-dashed line correspond to $(\frac{63}{64}\pi, \frac{1}{64}\pi)$ ('hot spot') and $(\frac{29}{64}\pi, \frac{27}{64}\pi)$ ('cold spot'), respectively.

The results for the single particle spectral weight and the DOS are shown in Fig. 4.3. In spite of the unconventional Fermi liquid behavior, the typical single peak structure appears in the

spectral weight. Thus, the picture of the quasi-particles holds in the nearly anti-ferromagnetic Fermi liquid. In particular, the pseudogap is not seen. The spectral weight is broad at the 'hot spot' and sharp at the 'cold spot' reflecting the momentum dependence of the quasi-particle's lifetime. The low energy states near $(\pi, 0)$ give the large DOS near the Fermi level. In this chapter a small constant damping is added in the self-energy when calculating the DOS in order to exclude the finite size effect. This treatment has no significant effect on the obtained results.

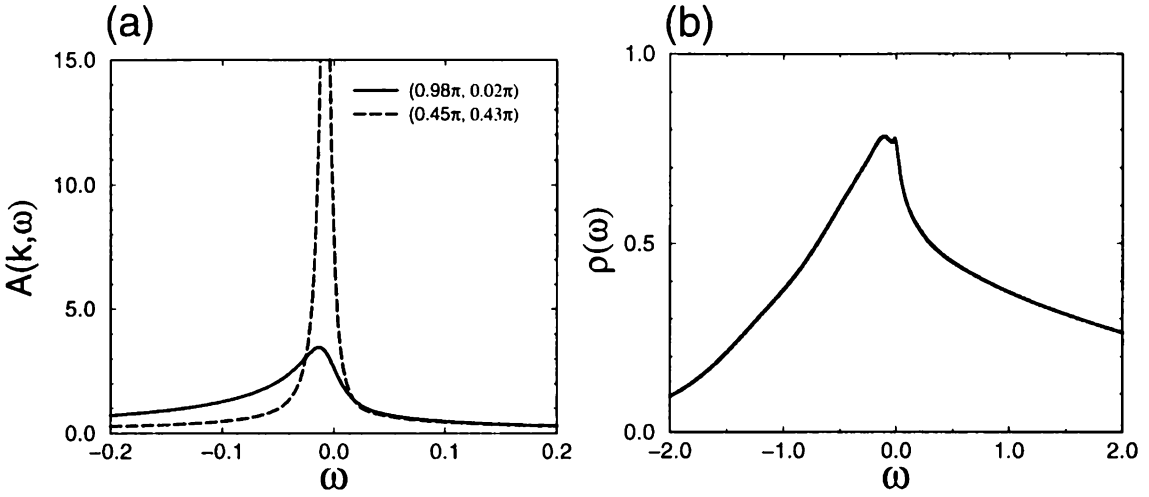

Figure 4.3: (a) The single particle spectral weight and (b) the DOS obtained by the FLEX approximation. The parameters are the same as those in the Fig. 4.2.

The obtained results for the superconducting critical temperature T_c are shown in Fig. 4.4. It is seen that the critical temperature increases with decreasing the doping concentration δ, or increasing the repulsive interaction U. In other words, the critical temperature increases with the development of the anti-ferromagnetic spin fluctuations. The critical temperature tends to be saturated in the large U and the small δ region. It is a common result of the FLEX calculation because the spin fluctuations have not only the pairing effects but also the de-pairing effects.

4.3 FLEX+T-matrix Approximation

Hereafter, we consider the superconducting fluctuations and their effects on the single particle properties and the magnetic properties. In our scenario, the superconducting fluctuations play a dominant role for the pseudogap phenomena. Therefore, we have to describe the superconducting fluctuations derived from the anomalous vertex $V_a(\boldsymbol{q}, i\Omega_n)$ given by the FLEX approximation. Although the calculation has been difficult [154], we succeed in the description fully including the momentum and frequency dependence of the anti-ferromagnetic spin fluctuations. We explain the method of the calculation bellow. The obtained results well explain the pseudogap phenomena including their doping dependence and some characteristic properties. In this section, the coupling constant U is fixed to $U = 1.6$ unless we specify.

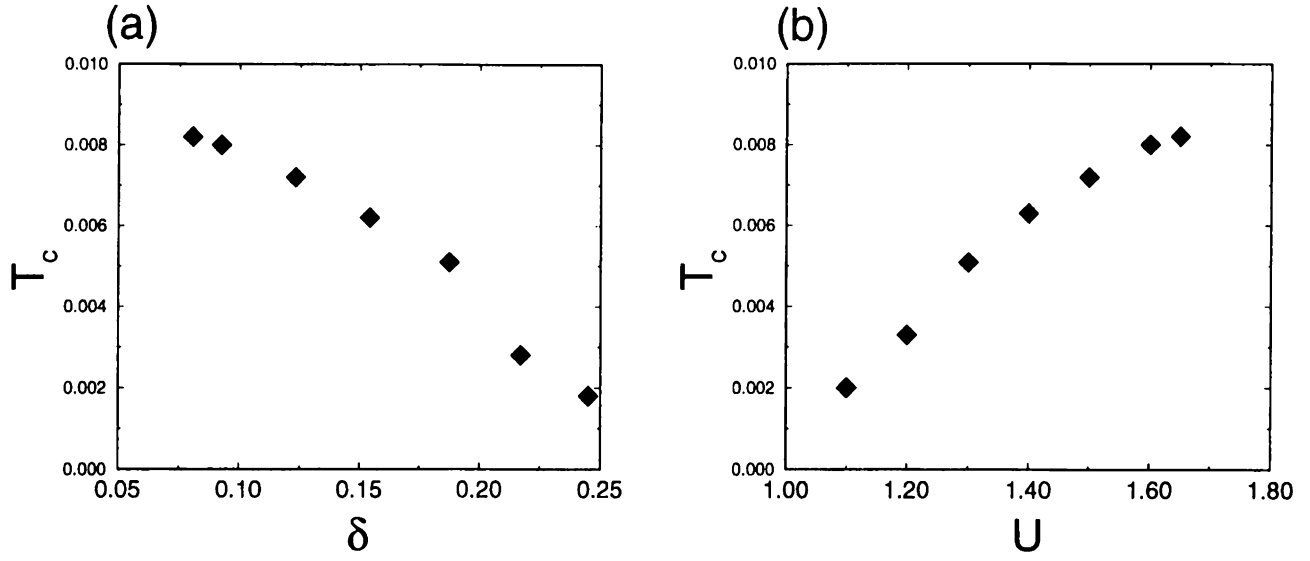

Figure 4.4: The superconducting critical temperature obtained by the FLEX approximation. (a) The doping concentration dependence for $U = 1.6$. (b) The repulsive interaction dependence for $\delta = 0.09$.

4.3.1 Formalism

First, we explain the formalism of the FLEX+T-matrix calculation which includes the effects of superconducting fluctuations within the lowest order. The superconducting fluctuations are generally represented by the T-matrix which is the propagator of the superconducting fluctuations. The T-matrix is expressed by the ladder diagrams in the particle-particle channel (Fig. 4.5 (a)) and is derived from the following Bethe-Salpeter equation.

$$\begin{aligned} T(\boldsymbol{k_1}, \mathrm{i}\omega_n : \boldsymbol{k_2}, \mathrm{i}\omega_m : \boldsymbol{q}, \mathrm{i}\Omega_n) &= V_{\mathrm{a}}(\boldsymbol{k_1} - \boldsymbol{k_2}, \mathrm{i}\omega_n - \mathrm{i}\omega_m) - T \sum_{\boldsymbol{k}, \omega_l} V_{\mathrm{a}}(\boldsymbol{k_1} - \boldsymbol{k}, \mathrm{i}\omega_n - \mathrm{i}\omega_l) \\ &\times G(\boldsymbol{k}, \mathrm{i}\omega_l) G(\boldsymbol{q} - \boldsymbol{k}, \mathrm{i}\Omega_n - \mathrm{i}\omega_l) T(\boldsymbol{k}, \mathrm{i}\omega_l : \boldsymbol{k_2}, \mathrm{i}\omega_m : \boldsymbol{q}, \mathrm{i}\Omega_n). \quad (4.9) \end{aligned}$$

Here, the pairing interaction is given by the anomalous vertex obtained by the FLEX approximation. Generally, it is difficult to solve the above integral equation except for the case where the separable pairing interaction is assumed [24, 25, 26, 27, 105]. Therefore, we carry out the following two approximations where the meaningful component as the $d_{x^2-y^2}$-wave superconducting fluctuations is properly taken out.

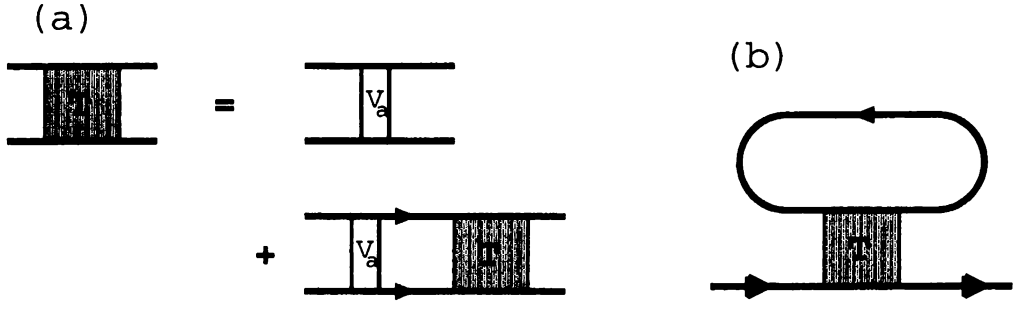

Figure 4.5: (a) The T-matrix. (b) The self-energy due to the superconducting fluctuations.

The T-matrix at $\boldsymbol{q} = \Omega_n = 0$ is approximately decomposed into the eigenfunction with their respective eigenvalues of the Éliashberg equation [155].

$$T(\boldsymbol{k}_1, \mathrm{i}\omega_n : \boldsymbol{k}_2, \mathrm{i}\omega_m : \boldsymbol{q} = \mathrm{i}\Omega_n = 0) = \sum_{\alpha} \frac{g_\alpha \phi_\alpha(\boldsymbol{k}_1, \mathrm{i}\omega_n)\phi^*_\alpha(\boldsymbol{k}_2, \mathrm{i}\omega_m)}{1 - \lambda_\alpha}. \tag{4.10}$$

The eigenvalue λ_α and the eigenfunction $\phi_\alpha(\boldsymbol{k}, \mathrm{i}\omega_n)$ are derived from the Éliashberg equation, eq. (4.7). The index α denotes each mode included in the T-matrix. Here, we take out the component with the maximum eigenvalue $\lambda_{\max}$ and the corresponding eigenfunction $\phi_{\max}$ which has the $d_{x^2-y^2}$-wave character. As is understood by considering that the superconducting transition is determined by the condition $\lambda_{\max} = 1$, the mode described by $\lambda_{\max}$ and $\phi_{\max}$ represents the $d_{x^2-y^2}$-wave superconducting fluctuations. The function $\phi_{\max}$ is the wave function of the fluctuating Cooper pairs in the fluctuating regime. Hereafter, we neglect the other modes since they have no significant effect on the superconducting fluctuations. Therefore, we neglect the index 'max' for simplicity. The approximation is justified when the superconducting fluctuations is strong. By using the above approximation, the T-matrix is expressed by the following equations [154].

$$T(\boldsymbol{k}_1, \mathrm{i}\omega_n : \boldsymbol{k}_2, \mathrm{i}\omega_m : \boldsymbol{q}, \mathrm{i}\Omega_n) = \frac{g(\boldsymbol{q}, \mathrm{i}\Omega_n)\phi(\boldsymbol{k}_1, \mathrm{i}\omega_n : \boldsymbol{q}, \mathrm{i}\Omega_n)\phi^*(\boldsymbol{k}_2, \mathrm{i}\omega_m : \boldsymbol{q}, \mathrm{i}\Omega_n)}{1 - \lambda(\boldsymbol{q}, \mathrm{i}\Omega_n)}. \tag{4.11}$$

The function $\lambda(\boldsymbol{q}, \mathrm{i}\Omega_n)$ is given by the maximum eigenvalue and $\phi(\boldsymbol{k}, \mathrm{i}\omega_n : \boldsymbol{q}, \mathrm{i}\Omega_n)$ is the corresponding eigenfunction of the following equation,

$$\begin{aligned}\lambda(\boldsymbol{q}, \mathrm{i}\Omega_n)\phi(\boldsymbol{k}, \mathrm{i}\omega_n : \boldsymbol{q}, \mathrm{i}\Omega_n) = & -T \sum_{\boldsymbol{p}, \mathrm{i}\omega_m} V_{\mathrm{a}}(\boldsymbol{k} - \boldsymbol{p}, \mathrm{i}\omega_n - \mathrm{i}\omega_m) \\ & G(\boldsymbol{p}, \mathrm{i}\omega_m)G(\boldsymbol{q} - \boldsymbol{p}, \mathrm{i}\Omega_n - \mathrm{i}\omega_m)\phi(\boldsymbol{p}, \mathrm{i}\omega_m : \boldsymbol{q}, \mathrm{i}\Omega_n).\end{aligned} \tag{4.12}$$

The function $1 - \lambda(\boldsymbol{q}, \mathrm{i}\Omega_n)$ describes the dispersion relation of the fluctuating Cooper pairs. In the above expression, the wave function is normalized as, $\sum_{\boldsymbol{k}, \mathrm{i}\omega_n} |\phi(\boldsymbol{k}, \mathrm{i}\omega_n : \boldsymbol{q}, \mathrm{i}\Omega_n)|^2 = 1$, and the coupling constant is given as, $g(\boldsymbol{q}, \mathrm{i}\Omega_n) = \sum_{\boldsymbol{k}_1, \mathrm{i}\omega_n} \sum_{\boldsymbol{k}_2, \mathrm{i}\omega_m} \phi^*(\boldsymbol{k}_1, \mathrm{i}\omega_n : \boldsymbol{q}, \mathrm{i}\Omega_n) V_{\mathrm{a}}(\boldsymbol{k}_1 - \boldsymbol{k}_2, \mathrm{i}\omega_n - \mathrm{i}\omega_m)\phi(\boldsymbol{k}_2, \mathrm{i}\omega_m : \boldsymbol{q}, \mathrm{i}\Omega_n)$.

Here, we perform one more approximation. We neglect the q- and Ω_n dependence of the eigenfunction $\phi(\boldsymbol{k}, \mathrm{i}\omega_n : \boldsymbol{q}, \mathrm{i}\Omega_n)$. The wave function is fixed to that at $q = \Omega_n = 0$. This approximation is well justified because the region around $q = \Omega_n = 0$ gives the dominant contribution as an effect of the superconducting fluctuations. Actually, the main q- and Ω_n dependence of the eigenvalue $\lambda(\boldsymbol{q}, \mathrm{i}\Omega_n)$ is derived from the differential of the Green function $G(\boldsymbol{q} - \boldsymbol{p}, \mathrm{i}\Omega_n - \mathrm{i}\omega_m)$ in eq. (4.12). In other words, the dispersion of the fluctuating Cooper pairs, $1 - \lambda(\boldsymbol{q}, \mathrm{i}\Omega_n)$ is insensitive to the change of the eigenfunction. It should be noticed that the wave function $\phi(\boldsymbol{k}, \mathrm{i}\omega_n : \boldsymbol{q}, \mathrm{i}\Omega_n)$ is independent of q and Ω_n when the separable paring interaction is considered (§3).

We have explicitly solved the eigenvalue equation (eq. (4.12)) and confirmed that the q- and Ω_n dependence of the eigenfunction $\phi(\boldsymbol{k}, \mathrm{i}\omega_n : \boldsymbol{q}, \mathrm{i}\Omega_n)$ is small in the region where the dominant contribution to the self-energy is yielded. In particular, it is confirmed that the value $1 - \lambda(\boldsymbol{q}, \mathrm{i}\Omega_n)$ is found within the error of 10-20 par cent by the above approximation. Thus, the second approximation only slightly underestimates the eigenvalue $\lambda(\boldsymbol{q}, \mathrm{i}\Omega_n)$ around $q = \Omega_n = 0$, since the precise eigenfunction is determined so as to optimize the eigenvalue. Needless to say, the precise eigenvalue is obtained at $q = \Omega_n = 0$. In other wards, the TDGL parameter (see eq. (4.18)) b is overestimated by the second approximation whereas t_0 is obtained precisely. The approximation slightly underestimates the effects of the superconducting fluctuations. Since the approximation is not precise for large q and Ω_n, the unphysical contribution to the self-energy is caused. Therefore, we eliminate the q- and Ω_n independent term $g\phi(\boldsymbol{k}_1, \mathrm{i}\omega_n)\phi^*(\boldsymbol{k}_2, \mathrm{i}\omega_m)$ in the T-matrix.

By using the above two approximations, the T-matrix is expressed as follows,

$$T(\boldsymbol{k}_1, \mathrm{i}\omega_n : \boldsymbol{k}_2, \mathrm{i}\omega_m : \boldsymbol{q}, \mathrm{i}\Omega_n) = \frac{g\lambda(\boldsymbol{q}, \mathrm{i}\Omega_n)\phi(\boldsymbol{k}_1, \mathrm{i}\omega_n)\phi^*(\boldsymbol{k}_2, \mathrm{i}\omega_m)}{1 - \lambda(\boldsymbol{q}, \mathrm{i}\Omega_n)}, \tag{4.13}$$

where

$$\lambda(\boldsymbol{q}, \mathrm{i}\Omega_n) = -T \sum_{\boldsymbol{k}, \mathrm{i}\omega_n} \sum_{\boldsymbol{p}, \mathrm{i}\omega_m} \phi^*(\boldsymbol{k}, \mathrm{i}\omega_n) V_{\mathrm{a}}(\boldsymbol{k} - \boldsymbol{p}, \mathrm{i}\omega_n - \mathrm{i}\omega_m) G(\boldsymbol{p}, \mathrm{i}\omega_m) G(\boldsymbol{q} - \boldsymbol{p}, \mathrm{i}\Omega_n - \mathrm{i}\omega_m) \phi(\boldsymbol{p}, \mathrm{i}\omega_m). \tag{4.14}$$

Here, the coupling constant g is defined as,

$$g = \sum_{\boldsymbol{k}_1, \mathrm{i}\omega_n} \sum_{\boldsymbol{k}_2, \mathrm{i}\omega_m} \phi^*(\boldsymbol{k}_1, \mathrm{i}\omega_n) V_{\mathrm{a}}(\boldsymbol{k}_1 - \boldsymbol{k}_2, \mathrm{i}\omega_n - \mathrm{i}\omega_m) \phi(\boldsymbol{k}_2, \mathrm{i}\omega_m), \tag{4.15}$$

and the wave function is normalized as,

$$\sum_{\boldsymbol{k}, \mathrm{i}\omega_n} |\phi(\boldsymbol{k}, \mathrm{i}\omega_n)|^2 = 1. \tag{4.16}$$

By taking out the freedom of the superconducting fluctuations, we obtain the pair susceptibility, $t(\boldsymbol{q}, \mathrm{i}\Omega_n) = g/(1 - \lambda(\boldsymbol{q}, \mathrm{i}\Omega_n))$ which we have termed the T-matrix in the previous chapter §3.

The self-energy due to the superconducting fluctuations is given by the one-loop diagram in the T-matrix approximation (Fig. 4.5(b)).

$$\Sigma_{\mathrm{S}}(\boldsymbol{k}, \mathrm{i}\omega_n) = T \sum_{\boldsymbol{q}, \mathrm{i}\Omega_n} T(\boldsymbol{k}, \mathrm{i}\omega_n : \boldsymbol{k}, \mathrm{i}\omega_n : \boldsymbol{q}, \mathrm{i}\Omega_n) G(\boldsymbol{q} - \boldsymbol{k}, \mathrm{i}\Omega_n - \mathrm{i}\omega_n). \tag{4.17}$$

In this section, we use the Green function determined by the FLEX approximation $G_{\mathrm{F}}(\boldsymbol{k}, \mathrm{i}\omega_n) = (\mathrm{i}\omega_n - \varepsilon_{\boldsymbol{k}} - \Sigma_{\mathrm{F}}(\boldsymbol{k}, \mathrm{i}\omega_n))^{-1}$ in calculating eqs. (4.13-17). That is to say, we calculate the lowest order correction due to the superconducting fluctuations on the FLEX approximation. We call the calculation FLEX+T-matrix approximation. The self-energy is determined by the summation, $\Sigma(\boldsymbol{k}, \mathrm{i}\omega_n) = \Sigma_{\mathrm{F}}(\boldsymbol{k}, \mathrm{i}\omega_n) + \Sigma_{\mathrm{S}}(\boldsymbol{k}, \mathrm{i}\omega_n)$. We show the results of the FLEX+T-matrix approximation in the following subsections. Since the calculation is carried out with the fixed chemical potential μ, the doping concentration δ decreases with decreasing the temperature T. However, the difference is smaller than 0.01 and has no significant effect.

In §4.4, we carry out the self-consistent calculation in which the fully dressed Green function $G(\boldsymbol{k}, \mathrm{i}\omega_n) = (\mathrm{i}\omega_n - \varepsilon_{\boldsymbol{k}} - \Sigma_{\mathrm{F}}(\boldsymbol{k}, \mathrm{i}\omega_n) - \Sigma_{\mathrm{S}}(\boldsymbol{k}, \mathrm{i}\omega_n))^{-1}$ is used everywhere. As a result of the self-consistency, the effect of the superconducting fluctuations are reduced. However, the qualitatively similar conclusions are obtained.

4.3.2 Pseudogap in the single particle properties

In this subsection the pseudogap, which is the main subject of this thesis, is derived. The calculated results well justify the pairing scenario based on the self-energy correction due to the superconducting fluctuations [24, 88]. On the basis of the model with a d-wave attractive interaction, it has been shown that the anomalous properties of the self-energy give rise to the pseudogap (§3.1). The characteristics of the self-energy leading to the pseudogap is that the real part has the positive slope and the imaginary part has the maximum absolute value at the Fermi level

$\omega = 0$. They are anomalous compared with the typical behavior in the Fermi liquid theory. The large imaginary part reduces the single particle spectral weight at the Fermi level and gives rise to pseudogap. The anomalous features seem to compete with the Fermi liquid behavior obtained by the FLEX calculations. In particular, the negative slope of the real part which is related to the renormalization factor Z_k^{-1} is generally increased by the strong electron correlation. However, the calculated results clearly show the important mechanism of the pseudogap formation in the strongly correlated electron systems. We show the obtained results for the analytically continuated self-energy $\Sigma^{\mathrm{R}}(\boldsymbol{k},\omega)$ in Fig. 4.6. Here, the doping concentration corresponds to the under-doped cuprates.

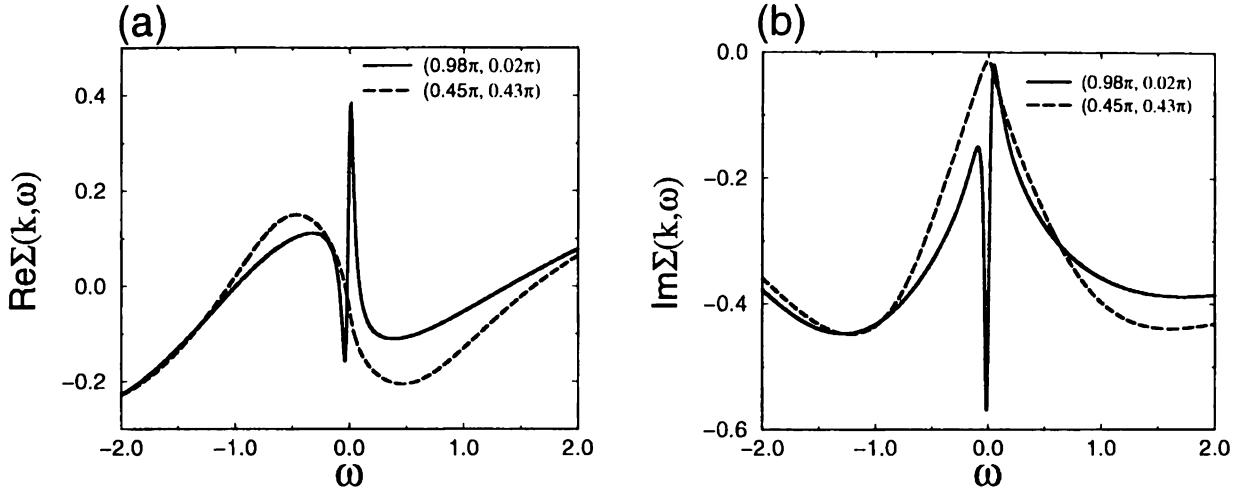

Figure 4.6: The self-energy obtained by the FLEX+T-matrix approximation. (a)The real part. (b) The imaginary part. Here, $U = 1.6$, $\delta = 0.095$ and $T = 0.010$. The solid line and the long-dashed line correspond to $(\frac{63}{64}\pi, \frac{1}{64}\pi)$ (hot spot) and $(\frac{29}{64}\pi, \frac{27}{64}\pi)$ (cold spot), respectively.

It should be noticed that the Fermi liquid behavior is seen when we look with the large energy scale $\omega \sim 0.5$. However, the anomalous behavior leading to the pseudogap is clearly seen in much smaller energy scale $\omega \sim 0.05$. The anomalous behavior vanishes around $(\pi/2, \pi/2)$ because of the $d_{x^2-y^2}$ wave symmetry of the fluctuating Cooper pairs.

It is the important point that the superconductivity and the pseudogap take place in the renormalized quasi-particles which have the small energy scale compared to the original band width. In other words, the pseudogap occurs with the much smaller energy scale than that of the electron systems. The above results clearly show the small energy scale and justify the calculation based on the model in which a d-wave attractive interaction acts on the renormalized quasi-particles. The superconducting fluctuations give the sufficiently strong effects on the low-energy quasi-particles and give rise to the pseudogap phenomena.

The results for the spectral weight are shown in Fig. 4.7. The pseudogap clearly appears in the single particle spectral weight (Fig. 4.7(a)) and the DOS (Fig. 4.7(b)). It is notable that the pseudogap is derived from the self-energy correction due to the superconducting fluctuations which are enhanced by the strong coupling superconductivity and the quasi-two dimensionality (§3). The ω-dependence of the wave function furthermore advances the pseudogap formation. Thus, our scenario based on the resonance scattering scenario is justified for the pseudogap phenomena. The $d_{x^2-y^2}$-wave form of the pseudogap is naturally obtained by the $d_{x^2-y^2}$-wave symmetry of the

superconducting fluctuations. The inset of Fig. 4.8 shows the much smaller energy scale of the pseudogap compared with the band width.

Moreover, the energy scale of the pseudogap is consistent with that of the superconducting gap. The experimental results show that the energy scale of the pseudogap is nearly the same as that of the superconducting gap [22, 23, 49]. That has been confirmed by the calculations in §3.3. The ratio $2\Delta_s/T_c \sim 12$ is obtained by the FLEX approximation in the optimally-doped region [117]. Here, Δ_s is the maximum value of the gap function in the ordered state. The larger ratio is expected in the under-doped region. Our results for the under-doped cuprates show the ratio $2\Delta_{pg}/T_c \sim 20$ (Fig. 4.7(a)). Here Δ_{pg} is the energy scale of the pseudogap. Thus, the pseudogap obtained by our calculation seems to have the relevant energy scale compared to the superconducting gap.

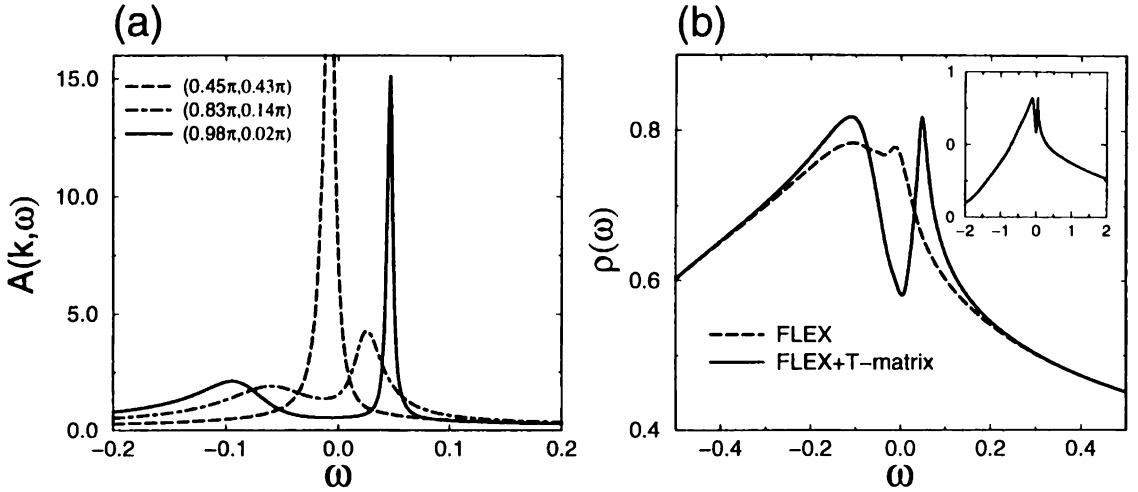

Figure 4.7: (a)The single particle spectral weight obtained by the FLEX+T-matrix approximation. The solid and long-dashed lines correspond to those in Fig. 4.6, respectively. The dash-dotted line corresponds to $(\frac{53}{64}\pi, \frac{9}{64}\pi)$. (b) The DOS obtained by the FLEX (long-dashed line) and the FLEX+T-matrix (solid line) approximations. The inset is the same result shown in the large frequency scale. The other parameters are the same as those in Fig. 4.6.

We show the detailed results for the DOS in Fig. 4.8. We choose the temperature $T = 1.25T_c$ in all figures of Fig. 4.8 in order to fix the distance to the critical point. The doping dependence is shown in Fig. 4.8(a). It is shown that the pseudogap becomes weak with increasing the hole-doping. The gap structure is filled up and the DOS near the Fermi level increases in the optimally-doped region. The effects of the superconducting fluctuations almost disappear in the over-doped region $\delta > 0.2$.

This is because both the critical temperature and the renormalization of the quasi-particles are reduced by the hole-doping. Since the ratio T_c^{MF}/ε_F decreases, the superconducting coupling is reduced. Therefore, the effects of the superconducting fluctuations are reduced. The above results justify our understanding for the phase diagram of High-T_c cuprates. It should be noticed that the pseudogap becomes well-defined near the optimally-doping $\delta \sim 0.15$. Thus, the pairing scenario properly explains the pseudogap in High-T_c cuprates including their doping dependence.

Here, the importance of the strong correlation is shown in Fig. 4.8(b). It is shown that the pseudogap becomes remarkable by increasing U. The reason is the same as that in the expla-

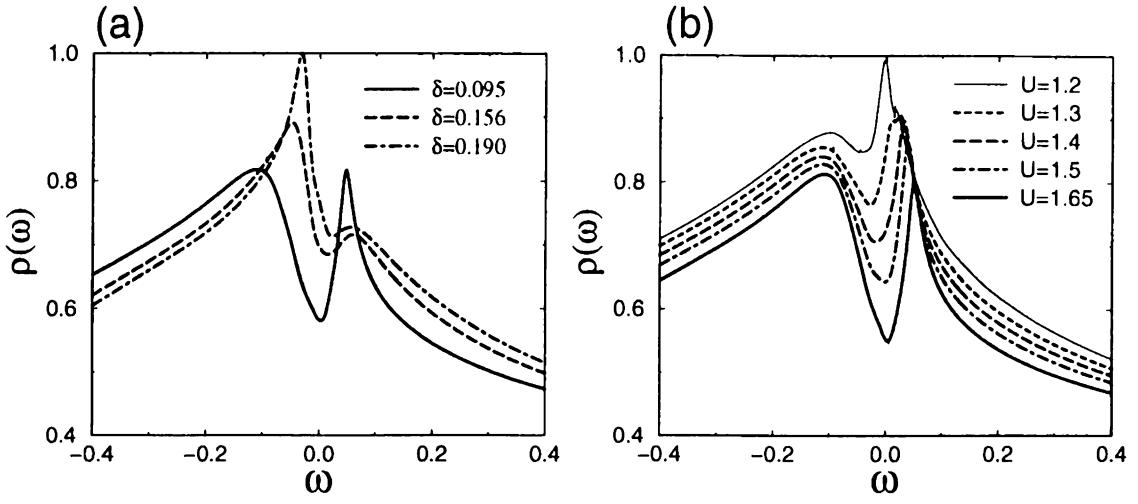

Figure 4.8: (a) The doping dependence of the DOS obtained by the FLEX+T-matrix approximation. The solid, long-dashed and dash-dotted lines correspond to $\delta = 0.095$, 0.156 and 0.190, respectively. (b) The density of state for the various strength of U. The thin solid, dashed, long-dashed, dash-dotted and thick solid lines correspond to $U = 1.2$, 1.3, 1.4, 1.5 and 1.65, respectively. In all figures, the temperature is chosen as $T = 1.25T_c$.

nation for Fig. 4.8(a). Thus, the strong coupling superconductivity, the strong superconducting fluctuations and the resultant pseudogap are the characteristics of the strongly correlated electron systems.

4.3.3 Superconducting fluctuations

Here, we discuss the character of the superconducting fluctuations in order to emphasize the importance of the strong coupling superconductivity.

In our pervious chapter describing the mechanism of the pseudogap, the TDGL expansion is used for the pair susceptibility as follows,

$$t(\boldsymbol{q},\omega) = \frac{g}{t_0 + b\boldsymbol{q}^2 - (a_1 + \mathrm{i}a_2)\Omega}, \tag{4.18}$$

where the factors arising from the wave function $\phi(\boldsymbol{k}, \mathrm{i}\omega_n)$ are neglected, namely $t(\boldsymbol{q}, \mathrm{i}\Omega_n) = \frac{g}{1-\lambda(\boldsymbol{q},\mathrm{i}\Omega_n)}$. In the notation of this chapter, the TDGL expansion corresponds to the expansion for the eigenvalue function $\lambda(\boldsymbol{q}, \Omega)$ as $1 - \lambda(\boldsymbol{q}, \Omega) = t_0 + b\boldsymbol{q}^2 - (a_1 + \mathrm{i}a_2)\Omega$.

The TDGL expansion parameters describe the character of the superconducting fluctuations. The detailed properties of the TDGL parameters are discussed in §3.1.1. Here, we discuss the TDGL parameters on the basis of the calculated results in this chapter. It is confirmed that the strong coupling superconductivity is realized as a result of the strong electron correlation.

The parameter $t_0 = 1-\lambda(\boldsymbol{0}, 0)$ represents the distance to the phase transition, and is sufficiently small near T_c. The parameter a_2 expresses the time scale of the fluctuations. The parameter a_1 is usually neglected within the weak coupling theory because it is higher order than a_2 with respect to the superconducting coupling T_c^{MF}/ε_F. However, the parameter a_1 has a significant effect in the strong coupling case §3.

The calculated results show that the sign of a_1 is negative in under-doped cuprates. This means the hole-like character of the superconducting fluctuations. The sign of a_1 which is determined

by the particle-hole asymmetry determines the sign of the fluctuating Hall conductivity [99]. The Hall anomaly [87] is phenomenologically explained by assuming the existence of the electron-like pre-formed pairs [84]. However, it has been pointed out in §3 that the explanation is not justified within the theory of the strong coupling superconductivity. It is confirmed in this chapter that the character of the superconducting fluctuations is not electron-like but hole-like in the under-doped region.

The effect of a_1 manifests in the particle-hole asymmetry of the pair susceptibility $t(\mathbf{0}, \Omega)$. It has been pointed out that the pair susceptibility can be measured by the pair tunneling current [106]. Although Ref. 106 shows the electron-like asymmetry on the basis of the electron gas model, the hole-like asymmetry should be measured in reality (see §3.1.5). The calculated results show that the asymmetry becomes strong with decreasing the doping concentration.

The parameter b represents the dispersion relation of the fluctuations and is related to the superconducting coherence length ξ_0, $b \propto \xi_0^2$. The small b generally means the strong superconducting fluctuations. Therefore, we show the results for the TDGL parameter b in Fig. 4.9.

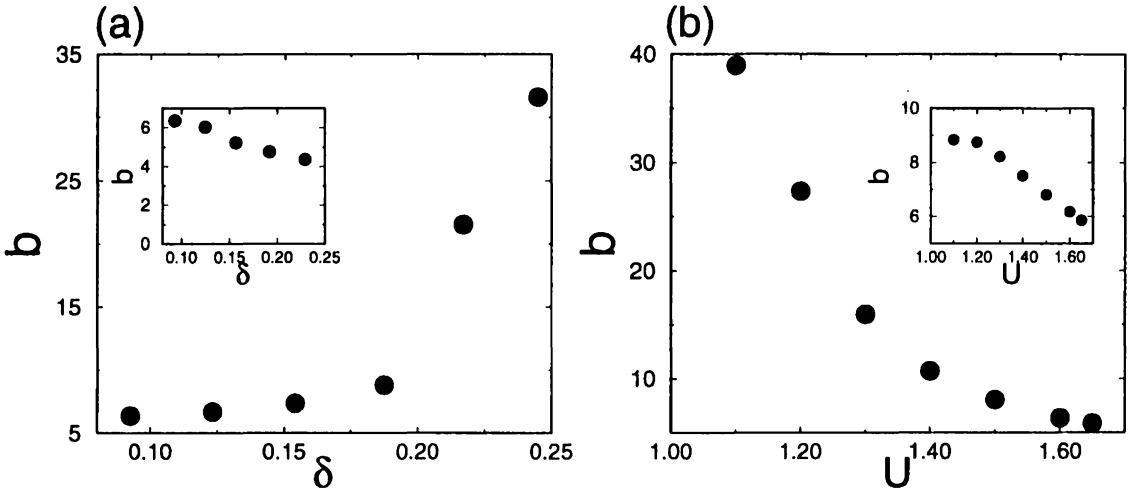

Figure 4.9: (a) The doping dependence of the TDGL parameter b at the critical point $T = T_c$. Here, the coupling constant is fixed to $U = 1.6$. The inset shows the same quantity at the fixed temperature $T = 0.0080$ (b) The TDGL parameter b for the various strength of U at $T = T_c$. Here the doping concentration is fixed to $\delta = 0.09$. The inset shows the same quantity at the fixed temperature $T = 0.0082$

The TDGL parameter b is expressed by the Fermi liquid description within the weak coupling theory as $b = g_d \tilde{\rho}_d(0) \frac{7\zeta(3)}{32\pi^2} \frac{\bar{v}_F^2}{T^2}$. Here, g_d is the d-wave component of the residual interaction $Z_k V_a(\boldsymbol{k} - \boldsymbol{k}') Z_{k'}$, namely $g_d = \sum_{\boldsymbol{k},\boldsymbol{k}'} \phi_d(\boldsymbol{k}) Z_k V_a(\boldsymbol{k} - \boldsymbol{k}') Z_{k'} \phi_d^*(\boldsymbol{k}')$. The effective density of state of the quasi-particles $\tilde{\rho}_d(\varepsilon)$ is defined as $\tilde{\rho}_d(\varepsilon) = \sum_{\boldsymbol{k}} \delta(\varepsilon - E_{\boldsymbol{k}}) |\phi_d(\boldsymbol{k})|^2$, which is enhanced by the renormalization. Here, $E_{\boldsymbol{k}}$ is the quasi-particle's energy $E_{\boldsymbol{k}} = Z_k(\varepsilon_{\boldsymbol{k}} + \mathrm{Re}\Sigma^R(\boldsymbol{k}, 0))$. The $\bar{v}_F$ is the effective Fermi velocity for the d-wave symmetry. This is defined as $\bar{v}_F^2 = \int_F \tilde{\rho}_{k_F} \tilde{v}(k_F)^2 dk_F / \tilde{\rho}_d(0)$, where the integration is carried out on the Fermi surface and $\tilde{\rho}_{k_F} = |\phi_d(k_F)|^2 / \tilde{v}(k_F)$. The velocity $\tilde{v}(k_F)$ is the absolute value of the quasi-particle's velocity $\tilde{\boldsymbol{v}}_{\boldsymbol{k}} = dE_{\boldsymbol{k}}/d\boldsymbol{k}$ on the Fermi surface. It should be noticed that the quasi-particle's velocity is reduced by the renormalization, especially around $(\pi, 0)$. Since the effective Fermi velocity $\bar{v}_F$ is mainly determined by the region around $(\pi, 0)$, $\bar{v}_F$ is remarkably reduced by the electron correlation.

It should be noticed that the TDGL parameter b is proportional to $\bar{v}_{\rm F}^2/T^2$, which is proportional to the inverse square of the superconducting coupling $T_{\rm c}^{\rm MF}/\varepsilon_{\rm F}$. That is to say, the TDGL parameter b decreases with increasing the superconducting coupling. We can see in Fig. 4.9 that the TDGL parameter b decreases with under-doping and/or with increasing U. It is because the critical temperature $T_{\rm c}$ increases and the renormalization for the effective Fermi velocity $\bar{v}_{\rm F}$ becomes remarkable. These effects reduce the TDGL parameter b in spite of the increasing coupling constant $g_{\rm d}\hat{\rho}_{\rm d}(0)$. The effects of the quasi-particle's renormalization is confirmed by showing the results at the fixed temperature. (see the inset in Fig. 4.9(b).) Although the coupling constant $g_{\rm d}\hat{\rho}_{\rm d}(0)$ increases and T is fixed, the parameter b decreases with increasing U. This is because the effective Fermi velocity $\bar{v}_{\rm F}$ is reduced. Thus, the superconductivity becomes strong coupling one and the pseudogap phenomena appear when the electron correlation is strong. The results clearly justify the doping dependence in our scenario for the pseudogap phenomena.

4.3.4 Magnetic properties

In this subsection, we show the results for the magnetic properties which are measured by NMR, neutron scattering and so on. The anti-ferromagnetic spin fluctuations are one of the important characters of High-$T_{\rm c}$ cuprates. The development of the spin fluctuations are well described by the FLEX approximation. One the other hand, the suppression of the low frequency spin fluctuations have been pointed out by NMR measurements [30, 31, 32, 33, 34, 35, 36]. The phenomena have been called 'spin gap' at an initial stage. At present, it is known that not only the spin channel but also the single particle properties show the gap-like features [22, 23, 49]. Therefore, the 'spin gap' is considered to be a result of the gap formation in the single particle properties, namely 'pseudogap'. In this chapter, the pseudogap in the magnetic properties are well explained by considering the effects of the superconducting fluctuations on the single particle properties.

In the FLEX+T-matrix approximation, the spin susceptibility $\chi_{\rm s}(\boldsymbol{q},\Omega)$ is obtained by extending the FLEX approximation,

$$\chi_{\rm s}^{\rm R}(\boldsymbol{q},\Omega) = \frac{\chi_0^{\rm R}(\boldsymbol{q},\Omega)}{1-U\chi_0^{\rm R}(\boldsymbol{q},\Omega)}, \tag{4.19}$$

$$\chi_0(\boldsymbol{q},{\rm i}\Omega_n) = -T\sum_{\boldsymbol{k},{\rm i}\omega_n} G(\boldsymbol{k},{\rm i}\omega_n)G(\boldsymbol{k}+\boldsymbol{q},{\rm i}\omega_n+{\rm i}\Omega_n), \tag{4.20}$$

where the Green function $G(\boldsymbol{k},{\rm i}\omega_n) = ({\rm i}\omega_n - \varepsilon_{\boldsymbol{k}} - \Sigma_{\rm F}(\boldsymbol{k},{\rm i}\omega_n) - \Sigma_{\rm S}(\boldsymbol{k},{\rm i}\omega_n))^{-1}$. The effects of the superconducting fluctuations are included in the self-energy, $\Sigma_{\rm S}(\boldsymbol{k},{\rm i}\omega_n)$.

The NMR spin-lattice relaxation rate $1/T_1$ and spin-echo decay rate $1/T_{2\rm G}$ are obtained by the following formula.

$$1/T_1T = \sum_{\boldsymbol{q}} F_\perp(\boldsymbol{q})[\frac{1}{\omega}{\rm Im}\chi_{\rm s}^{\rm R}(\boldsymbol{q},\omega)\mid_{\omega\to 0}], \tag{4.21}$$

$$1/T_{2G}^2 = \sum_{\boldsymbol{q}}[F_\parallel(\boldsymbol{q}){\rm Re}\chi_{\rm s}^{\rm R}(\boldsymbol{q},0)]^2 - [\sum_{\boldsymbol{q}} F_\parallel(\boldsymbol{q}){\rm Re}\chi_{\rm s}^{\rm R}(\boldsymbol{q},0)]^2. \tag{4.22}$$

Here, $F_\perp(\boldsymbol{q}) = \frac{1}{2}[\{A_1+2B(\cos q_x+\cos q_y)\}^2 + \{A_2+2B(\cos q_x+\cos q_y)\}^2]$ and $F_\parallel(\boldsymbol{q}) = \{A_2+2B(\cos q_x+\cos q_y)\}^2$. The hyperfine coupling constants A_1, A_2 and B are evaluated as $A_1 = 0.84B$ and $A_2 = -4B$ [112].

The calculated results for the NMR $1/T_1T$, $1/T_{2\rm G}$ and the static spin susceptibility are shown in Fig. 4.10. The results show the pseudogap in the NMR $1/T_1T$ (Fig. 4.10(a)). In the FLEX

calculation, the NMR $1/T_1T$ increases with decreasing the temperature owing to developing the spin fluctuations. (see the inset in Fig 10(a).) In the FLEX+T-matrix calculation, the NMR $1/T_1T$ increases with decreasing the temperature from high temperature, shows its peak at T^* and decreases with decreasing the temperature. This decrease above the critical point $T = T_c$ is the well-known pseudogap in NMR measurements. This phenomenon is caused by the superconducting fluctuations. Since the DOS is reduced by the superconducting fluctuations, the low frequency spin fluctuations are suppressed as a result. Since the NMR $1/T_1T$ measures the low frequency component of the spin fluctuations, $1/T_1T$ decreases with approaching the critical point. Thus, the pseudogap observed in NMR $1/T_1T$ takes place through the pseudogap in the single particle states.

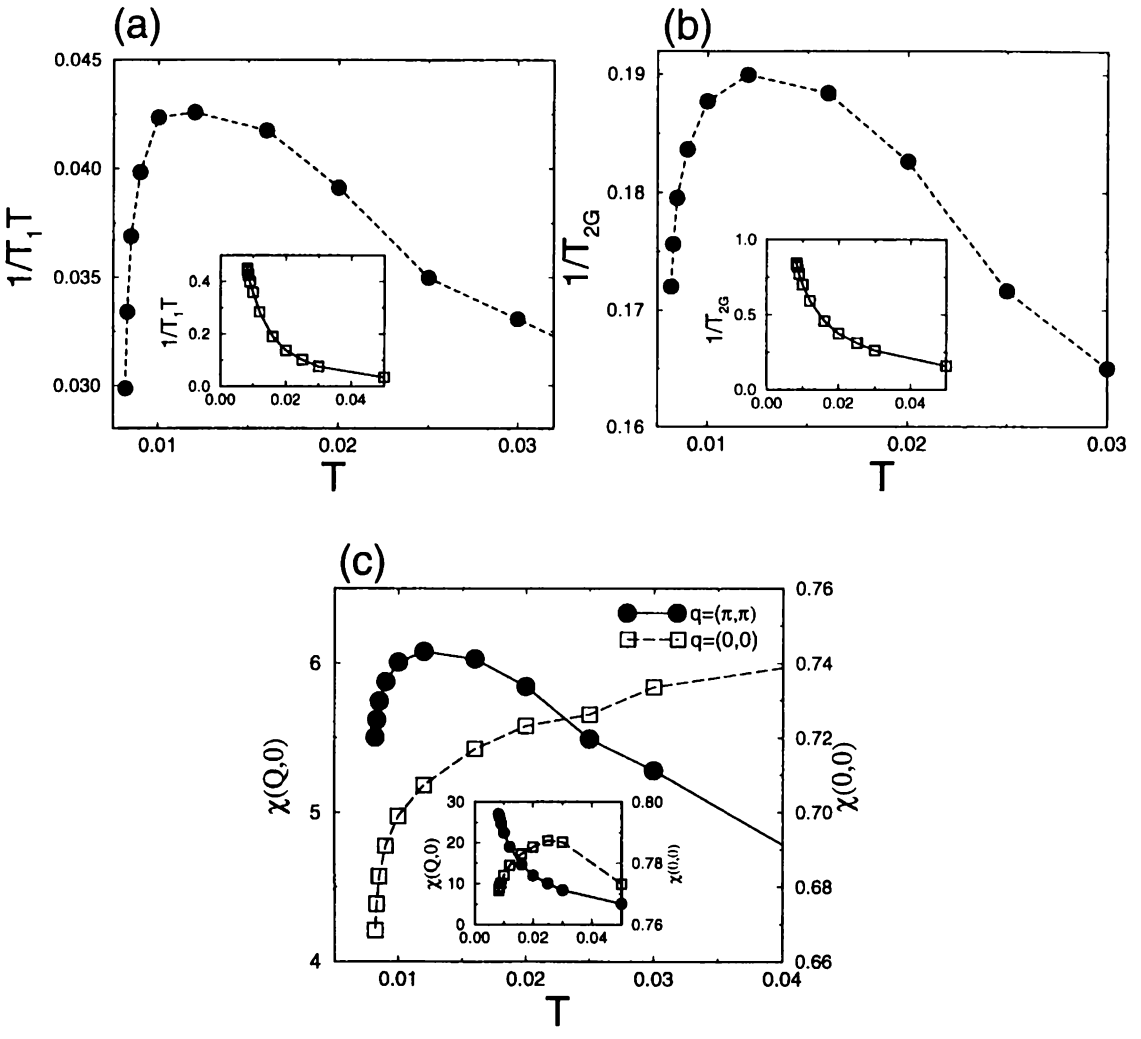

Figure 4.10: The temperature dependence of (a) the NMR $1/T_1T$ and (b) the NMR $1/T_{2G}$ calculated by the FLEX+T-matrix approximation. (c) The temperature dependence of static spin susceptibility $\chi_s^R(\boldsymbol{q}, 0)$ at $\boldsymbol{q} = (0, 0)$ (Open squares) and at $\boldsymbol{q} = (\pi, \pi)$ (Closed circles). Here, the doping concentration is fixed to the under-doped region $\delta = 0.093 \sim 0.103$. The inset in (a), (b) and (c) shows the same quantities calculated by the FLEX approximation.

The NMR $1/T_{2G}$ also shows the pseudogap (Fig. 4.10(b)) with the same onset temperature T^* as that in $1/T_1T$. The NMR $1/T_{2G}$ decreases with approaching the critical point. This is an effect of the superconducting fluctuations. However, the pseudogap in the NMR $1/T_{2G}$ is weak compared

with that in the NMR $1/T_1T$ because the NMR $1/T_{2G}$ measures the static spin susceptibility which reflects the total weight of the spin fluctuations (§3.2 and §3.3). It should be noticed that the pseudogap suppresses only the low frequency component of the spin fluctuations. It is a natural result because the superconductivity has a smaller energy scale than that of the spin fluctuations. Thus, it is no wonder that the scaling relation of the spin fluctuations is violated in the pseudogap state.

The similar features of the NMR $1/T_1T$ and $1/T_{2G}$ have been observed in the superconducting state [30, 31, 32, 33, 34, 35, 36]. In particular, the $1/T_{2G}$ remains even in the low temperature, although the $1/T_1T$ rapidly decreases. These features are the characteristics of the d-wave superconductivity [27, 113]. Therefore, the above results for the pseudogap state are natural because the pseudogap is a precursor of the d-wave superconductivity. The above results for the NMR give the qualitatively consistent explanation for the experimental results [30, 31, 32, 33, 34, 35, 36].

While the many quantities show the pseudogap with the same onset temperature T^* [43], the uniform spin susceptibility $\chi_s^R(\mathbf{0},0)$ decreases from the much higher temperature than T^* [34, 54], However, the decrease of the uniform susceptibility becomes more rapid near T^* [34]. We consider that the rapid decrease is caused by the superconducting fluctuations. The calculated results confirm the consideration. We show the results for the uniform susceptibility $\chi_s^R(\mathbf{0},0)$ and the staggard susceptibility $\chi_s^R(\boldsymbol{Q},0)$ in Fig. 4.10(c). The staggard susceptibility shows the pseudogap at the pseudogap onset temperature T^* observed in $1/T_1T$. On the other hand, the uniform susceptibility $\chi_s^R(\mathbf{0},0)$ decreases with decreasing the temperature from much higher temperature. The decrease becomes rapid near T^*. The above results well explain results of the NMR measurements [34].

The decrease of the uniform susceptibility is shown even in the FLEX approximations. (see the inset in Fig. 4.10(c).) Therefore, the decrease of the uniform susceptibility is not necessarily attributed to the superconducting fluctuations. However, the superconducting fluctuations significantly affect the uniform susceptibility and remarkably reduce the quantity near the critical point.

The frequency dependence of the spin susceptibility well describes the character of the pseudogap in the magnetic properties. The results for the dynamical spin susceptibility $\chi_s^R(\boldsymbol{q},\Omega)$ at $\boldsymbol{q} = \boldsymbol{Q}$ is shown in Fig 11. The real part is suppressed at the low frequency in the pseudogap state ($T = 0.0082$ in Fig. 4.11(a)). Thus, the magnetic order is suppressed by the superconducting fluctuations.

The imaginary part has been measured by the inelastic neutron scattering and shows the pseudogap [119]. The calculated results show that the imaginary part is remarkably suppressed at the low frequency in the pseudogap state (Fig. 4.11(b)). This is the pseudogap observed in the neutron scattering. On the other hand, the spin fluctuations develop in higher frequency region. In other words, the pseudogap transfers the spectral weight of the spin fluctuations from the low frequency region to the high frequency region. Therefore, the total weight is not so reduced by the pseudogap. These features coincide with the above explanation for the NMR $1/T_1T$ and $1/T_{2G}$. It is notable that the pairing interaction arising from the spin fluctuations originates in the relatively wide frequency region. Therefore, the d-wave pairing interaction is not so reduced by the pseudogap.

In the remaining part of this subsection, we discuss the commensurate and incommensurate structure of the spin fluctuations. The incommensurability has been pointed out by the inelastic neutron scattering measurements for the Y-based compounds, and has been discussed in connection with the stripe phase [38].

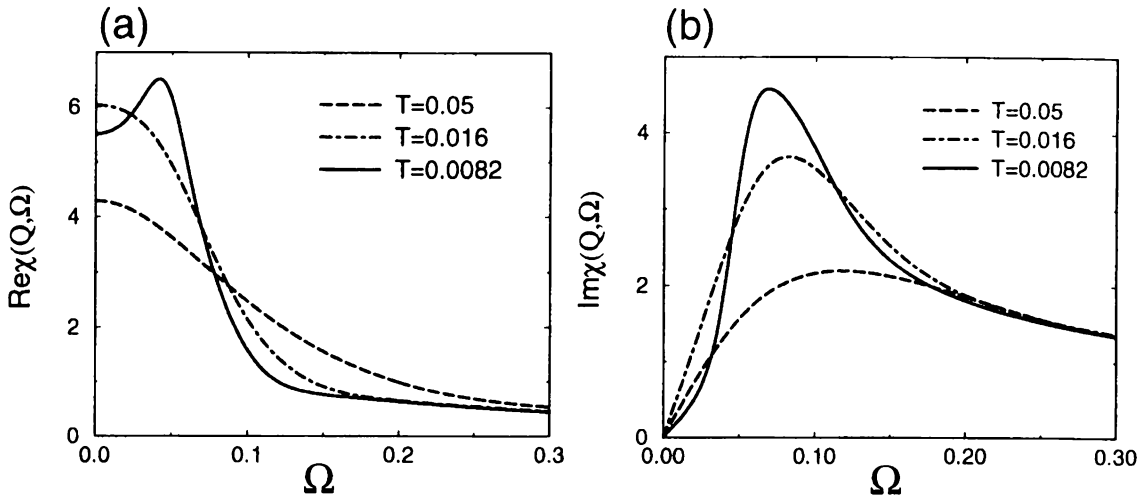

Figure 4.11: The frequency dependence of the staggard spin susceptibility $\chi_s^R(\boldsymbol{Q}, \Omega)$ calculated by the FLEX+T-matrix approximation for under-doped cuprates. (a) The real part. (b) The imaginary part. The solid line, the dash-dotted line and the long-dashed line correspond to $T = 0.0082$, $T = 0.016$ and $T = 0.05$, respectively.

The stripe phase has been measured by the elastic neutron scattering for the La-based compounds and has been actively discussed lately [156, 157, 158, 159, 160, 161, 162].

It should be noticed that both commensurate and incommensurate peaks in the spin susceptibility $\mathrm{Im}\chi_s^R(\boldsymbol{q}, \Omega)$ are obtained within the FLEX approximation (Figs. 4.12(a) and 4.12(c)). The incommensurability δ_{inc} is defined by the peak position of the dynamical spin susceptibility $\boldsymbol{Q}_p = (\pi \pm \delta_{\mathrm{inc}}, \pi)$ and $(\pi, \pi \pm \delta_{\mathrm{inc}})$. Whether the spin fluctuations are commensurate or incommensurate is determined by the chosen parameters, t', δ and U. One of the general results in our calculation is that the incommensurability δ_{inc} increases with the doping concentration δ. The results are consistent with the experiments, qualitatively [39]. The detailed agreement with the experimental results has been obtained by the FLEX calculation in the normal state [163].

The other general result is that the superconducting fluctuations enhance the incommensurability. Although the commensurate peak is obtained by the FLEX approximation in under-doped cuprates (Fig. 4.12(a)), it becomes incommensurate by the effects of the superconducting fluctuations (Fig. 4.12(b)). The incommensurability δ_{inc} increases in the FLEX+T-matrix approximation in optimally-doped cuprates (Fig. 4.12(d)). The above effect also originates in the pseudogap formation around $(\pi, 0)$. The results well explain the experimental results of the inelastic neutron scattering. The neutron scattering experiments show that the spin fluctuations change from incommensurate to commensurate with increasing the measured frequency and the temperature [38]. The effect of the pseudogap disappears when the measurement is done at the higher frequency than the energy scale of the pseudogap. Thus, the incommensurate peak in the inelastic neutron scattering can be explained without any assumption of the charge and/or spin spatial modulation.

It is expected from the above results that the incommensurate structure tends to appear in the superconducting state where the measurements are carried out in many cases. This is because the pseudogap is a precursor of the superconductivity and has the same $d_{x^2-y^2}$-wave form. Therefore, the calculation including the superconducting order is desired for the detailed agreement with the experimental results.

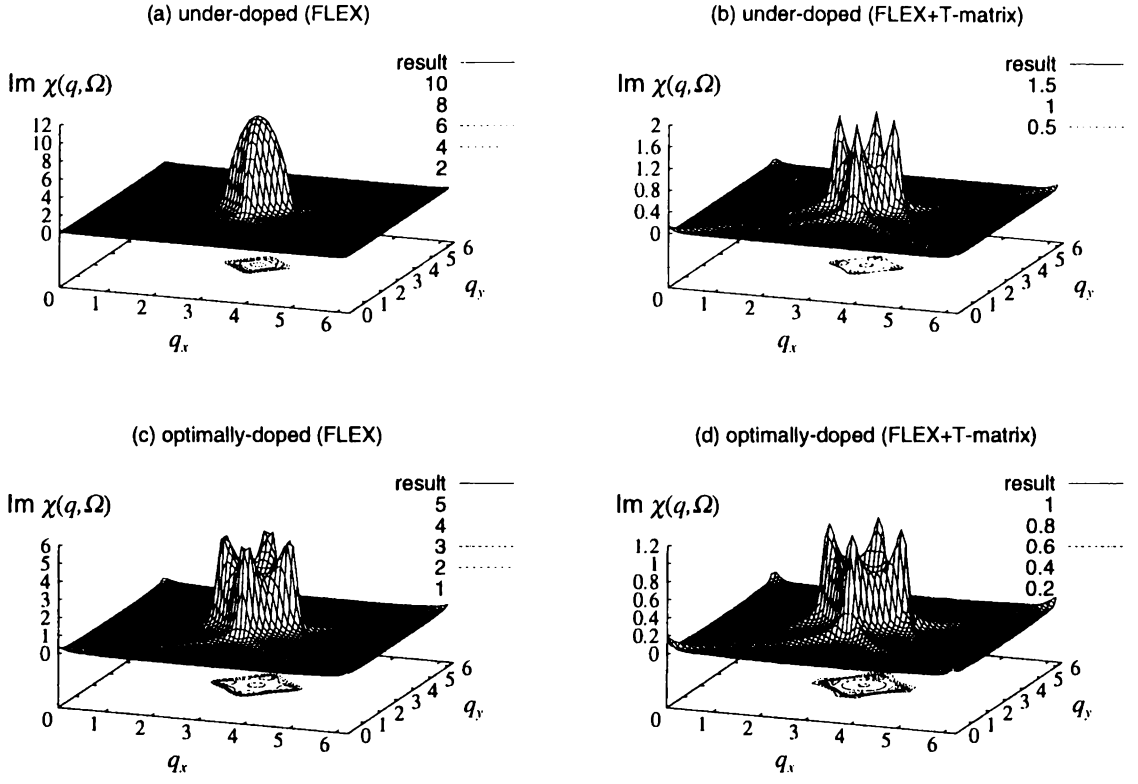

Figure 4.12: The momentum dependence of the dynamical spin susceptibility $\mathrm{Im}\chi_{\mathrm{s}}^{\mathrm{R}}(\boldsymbol{q},\Omega)$ at $\Omega = 0.01$. The results for under-doped cuprates ($\delta = 0.095$ and $T = 0.010$) (a) by the FLEX approximation and (b) by the FLEX+T-matrix approximation. The results for optimally-doped cuprates ($\delta = 0.156$ and $T = 0.0078$) (c) by the FLEX approximation and (d) by the FLEX+T-matrix approximation.

4.3.5 Electron-doped cuprates

In this subsection, we apply the above calculation to the electron-doped cuprates. It is well known that not only the hole-doped cuprates but also the electron-doped cuprates such as $Nd_{2-x}Ce_xCuO_{4-y}$ and $Pr_{2-x}Ce_xCuO_{4-y}$ are the superconductors [29]. The electron-hole symmetry is expected within the simple Hubbard model including only the nearest-neighbor hopping. However, some different properties from the hole-doped cuprates are pointed out for the electron-doped cuprates. The anti-ferromagnetic ordered state is robust against the carrier doping in the electron-doped cuprates rather than the hole-doped ones. The relatively low superconducting critical temperature T_c is observed in the narrow doping range [29].

It has been believed for a long time that the electron-doped cuprates are an s-wave or the other node-less superconductor. Some experiments have supported the node-less superconductivity. The exponential dependence of the magnetic penetration depth has been reported [164]. The absence of the zero bias conductance peak is also reported [165] while it should exist in the d-wave superconductor [166]. The possibility of some node-less superconductivity has been proposed theoretically [167]. However, some recent experimental results support the $d_{x^2-y^2}$-wave superconductivity also in the electron-doped cuprates. The power law of the magnetic penetration depth [168] and the zero bias conductance peak [169] are shown. The $d_{x^2-y^2}$-wave form of the superconducting gap is directly measured by the ARPES [170]. Moreover, the phase sensitive evidence for the d-wave superconductivity is also reported by the SQUID microscope [171].

We consider that the hole- and electron-doped cuprates should be understood comprehensively by the theory including their respective characters. The anomalous properties of the Hall coefficient are well explained for not only hole- but also electron-doped cuprates on the basis of the same formalism treating the spin fluctuations [58, 59]. Therefore, it is natural to expect the same mechanism for the superconductivity arising from the spin fluctuations in the electron-doped cuprates. Recently, the d-wave superconductivity mediated by the spin fluctuations has been calculated theoretically [172].

We consider that the application to the electron-doped cuprates is an important test of theories of High-T_c cuprates. Here, it is shown that our theory properly describes the important properties of the electron-doped cuprates. The features of the electron-hole asymmetry are naturally explained by our calculations. The electron-hole asymmetric properties are introduced by the next-nearest-neighbor hopping term t' in our model. Moreover, some theoretical expectations are proposed below. The more experimental verification is desirable.

The main difference between the electron- and hole-doped cuprates results from the shape of the Fermi surface and the distance from the Fermi level to the Van-Hove singularity. The Fermi surface of the electron-doped cuprates is obtained by lifting the chemical potential μ (Fig. 4.13). As a result, the Fermi level is lifted from the Van-Hove singularity $(\pi, 0)$ where the dispersion is flat. Therefore, the DOS is rather small in the electron-doped cuprates. The small DOS means that the electron correlation is effectively weak. On the other hand, the nesting around $(\pi/2, \pi/2)$ is enhanced and the tendency toward the anti-ferromagnetic order is robust. In the light of the d-p model, the carrier is confined in the Cu-site in the electron-doped cases, while it is in the O-site in the hole-doped ones. This fact probably contributes to the robustness of the anti-ferromagnetic order. The difference may affect the parameter of the Hubbard model which is an effective model of the d-p model in the metallic phase. However, the essential difference is included in the properties of the band structure since only the vicinity of the Fermi surface is important for the low energy physics.

Since we define the doping concentration as $\delta = 1 - n$, it is negative in the electron-doped case.

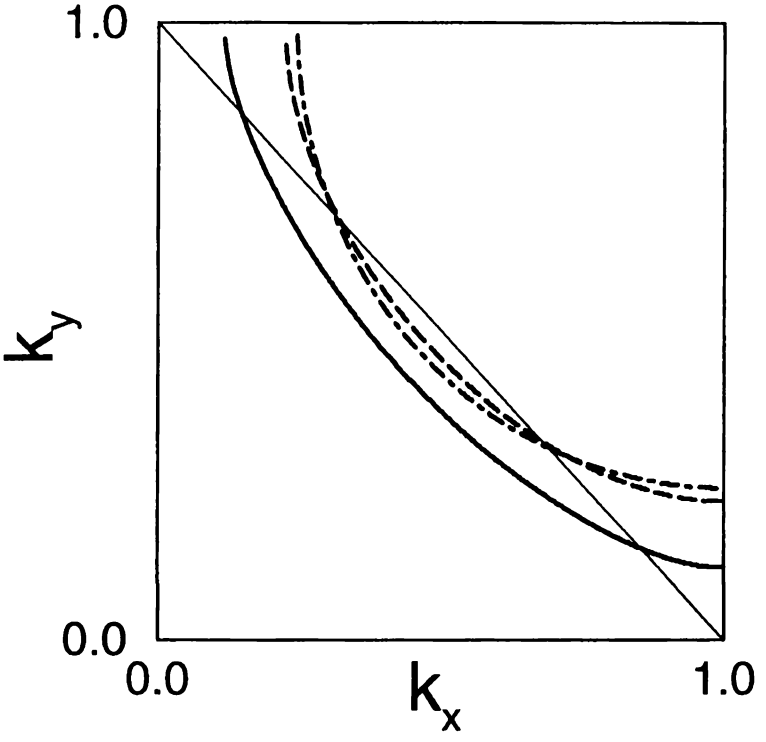

Figure 4.13: The Fermi surface of the hole- and the electron-doped cuprates. The thick solid line shows the Fermi surface of the hole-doped case $\delta = 0.10$. The long-dashed and the dash-dotted lines show the Fermi surface of the electron-doped case $\delta = -0.10$. The long-dashed and the dash-dotted lines correspond to case $t' = -0.25t$ and $t' = -0.35t$, respectively. The thin solid line shows the magnetic Brillouin zone. It should be mentioned that this figure shows the non-interacting Fermi surface. Actually, the electron correlation transforms the Fermi surface. The transformation is remarkable when the anti-ferromagnetic spin fluctuations are strong. The transformation is actually shown in Fig. 3.35.

We should note that the numerical calculation is not so correct for the electron-doped cases as for the hole-doped ones because of some reasons. The main reason is the finite size effects which are serious due to the large velocity, the weak correlation and the low temperature. The finite size effects on the spin- and superconducting fluctuations are also serious by the same reasons. Therefore, we divide the first Brillouin zone into 128×128 lattice points in calculation for the electron-doped cuprates.

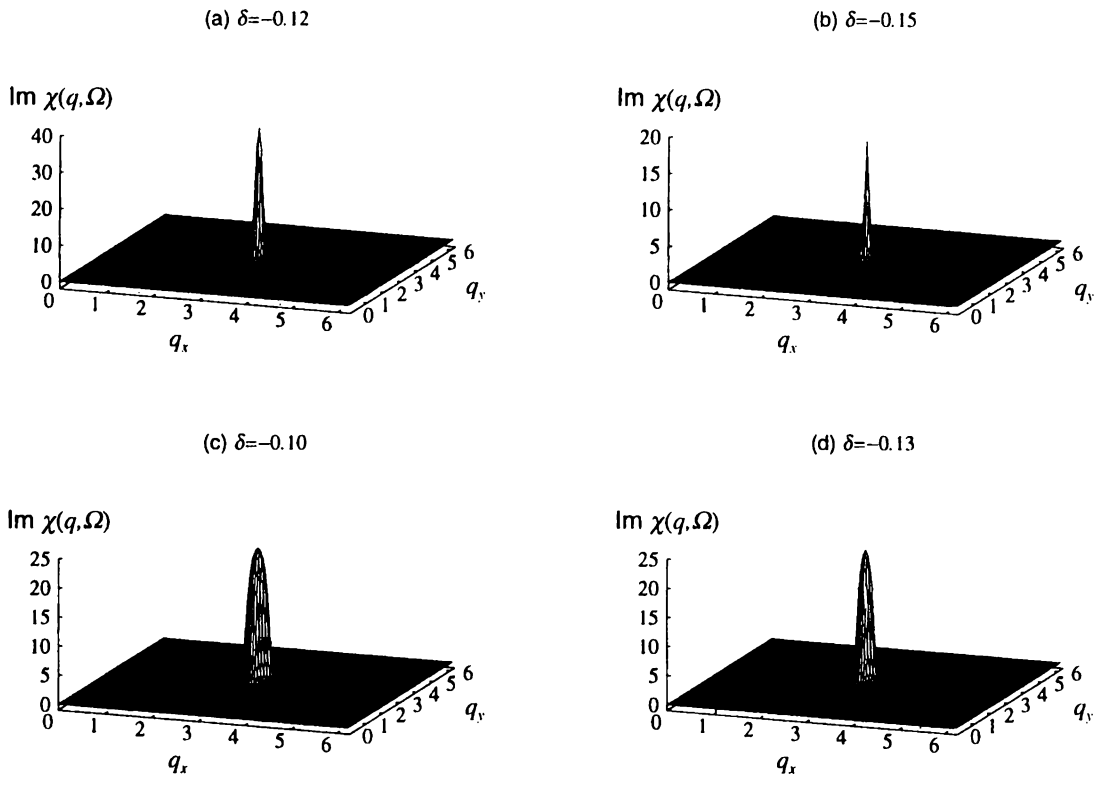

Figure 4.14: The momentum dependence of the dynamical spin susceptibility $\mathrm{Im}\chi_{\mathrm{s}}^{\mathrm{R}}(\boldsymbol{q}, \Omega)$ at $\Omega = 0.01$ calculated by the FLEX approximation. (a) $\delta = -0.123$ and (b) $\delta = -0.150$ at $t' = -0.25t$ and $T = 0.01$. (c) $\delta = -0.104$ and (d) $\delta = -0.130$ at $t' = -0.35t$ and $T = 0.005$.

For example, the difference from the hole-doped cuprates appears in the magnetic properties. We show the results of the FLEX approximation for the momentum dependence of the dynamical spin susceptibility in Figs. 4.14 (a) and (b) by using the same parameters t, t' and U. A remarkable feature of the spin correlation is that the range of the spin fluctuations is narrow in the momentum space. The width of the range and the strength of the anti-ferromagnetic correlation is reduced by the electron-doping. The spin correlation is always commensurate in the electron-doped cases. That is consistent with the recent experiments [173].

It is notable that the FLEX calculation is difficult untill the electron-doping $|\delta| \sim 0.12$ because the anti-ferromagnetic correlation is too strong. This fact implies that the anti-ferromagnetic order is robust in the electron-doped cuprates than in the hole-doped ones.

The narrow range of the spin fluctuations means that the mode coupling effects are small in the electron-doped cuprates. This favors the anti-ferromagnetic order. Actually, the other factors probably contribute to the robustness of the anti-ferromagnetism. For example, the anti-ferromagnetic order is robust when the three dimensionality (or the interlayer coupling) is strong.

Moreover, the frustration due to the carrier doping is weak when the carrier enters the Cu-site.

Hereafter, we discuss the superconductivity and the pseudogap in the electron-doped cuprates. The superconductivity mediated by the spin fluctuations is also derived by using the FLEX approximations. The most favorable superconductivity is the $d_{x^2-y^2}$-wave. However, the superconducting critical temperature is very low. The critical temperature T_c higher than 0.002 is not obtained within our numerical calculation. It is simply understood that the pairing interaction from the spin fluctuations is weak in the electron-doped cuprates because of the narrow range of the spin fluctuations. It should be noticed that the pairing interaction in the hole-doped cuprates results from the relatively wide range of the spin fluctuations around $\boldsymbol{Q} = (\pi, \pi)$. In addition to this, the small DOS remarkably reduces the critical temperature.

We can obtain a higher critical temperature T_c by choosing the hopping parameter t' so as to reproduce the Fermi surface of $Nd_{2-x}Ce_xCuO_{4-y}$ with more accuracy. Here, we choose $t' = 0.35t$ and $U = 2.0$. The commensurate spin fluctuations over a wider range are obtained (Figs. 4.14(c) and (d)). The spin fluctuations give rise to the $d_{x^2-y^2}$-wave superconductivity (Fig. 4.15). However, the critical temperature is low and the doping range in which the superconductivity occurs is remarkably narrow compared with the hole-doped ones (see the inset of Fig. 4.15). The maximum value of the obtained critical temperature is $T_c = 0.0045$. The doping range is $\delta = -0.102 \sim -0.107$. The results for the superconductivity are qualitatively consistent with the experimental results [29].

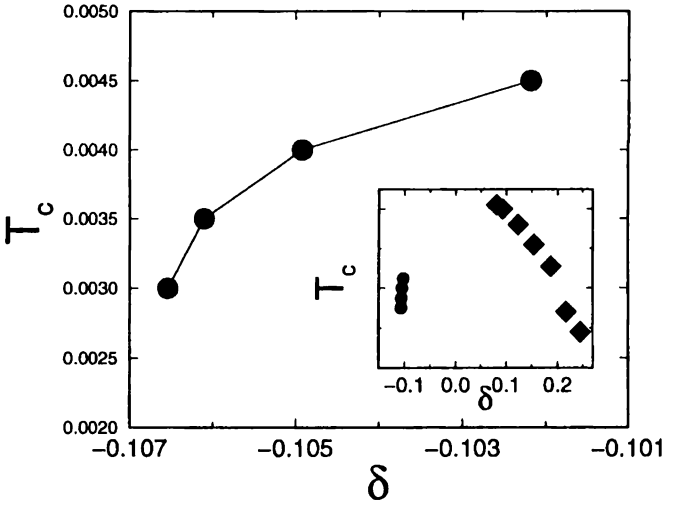

Figure 4.15: The obtained critical temperature T_c for the electron-doped cuprates. The inset shows the phase diagram including both hole- and electron-doped cases.

We show the momentum dependence of the wave function of the superconductivity $\phi(\boldsymbol{k}, i\omega_n)$ in Fig. 4.16. Fig. 4.16(a) clearly shows the d-wave superconductivity with the node in the diagonal direction. It is a notable difference between the electron- and hole-doped cuprates that a wave function shows the sharp momentum dependence in the electron-doped cuprates (Fig. 4.16(a)). This is because the quasi-particle and the Fermi surface are more clearly defined in the electron-doped cases. In the hole-doped cuprates, the many low energy states lie around $(\pi, 0)$ where the quasi-particles are broad because of the strong correlation and the high temperature. On the other hand, the electron correlation is effectively weak in the electron-doped case. Therefore, the order parameter has a large value only in the vicinity of the Fermi surface. The effectively

weak correlation is consistent with the T-square resistivity in the electron-doped cuprates [29]. Our calculation shows the ω-square dependence of the imaginary self-energy $\mathrm{Im}\Sigma_{\mathrm{F}}^{\mathrm{R}}(\boldsymbol{k},\omega)$ which implies the T-square resistivity. The incommensurate spin fluctuations have been regarded to give rise to the above momentum dependence of the wave function in electron-doped cuprates [172]. However, it is actually not the main reason. Actually, the spin fluctuations are always commensurate in the electron-doped cuprates within our calculations.

Thus, the FLEX approximation gives the $d_{x^2-y^2}$-wave order parameter $\phi(\boldsymbol{k}, \mathrm{i}\omega_n)$ for the electron-doped cuprates although the critical temperature is low compared to that of the hole-doped cuprates. The comprehensive understanding for the phase diagram furthermore support the $d_{x^2-y^2}$-wave superconductivity mediated by the anti-ferromagnetic spin fluctuations.

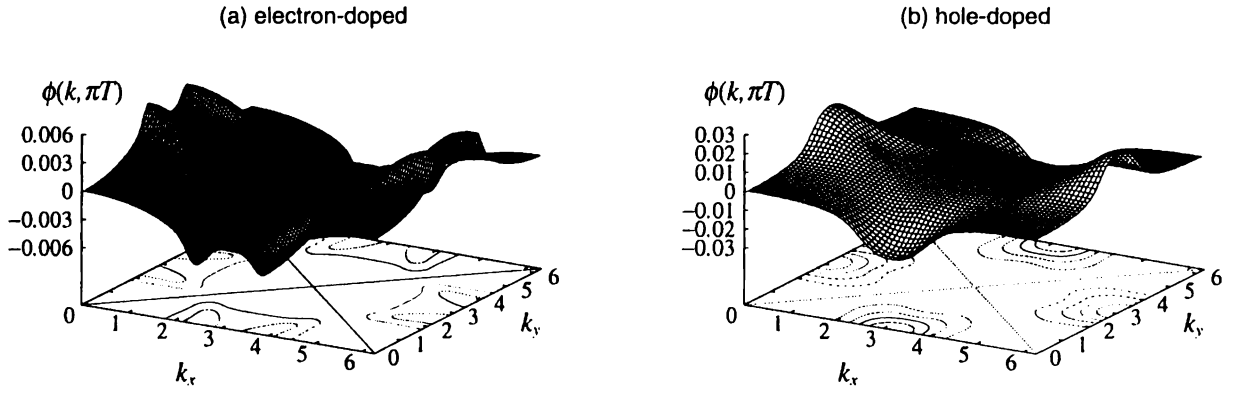

Figure 4.16: The momentum dependence of the wave function of the superconductivity (a) in the electron-doped cuprates ($\delta = -0.105$ and $T_{\mathrm{c}} = 0.0040$) and (b) in hole-doped cuprates ($\delta = 0.093$ and $T_{\mathrm{c}} = 0.0080$).

From the above results, we understand that the pseudogap has not been observed in the electron-doped cuprates [170, 173]. Because of the low T_{c} and the weak electron correlation, the superconducting coupling $T_{\mathrm{c}}^{\mathrm{MF}}/\varepsilon_{\mathrm{F}}$ is small. Actually, the large TDGL parameter $b = 30$ is obtained for the parameter set used in Fig. 4.16(a). Therefore, the superconducting fluctuations have no significant role as well as in the standard BCS superconductor. The calculated self-energy shows only the weak effects which are the same order as those in over-doped cuprates. For example, the damping $-\mathrm{Im}\Sigma^{\mathrm{R}}(\boldsymbol{k}, 0)$ at $T = 0.005$ and $\delta = -0.104$ is about 1/40 of that for the under-doped cuprates in Fig. 4.6. Therefore, the pseudogap due to the superconducting fluctuations is expected to be weak in the electron-doped cuprates, even if it is seen by some experiments. The weak effects give rise to the weak pseudogap in our calculation. However, the finite size effect seriously overestimates the effects of the superconducting fluctuations because of the large b. Therefore, the effects are precisely much weaker. The results are consistent with the experimental results of ARPES [170] and the neutron scattering [173] which do not show the pseudogap in the electron-doped cuprates.

Thus, our calculation naturally explain the doping dependence of High-T_{c} cuprates including the particle-hole asymmetry. The comprehensive understanding including both the hole- and electron-doped systems rather supports the pairing scenario for the pseudogap.

4.4 Self-Consistent Calculation

In this section, we carry out the self-consistent calculation including the spin fluctuations, superconducting fluctuations, and the single-particle properties. In the self-consistent calculation (We call the SC-FLEX+T-matrix calculation), eqs. (4.3-8) and (4.13-17) are solved self-consistently where the fully dressed Green function $G(\boldsymbol{k}, \mathrm{i}\omega_n) = (\mathrm{i}\omega_n - \varepsilon_{\boldsymbol{k}} - \Sigma(\boldsymbol{k}, \mathrm{i}\omega_n))^{-1}$ is used. By the self-consistent calculation, we calculate the critical temperature T_c reduced by the superconducting fluctuations. As is described in the previous chapter §3, there exists the singularity arising from the two-dimensionality. The singularity is actually removed by the weak three dimensionality which surely exists in the real systems. Therefore, we determine the critical temperature as the temperature at which $\lambda(\mathbf{0}, 0) = 0.98$ in order to avoid the unphysical singularity. The finite critical temperature is obtained by this operation. The method of the determination makes no significant difference on the following results. Hereafter, we consider the hole-doped cuprates.

4.4.1 Spin fluctuation and superconducting fluctuation

First, we clarify the relation between the spin fluctuations and the superconducting fluctuations. The two fluctuations complicatedly couple to each other through the single particle properties. Here, we digest the important factors of the relations.

The superconducting fluctuations as well as the superconductivity result from the spin fluctuations which act as the d-wave attractive interaction. The spin fluctuations give rise to the renormalization of the quasi-particles especially around $(\pi, 0)$. The renormalization reduces the effective Fermi energy ε_{F} for the d-wave superconductivity as well as the critical temperature T_c. Therefore, the strong superconducting fluctuations are obtained at the reasonable critical temperature.

The effects of the superconducting fluctuations on the spin fluctuations have been investigated in §4.3.4. The superconducting fluctuations suppress the low frequency spin fluctuations and the anti-ferromagnetic order (see Fig. 4.11). A residual question is whether the feedback effects of the pseudogap on the spin fluctuations suppress the superconductivity itself.

In order to answer the question, we calculate the feedback effect on the critical temperature T_c. We carry out the Modified FLEX (M-FLEX) calculation in which the fully dressed Green function is used only in eq. (4.6). In the other equations $G^{\mathrm{F}}(\boldsymbol{k}, \mathrm{i}\omega_n) = (\mathrm{i}\omega_n - \varepsilon_{\boldsymbol{k}} - \Sigma_{\mathrm{F}}(\boldsymbol{k}, \mathrm{i}\omega_n))^{-1}$ is used. Thus, the effects of the superconducting fluctuations on the spin fluctuations are included, however those on the single particle properties are not included. The eqs. (4.3-8) and (4.12-17) are solved self-consistently in the M-FLEX approximation. The results of the FLEX, M-FLEX and SC-FLEX+T-matrix calculations are shown in Table 4.1. Here, we determine the critical temperature by the condition $\lambda(\mathbf{0}, 0) = 0.98$ in the respective calculations for an equity.

In order to understand the results, it is important that the spin fluctuations have not only the paring effect but also the de-pairing effect. The former is from the relatively wide frequency region, and the latter is from the low frequency component. The pseudogap remarkably suppresses the low frequency component, however the total weight is not so reduced (Fig. 4.11). Thus, the de-pairing effect is reduced by the pseudogap rather than the pairing effect. Therefore, the higher critical temperature $T_c = 0.0098$ is obtained by the M-FLEX calculation where $T_c = 0.0084$ in the FLEX calculation. In other words, the feedback effects are advantageous to the superconductivity. Thus, only the properties of the low frequency component are not sufficient in order to understand the relation between the spin and superconducting fluctuations.

	FLEX	M-FLEX	SC-FLEX+T-matrix
T_c	0.0084	0.0098	0.0031
$g\phi^2_{\max}$	24.18	14.23	20.1529
γ_h	0.06970	0.02747	0.04277
γ_c	0.00995	0.00971	0.00298

Table 4.1: The comparison among the FLEX, M-FLEX and SC-FLEX+T-matrix approximations. The critical temperature T_c, the effective pairing interaction $g\phi^2_{\max}$, the damping at 'hot spot' γ_h and that at 'cold spot'γ_c at $T = T_c$ are shown. The parameters are $U = 1.6$ and $\delta = 0.083 \sim 0.096$. Here, the self-energy in the M-FLEX approximation is $\Sigma^R_F(\boldsymbol{k}, \omega)$.

Needless to say, the pseudogap itself in the single particle properties reduces the critical temperature. The lower critical temperature $T_c = 0.0031$ is obtained by the SC-FLEX+T-matrix calculation. The de-paring effect from the superconducting fluctuations is rather drastic than that from the spin fluctuations. (Therefore, the pseudogap is easily caused by the superconducting fluctuations.)

In order to make the above understanding clear, we show the quantities $g\phi^2_{\max}$, γ_h and γ_c in Table 4.1. Here, $\phi_{\max}$ is the maximum value of $\phi(\boldsymbol{k}, i\omega_n)$ and $g\phi^2_{\max}$ represents the strength of the pairing interaction.

The damping at the 'hot spot' $\gamma_h = -\mathrm{Im}\Sigma^R(\boldsymbol{k}_h, 0)$ at $T = T_c$ represents the strength of the de-pairing effect. Here, $\boldsymbol{k}_h = (0.98\pi, 0.02\pi)$. In should be noticed that the obtained γ_h by the M-FLEX calculation has the minimum value in Table 4.1, although the temperature is highest. This fact shows the reduction of the de-pairing effect from the spin fluctuations.

The damping at the 'cold spot' $\gamma_c = -\mathrm{Im}\Sigma^R(\boldsymbol{k}_c, 0)$ determines the in-plane transport [57, 56, 69]. Here, $\boldsymbol{k}_c = (0.45\pi, 0.42\pi)$. The Table 4.1 shows that the value γ_c is not so reduced in the M-FLEX calculation from the FLEX calculation. Thus, the feedback effects through the spin fluctuations are small around the 'cold spot'. Since the self-energy from the superconducting fluctuations $\Sigma^R_S(\boldsymbol{k}_c, \omega)$ vanishes at the 'cold spot', we can understand that the effect of the pseudogap on the in-plane transport is small (§3.4.2), as is observed experimentally [33, 43]. The slope of the T-linear resistivity is slightly reduced by the feedback effects. The anisotropy γ_h/γ_c increases due to the superconducting fluctuations. This is important for the incoherent c-axis transport in the pseudogap state because the c-axis transport is determined by the 'hot spot' [57, 69].

4.4.2 Results of the SC-FLEX+T-matrix calculation

In this subsection, we show the results of the SC-FLEX+T-matrix approximation. The qualitatively similar results to the FLEX+T-matrix approximation are obtained, although the effects of the superconducting fluctuations are reduced by the self-consistency. It is notable that the calculation treating a stronger electron-electron interaction U is possible because the superconducting fluctuations suppress the anti-ferromagnetic order. Here, we choose the interaction $U = 2.4$.

In Fig. 4.17, we show the self-energy calculated for the under-doped case $\delta = 0.073$. The competition between the pseudogap and the Fermi liquid behavior is shown. The small imaginary part and the positive slope of the real part are obtained in the narrow region around the Fermi level.

The anomalous features due to the superconducting fluctuations are shown in larger energy scale. These features are qualitatively the same as those obtained within the model with an attractive interaction in §3.1. It should be noticed that this behavior is given by the self-consistency between the superconducting fluctuations and the single particle properties. The necessity of the behavior has been explained in §3.1.

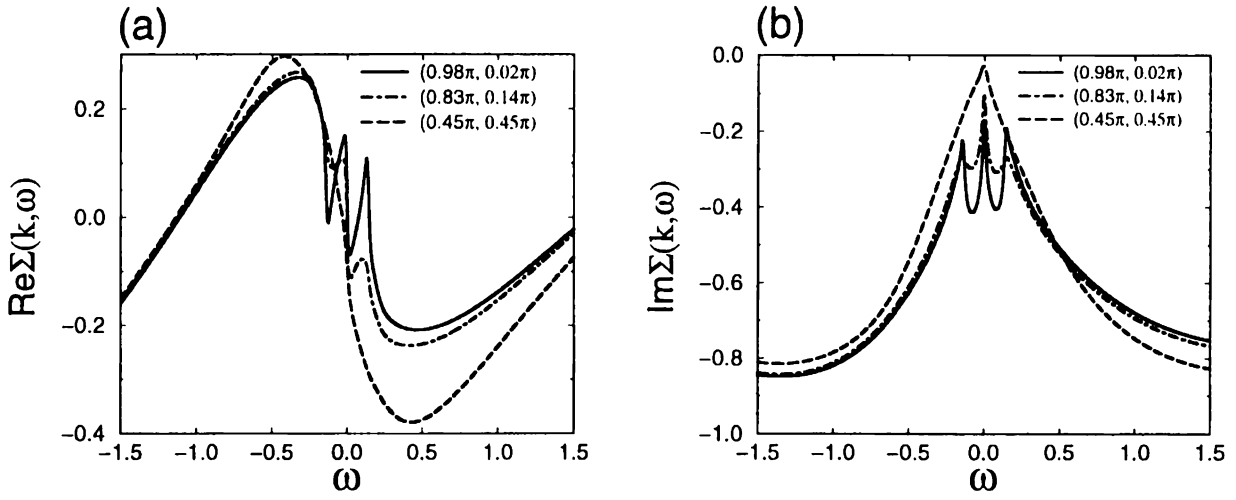

Figure 4.17: The self-energy obtained by the SC-FLEX+T-matrix approximation. (a) The real part. (b) The imaginary part. Here, parameters are $U = 2.4$, $\delta = 0.073$ and $T = 0.004$. The solid, dash-dotted and long-dashed lines are correspond to $(\frac{63}{64}\pi, \frac{1}{64}\pi)$, $(\frac{53}{64}\pi, \frac{9}{64}\pi)$ and $(\frac{47}{64}\pi, \frac{13}{64}\pi)$, respectively.

The obtained spectral weight is shown in Fig. 4.18. The peak is shown near the Fermi level at the momentum around $(\pi, 0)$. This reflects the Fermi liquid behavior of the self-energy in Fig. 4.17. The typical three peak structure shown in the under-doped case $\delta = 0.073$ (Fig. 4.18(a)) is a common feature to the results based on the model with an attractive interaction (§3.1.3). It should be noticed that the weight around the Fermi level is remarkably reduced. This is an effect of the superconducting fluctuations which give the large self-energy around the Fermi level. As is shown in the inset of Fig. 4.18(a), the usual single peak structure is obtained by neglecting the self-energy due to the superconducting fluctuations $\Sigma_{\rm S}(\boldsymbol{k}, \mathrm{i}\omega_n)$, namely $G(\boldsymbol{k}, \mathrm{i}\omega_n) = (\mathrm{i}\omega_n - \varepsilon_k - \Sigma_{\rm F}(\boldsymbol{k}, \mathrm{i}\omega_n))^{-1}$. The spectral weight is recovered and the three peak structure vanishes when the momentum leaves $(\pi, 0)$ along the Fermi surface. Similarly, the effects of the superconducting fluctuations are reduced by the hole-doping (Fig. 4.18(b)). The single peak structure is obtained for $\delta = 0.165$ (the inset in Fig. 4.18(b)). In other words, the pseudogap is reduced by the hole-doping because the superconducting fluctuations are suppressed.

The above effect of the superconducting fluctuations becomes more clear by showing the DOS in Fig. 4.19. The DOS near the Fermi level is reduced by the superconducting fluctuations and the gap structure appears in the under-doped case (solid line). It is confirmed by showing the result in which $\Sigma_{\rm S}(\boldsymbol{k}, \mathrm{i}\omega_n)$ is neglected (long-dashed line) that the pseudogap in the DOS is caused by the superconducting fluctuations. The pseudogap is suppressed by the hole-doping, similarly (dash-dotted line). Thus, the pseudogap is properly obtained by the self-consistent calculation including their doping dependence.

At last, we show the obtained phase diagram in Fig. 4.20. By the self-consistent calculation,

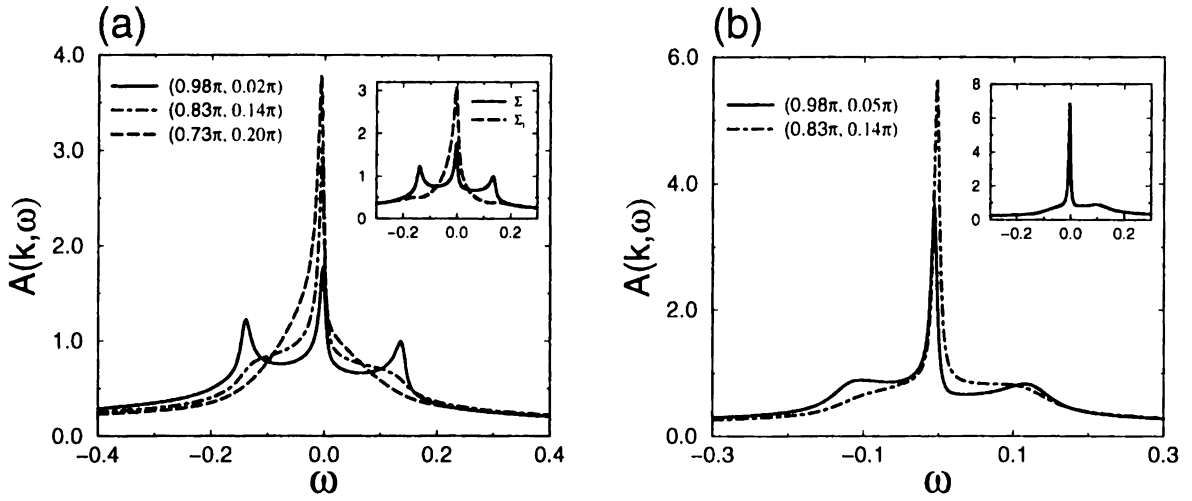

Figure 4.18: The single particle spectral weight obtained by the SC-FLEX+T-matrix approximation. (a) The under-doped case, $\delta = 0.073$ and $T = 0.004$. Here, $T_c = 0.0032$. The solid, dash-dotted and long-dashed lines are correspond to $(\frac{63}{64}\pi, \frac{1}{64}\pi)$, $(\frac{53}{64}\pi, \frac{9}{64}\pi)$ and $(\frac{29}{64}\pi, \frac{29}{64}\pi)$, respectively. In the inset, the solid line shows the same results as the main figure. The long-dashed lines show the result by neglecting $\Sigma_S(\boldsymbol{k}, i\omega_n)$. (b) The optimally-doped case, $\delta = 0.119$ and $T = 0.004$. Here, $T_c = 0.0035$. The solid and dash-dotted lines correspond to $(\frac{63}{64}\pi, \frac{3}{64}\pi)$ and $(\frac{53}{64}\pi, \frac{9}{64}\pi)$, respectively. The inset shows the result for the over-doped case, $\delta = 0.165$, $T = 0.0035$ and $\boldsymbol{k} = (\frac{63}{64}\pi, \frac{5}{64}\pi)$.

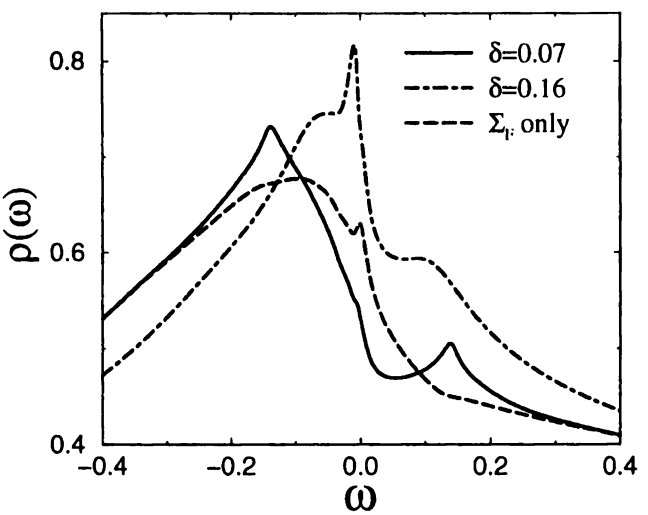

Figure 4.19: The DOS obtained by the SC-FLEX+T-matrix approximation. The solid and dash-dotted lines show the under-doped case ($\delta = 0.073$ and $T = 0.004$) and the over-doped case ($\delta = 0.165$ and $T = 0.0035$), respectively. The long-dashed line shows the result for the under-doped case obtained by neglecting the self-energy $\Sigma_S(\boldsymbol{k}, i\omega_n)$.

the superconducting critical temperature T_c suppressed by the superconducting fluctuations is calculated. It should be noticed that the suppression of T_c from the mean field value becomes remarkable with under-doping. This is a natural result because the superconducting fluctuations become strong with under-doping. In other words, the pseudogap develops with under-doping and the reduced DOS gives the reduced critical temperature. An important result is that the critical temperature has the maximum value at $\delta \sim 0.11$ and decreases with under-doping in the SC-FLEX+T-matrix calculation for $U = 2.4$, whereas T_c goes on increasing in the FLEX calculation. In other words, the mean field critical temperature given by the anti-ferromagnetic spin fluctuations develops with under-doping, however, the strong superconducting fluctuations decreases the critical temperature with under-doping in the under-doped region.

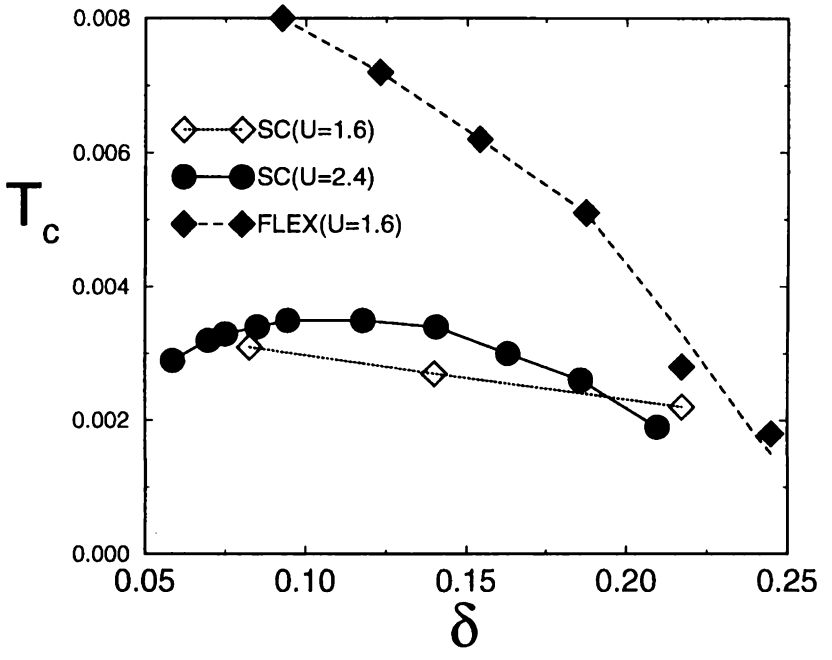

Figure 4.20: The phase diagram obtained by the FLEX and the SC-FLEX+T-matrix approximations. The closed circles show the results of the SC-FLEX+T-matrix approximation for $U = 2.4$. The closed and open diamonds show the results of the FLEX and the SC-FLEX+T-matrix approximations for $U = 1.6$.

It is notable to write again that the strength of the superconducting coupling is indicated by the ratio T_c^{MF}/ϵ_F, and not by T_c. Since the effective Fermi energy ϵ_F decreases, the superconducting coupling becomes strong with under-doping in spite of the decreasing T_c. Thus, the decreasing T_c in the under-doped region is obtained by considering the superconducting fluctuations.

We can see from Fig. 4.20 that the critical temperature for $U = 1.6$ does not decrease with under-doping even in the SC-FLEX+T-matrix calculation. Thus, the strong renormalization of the quasi-particles by the electron correlation plays an important role for describing the under-doped cuprates. It is important that we can treat the strong correlation by considering the superconducting fluctuations which suppresses the anti-ferromagnetic order.

4.5 Summary

In this chapter, we have investigated the pseudogap phenomena starting from the Hubbard model. We have succeeded in deriving the pseudogap phenomena from the on-site repulsive interaction. The renormalized quasi-particles and the pairing interaction via the anti-ferromagnetic spin fluctuations are calculated by using the FLEX approximation. The anti-ferromagnetic spin fluctuations give rise to the strong renormalization around the 'hot spot'. Therefore, the effective Fermi energy $\varepsilon_{\rm F}$ for the d-wave symmetry is strongly renormalized. Because of the high critical temperature $T_{\rm c}$ and the renormalized Fermi energy $\varepsilon_{\rm F}$, the superconducting coupling $T_{\rm c}^{\rm MF}/\varepsilon_{\rm F}$ becomes strong in the under-doped region. As a result, the pseudogap phenomena occurs owing to the self-energy correction by the strong superconducting fluctuations. The results support the scenario which is described within the model with a d-wave attractive interaction (§3).

An important progress is that the pseudogap is described as a phenomenon near the Fermi surface. Because the obtained pairing interaction affects only the quasi-particles near the Fermi surface, it is naturally described that the superconducting fluctuations and the pseudogap have the small energy scale compared with the electron correlation. These results support the picture in which the pairing interaction becomes effectively strong for the renormalized quasi-particles.

Moreover, it should be emphasized that the calculation in this chapter properly describes the doping dependence of the pseudogap phenomena. The superconducting coupling becomes weak with hole-doping since the Fermi energy increases and the mean field critical temperature $T_{\rm c}^{\rm MF}$ decreases. Therefore, the superconducting fluctuations gradually become insignificant with hole-doping and negligible in under-doped region. The doping dependence well explains the phase diagram of the High-$T_{\rm c}$ superconductors. The obtained doping dependence of the TDGL parameter b has confirmed the above picture and gives the comprehensive understanding of the magnetic field dependence of the pseudogap phenomena (§3.2).

The application of the calculation to the electron-doped cuprates gives a consistent understanding with the experimental results [29, 168, 169, 170, 171, 173]. We have obtained the $d_{x^2-y^2}$-wave superconductivity with low critical temperatures within the narrow doping range. It is shown that the pseudogap is not observed in the electron-doped cuprates. The difference from the hole-doped case is derived from the particle-hole asymmetry of the band structure. The band structure obtained by the band calculation and observed by the ARPES naturally leads to the particle-hole asymmetric properties. It is surprising that such simple explanation is given for the complicated problems. The comprehensive understanding including the particle-hole asymmetry furthermore supports our scenario for High-$T_{\rm c}$ cuprates.

The pseudogap in the magnetic properties has been investigated and explained properly. We have calculated the quantities observed by the NMR and the neutron scattering. Our calculation has naturally explained the characteristics of the pseudogap phenomena which are subtly different from each other.

We have clarified the relation between the spin fluctuations and the superconducting fluctuations which are complicatedly connected with each other. It is shown that the feedback effects of the superconducting fluctuations on the spin fluctuations *do not* suppress but enhance the superconducting correlation. Therefore, the strong coupling superconductivity is not suppressed by the feedback effect. Since the relation of the spin- and superconducting fluctuations are complicated, we have to understand the different energy scale of the two phenomena, the superconductivity and the magnetism in order to clarify it.

Of course, the superconducting fluctuations themselves suppress the superconducting transi-

tion. This effect is so strong and the critical temperature is remarkably reduced in the under-doped region. We have calculated the reduced critical temperature by the SC-FLEX+T-matrix calculation in which the single particle properties, the spin fluctuations and the superconducting fluctuations are determined self-consistently. Qualitatively the same results for the pseudogap phenomena have been obtained by the SC-FLEX+T-matrix calculation. The calculated critical temperature shows the maximum value near $\delta \sim 0.11$, and decreases with under-doping, although it keeps increasing in the FLEX calculation. Thus, we have succeeded in describing the under-doped cuprates by considering the strong superconducting fluctuations in the strongly correlated electron systems.

Finally, it should be stressed that the calculation in this chapter starts from the Fermi liquid state and properly describes the High-T_c cuprates including the under-doped region. The comprehensive understanding of High-T_c cuprates has been obtained including their doping dependence.

Chapter 5

Conclusion

In this thesis, we have given an explanation of the pseudogap phenomena in High-T_c cuprates which are the remained highlight of the High-T_c superconductivity. So far, many arguments have been given for the anomalous properties in the normal state High-T_c cuprates. Many of them have been based on the anomalous state far from the Fermi liquid state. The pseudogap phenomena are the main topics among the 'anomalous' properties. In this thesis, we have started from the Fermi liquid state and taken into account the strong electron correlation and the resulting superconducting fluctuations. The obtained results have properly described the 'anomalous' properties in the under-doped region. The pseudogap phenomena result from the strong superconducting fluctuations. The origin of the strong superconducting fluctuations are the strong electron correlation, the high critical temperature and the quasi-two dimensionality. These important factors are the characteristics of High-T_c cuprates. Therefore, it is considered that the derived answer is reasonable.

It should be stressed that the reasonable explanation is obtained by starting from the Fermi liquid state, although the resulting electronic state is far from the conventional Fermi liquid theory. This result strongly indicates the universality of the Fermi liquid theory. The concept of the Fermi liquid theory is not restricted within the conventional Fermi liquid state. The continuous change from the under-doped region to the over-doped region suggests the validity of the starting point based on the Fermi liquid state. In particular, the starting point is necessary for the comprehensive description of the High-T_c superconductivity. It should be noticed that the anomalous behavior observed in the under-doped region is not essential for the High-T_c superconductivity because the superconductivity occurs even in the over-doped region. It is reasonable that the normal state is also described by starting from the Fermi liquid state. However, the description has been important but difficult problem so far. Although the several problems are solved, the main topics (that is, pseudogap phenomena) are remained to be understood. We think that the answer is obtained by considering the superconducting fluctuations. It should be stressed that the results obtained in this thesis gives the answer and shows the comprehensive description of the High-T_c superconductivity.

The important and remained problem is the description of the under-doped limit. The calculation in this chapter can not be applied to the limit because the FLEX approximation does not describe the Mott transition. Although the calculation describing the Mott transition is difficult at present, we think that the essence of the metallic state of High-T_c cuprates has been explained in this thesis.

Bibliography

[1] J. G. Bednortz and K. A. Müller: Z. Phys. B**64** (1986) 189.

[2] J. Bardeen, L. Cooper and J. R. Schrieffer: Phys. Rev. **108** (1957) 1175.

[3] For example, K. Ishida, Y. Kitaoka, N. Ogata, T. Kamino, K. Asayama, J. R. Cooper and N. Athanassopoulou: J. Phys. Soc. Jpn. **62** (1993) 2803.

[4] S. Fujimoto: J. Phys. Soc. Jpn. **61** (1992) 765; Prog. Theor. Phys. **89** (1993) 333.

[5] M. Sigrist and T. M. Rice: J. Phys. Soc. Jpn. **61** (1992) 4283.

[6] C. C. Tsuei, J. R. Kirtley, C. C. Chi, L. S. Yu-Jahnes A. Gupta, T. Shaw, J. Z. Sun and M. B. Ketchen : Phys. Rev. Lett. **73** (1994) 593.

[7] T. Moriya, Y. Takahashi and K. Ueda: J. Phys. Soc. Jpn **59** (1990) 2905; K. Ueda, T. Moriya and Y. Takahashi: J. Phys. Chem. Solids **53** (1992) 1515.

[8] P. Monthoux, A. V. Balatsky and D. Pines: Phys. Rev. B **46** (1992) 14803.

[9] D. Pines: Z. Phys. B **103** (1997) 129 and references there in.

[10] T. Moriya and K. Ueda: Adv. Phys. **49** (2000) 555.

[11] P. W. Anderson: Science. **235** (1987) 1196.

[12] H. Fukuyama: Prog. Theor. Phys. Suppl. **108** (1992) 287.

[13] H. Yokoyama and H. Shiba: J. Phys. Soc. Jpn. **57** (1988) 2482.

[14] H. Yokoyama and M. Ogata: J. Phys. Soc. Jpn. **65** (1996) 3615.

[15] A. Himeda and M. Ogata: Phys. Rev. B **60** (1999) R9935.

[16] For example, P. Nozières: *Theory of Interacting Fermi Systems* (Addison Wesley, 1964).

[17] A. Kampf and J. R. Schrieffer: Phys. Rev. B **41** (1990) 6399.

[18] T. Dahm and L. Tewordt: Phys. Rev. B. **52** (1995) 1297.

[19] A. V. Chubukov, D. K. Morr and K. A. Shakhnovich: Philos. Mag. B **74** (1996) 563; A. V. Chubukov and J. Schmalian: Phys. Rev. B **57** (1998) 11085.

[20] C. A. R. Sá de Melo, M. Randeria and J. R. Engelbrecht: Phys. Rev. Lett. **71** (1993) 3202; M. Randeria: *Bose-Einstein Condensation* ed. A. Griffin, D. Snoke and S. Stringari (Cambridge, Cambridge University Press, 1994); M. Randeria: preprint (cond-mat/9710223) and references there in.

[21] V. J. Emery and S. A. Kivelson: Phys. Rev. Lett. **74** (1995) 3253.

[22] H. Ding, T. Yokoya, J. C. Campuzano, T. Takahashi, M. Randeria, M. R. Norman, T. Mochiku, K. Kadowaki and J. Giapintzakis: Nature. **382** (1996) 51; M. R. Norman, H. Ding, M. Randeria, J. C. Campuzano, T. Yokoya, T. Takeuchi, T. Takahashi, T. Mochiku, K. Kadowaki, P. Guptasarma and D. G. Hinks: Nature. **392** (1998) 157.

[23] A. G. Loeser, Z. X. Shen, D. S. Dessau, D. S. Marshall, C. H. Park, P. Fournier and A. Kapitulnik: Science. **273** (1996) 325.

[24] Y. Yanase and K. Yamada: J. Phys. Soc. Jpn. **68** (1999) 2999.

[25] Y. Yanase and K. Yamada: J. Phys. Soc. Jpn. **69** (2000) 2209.

[26] T. Jujo, Y. Yanase and K. Yamada: J. Phys. Soc. Jpn. **69** (2000) 2240.

[27] Y. Yanase, T. Jujo and K. Yamada: J. Phys. Soc. Jpn. **69** (2000) 3664.

[28] Y. Yanase and K. Yamada: preprint.

[29] Y. Tokura, H. Takagi and S. Uchida: Nature. **337** (1989) 345; H. Takagi, S. Uchida and Y. Tokura: Phys. Rev. Lett. **62** (1989) 1197.

[30] H. Yasuoka, T. Imai and T. Shimizu: *Strong Correlation and Superconductivity* (Springer Verlag, Berlin 1989), p. 254.

[31] For example, W. W. Warren, R. E. Walstedt, G. F. Brennert, R. J. Cava, R. Tycko, R. F. Bell and G. Dabbagh: Phys. Rev. Lett. **62** (1989) 1193; M. Takigawa, A. P. Reyes, P. C. Hammel, J. D. Thompson, R. H. Heffner, Z. Fisk and K. C. Ott: Phys. Rev. B **43** (1991) 247. M. H. Julien, P. Carretta, M. Horvatić: Phys. Rev. Lett. **76** (1996) 4238;

[32] M. Takigawa: Phys. Rev. B **49** (1994) 4158.

[33] Y. Itoh, T. Machi, S. Adachi, A. Fukuoka, K. Tanabe and H. Yasuoka: J. Phys. Soc. Jpn. **67** (1998) 312.

[34] K. Ishida, K. Yoshida, T. Mito, Y. Tokunaga, Y. Kitaoka, K. Asayama, Y. Nakayama, J. Shimoyama and K. Kishio: Phys. Rev. B **58** (1998) R5960.

[35] Y. Tokunaga, K. Ishida, K. Yoshida, T. Mito, Y. Kitaoka, Y. Nakayama, J. Shimoyama, K. Kishio, O. Narikiyo and K. Miyake: Physica B **284-288** (2000) 663.

[36] A. Goto and T. Shimizu: Physica B **281&282** (2000) 810; A. Goto and T. Shimizu: Phys. Rev. B **57** (1998) 7977; A. Goto and T. Shimizu: Physica B **259-261** (1999) 468.

[37] J. Rossat-Mignod, L. P. Regnault, C. Vettier, P. Burlet, J. Y. Henry and G. Lapertot: Physica B **169** (1991) 58.

[38] P. Dai, H. A. Mook, and F. Doğgan: Phys. Rev. Lett. **80** (1998) 1738; M. Arai, T. Nishijima, Y. Endoh, T. Egami, S. Tajima, K. Tomimoto, Y. Shiohara, M. Takahashi, A. Garrett and S. M. Bennington: Phys. Rev. Lett. **83** (1999) 608.

[39] K. Yamada, C. H. Lee, K. Kurahashi, J. Wada, S. Wakimoto, S. Ueki, H. Kimura, Y. Endoh, S. Hosoya, G. Shirane, R. J. Birgeneau, M. Greven, M. A. Kastner, and Y. J. Kim: Phys. Rev. B. **57** (1998) 6165.

[40] The experimental results for the transport properties are reviewed in, Y. Iye: *Physical Properties of High Temperature Superconductors III*, ed. D.M.Ginsberg, (World Sci. Pub., Singapore, 1992), pp.285-361.

[41] H. Takagi, T. Ido, S. Ishibashi, M. Uota, S. Uchida and Y. Tokura: Phys. Rev. B **40** (1989) 2254.

[42] For example, T. Ito, K. Takenaka and S. Uchida: Phys. Rev. Lett. **70** (1993) 3995; K. Mizuhashi, K. Takenaka, Y. Fukuzumi and S. Uchida: Phys. Rev. B **52** (1995) R3884.

[43] M. Oda, K. Hoya, R. Kubota, C. Manabe, N. Momono, T. Nakano and M. Ido: Physica C **281** (1997) 135.

[44] For example, J. Takeda, T. Nishikawa and M. Sato: Physica C **231** (1994) 293; T. Nishikawa, J. Takeda and M. Sato: J. Phys. Soc. Jpn **63** (1994) 1441. H. Y. Hwang, B. Batlogg, H. Takagi, H. L. Kao, J. Kwo, R. J. Cava, J. J. Krajewski and W. F. Peck, Jr: Phys. Rev. Lett. **72** (1994) 2636.

[45] For example, K. Takenaka, K. Mizuhashi, H. Takagi and S. Uchida: Phys. Rev. B **50** (1994) 6534.

[46] C. C. Homes, T. Timusk, R. Liang, D. A. Bonn and W. H. Hardy: Phys. Rev. Lett. **71** (1993) 1645.

[47] D. N. Basov, R. Liang, B. Dabrowski, D. A. Bonn, W. N. Hardy and T. Timusk: Phys. Rev. Lett. **77** (1996) 4090.

[48] S. Tajima, J. Schützmann, S. Miyamoto, I. Terasaki, Y. Sato and R. Hauff: Phys. Rev. B **55** (1997) 6051.

[49] Ch. Renner, B. Revaz, J.-Y. Genoud, K. Kadowaki and Ø. Fischer: Phys. Rev. Lett. **80** (1998) 149.

[50] N. Miyakawa, P. Guptasarma, J. F. Zasadzinski, D. G. Hinks and K. E. Gray: Phys. Rev. Lett. **80** (1998) 157.

[51] J. W. Loram, K. A. Mirza, J. M. Wade, J. R. Cooper and W. Y. Liang: Physica C **235&240** (1994) 134.

[52] N. Momono, T. Matsuzaki, T. Nagata, M. Oda and M. Ido: to be published in J. Low. Temp. Phys.

[53] T, Timusk and B. Statt: Rep. Prog. Phys. **62** (1999) 61.

[54] M. Oda, H. Matsuki and M. Ido: Solid State Commun. **74** (1990) 1321.

[55] R. Hlubina and T. M. Rice: Phys. Rev. B **51** (1995) 9253.

[56] B. P. Stojković and D. Pines: Phys. Rev. Lett. **76** (1996) 811; B. P. Stojković and D. Pines: Phys. Rev. B **55** (1997) 8576.

[57] Y. Yanase and K. Yamada: J. Phys. Soc. Jpn **68** (1999) 548.

[58] K. Kanki and H. Kontani: J. Phys. Soc. Jpn **68** (1999) 1614.

[59] H. Kontani, K. Kanki and K. Ueda: Phys. Rev. B **59** (1999) 14723.

[60] H. Kohno and K. Yamada: Prog. Theor. Phys. **80** (1988) 623.

[61] Ch. Renner, B. Revaz, K. Kadowaki, I. Maggio-Aprile and Ø. Fischer: Phys. Rev. Lett. **80** (1998) 3606.

[62] M. Franz and Z. Tesanovic: Phys. Rev. Lett. **80** (1998) 4763.

[63] K. Yasui and T. Kita: Phys. Rev. Lett. **83** (1999) 4168.

[64] I. Maggio-Aprile, Ch. Renner, A. Erb, E. Walker, and Ø. Fischer: Phys. Rev. Lett. **75** (1995) 2754.

[65] S. H. Pan, E. W. Hudson, A. K. Gupta, K. W. Ng, H. Eisaki, S. Uchida and J. C. Davis: Phys. Rev. Lett. **85** (2000) 1536.

[66] A. Himeda, M. Ogata, Y. Tanaka and S. Kashiwaya: J. Phys. Soc. Jpn **66** (1997) 3367.

[67] C. Wu, T. Xiang and Z. Su: Phys. Rev. B **62** (2000) 14427.

[68] O. K. Anderson, A. I. Liechtenstein, O. Jepsen and F. Paulsen: J. Phys. Chem. Solids. **56** (1995) 1573.

[69] L. B. Ioffe and A. J. Millis: Phys. Rev. B **58** (1998) 11631; V. B. Geshkenbein, L. B. Ioffe and A. J. Millis: Phys. Rev. Lett. **80** (1998) 5778.

[70] T. Nakano, N. Momono, M. Oda and M. Ido: J. Phys. Soc. Jpn **67** (1998) 2622.

[71] L. G. Aslamazov and A. I. Larkin: Fiz. Tverd. Tela. **10** (1968) 1104. [Sov. Phys. Solid State **10** (1968) 875.]

[72] K. Maki: Prog. Theor. Phys **40** (1968) 193.; R. S. Thompson: Phys. Rev. B **1** (1970) 327.

[73] A. J. Leggett: *Modern Trends in the Theory of Condensed Matter* ed. A. Pekalski and R. Przystawa (Springer-Verlag, Berlin, 1980).

[74] P. Nozières and S. Schmitt-Rink: J. Low Temp. Phys. **59** (1985) 195.

[75] S. Schmitt-Rink, C. M. Varma and A. E. Ruckenstein: Phys. Rev. Lett. **63** (1989) 445.

[76] A. Tokumitu, K. Miyake and K. Yamada: Prog. Theor. Phys. Suppl. **106** (1991) 63.

[77] R. Haussmann: Phys. Rev. B **49** (1994) 12975.

[78] R. Micnas, M. H. Pedersen, S. Schafroth, T. Schneider, J. J. Rodríguez-Núñez and H. Beck: Phys. Rev. B **52** (1995) 16223.

[79] S. Stintzing and W. Zwerger: Phys. Rev. B **56** (1997) 9004.

[80] J. R. Engelbrecht, A. Nazarenko, M. Randeria and E. Dagotto: Phys. Rev. B **57** (1998) 13406.

[81] T. Hotta, M. Mayr and E. Dagotto: Rev. B **60** (1999) 13085.

[82] S. Koikegami and K. Yamada: J. Phys. Soc. Jpn. **67** (1998) 1114.

[83] A. Kobayashi, A. Tsuruta, T. Matsuura and Y. Kuroda: J. Phys. Soc. Jpn. **67** (1998) 2626.

[84] V. B. Geshkenbein, L. B. Ioffe and A. I. Larkin: Phys. Rev. B **55** (1997) 3173.

[85] J. Ranninger and J. -M. Robin: Phys. Rev. B **53** (1996) R11961; Phys. Rev. B **56** (1997) 8330.

[86] A. Perali, C. Castellani, C. Di Castro, M Grilli, E. Piegari and A. A. Varlamov: Phys. Rev. B **62** (2000) R9295.

[87] T. Nagaoka, Y. Matsuda, H. Obara, A. Sawa, T. Terashima, I. Chong, M. Takano and M. Suzuki: Phys. Rev. Lett. **80** (1998) 3594; A. G. Aronov and A. B. Rapoport: Mod. Phys. Lett. B **6** (1992) 1083.

[88] B. Jankó, J. Maly and K. Levin: Phys. Rev. B **56** (1997) 11407; J. Maly, B. Jankó and K. Levin: Physica C **321** (1999) 113.

[89] M. Franz and A. J. Millis: Phys. Rev. B **58** (1998) 14572;

[90] H-J. Kwon and A. T. Dorsey: Phys. Rev. B **59** (1999) 6438.

[91] Z. A. Xu, N. P. Ong, Y. Wang, T. Kakeshita and S. Uchida: Nature **406** (2000) 486.

[92] K. Kuboki and H. Fukuyama: J. Phys. Soc. Jpn **58** (1989) 376.

[93] J. Heym: J. Low Temp. Phys. **89** (1992) 869.

[94] M. Randeria and A. A. Varlamov: Phys. Rev. B **50** (1994) 10401.

[95] C. Di Castro, R. Raimondi, C. Castellani and A. A. Varlamov: Phys. Rev. B **42** (1990) 10221.

[96] A. A. Varlamov, G. Balestrino, E. Milani and D. V. Livanov: Adv. Phys. **48** (1999) 655.

[97] M. Eschrig, D. Rainer and J. A. Sauls: Phys. Rev. B **59** (1999) 12095.

[98] O. Tchernyshyov: Phys. Rev. B **56** (1997) 3372.

[99] H. Ebisawa and H. Fukuyama: Prog. Theor. Phys **46** (1971) 1042; H. Fukuyama, H. Ebisawa and T. Tsuzuki: Prog. Theor. Phys **46** (1971) 1028. It has been point out that the sign of the Hall coefficient is wrong in these papers.

[100] M. R. Norman, M. Randeria, H. Ding and J. C. Campuzano: Phys. Rev. B **57** (1998) 11093.

[101] M. Randeria, H. Ding, J. C. Campuzano, A. Bellman, G. Jennings, T. Yokoya, T. Takahashi, H. Katayama-Yoshida, T. Mochiku and K. Kadowaki: Phys. Rev. Lett. **74** (1995) 4951.

[102] T. Ichinomiya and K. Yamada: J. Phys. Soc. Jpn. **68** (1999) 981.

[103] A. Kobayashi, A. Tsuruta, T. Matsuura and Y. Kuroda: J. Phys. Soc. Jpn. **68** (1999) 2506.

[104] A. Kawamoto, K. Miyagawa, Y. Nakazawa and K. Kanoda: Phys. Rev. Lett. **74** (1995) 3455.

[105] T. Jujo and K. Yamada: J. Phys. Soc. Jpn. **68** (1999) 2198.

[106] B. Jankó, I. Kosztin, K. Levin, M. R. Norman and D. Scalapino: Phys. Rev. Lett. **82** (1999) 4304.

[107] D. J. Scalapino: Phys. Rev. Lett. **24** (1970) 1052. H. Takayama: Prog. Theor. Phys. **46** (1971) 1.

[108] G-q. Zheng, W. G. Clark, Y. Kitaoka, K. Asayama, K. Kodama, P. Kuhns and W. G. Moulton: Phys. Rev. B **60** (1999) R9947.

[109] K. Gorny, O. M. Vyaselev, J. A. Martindale, V. A. Nandor, C. H. Pennington, P. C. Hammel, W. L. Hults, J. L. Smith, P. L. Kuhns, A. P. Reyes and W. G. Moulton: Phys. Rev. Lett. **82** (1999) 177.

[110] G-q. Zheng, H. Ozaki, W. G. Clark, Y. Kitaoka, P. Kuhns, A. P. Reyes, W. G. Moulton, T. Kondo, Y. Shimakawa and Y. Kubo: Phys. Rev. Lett. **85** (2000) 405.

[111] P. Fulde and R. A. Ferrell: Phys. Rev. **135** (1964) A550; A. I. Larkin and Y. N. Ovchinnikov: Sov. Phys. -JETP **20** (1965) 762.

[112] V. Barzykin and D. Pines: Phys. Rev. B **52** (1995) 13585.

[113] N. Bulut and D. J. Scalapino: Phys. Rev. Lett. **67** (1991) 2898.

[114] E. Abrahams and T. Tsuneto: Phys. Rev. **152** (1966) 416.

[115] J. R. Engelbrecht, M. Randeria and C. A. R. Sá de Melo: Phys. Rev. B **55** (1997) 15153.

[116] P. W. Anderson: Phys. Rev. **112** (1958) 1900. *ibid* **112** (1958) 795.

[117] T. Takimoto and T. Moriya: J. Phys. Soc. Jpn **67** (1998) 3570.

[118] T. Sato, T. Yokoya, Y. Naitoh, T. Takahashi, K. Yamada, and Y. Endoh: Phys. Rev. Lett. **83** (1999) 2254.

[119] For example, J. Rossat-Mignod, L. P. Regnault, C. Vettier, P. Bourges, P. Burlet, J. Bossy, J. Y. Henry and G. Lapertot: Physica C **185&189** (1991) 86; H. A. Mook, M. Yethiraj, G. Aeppli, T. E. Mason and T. Armstrong: Phys. Rev. Lett. **70** (1993) 3490; H. F. Fong, B. Keimer, P. W. Anderson, D. Reznik, F. Dogan and I. A. Aksay: Phys. Rev. Lett. **75** (1995) 316; P. Bourges, L. P. Regnault, Y. Sidis and C. Vettier: Phys. Rev. B **53** (1996) 876; P. Dai, M. Yethiraj, H. A. Mook, T. B. Lindemer and F. Dogan: Phys. Rev. Lett. **77** (1996) 5425.

[120] P. Dai, H. A. Mook, S. M. Hayden, G. Aeppli, T. G. Perring, R. D. Hunt and F. Dogan: Science **284** (1999) 1344; H. F. Fong, P. Bourges, Y. Sidis, L. P. Regnault, J. Bossy, A. Ivanov, D. L. Milius, I. A. Aksay and B. Keimer: Phys. Rev. B **61** (2000) 14773.

[121] H. Yoshikawa and T. Moriya: J. Phys. Soc. Jpn **68** (1999) 1340.

[122] D. K. Morr and D. Pines: Phys. Rev. Lett. **81** (1998) 1086; Ar. Abanov and A. V. Chubukov: Rev. Lett. **83** (1999) 1652; (E) Rev. Lett. **84** (2000) 398.

[123] A. Rosch: Phys. Rev. Lett. **82** (1999) 4280; A. Rosch: Physica B **280** (2000) 341.

[124] N. E. Hussey, J. R. Cooper, J. M. Wheatley, I. R. Fisher, A. Carrington, A. P. Mackenzie, C. T. Lin and O. Milat: Phys. Rev. Lett. **76** (1996) 122.

[125] H. Kohno and K. Yamada: Prog. Theor. Phys. **85** (1991) 13.

[126] K. Yamada and K. Yosida: Prog. Theor. Phys. **76** (1986) 621.

[127] T. Dahm, D. Manske and L. Tewordt: Phys. Rev. B **60** (1999) 14888.

[128] P. J. Hirschfeld, S. M. Quinlan and D. J. Scalapino: Phys. Rev. B **55** (1997) 12742.

[129] L. B. Ioffe and A. J. Millis: Science. **285** (1999) 1241; L. B. Ioffe and A. J. Millis: Phys. Rev. B **61** (2000) 9077.

[130] T. Xiang, C. Panagopoulos and J. R. Cooper: Int. J. Mod. Phys. B **12** (1998) 1007.

[131] S. Kamal, R. Liang, A. Hosseini, D. A. Bonn and W. N. Hardy: Phys. Rev. B **58** (1998) R8933; C. Panagopoulos, B. D. Rainford, J. R. Cooper, W. Lo, J. L. Tallon, J. W. Loram, J. Betouras, Y. S. Wang and C. W. Chu: Phys. Rev. B **60** (1999) 14617.

[132] Y. J. Uemura *et al.*: Phys. Rev. Lett. **62** (1989) 2317.

[133] A. J. Millis, S. M. Girvin, L. B. Ioffe and A. I. Larkin: J. Phys. Chem. Solids. **59** (1998) 1742.

[134] J. Mesot, M. R. Norman, H. Ding, M. Randeria, J. C. Campuzano, A. Paramekanti, H. M. Fretwell, A. Kaminski, T. Takeuchi, T. Yokoya, T. Sato, T. Takahashi, T. Mochiku and K. Kadowaki: Phys. Rev. Lett. **83** (1999) 840.

[135] A. Paramekanti, M. Randeria, T. V. Ramakrishnan and S. S. Mandal: Phys. Rev. B **62** (2000) 6786; L. Benfatto, S. Caprara, C. Castellani, A. Paramekanti and M. Randeria: preprint (cond-mat/0008100)

[136] A. J. Legget: Phys. Rev. **140** (1965) A1869.

[137] T. Okabe: J. Phys. Soc. Jpn **67** (1998) 2792; *ibid* 4178.

[138] H. Maebashi and H. Fukuyama: J. Phys. Soc. Jpn **66** (1997) 3577; *ibid* **67** (1998) 242.

[139] N. E. Bickers, D. J. Scalapino and S. R. White: Phys. Rev. Lett. **62** (1989) 961; N. E. Bickers and D. J. Scalapino: Ann. Phys. (N.Y.) **193** (1989) 206.

[140] G. Baym and L. P. Kadanoff: Phys. Rev. **124** (1961) 287.

[141] T. Moriya: *Spin Fluctuations in Itinerant Electron Magnetism* (Springer-Verlag, 1985).

[142] P. Monthoux and D. J. Scalapino: Phys. Rev. Lett. **72** (1994) 1874.

[143] C.-H. Pao and N. E. Bickers: Phys. Rev. Lett. **72** (1994) 1870; Phys. Rev. B **51** (1995) 16310.

[144] T. Dahm and L. Tewordt: Phys. Rev. Lett. **74** (1995) 793; Phys. Rev. B **52** (1995) 1297.

[145] M. Langer, J. Schmalian, S. Grabowski and K. H. Bennemann: Phys. Rev. Lett. **75** (1995) 4508.

[146] J. J. Deisz, D. W. Hess and J. W. Serene: Phys. Rev. Lett. **76** (1996) 1312.

[147] S. Koikegami, S. Fujimoto and K. Yamada: J. Phys. Soc. Jpn **66** (1997) 1438.

[148] T. Takimoto and T. Moriya: J. Phys. Soc. Jpn **66** (1997) 2459.

[149] H. Kino and H. Kontani: J. Phys. Soc. Jpn. **67** (1998) 3691.

[150] H. Kondo and T. Moriya: J. Phys. Soc. Jpn. **67** (1998) 3695.

[151] J. Schmalian: Phys. Rev. Lett. **81** (1998) 4232.

[152] H. Kontani and K. Ueda: Phys. Rev. Lett. **80** (1998) 5619.

[153] K. Miyake and O. Narikiyo: J. Phys. Soc. Jpn **63** (1994) 3821.

[154] S. Koikegami and K. Yamada: J. Phys. Soc. Jpn. **69** (2000) 768; J. Phys. Soc. Jpn. **69** (2000) 1950.

[155] T. Dahm, D. Manske and L. Tewordt: Phys. Rev. B **55** (1997) 15274.

[156] J. M. Tranquada, B. J. Sternlieb, J. D. Axe, Y. Nakamura and S. Uchida: Nature **375** (1995) 561; J. M. Tranquada, J. D. Axe, N. Ichikawa, Y. Nakamura, S. Uchida and B. Nachumi: Phys. Rev. B **54** (1996) 7489.

[157] J. Zaanen and A. M. Oleś: Ann. Phys. **5** (1996) 224.

[158] V. J. Emery, S. A. Kivelson and O. Zachar: Phys. Rev. B. **56** (1997) 6120.

[159] S. R. White and D. J. Scalapino: Phys. Rev. Lett. **80** (1998) 1272.

[160] T. Mizokawa and A. Fujimori: Phys. Rev. Lett. **80** (1998) 1320.

[161] H. Yamase, H. Kohno, H. Fukuyama and M. Ogata: J. Phys. Soc. Jpn **68** (1999) 1082.

[162] K. Machida and M. Ichioka: J. Phys. Soc. Jpn **68** (1999) 2168; M. Ichioka and K. Machida: J. Phys. Soc. Jpn **68** (1999) 4020.

[163] K. Kuroki, R. Arita and H. Aoki: Phys. Rev. B. **60** (1999) 9850.

[164] D. H. Wu, J. Mao, S. N. Mao, J. L. Peng, X. X. Xi, T. Venkatesan, R. L. Greene, and S. M. Anlage: Phys. Rev. Lett. **70** (1993) 85; A. Andreone, A. Cassinese, A. Di Chiara, R. Vaglio, A. Gupta, and E. Sarnelli: Phys. Rev. B. **49** (1994) 6392; C. W. Schneider, Z. H. Barber, J. E. Evetts, S. N. Mao, X. X. Xi and T. Venkatesan: Physica C **233** (1994) 77; S. M. Anlage, D.-H. Wu, J. Mao, S. N. Mao, X. X. Xi, T. Venkatesan, J. L. Peng, and R. L. Greene: Phys. Rev. B. **50** (1994) 523; L. Alff, S. Meyer, S. Kleefisch, U. Schoop, A. Marx, H. Sato, M. Naito, and R. Gross: Phys. Rev. Lett. **83** (1999) 2644.

[165] S. Kashiwaya, T. Ito, K. Oka, S. Ueno, H. Takashima, M. Koyanagi, Y. Tanaka, and K. Kajimura: Phys. Rev. B. **57** (1998) 8680; L. Alff, A. Beck, R. Gross, A. Marx, S. Kleefisch, Th. Bauch, H. Sato, M. Naito, and G. Koren: Phys. Rev. B. **58** (1998) 11197.

[166] Y. Tanaka and S. Kashiwaya: Phys. Rev. Lett. **74** (1995) 3451; S. Kashiwaya, Y. Tanaka, M. Koyanagi, H. Takashima and K. Kajimura: Phys. Rev. B. **51** (1995) 1350; S. Kashiwaya, Y. Tanaka, M. Koyanagi and K. Kajimura: Phys. Rev. B. **53** (1996) 2667.

[167] M. Ogata: J. Phys. Soc. Jpn **66** (1997) 3375; K. Kuroki and H. Aoki: J. Phys. Soc. Jpn **67** (1998) 1533.

[168] J. D. Kokales, P. Fournier, L. V. Mercaldo, V. V. Talanov, R. L. Greene, S. M. Anlage: Phys. Rev. Lett. **85** (2000) 3696; R. Prozorov, R. W. Giannetta, P. Fournier, R. L. Greene: Rev. Lett. **85** (2000) 3700.

[169] F. Hayashi, E. Ueda, M. Sato, K. Kurahashi and K. Yamada: J. Phys. Soc. Jpn **67** (1998) 3234.

[170] T. Takahashi and T. Sato: private communications.

[171] C. C. Tsuei and J. R. Kirtley: Phys. Rev. Lett. **85** (2000) 182.

[172] D. Manske, I. Eremin and K. H. Bennemann: Phys. Rev. B. **62** (2000) 13922.

[173] K. Yamada: private communications.